June 2019

IMPACTS OF URBAN DEVELOPMENT PATTERN ON RUNOFF PEAK FLOWS AND STREAMFLOW FLASHINESS OF PERI-URBAN CATCHMENTS: ASSESSING THE PERFORMANCE OF PHYSICAL AND DATA-DRIVEN MODELS FOR REAL-TIME ENSEMBLE FLOOD FORECASTING

Babak Kasaee Roodsari
Syracuse University

Abstract

Urban growth is a global phenomenon, and the associated impacts on hydrology from land development are expected to increase, especially in peri-urban catchments, which are newly developing catchments in proximity of growing cities. In northern climates, hydrologic response of peri-urban catchments change with the water budget and climatic conditions. As a result, runoff response of northern peri-urban catchments can vary immensely across seasons. During warm seasons, the evapotranspiration (ET) and infiltration rates are high, so urban floods are expected to occur during high intensity, low duration storm events. During cold seasons and below freezing temperatures, surficial soils are typically frozen and nearly impervious. In addition, the ET rate is low throughout winter. Therefore, the difference in runoff response between peri-urban and natural catchments is least in winter. Furthermore, winter snow redistribution by plowing and endogenous urban heat affect the snowmelt timing and frequency. Due to the limited availability of data on snow removal and redistribution activities in northern peri-urban catchments, cold-season hydrologic modeling for peri-urban catchments remains a challenging task in urban hydrology.

Research on the cold season hydrologic response of peri-urban catchments are mostly limited to Finland, Sweden, and Canada. The resulting research gap on seasonal change in hydrologic response of peri-urban catchments is common to many northern settings. In the first phase of this study, I use intensive discharge monitoring records at several peri-urban catchments near Syracuse, NY to calculate and compare seasonal runoff peak flows among several peri-urban catchments. These are selected to provide a range of drainage area and imperviousness to clarify

the impact of urban development and catchment size on seasonal hydrologic behavior of peri-urban catchments.

It is well understood that greater peak flows and higher stream flashiness are associated with increased surface imperviousness and storm location. However, the effect of the distribution of impervious areas on runoff peak flow response and stream flashiness of peri-urban catchments has not been well studied. In the second phase of this dissertation, I define a new geometric index, Relative Nearness of Imperviousness to the Catchment Outlet (RNICO), to correlate imperviousness distribution of peri-urban catchments with runoff peak flows and stream flashiness. The study sites for this phase of the study include ninety peri-urban catchments in proximity of 9 large US cities: New York, NY (NYC), Syracuse, NY, Baltimore, MD, Portland, OR, Chicago, IL, Austin, TX, Houston, TX, San Francisco, CA, and Los Angeles, CA. Based on RNICO, all development patterns are divided into 3 classes: upstream, centralized, and downstream. Analysis results showed an obvious increase in runoff peak flows and decrease in time to peak as the centroid of imperviousness moves downstream. This indicates that RNICO is an effective tool for classifying urban development patterns and for macroscale understanding of the hydrologic behavior of small peri-urban catchments, despite the complexity of urban drainage systems. Results for nine cities show strong positive correlations between RNICO and runoff peak flows and stream flashiness index for small peri-urban catchments. However, the area threshold used to distinguish small and large catchments differs slightly by location. For example, for Chicago, IL, NYC, NY, Baltimore, MD, Houston, TX, and Austin, TX area threshold values of 55, 40, 50, 42, and 32 km^2 emerged, runoff peak flows in catchments with drainage area below these values were positively correlated to RNCIO. This first phase of this study suggests that RNICO is a stronger predictor of runoff peak flow and stream-flow regime in

humid northern and southern US study sites, compared to more arid western US study sites. This difference is likely due to the greater precipitation rates and greater antecedent soil moisture contents for humid climates. The extent of urban infrastructure is less likely to control the effectiveness of RNICO for predicting runoff peak flows and R-B flashiness index for the selected study sites, due to the relatively similar urban development level within the peri-urban study catchments.

Consistent forecast of peak flows across scales in flood hydrographs remains a challenge for most hydrologic models. Urbanization increases the magnitude and frequency of peak flows, often challenging the forecast ability for real-time flood prediction. Following advances in satellite and ground-based meteorological observations, global and continental real-time ensemble flood forecasting systems use a variety of physical hydrology models to predict urban peak flows. Artificial intelligence (AI) models provide an alternative approach to physical hydrology models for real-time flood forecasting. Despite recent advances in AI techniques for hydrologic prediction, ensemble stream-flow prediction by these methods has been limited. In addition, application of AI models for flood forecasting has been limited to large river basins, with very limited research on use of AI models for small peri-urban catchments. Flood forecasting in small urban catchments can be a critical task to urban safety due to the short time of concentration and quick precipitation runoff response. AI flood forecasting models typically apply upstream streamflow measurements to forecast downstream flood discharge. Therefore, the storm direction may change the flood travel time and time to peak, which challenges accurate flood forecasting. For example, if the storm direction is upstream through an AI model trained on the upstream gage data may fail to accurately predict peak flow magnitude and timing, at the

outlet, this is due to the quicker runoff response of the downstream gage compared to the upstream station. There has been very limited focus on the impact of storm direction on peak flow response of urban catchments and available literature are limited to lab-scale prototypes and rainfall simulators. These may not fully represent real-world flooding scenarios. Therefore, the impact of storm direction on flood forecasting performance of peri-urban catchments is another important research gap in real-time urban flood forecasting.

In the third phase of my dissertation project, I initially assess the impact of storm direction on the flood forecasting performance of an Adaptive Neuro Fuzzy Inference System (ANFIS) at a peri-urban catchment in proximity of Syracuse, NY. Next, I compare the relative utility of physical hydrology and AI approaches to predict flood hydrograph in peri-urban catchments. For this comparison, I selected ANFIS, and Sacramento Soil Moisture Accounting Model (SAC-SMA) for real-time ensemble re-forecasting of streamflow in several small to medium size suburban catchments near NYC for Hurricane Irene and a smaller storm event. The SAC-SMA model is a physical hydrology model that was initially developed by Burnash et al. (1973). The National Oceanic and Atmospheric Administration (NOAA) selected the SAC-SMA lumped model as a comparison baseline for participating distributed hydrologic models in the Distributed Model Intercomparison Project (DMIP), which aimed to identify the most suitable model for National Weather Service (NWS) streamflow prediction across the US (http://www.nws.noaa.gov/ohd/hrl/dmip/). More importantly, the NWS is currently using the lumped form of SAC-SMA for ensemble flood forecasting across the US (Emerton et al., 2016). For these reasons, I chose to employ a lumped version of SAC-SMA in my dissertation project. SAC-SMA performed well for both large and small events and for lead times of three to 24 hours, but ANFIS predicted the Hurricane Irene flood discharge well only for short lead times in

small study catchments. ANFIS had reasonable percent bias (*PBIAS*) for predicting the small storm event for all lead times, indicating the utility of ANFIS for small events. In addition, the accuracy of both SAC-SMA and ANFIS models for ensemble flood prediction did not change significantly with catchment size and imperviousness. Overall, results of the third phase of this study suggest that the lumped SAC-SMA model may be a reliable option for local urban flood forecasting for evacuation plan lead time up to 24 hours. Due to the uncertainties in future climatic conditions, my study emphasizes the importance of using physical hydrology models for real-time flood forecasting of large events in small urban catchments. This recommendation is based on the finding that the performance of data-driven models may greatly decrease with the storm scale if the training period includes storms of magnitude less than storms in the validation period.

IMPACTS OF URBAN DEVELOPMENT PATTERN ON RUNOFF PEAK FLOWS AND STREAMFLOW FLASHINESS OF PERI-URBAN CATCHMENTS: ASSESSING THE PERFORMANCE OF PHYSICAL AND DATA-DRIVEN MODELS FOR REAL-TIME ENSEMBLE FLOOD FORECASTING

by

Babak Kasaee Roodsari

B.S., Ferdowsi University, Mashhad, Iran, 2005
M.S., Ferdowsi University, Mashhad, Iran, 2008

Dissertation
Submitted in partial fulfillment of the requirements for the degree of
Doctor of Philosophy in Civil Engineering

Syracuse University
June 2019

To

my parents, Seifollah and Tahereh,

and my siblings.

Acknowledgment

I would like to express my special appreciation and thanks to my PhD advisor, David G. Chandler. He kindly supported me through this dissertation project and taught me many important concepts of physical hydrology. I am very grateful to him for his insightful scientific discussions and suggestions.

I will forever be thankful to my committee members, Charles N. Kroll, Christa Kelleher, Chris E. Johnson, and Shobha K. Bhatia for serving as my committee members. I would like to acknowledge the remarkable help and technical advice I received from you. I want to thank you for your many insightful comments and suggestions.

I am very thankful of Dr. Chilukuri Mohan for serving as the chair committee of my defense.

I would also want to thank our department staff for their assistance at Syracuse University: Elizabeth Buchanan, Heather Kirkpatrick, Maureen Hale, and Morgan Narkiewicz.

I am very thankful for the financial support provided by the Department of Civil & Environmental Engineering at Syracuse University in the form of fellowship and teaching assistantships. Some parts of my research were conducted with funds from grants provided by the National Science Foundation, Grant/Award Number: SBE-1444755 and 1417542.

Table of Contents

List of Tables

List of Figures

1. Chapter 1 (Introduction)

1.1. Motivation

1.1.1. Impacts of urbanization on peak flows in northern climates

Urban floods endanger human lives, damage private property, and cause a cascade of environmental impacts (Jha et al., 2012; World Bank, 2013). For example, floods release pollutants and heavy metals into groundwater and rivers, impairing water quality (Markantonis et al., 2013). Furthermore, flooding can cause significant disruption to urban services such as transportation, water provision, housing, and education (Hammond et al., 2015).

Global urban growth increases land surface imperviousness and elevates the flooding potential of urban catchments. The United Nations reported that approximately 70% of the world's population will live in urban areas by 2050 (United Nations, 2010). As a consequence of rapid urbanization in the absence of a reliable stormwater management system, many urban watersheds worldwide have been threatened by flooding due to increased surface imperviousness (Miguez et al., 2015; Smith et al., 2005). Consequently, the study of the influence of urbanization and increased imperviousness on hydrologic behavior of peri-urban catchments, which are newly developed urban catchments in proximity of large growing cities.

In northern urban catchments, stormwater runoff peak flows vary throughout the year in response to the water and energy budgets. Typically, evapotranspiration, infiltration, and available soil water storage capacity are minimized during the cold season with a

resulting decrease in runoff peak flows. This is largely due to storage of a significant fraction of precipitation in northern catchments as snow (Heino and Hellsten, 1983; Valtanen et al., 2014). As a result, spring snowmelt is a large part of annual runoff (Koivusalo et al., 2006; Taylor, 1982, 1977). Urban snow is often redistributed or removed by human activities (Bengtsson and Westerström, 1992; Buttle and Xu, 1988; Ho and Valeo, 2005; Semádeni-Davies, 2000; Semádeni-Davies and Bengtsson, 1999). Study of snowmelt runoff from a rural and a suburban catchment in Peterborough, Ontario showed that suburban catchment reacts more quickly to snowmelt and rain-on-snow event and produces more initial quick flow due to the microclimatic and hydraulic alterations caused by human activities (Buttle and Xu, 1988). Bengtsson and Westerström (1992) showed that daily melt rates in Lalea, Sweden is about 10 mm greater in the city than in rural areas as a result of increased long wave radiation. In addition, infiltration rate of urban soil significantly decreased in the cold season and snowmelt runoff from pervious and impervious areas were almost the same. Similar results were indicated by Ho and Valeo (2005) in an urban snow properties study at Calgary, Canada. They found that both the urban snow removal activities and the physical characteristic changes in urban environment largely influence the energy-balance of snowpacks. Antecedent soil moisture was found to have very little effect on frozen ground and pervious areas act nearly as impervious. Additionally, the timing of snowmelt in northern urban catchments can be altered by application of deicers to roadways and heat loss from the roof tops and other infrastructure. However, data available for human snow redistribution and removal activities are limited and snowmelt peak flow analysis remains a challenging problem in urban hydrology.

The influence of urbanization on magnitude and seasonality of peak flows in cold climates is not well addressed and previous studies have been mostly limited to Finland, Sweden, and Canada (Eimers and McDonald, 2015; Sillanpää and Koivusalo, 2015; Valtanen et al., 2014). Valtanen et al. (2014) studied seasonal runoff volume and peak flows at three urbanized catchments in southern Finland representing low, medium, and high urbanization levels, respectively. They found that the medium and high urbanized catchments produce more runoff during warm season, whereas less urbanized catchments have greatest runoff generation during cold season. The spring snowmelt freshet started a few weeks earlier in the two most urbanized catchments and the snowmelt runoff rates in these catchments were smaller than during summer storms. The result from this study suggested that the stormwater runoff in cold climates is season dependent and the impact of imperviousness is much less during cold season than during summer. Similarly, studies on a developing catchment in the city of Espoo in southern Finland (Sillanpää and Koivusalo, 2015) and nine urbanized catchments in southern Ontario, Canada (Eimers and McDonald, 2015) indicated less pronounced impact of imperviousness on peak flows during cold season.

The first phase of this dissertation project demonstrates the impacts of urbanization on seasonal runoff peak flow response of northern peri-urban catchments. This is based on intensive field work to develop discharge records for five sub-catchments of Onondaga Lake watershed, in central New York State, representing a range of imperviousness from eleven to 48 percent. The collected discharge data are used to calculate peak flow magnitudes for a range of event magnitudes in the study period. The calculated peak

flows are then classified into four seasons and compared for different stations to study the impacts of urbanization on seasonal peak flows. The results support understanding of changes in hydrologic response of northern peri-urban catchments with changing climatic conditions. Study sites are in the proximity of Syracuse, NY and generate runoff from both spring snowmelt, which includes significant annual accumulation of lake effect snow and from convective summer storms, both of which cause flash floods. These attributes make the region a good study case for comparison of seasonal flooding.

Stormwater runoff management in northern peri-urban catchments is often challenging due to the great seasonal variations in water budget in these catchments. Furthermore, many northern US cities, such as Syracuse, NY, have old stormwater infrastructures with combined sewer overflows that can potentially impair water quality in rivers and lakes, and impose significant potential costs to the municipalities. Understanding the seasonal variations in urban runoff volumes and peak flow magnitudes is expected to help municipalities better develop stormwater management plans to efficiently mitigate runoff peak flows, in order to reduce costs associated with urban floods and CSOs. For example, seasonal peak flow data could be used for real-time control of slow release valves in rainwater harvesting cisterns. If the magnitude of historical seasonal runoff peak flows is introduced to an automated flow control valve, the system could release a enough stored water into the sewer system before the start of a new storm event to reduce the chance of CSO during each season.

1.1.2. Impacts of urban development pattern on runoff peak flows

The impact of increased fractional impervious area on flooding potential of urbanized catchments has been assessed across several international studies with a wide range of catchment sizes and climatic settings in several empirical and modeling studies. Example study locations in northern climates include several peri-urban catchments in Canada and Finland. For example, Nirupama and Simonovic (2007) found approximately 270% increase in peak flow magnitudes associated with extensive urban growth over a 27-year period for a large Canadian river basin. Similarly, stormwater runoff peak flows during summer and spring snowmelt at a small, highly impervious catchment in southern Finland were approximately 100% to 300% greater than those for a slightly pervious catchment over a 2-year study period (Valtanen et al., 2014). Flood peak discharge of another small Finnish catchment increased by about 50 times over the predevelopment condition during five years of heavy urbanization (Sillanpää and Koivusalo, 2015). Similarly, increased stream flashiness and in large increase in quick flows (300%) were associated with catchment imperviousness at several medium to large Canadian catchments in both rural and urban settings over a 9-year period (Eimers and McDonald, 2015). Furthermore, runoff peak flows of a medium-size, highly urbanized catchment in Georgia, USA, were 30% to 100% greater than those for low development density catchments for the 25 largest events of a 39-year study period (Rose and Peters, 2001). In contrast, Zope et al. (2015) projected a marginal urbanization impact on peak flows in a major catchment in Mumbai City, India over 40 years of urban development but warned about the importance of these impacts when combined with tidal influences. Modeling efforts projected increased flood stage and inundated areas for a medium-size urban

catchment (300 km^2) in Chennai Metropolitan City, India due to 30-year urban growth (Suriya and Mudgal, 2012) and in a large Chinese river basin (19,354 km^2) over nine years of urbanization (Wang and Yang, 2013). The increased daily peak discharge was linked to the increased fractional impervious area in a medium-size highly urbanized catchment (78 km^2) in Qinhuai River basin, China over a 30-year study period (Du et al., 2015).

Stream flashiness typically refers to the frequency, magnitude, and duration of short-term variations in water level and discharge. These typically increase with urbanization and increased imperviousness (Baker et al., 2004; Eimers and McDonald, 2015; Julian and Gardner, 2014). To compare these streamflow attributes across sites and time, Baker et al. (2004) developed a dimensionless stream flashiness index, Richards–Baker index (R-B index):

$$R-B\ Index = \frac{\sum_{i=1}^{n} |q_i - q_{i-1}|}{\sum_{i=1}^{n} q_i} \qquad \text{(Eq. 1)}$$

Where q_i is the daily mean discharge of the *ith* day (m^3/s) and n is the number of days in the study period.

The application of the R-B Index (Equation 1) to data from 515 United States Geological Survey (USGS) stream gages over a 27-year period showed that the R-B index is negatively correlated with catchment drainage area and positively correlated with catchment imperviousness (Baker et al., 2004). They showed statistically significant

increases in flashiness from 1974 to 2001 due to increased imperviousness in urban catchments including Milwaukee, Chicago, and Detroit (Baker et al., 2004).

Increased frequency and magnitude of peak flows in urbanized catchments are commonly attributed to increased area of imperviousness (Arnold and Gibbons, 1996; Cheng et al., 2010). Generally, as more natural land cover is converted to impervious surface, the evapotranspiration (Grimmond and Oke, 1999), infiltration (Valtanen et al., 2014), and soil storage capacity (Bhaskar and Welty, 2012) are reduced. The result of these alterations to the water balance often increases the quantity of runoff and decreases travel time to the catchment outlet, leading to greater peak flows. Although the fractional area of imperviousness has been widely studied as a control criterion for urban peak flows, this metric does not address the complexity of imperviousness distribution in the catchment (Du et al., 2015). For example, Mejía and Moglen (2009, 2010a, 2010b) and Yang et al. (2011) found that the spatial distribution of impervious areas is an important control on the hydrologic response of urban catchments. Mejía and Moglen (2009) defined several water resources-based objective functions to optimize imperviousness distribution in a hypothetical catchment and concluded that applying imperviousness threshold policies that limit the areas of surface impervious to 10% (Schueler, 1994; Valtanen et al., 2014) may cause an unintended low-density sprawl across the catchment. Yang et al. (2011) assessed the impact of spatial distribution of imperviousness on runoff peak flows of several catchments in Indiana, USA, using a combined GIS and hydrologic modeling approach. They concluded that the spatial distribution of imperviousness is scale dependent; at the urban catchment scale, the effect of greater imperviousness is

manifested through changes to processes affecting runoff, whereas at the watershed scale, the influence of the urban runoff contribution is more closely related to runoff travel time to the point of measurement.

Previous studies of the impact of imperviousness distribution on peak flows in urban catchments have suggested greater hydrologic impacts from land development closer to streams (Su et al., 2014). The physical rationale for the linkage between impervious surface location and peak flow can be explained by surface runoff travel time (Meierdiercks et al., 2010). During extreme rainfall events, impervious areas generate runoff earlier than pervious areas due to lower infiltration rates and more hydraulically efficient flow paths. As a result, they transmit early flood waves to the catchment outlet (Arnold and Gibbons, 1996; Du et al., 2015). These early flood waves travel through the catchments soil and streambed (Liebe et al., 2009) and are attenuated through time (Lamberti and Pilati, 1996) by losses to storage. The travel time of flood waves from the source to the outlet point depends on the flow path length and the proximity of contributing impervious areas to the catchment outlet. Therefore, the distance from impervious areas to the stream and then the stream outlet is the major control on flood wave travel time and peak flood stage (Du et al., 2015). It is well understood that impervious areas close to the outlet contribute greater discharge to the rising limb and peak of the hydrograph than impervious areas farther from the outlet.

Climate and storm event characteristics such as depth, duration, and intensity may also impact runoff peak flow response of urban catchments. Urban catchments in

Mediterranean climate cities Los Angeles, CA and San Francisco, CA are typically flooded during long winter rainfall events from the Pacific Ocean to the land surface. On the other hand, urban flooding in the northeastern US typically occurs during summer storms and spring snowmelt events. In both western and northeastern US cites, runoff peak flows and flood travel time can be influenced by many parameters such as stormwater systems (Miller et al., 2014), catchment drainage area, imperviousness, and development pattern. This dissertation is motivated by the importance of understanding how development patterns impact flooding across several US peri-urban catchments with different climate conditions. I compare groups of western, northern, southern US peri-urban catchments with a wide range of imperviousness and drainage areas to provide insight into the combined impact of climate and imperviousness on runoff peak flow response of urban catchments.

Few assessments have been published on the impact of land development pattern and spatial distribution of impervious surfaces on peak flows in urbanized catchments. Whereas most existing studies have used physical hydrology modeling approaches to analyze different land development scenarios (Du et al., 2015; Su et al., 2014; Yang et al., 2011; Zhang and Shuster, 2014). Calibration and validation of physical hydrology models require quantitative information and high-quality input datasets, and significant knowledge of hydrologic processes and modeling. Many urban municipalities and government authorities are interested in macro-management of urban watersheds but may not have enough capacity for calibrating hydrologic models. Although physical hydrology models can provide some insight into the behavior of natural systems, they are

limited by uncertainty (Jakeman and Hornberger, 1993; Singh and Dutta, 2017) and errors due to simplification, calibration, and validation (Yen et al., 2015) and scale effects (Carpenter and Georgakakos, 2006; Grayson et al., 1992; Koren et al., 1999). For example, stream-flows in small first-order catchments may be more responsive to small events than stream-flow of large catchments due to the closer match between the scale of the storm and catchment time of concentration (Nicótina et al., 2008; Wilson et al., 1979) and catchment storage capacity (Sapriza-Azuri et al., 2015). Therefore, models developed for a specific scale may not closely represent the processes and behavior of small urban catchments.

In the second phase of my dissertation, I overcome these limitations by developing a new geometric index which can be used for urban planning. For this purpose, I took advantage of my field monitoring data at Onondaga lake watershed sub-catchments, comprehensive discharge records at several USGS gages, and the National Land Cover Dataset 2011. These datasets enabled simple calculation of the impact of distribution of impervious areas on peak flows, using geometric and statistical analysis approaches. To accomplish this goal, I defined a new geometric index, Relative Nearness of Imperviousness to the Catchment Outlet (RNICO), based on the distribution of impervious surfaces in the catchment and the location of catchment centroid. Based on early results, I hypothesized that RNICO is a broadly applicable index to classify the peak flow response of small to medium size study catchments ($A< 40$ km^2). I selected 90 peri-urban catchments in proximity of nine large growing western, northern, and southern US cities to perform the analysis for different climate conditions and over a wider range of urban catchment

scales. To demonstrate the method, I calculated RNICO for the study sites and correlated it to runoff peak flows and streamflow regime indices.

Results of this phase of my dissertation studies may be valuable for macro-scale management of urban development patterns in growing peri-urban catchments. Urban planners and municipalities can use the RNICO index to develop hydrologically sustainable development strategies for growing cites instead of allowing random urban sprawl. A great advantage of the RNICO index is the simplicity of the calculation based on land cover maps and discharge records that are typically available for many urban catchments worldwide.

1.1.3. Low Impact Development (LID)

One practical solution proposed for mitigating flood damage during high intensity, low duration storm events is the investment in LID to complement centralized water infrastructures (Sapkota et al., 2014; Tjandraatmadja et al., 2005). LIDs are small to medium scale structures that mitigate or capture stormwater runoff at the source. The captured water may be reused for local indoor and outdoor purposes (Domínguez et al., 2017; Sojka et al., 2016; Younos, 2011). Typical examples of LID are bioretention systems, green roofs, detention and retention ponds, rain barrels, porous asphalts, and rain gardens. A primary reason for adopting LID is the positive impacts of these systems on the environment (Mao et al., 2017), and water resources (van Roon, 2007). For example, LID strategies can mitigate the stormwater runoff volume and peak flow to prevent local flooding in urban areas (Alves et al., 2018), improve the stormwater runoff quality before percolating to the groundwater (Dietz and Chester, 2018), and mitigate the

impact of urban heat island in urban areas by increasing the green space (Herath et al., 2018). In addition, LID improves water security, strengthens local economy, regenerate and protect the natural environment in urbanized areas, and supports community well-being (Biggs et al., 2009).

The hydrologic performance of LID in northern climates may change seasonally due to variability across climatic and hydrologic conditions (Driscoll et al., 2015). There has been limited focus on assessing the seasonal performance of LID technologies in previous literature (Khan et al., 2013; Muthanna et al., 2008; Roseen et al., 2009). Roseen et al. (2009) have shown great potentials of LID in mitigating runoff peak flow magnitude and reducing detention time, but most of their performances used in their study cannot be easily translated to simple runoff volume and peak flow reduction metrics (Driscoll et al., 2015). In the third phase of this dissertation, I synthesize the current knowledge on seasonal change in runoff reduction performance of bioretention cells and green roofs.

Although LID approaches hold the promise of mitigating surface runoff, reliability of such systems depends on the expected design storm's return period. For example, a stormwater detention pond that is designed to operate for a precipitation event with return period of 25 years may fail to operate efficiently during 100- or 500-year events. One non-structural alternative to investments in decentralized stormwater systems is implementation of an early warning system to predict flooding events with an appropriate time lag (Jayawardena et al., 2014). A great challenge for real-time flood forecasting models is model selection. Previous studies on urban flood forecasting have argued that

AI models can be used as an advanced alternative to process-based models to improve the accuracy of real-time flood forecasting. However, practical application of AI models in real-time flood forecasting systems for small peri-urban catchments has been limited. This motivated me to compare the performance of an AI and a physical model for real-time flood forecasting in small peri-urban catchments over the next phase of my dissertation project.

1.1.4. Model selection challenge for real-time flood forecasting in small peri-urban catchments

Real-time flood forecast systems attempt to provide emergency management authorities sufficient lead time to execute plans for evacuation and asset protection in urban watersheds during extreme rainfall events. However, developing these systems is complicated by spatial and temporal variations and uncertainty in rainfall distributions and complex rainfall-runoff relationships. As such, flood forecasting remains one of the most challenging tasks in hydrology (Chang et al., 2007; Wood et al., 2017).

Many contemporary local and continental flood forecasting systems exploit recent advances in satellite and ground-based meteorological observations through probabilistic streamflow forecasting approaches (Cloke and Pappenberger, 2009; Day, 1985; Emerton et al., 2016; Gouweleeuw et al., 2005). Probabilistic flood forecasting systems, often called Ensemble Streamflow Prediction (ESP) systems, typically include a Numerical Weather Prediction (NWP) unit and a physical flood forecasting model component. The NWP generates a series of meteorological forecast ensembles based on different future climate assumptions. The NWP forecast ensembles are used to generate a series of future

hydrographs, called a spaghetti hydrograph (Emerton et al., 2016). This procedure is performed on a real-time basis and the flood forecast model component is continuously calibrated up to the current time using historical weather and streamflow observations. A great benefit of a probabilistic approach over the traditional single-run deterministic modeling approach is the generation of an ensemble of predicted flood hydrographs that facilitate uncertainty analyses (Day, 1985). A spaghetti hydrograph informs emergency managers about possible future flooding scenarios and guides strategies for evacuation and rescue.

Local and global real-time flood forecasting systems have typically used physical hydrology models for ensemble flood prediction during extreme events. Two important concerns when applying physical hydrology models in real-time flood forecasting systems are over-parameterization and equifinality (Beven, 2006, 2018). Physical hydrology models require several input variables including topography, land use, meteorological data, and soil characteristics. The calibration of these multiple input parameters increases uncertainty of estimated hydrologic variables due to the uncertainty of measuring or approximating model input datasets. In this case, the calibration process may converge to several independent model input parameter sets that converge to a similar value for the calibration objective function. As a result, a new challenge for model calibration is to identify the best of several equifinal parameter sets (Foulon and Rousseau, 2018), which may require human inspection on the calibration process.

Artificial Intelligence (AI) models are a suggested alternative to physical hydrology models (Napolitano et al., 2010); AI models decrease the degrees of freedom and the risk of equifinality in the real-time flood forecasting systems. Input data for AI models used for real-time flood forecasting typically include observed discharge and predicted precipitation (Chang et al., 2007; Nayak et al., 2005).

The recent increases in the use of AI models for hydrologic applications reflects the greater computational efficiency and ease of real-time analysis within the structure of AI models (Adamowski, 2008; Jain et al., 2001). AI models apply mathematical equations analyzing concurrent input and output time series rather than simulating physical processes in the watershed (Nourani et al., 2014; Solomatine and Ostfeld, 2008). Artificial Neural Networks (ANNs) and Adaptive Neuro-Fuzzy Inference Systems (ANFISs) are two of the most commonly used AI models in flood forecasting (Campolo et al., 2003; Chang et al., 2007; Chiang et al., 2007; Deshmukh and Ghatol, 2010; Khac-Tien Nguyen and Hock-Chye Chua, 2012; Nayak et al., 2005; Rezaeianzadeh et al., 2014).

Despite the advances in technique and availability of model input data, there has been very limited focus on applying physical hydrology and data-driven models for local flood forecasting in small peri-urban catchments. Streamflow is flashier in small peri-urban catchments than in large catchments due to shorter response times (Epstein et al., 2016; Walsh et al., 2005). Additionally, studies have shown that the statistical correlation between the antecedent streamflow discharge and the current discharge decreases with lead times (Campolo et al., 2003). Therefore, AI models that are trained with only antecedent discharge may not accurately forecast flood peak magnitude and timing for

long forecast lead times in these small catchments. However, I hypothesize that data-driven models that are trained using the antecedent discharge and precipitation inputs may perform more accurately for long lead times due to the strong correlation between rainfall and runoff timing. As an alternative to AI models, physical hydrology models provide some insight into the hydrologic behavior of small urban catchments, but they are limited by uncertainty (Jakeman and Hornberger, 1993) and errors because of simplification, calibration (Yen et al., 2015), and scale impacts (Carpenter and Georgakakos, 2006; Grayson et al., 1992; Koren et al., 1999). For example, first-order streamflows in small urban catchments may be more responsive to small storm events compared to large catchments because of the closer match between the storm scale, catchment time of concentration (Nicótina et al., 2008; Wilson et al., 1979), and catchment storage capacity (Sapriza-Azuri et al., 2015). Consequently, physical hydrology models established for a specific scale, may not closely represent the hydrological processes and behavior of small urban catchments. Thus, several questions remain regarding the performance of AI and physical hydrology models in small catchments, especially in terms of relative utility. Further knowledge about the performance of physical hydrology and data-driven models for flood forecasting in small urban catchments is expected to be valuable for local urban flood emergency management at peri-urban catchments, which are the newly developed urban catchments in proximity of large growing cities worldwide.

Storm direction may also influence the performance of real-time flood forecasting models in small catchments by changing the time of concentration. For example, for storms that

move in a downstream direction through the catchment, early flood measurements at the upstream gage can be used by the data-driven model to forecast downstream flood intensity with an appropriate lead time. In contrast, for storms moving downstream to upstream the stage increases earlier downstream, so the delayed upstream response may not appropriately predict the downstream peak flows sufficiently. Investigating this linkage is aimed to help understanding the strengths and limitations of data-driven models for flood forecasting in small urban catchments.

In the fourth phase of my dissertation project, I 1) assess the impact of storm direction on predictability performance of the ANFIS flood forecasting model in Ley Creek; 2) compare the performance of ANFIS, SWMM, and SAC-SMA for deterministic real-time flood forecasting in Ley Creek, and 3) compare the performance of ANFIS and SAC-SMA models for real-time ensemble flood prediction at several small to medium sized suburban catchments (17 km^2-150 km^2) near NYC (Roodsari et al., 2018). To assess the impact of storm direction on flood forecasting performance of ANFIS model, the model is trained with different combinations of storm direction and model validation errors are compared among different scenarios. To evaluate the performance of ANFIS, SWMM, and SAC-SMA for deterministic real-time flood forecasting, all three models are used for a real-time flood forecasting scenario at Ley Creek catchment. To compare the skill of ANFIS and SAC-SMA for real-time flood forecasting during large- and small-scale storm events, I apply both models to re-forecast the flood hydrograph of a disastrous historical extreme event, Hurricane Irene, and another small storm that occurred a few weeks after Hurricane Irene. The models are calibrated using the historical streamflow

and meteorological records prior to the start day of the storm events (27 August 2011 for Hurricane Irene and 23 September 2011 for the small event). These models are then validated using streamflow prediction for three years following the event start dates to validate the strength of model calibration. The calibrated/validated models are then used for ensemble flood forecasting during the events (27-29 August 2011 and 23-25 September 2011) using 2nd-generation NOAA Global Ensemble Forecast Re-forecast (GEFS/R) precipitation data (Hamill et al., 2013). I will use this analysis to test the hypothesis that ANFIS performs as accurately as SAC-SMA for ensemble flood forecasting in relatively small urban catchments for forecast lead times of three to 24 hours.

Results of this phase of my dissertation are aimed at understanding the strengths and limitations of AI models for use in local real-time flood forecasting systems in small peri-urban catchments. In addition, research on the impact of storm direction on flood forecasting performance of AI models has been very limited and use of such models in peri-urban catchments is a frontier in flood prediction. Previous research in this area depended on lab-scale prototypes and rainfall simulators to address the impact of storm direction on runoff peak flow (Seo et al., 2012), and may not fully represent the actual flooding scenarios. Research on the impact of storm direction on flood forecasting models may advance emergency management related to urban flooding.

1.2. Objectives

The goals of this dissertation are:

1) a) to study the hydrologic behavior of peri-urban catchments during cold season, and b) to study the impact of urbanization and increased areas of imperviousness on runoff peak flows in peri-urban catchments during cold season.

2) a) to address the impact of urban development pattern or distribution of impervious surfaces on runoff peak flows and stream-flow flashiness in relatively small peri-urban catchments ($A < 260\ km^2$), b) to develop a simple geometric index to quantify the distribution of impervious surfaces for macro-scale management and classification of urban development patterns in small peri-urban catchments, c) to apply the developed geometric index to predict urban runoff peak flows and stream flashiness in small peri-urban catchments, d) to assess the effectiveness of the developed index under different catchments scales, and geologic and climatic conditions.

3) To perform a statistical correlation analysis between the average runoff peak flows with several measurable surface properties of peri-urban catchments at different climatic and geologic conditions.

4) to study the seasonal change in hydrologic performance of LIDs.

5) To assess the impact of storm direction on the performance of ANFIS flood forecasting model.

6) To apply SWMM, ANFIS, and SAC-SMA for real-time deterministic flood forecasting.

7) a) to apply ANFIS and SAC-SMA for real-time ensemble stream-flow prediction of the Hurricane Irene flood hydrograph in several small to medium sized peri-urban

catchments (17 km^2-150 km^2) near NYC, b) to apply both models for real-time ensemble flood forecasting of a small storm event at the NYC study catchment to assess the impact of storm scale on models performance, c) to quantify the performance of ANFIS and SAC-SMA for ensemble streamflow prediction of the two study storm events using several quantitative performance indices, d) to address the impact of catchments scale and physical properties on models performance for ensemble flood forecasting.

I accomplished these goals via field observations, statistical analysis of my field data and input data from many additional USGS monitoring catchment across the US, and by testing physical hydrology and AI models. These efforts support the following research questions:

1.3. Research questions

Question 1: Does the cold-season hydrologic response of peri-urban catchments change with increased area of imperviousness? If so, how does the fractional impervious area impact the seasonal runoff peak flows in peri-urban catchments?

Question 2: Does the distribution of imperviousness in peri-urban catchments impact runoff peak flow and stream flashiness? If so, how can we characterize these impacts? Can we use a simple geometric index that relates the location of the imperviousness to the catchment outlet?

Question 3: Do Artificial Intelligence (AI) models perform as well as lumped physical hydrology models for ensemble flood forecasting in relatively small peri-urban

catchments? If so, how do storm size, catchment drainage area, and fractional impervious area affect each of the model types for ensemble flood forecasting?

Five additional minor research questions are presented in Appendix S.

1.4. Approach

This dissertation project includes two different phases: field monitoring and data analysis. In the field monitoring phase, I performed intensive water level and stream-flow (discharge) monitoring at several subcatchments of Ley Creek, a highly urbanized peri-urban catchment in proximity of Syracuse, NY. I used these field observations and stream-flow discharge records from many additional USGS catchments across the US to address the impact of urban development pattern on hydrologic behavior of peri-urban catchments. The data analysis phase of this dissertation was comprised of two parts: statistical analysis and modeling. The statistical analysis phase consisted of a literature review on the seasonal performance of LID and calculated average runoff peak flow and volume reduction of bioretention cells and green roofs, based on prior studies. I calculated the average seasonal peak flows in Ley Creek subcatchments using field monitoring data. Next, I studied the impact of imperviousness distribution on runoff peak flows and stream-flow flashiness for 90 peri-urban catchments in nine large growing cities of the US using a newly developed geometric index (RNICO). In the modeling phase, I initially studied the impact of storm movement direction on the performance of ANFIS flood forecasting model. Next, I applied ANFIS, SAC-SMA, and SWMM for deterministic real-time flood forecasting at Ley Creek. Finally, I applied ANFIS and SAC-SMA models for ensemble stream-flow forecasting of the Hurricane Irene flood

hydrograph at the outlet point of nine NYC peri-urban catchments. I present the details of the study sites and approaches used in this dissertation in Chapter 3.

2. Chapter 2 (Literature review)

2.1. Impacts of urbanization on flooding

Global urban growth and conversion of green space to impervious areas increases the likelihood of flood in many urban catchments (Jha et al., 2012). Urban floods threaten human lives, damage property, and cause a cascade of environmental impacts in urban catchments. These events impose substantial financial investments to municipalities and emergency managers to protect urban infrastructures from flooding. Therefore, there has been recent increased interest in the study of impacts of urbanization on runoff peak flows in urban catchments.

Seasonal variations in energy and water budget, and the influence of human activities on snowmelt processes can greatly influence peak flow response of northern urban catchments. Flood events in northern catchments commonly occur during summer flash floods and spring snowmelt in mid-April through early March. Previous studies in northern urban environments agree on the significant influence of human activities on snowmelt processes (Koivusalo et al., 2006; Taylor, 1982, 1977). For example, urban snow is typically removed or re-distributed in northern urban catchments (Bengtsson and Westerström, 1992; Buttle and Xu, 1988; Ho and Valeo, 2005; Semádeni-Davies, 2000; Semádeni-Davies and Bengtsson, 1999). Furthermore, application of road salt and deicers on the streets, which transfer heat from the urban infrastructures to the snow, can alter the snowmelt timing and peak flow magnitude. Due to the limited knowledge on snow

removal/redistribution activities, seasonal peak flow analysis remains a challenge in urban hydrology.

Previous studies on seasonal peak flow analysis for peri-urban catchments in Canada, Sweden, and Finland found greater daily snowmelt rates and significantly less infiltration rates during cold seasons and associated these effects with human activities (Bengtsson and Westerström, 1992; Ho and Valeo, 2005). For example, a comparison study of snowmelt runoff from a rural and a suburban catchment in Peterborough, Ontario showed that the suburban catchment reacts more quickly to snowmelt and rain-on-snow event. This supports the concept that greater initial quick flow is related to microclimatic and hydraulic alterations caused by human activities (Buttle and Xu, 1988). In another similar study, Bengtsson and Westerström (1992) showed that daily snowmelt rates in Lalea, Sweden are nearly 10 mm greater than in rural areas, as a result of increased absorbed radiative energy. In addition, urban infiltration rates into soil significantly decreased during the cold season so that snowmelt runoff from pervious and impervious areas were similar. Ho and Valeo (2005) show similar response in urban snowmelt studies in Calgary, Canada, i.e. urban snow removal activities and differences in in urban environment largely influence the energy-balance of snowpacks. Nevertheless, antecedent soil moisture had very little effect on runoff from frozen soil which behaved similarly to impervious surfaces.

Most studies on urban runoff peak flows in cold climates have been limited to Canada, Sweden, and Finland, with much of the available literature focused on snowmelt runoff. There has been limited focus on seasonal comparison of runoff peak flows. To fill this research gap, I study the seasonal changes in runoff peak flows in several northeastern

US peri-urban catchments. I use a set of intensive field observations and discharge monitoring records from a network at several subcatchments of Onondaga Lake watershed to calculate seasonal runoff changes in runoff peak flows within the study sites. My study catchments include a wide range of fractional impervious area from 11 to 48 %, which supports study of the impact of increased area of imperviousness on the magnitude and frequency of runoff peak flows.

2.2. Impacts of urban development pattern on flooding

Increased surface imperviousness can increase urban runoff peak flows by a factor of up to fifty, as shown by both empirical and modeling approaches across climates. A longitudinal study of urban development in a large Canadian basin (5825 km^2) showed increased runoff peak flow magnitudes by three times the pre-development condition (Nirupama and Simonovic, 2007). A paired study of summer and spring discharge from highly developed urban (0.06 km^2) and rural (0.13 km^2) catchments in Finland also showed up to a threefold increase in peak flows with urbanization (Valtanen et al., 2014). Also in Finland, five years of heavy urbanization in a small (0.13 km^2) catchment increased peak flows by a factor of fifty over 5 years (Sillanpää and Koivusalo, 2015). Similarly, increased imperviousness caused significantly greater high flow frequency and increased stream flashiness in several medium to large (43-205 km^2) rural and urban Canadian catchments for a nine-year study period (Eimers and McDonald, 2015). Flood peak discharge of large storm events over a 39-year study period in a large (225 km^2), highly developed urban catchment in Georgia, USA were up to two times greater than for several large rural catchments (187-1015 km^2) (Rose and Peters, 2001). In contrast, Zope et al. (2015) found a negligible effect of four decades of urban growth or about 60 %

increase in built-up areas in a medium size (73 km^2) catchment in India, but cautioned about the combined impacts of urban development and coastal tides. Suriya and Mudgal (2012) predicted elevated flood levels and increased inundated areas due to a thirty-year urban sprawl in a large (300 km^2) urban basin in India.

Historically, the fractional impervious area is linked to increased magnitude and frequency of urban runoff peak flows (Arnold and Gibbons, 1996; Cheng et al., 2010). Conversion of green space to impervious surface generally decreases infiltration (Valtanen et al., 2014), evapotranspiration (Grimmond and Oke, 1999), and catchment soil storage volume (Bhaskar and Welty, 2012). These alterations to the water balance are manifested as decreased flood travel time and elevated surface runoff volume and more intense peak flows. Fractional impervious area has been widely used for assessing the impact of urbanization on flooding in urban catchments, but this criterion may not fully represent the complexity of the distribution of impervious surfaces within urban catchments (Du et al., 2015). It is well understood that the distribution of impervious areas within urban catchments can affect peak flows (Mejía and Moglen, 2010a, 2010b, 2009; Yang et al., 2011). For example, Mejia and Moglen (2010) used several water resources objective functions to optimize the distribution of impervious areas in several hypothetical urban catchments and found that restraining catchment imperviousness to 10% , as defined in previous literature (Schueler et al., 2009; Schueler, 1994; Valtanen et al., 2014), may lead to an unplanned low density urban growth within the catchment. Yang et al. (2011) used a GIS-bases physical hydrology model approach to address the impact of the distribution of impervious areas on peak flows in several urban catchments in Indiana, USA. They found a significant impact of runoff processes on urban peak

flows for catchment scales and higher influence of runoff travel time to the catchment outlet for large river basins.

The concept that urban development patterns can alter runoff peak flows and stream flashiness through the location of impervious areas within the catchment in urban catchments is not new (Mejía and Moglen, 2010a, 2010b, 2009; Yang et al., 2011), a deterministic approach to address such impacts has not been developed for general use. Most studies have focused on site-specific hydrological modeling approaches to address the impact of different hypothetical urban sprawl scenarios. Although physical models can provide insight into the behavior of a natural system, they are limited by uncertainty of data input and model parameter calibration. To overcome this limitation and fill this research gap, I developed a new simple geometric index (RNICO) to account for the relative proximity of impervious areas within urban catchments to the catchment outlet. An advantage of RNICO compared to modeling approaches presented in previous literature is that it only requires land cover maps and stream-flow discharge records. These are typically accessible for most urban catchments worldwide. More importantly, the simplicity of calculating RNICO supports broad-scale planning and management of urban development in peri-urban catchments. Such an approach could be an important tool for urban planners and municipalities with limited knowledge of hydrology and modeling.

2.2. Real-time flood forecasting

Historically, local ensemble stream-flow prediction systems have applied different physical hydrology models and numerical weather prediction data sources for simulating rainfall-runoff processes during extreme events such as flash floods or hurricanes. For

example, Marty et al. (2013) used the lumped TOPSIMPL model and Probabilistic Quantitative Precipitation Forecast (PQPF) at daily and sub daily (six hours) time steps to re-forecast the flood hydrographs of five major flash flood events in southern France between 2005 and 2008. They generated hourly streamflow forecast ensembles for lead times of up to 48 hours for a range of catchment scales from 100 to 600 km^2 and indicated that streamflow forecasts depend on the accuracy of PQPF, while using both daily and sub daily weather sources considerably increased the TOPSIMPL model performance. A semi-distributed rainfall-runoff model (PREVAH) and weather forecast ensembles of two radars (NORA and REAL-C2) were used to re-forecast several flash flood event hydrographs in the southern Swiss Alps between 2007 and 2010 (Liechti et al., 2013) and found that the REAL-C2 radar forecast ensembles provided a better performance results compared to the NORA radar. More recently, Hally et al. (2015) used a multi-model software, Meteorological Model Bridge (MMB), that applied multiple semi-distributed physical hydrologic and atmospheric prediction models to re-forecast the hydrograph of the tragic flood event on 4 November, 2011 at Genoa, Italy. They found that the multi-modeling aspect of MMB model is a is a useful tool to generate more accurate predictions during large storm events. Similarly, Mengual et al. (2015) used the semi-distributed Hydrologic Modeling System (HEC-HMS) and rain gage data through both probabilistic and deterministic approaches to re-forecast the hydrograph of the disastrous flash flood event of 28 September, 2012 in Murcia, Spain. Based on the forecast results for lead times of 48 hours, they emphasized the benefit of a probabilistic approach that accounts for weather prediction uncertainties for short-term flood prediction systems. Similarly, Saleh et al. (2016) applied the semi-distributed HEC-HMS

model and 21 precipitation ensembles of the Global Ensemble Forecast System (GEFS/R) for short-term flood forecasting in the Hudson River Basin, New York during Hurricane Irene. They generated streamflow forecast ensembles for lead times of 24 to 72 hours and showed that the probabilistic approach improves short-term streamflow predictions by carrying more useful information than a traditional single-run deterministic modeling approach. These studies support the use of ensemble flood prediction to develop improve flood forecasts over traditional deterministic modeling approaches, especially for river basins greater than 100 km^2. However, the effectiveness of the ensemble flood forecasting approach for urban catchments less than 100 km^2 remains unclear due to the limited number small catchment studies in urban settings.

Continental flood forecasting systems worldwide use a variety of rainfall-runoff models based on deterministic and probabilistic approaches. In Europe, the European Flood Awareness System (EFAS) applies Lisflood (Knijff et al., 2010) and the European Hydrological Predictions for the Environment (E-HYPE) uses the HYPE model (Lindström et al., 2010). Lisflood uses precipitation, temperature, and evaporation forecast ensembles as input to simulate hydrologic and flow routing processes (Emerton et al., 2016). The model simulates twenty-two years of historical discharge using Lisflood to find reference flooding thresholds. In contrast, E-HYPE applies deterministic Numerical Weather Prediction (NWP) as input for a distributed rainfall-runoff HYPE model to simulate hydrologic processes such as evapotranspiration, snowmelt, and groundwater recharge. In Australia, the Flood Forecasting and Warning Service (FFWS) uses a combination of GR4J, GR4H, and Unified River Basin Simulator (URBS) models

for rainfall-runoff simulation and a Muskingum approach for channel routing (Emerton et al., 2016). In the United States, the NWS runs the Hydrologic Ensemble Forecast System (HEFS) using the lumped Sacramento Soil Moisture Accounting (SAC-SMA) model (Burnash et al., 1973). HEFS receives forecast ensembles of precipitation and temperature to simulate rainfall-runoff in hourly to seasonal time steps. Although most continental flood forecasting systems use physical hydrology models, there is no single recommended approach for using data-driven models for ensemble flood forecasting.

Several previous studies have used AI models for deterministic flood forecasting in large river basins. For example, Campolo et al. (2003) used an ANN model for real-time flood stage prediction at a large river basin (4000 km^2) in Italy using rainfall, hydrometric and dam operation information and indicated accurate forecast results for lead times of up to six hours. Results of training ANFIS and ANN models for hourly flood forecasting in a large Indian river basin (1350 km^2) using antecedent rainfall and runoff input datasets showed better performance of ANFIS compared to ANN (Nayak et al., 2005). Using a combination of satellite and rain gage precipitation records as input for a recurrent neural network (RNN) showed an increase in the accuracy of forecasting typhoon flood peaks at a medium size river basin (204 km^2) in Taiwan (Chang et al., 2007). However, the effectiveness of this improvement in model performance decreased by increasing the number of rain gages. For daily flood stage forecasts, ANFIS was shown to have excellent performance for predicting flood stage at a very large river basin (790,000 km^2) in Laos (Khac and Chua, 2012).

Storm direction can affect the hydrologic response of small catchments by changing the time of concentration (Seo et al., 2012). This difference in storm direction may change the prediction performance of data-driven models trained by upstream gage. For example, for storms that move downstream through the catchment, early flood measurements at the upstream gage can inform a data-driven model to forecast the downstream flood intensity if provided sufficient lead time. In contrast, for storms moving upstream, the stage increases earlier downstream, so the delayed upstream response may not predict the downstream peak flows sufficiently. There has been very limited research on the impact of storm direction on the performance of flood forecasting models. Previous research in this area depended on lab-scale prototypes and rainfall simulators (Seo et al., 2012), and may not fully represent the actual flooding scenarios. Investigating this linkage helps understanding the strengths and limitations of data-driven models for flood forecasting in small urban catchments. I study the impact of storm direction on the performance of data-driven models for flood forecasting in small urban catchments as part of the second phase of this dissertation.

The previous literature indicates that the practical application of AI models has been limited for real-time flood forecasting systems due to limited trust in training algorithms for these models. This is especially the case for small peri-urban catchments, where the time of concentration is short and catchments response time to precipitation events is great, model selection for real-time flood forecasting is an important concern. To address this concern, I will compare the performance of AI and physical models for small urban catchments. Therefore, the second phase of this dissertation demonstrates the use of ANFIS and SAC-SMA models in real-time flood forecasting systems. I chose to re-

forecast the Hurricane Irene flood hydrograph at the outlet of nine peri-urban catchments near NYC which were extensively flooded and damaged during the event. Results of this phase of the study demonstrate relative performance of AI and physical model for an important flood event. Ideally, this demonstration demonstrates the benefits and drawbacks of AI models as an alternative to physical hydrology models in practical real-time flood forecasting systems.

3. Chapter 3 (Methods)

3.1. Field monitoring

3.1.1. Study sites

Ley Creek is an urbanized catchment, in the eastern part of Onondaga lake watershed north of the city of Syracuse, New York (43°04'38", 76°10'13"). The catchment drains 78 km^2 of low-gradient glaciated lake margin with elevations ranging from 111 to 208 m. About 40 % of the catchment is impervious due to the presence of a central commercial district and Hancock International Airport (Table 1). Ley Creek outlet is a third order stream with three main sub-branches: north branch, south branch, and main branch. North and south branches converge near I-90 to form the main branch (Figure 1). Except for the natural wetlands and forests on northeastern side of the catchment, the watershed has extensive areas of impervious land covers including residential, commercial, and local industries (Figure 2). Additionally, most soils the catchment are characterized as having low to moderate drainage potential. Much of the catchment is equipped with drainage infrastructure. The area has a humid continental climate with the thirty-year average annual, minimum, and maximum temperatures of 9, −10, and 28 ◦C respectively (NOAA, 2000). The annual average effective depth of precipitation and snow for the period 1948-2014 are 980 and 2970 mm, respectively (Figure 3).

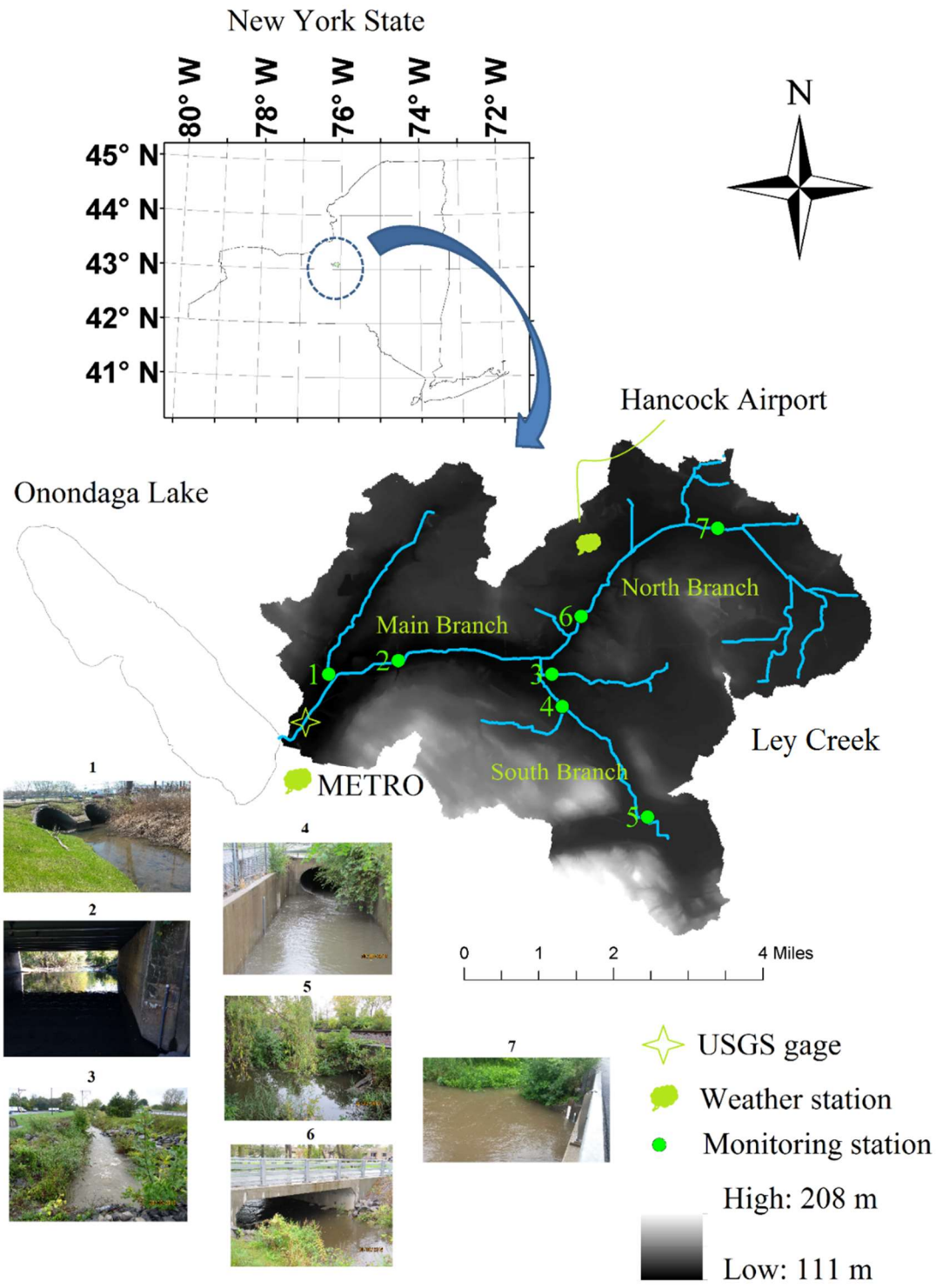

Figure 1. Topography and the location of monitoring stations at Ley Creek.

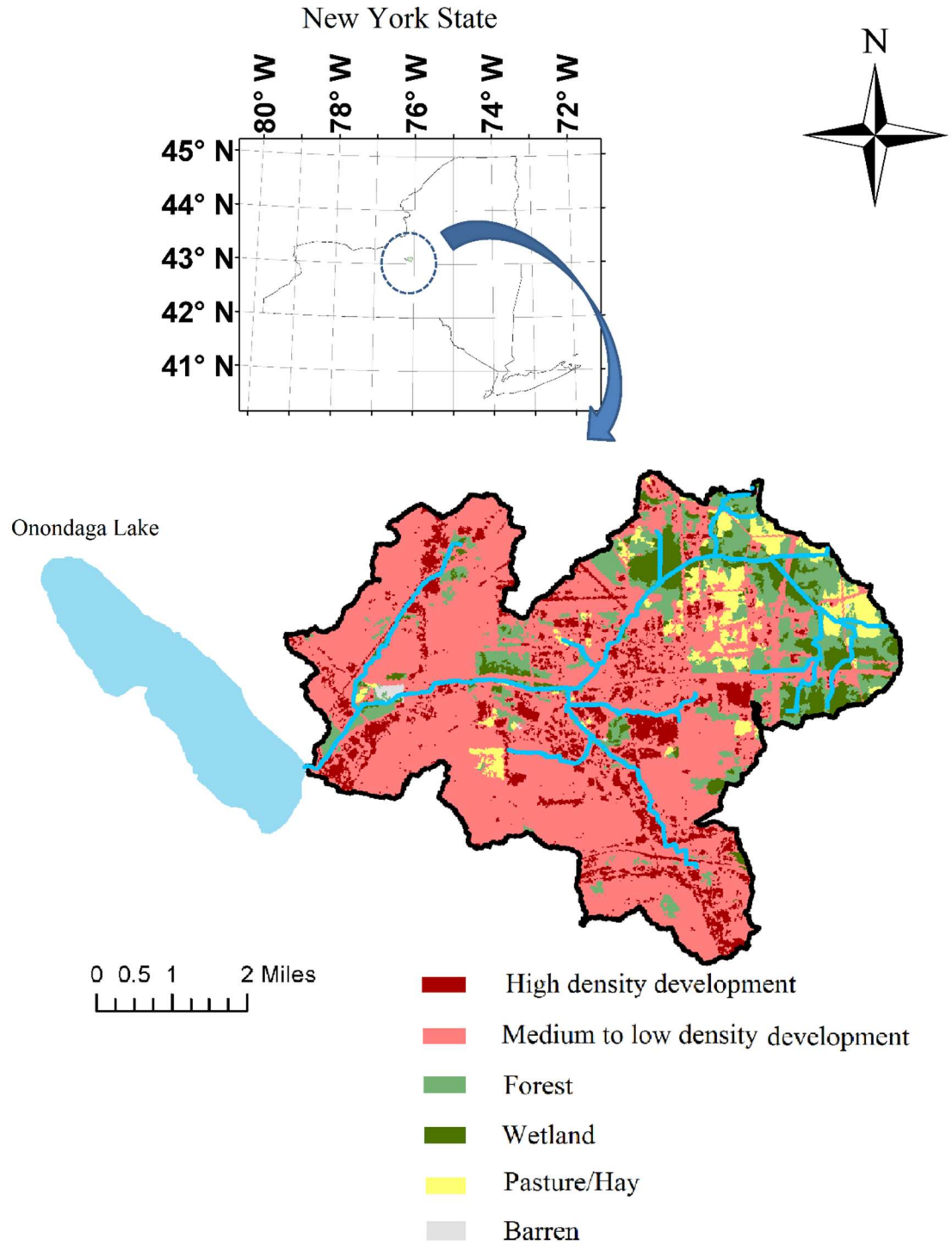

Figure 2. Land cover classification map in Ley Creek (NLCD, 2011)

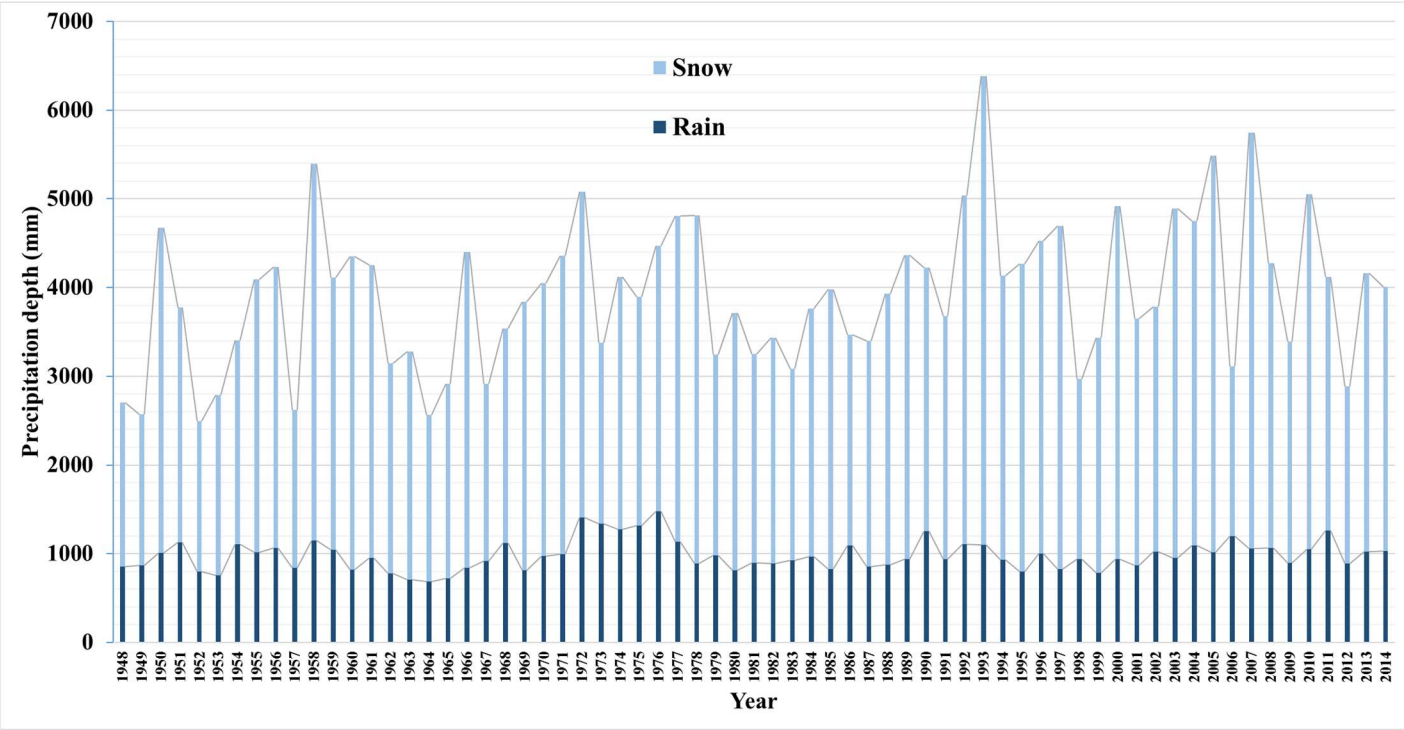

Figure 3. Annual precipitation records at Hancock International Airport, Syracuse, NY (NOAA, 2016)

Table 1. Descriptions of the eight study subcatchments at Ley Creek, Syracuse, NY

Gage ID	Subcatchment name	Area (km^2)	Imperviousness (%)
1	Ley Creek Dr.	10	36
2	Lemoyne Ave	58	33
3	Deere Rd.	7	43
4	Old Ct. St.	5	49
5	Stm Pond	5	48
6	Thompson Rd.	24	17
7	Fly Rd.	11	11
8	Park St. USGS	72	34

Poor channel conditions and rapid urbanization have contributed to several floods in Ley Creek from 1950 to 1970. Spring snowmelt flooding caused extensive damage in March 1950, March 1960, and March 1964 (FEMA, 2012). The Onondaga County Department of Drainage and Sanitation responded by increasing the channel dimensions and rerouting Ley Creek through the Town of Salina Landfill in 1970. These flood mitigation plans have shown relatively positive outcomes, however Ley Creek continues to flood beyond its banks periodically (USEPA, 2014) (Figure 4). The high flood potential, present condition of the catchment, and likely future increases in summer precipitation intensity, warrants research on land use management and stormwater control strategies to reduce the flood risk in Ley Creek, and as an example study for flood forecasting in other small urban catchments.

(a)

(b)

(c)

(d)

Figure 4. Images from the flooding event at Ley Creek on 7 July 2015. Panels a and b show the road closure due to flooding at the intersection of Ley Creek Dr. and 7th N. St. and panels b and c show backwater pooling at bridges near the intersection of Thompson Rd. and E. Molloy Rd in De Witt, NY.

3.1.2. Monitoring stations

Water level was monitored at the culvert inlets at screened wells constructed of 5 cm diameter PVC using HOBO U20-L temperature and pressure sensors (Onset Computer, Bourne MA USA). Stream conditions varied widely between base flow and peak flows, so two gaging methods were combined to estimate discharge over the range of observed stage and velocity at non-USGS monitoring stations. For base flows, stream discharge

ranging from 0.004 to 1.72 m^3/s was measured with ultrasonic Doppler gaging device (Sontek YSI, San Diego CA) using USGS stream-gaging technique (Buchanan and Somers, 1969) and stage discharge relationships were developed using stream gaging records (Rantz S. E. et al., 1982):

$$Q=a(G-c)^b \quad \text{(Eq. 2)}$$

Where Q: Discharge (m^3/s); G: recorded stream depth (m); a & b: rating curve coefficients; and c: gage height in which discharge equals zero at the station. km^2

The inlet control assumption was applied to calculate high flows for unsubmerged culvert conditions from geometry of the inlet using standard hydraulic formulae (Haderlie and Tullis, 2008, 2008; Norman J. M. et al., 2001; Tullis and Anderson, 2010):

$$\frac{H_W}{D} = \frac{H_c}{D} + K\left(\frac{K_u Q}{AD^{0.5}}\right)^M - 0.5S \quad \text{(Eq. 3)}$$

Where H_w: headwater depth (m)

D: interior height of the culvert (m)

A: culvert intersection area, (m^2);

H_c: specific head at critical depth ($dc + \frac{V_c^2}{2g}$), m;

M: 1.811 for SI units;

S: culvert slope, $\frac{m}{m}$;

K and M: constants (function of culvert type and geometry).

3.2. Data analysis

3.2.1. Seasonal peak flow analysis for Ley Creek

3.2.1.1. Study sites

Five subcatchments of Onondaga Lake watershed were selected for the first part of the study (Table 2, Figure 5): three low urbanized (imperviousness of 11 % to 17 %, LOW1, LOW2, and LOW3) and two moderately urbanized (imperviousness of 34 % and 48 %, INT1 and INT2). These study sites have a relatively low-gradient topography and more than half of the catchments (on the downstream part) is urbanized. All subcatchments are partially developed with relatively high density residential and commercial land uses except for LOW1 (imperviousness of 11%) which is predominantly wetlands.

Table 2. Descriptions of the five study subcatchments at Onondaga Lake Watershed

Gage ID	Site category	Subcatchment name	Area (km^2)	Average Imperviousness (%)
LOW1	Low Urbanization	Ley Creek North-Fly Rd.	11	11
LOW2		Upstream Harbor Brook USGS gage	25	12
LOW3		Downstream Harbor Brook USGS gage	28	17
INT1	Intermediate Urbanization	Park St. USGS gage	72	34
INT2		Ley Creek South-Stormwater Pond	5	48

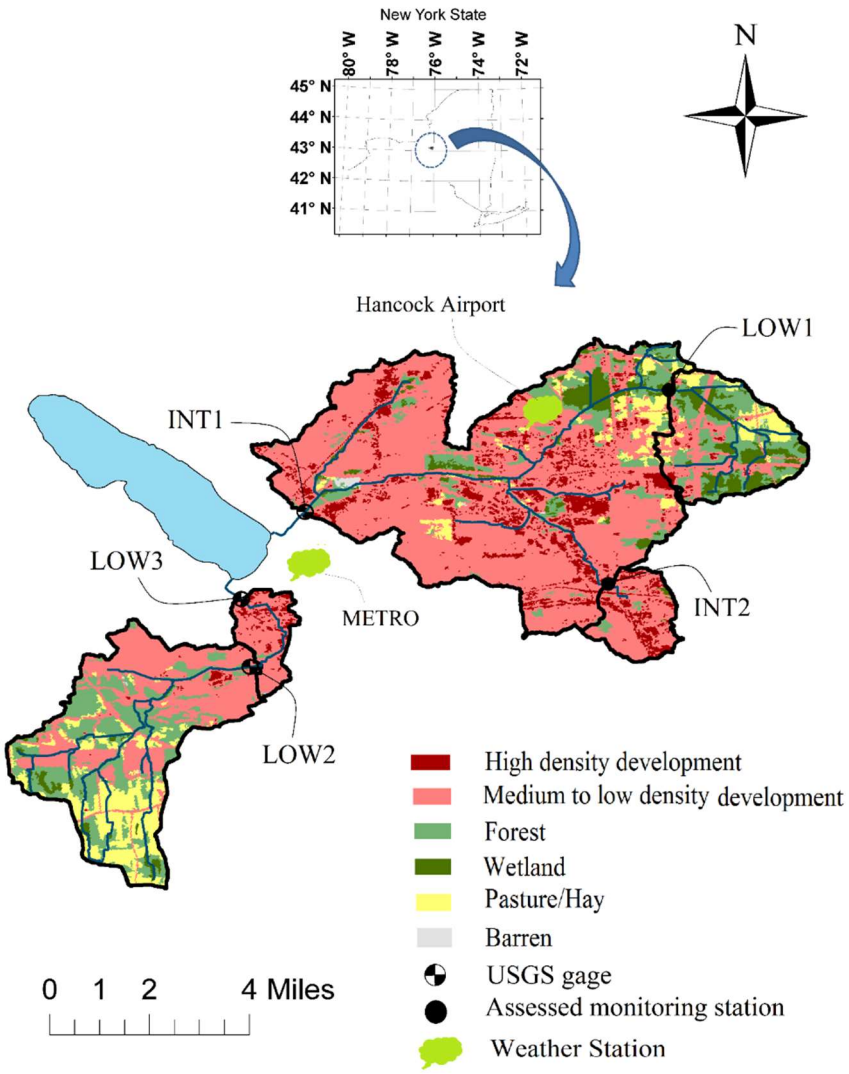

Figure 5. The location and land cover map of the study subcatchments at Onondaga Lake watershed, at Syracuse, New York

3.2.1.2. Seasonal runoff peak flow calculation

I selected seventy-nine runoff events from October 2014 to December 2015 for analysis. Each individual storm event was defined by measured rainfall of more than 3 mm followed by no rain at least four hours. Events were classified into four seasons based on Equinox and Solstice dates (20 March, 21 June, 22 September, and 21 December). Snowmelt events were indicated by hydrograph peaks associated with periods of positive

temperature or rain-on-snow events during March and early April 2015. Average seasonal and annual peak flow magnitudes were calculated for each subcatchment.

Land cover in each subcatchment was determined by delineating the watershed with ARC-HYDRO extension of ARCMAP10.3 and overlaying it with land cover shape file. Geographic site information including catchment boundary, water bodies, rivers, land use, and land cover layers were obtained from National Land Cover Dataset and Digital Elevation Model (DEM) maps were obtained from Cornell University Geospatial Information Repository. The DEM maps and watershed boundary layers were exported to ARCMAP 10.3. Monitoring station locations were specified and subcatchments corresponding to different monitoring stations were delineated with ARC-HYDRO. Land cover layers were clipped to the extension of delineated subcatchments. NLCD Land cover maps are in .tiff format which is not suitable for geometric calculations. Therefore, raster-to-polygon command in ARCMAP was used to convert .tiff to polygon for each subcatchment. Based on the definition of color codes, corresponding fractional impervious areas were calculated for different subcatchments (Table 2).

3.2.2. Impacts of urban development pattern on peak flows

3.2.2.1. Study sites

Ninety peri-urban catchments in proximity of nine large growing western, northern, and southern US cities are selected for analysis (Figure 6 and Table 3). Site IDs for each city are assigned based on the drainage area while the smallest catchment has ID=1 and the largest site has the greatest ID number. The drainage area of the study catchments range of from 1 to 255 km^2 and imperviousness from 4 to 56 %.

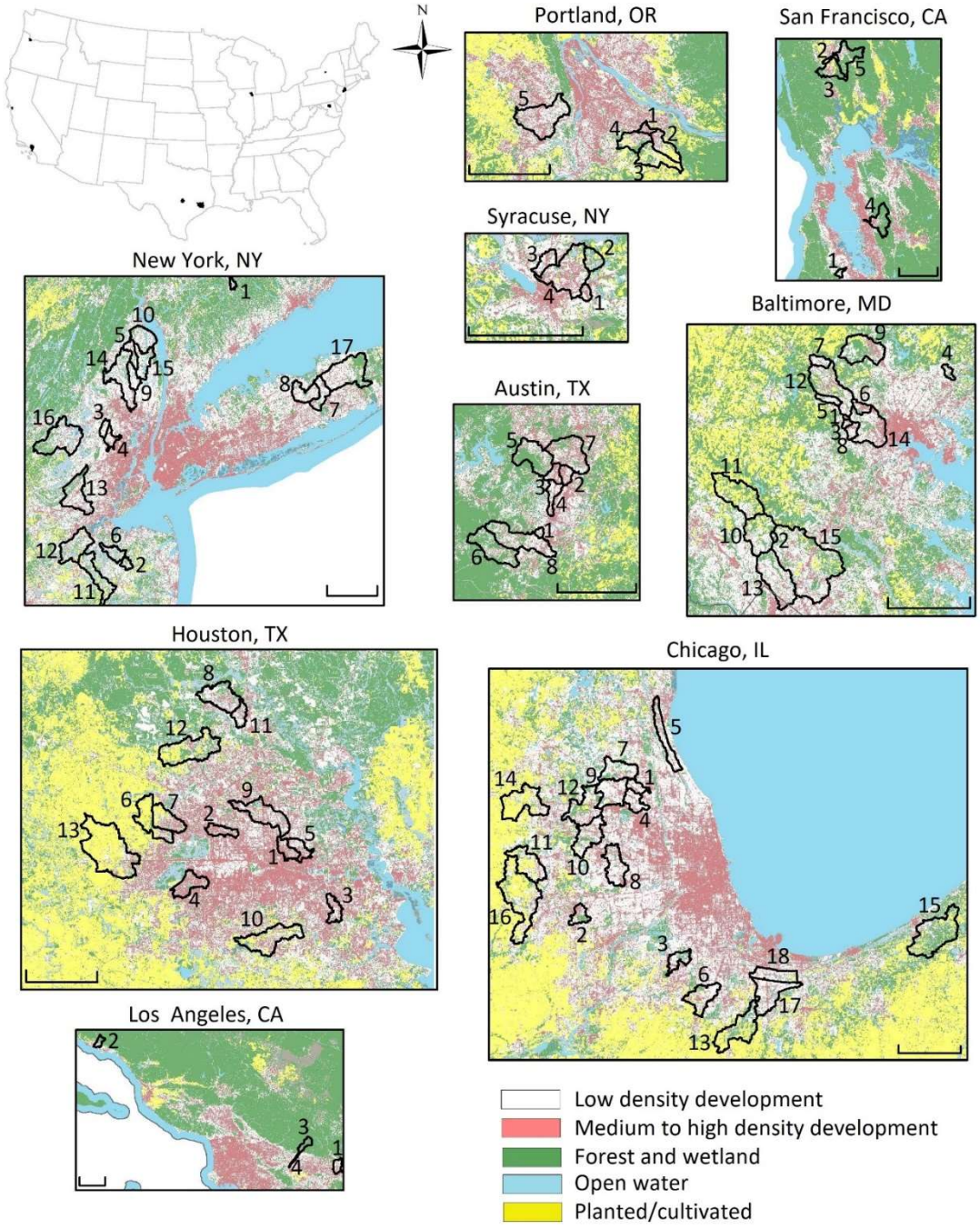

Figure 6. Land cover maps and location of the study catchments: NYC, Syracuse, NY, Chicago, IL, Baltimore, MD, Austin, TX, Houston, TX, Portland, OR, San Francisco, CA, and Los Angeles, CA. The background colors which are described in the legend are defined based on the NLCD 2011 land cover dataset. Catchment boundaries are presented with solid black lines. Numbers on the maps represent catchment IDs. Scale bars for each city represents 20 kilometers.

Table 3. Study site characteristics

City	ID	USGS gage #	Area (km^2)	Fractional impervious area	City	ID	USGS gage #	Area (km^2)	Fractional impervious area	City	ID	USGS gage #	Area (km^2)	Fractional impervious area
New York, NY	1	012095493	8.8	0.13	Chicago, IL	1	5529500	20.3	0.40	Baltimore, MD	1	1589317	1.3	0.52
	2	01407290	16.6	0.12		2	5540275	25.6	0.34		2	1649150	2.7	0.08
	3	01389550	20.3	0.19		3	5536500	29.2	0.31		3	1589320	4.9	0.45
	4	01392500	30.0	0.34		4	5530000	33.0	0.39		4	1585104	6.0	0.16
	5	01377370	34.7	0.20		5	5535070	54.2	0.30		5	1589290	8.7	0.22
	6	01406050	41.4	0.14		6	5536255	60.1	0.32		6	1589305	9.8	0.37
	7	01306460	56.7	0.29		7	5528500	61.1	0.26		7	1589197	10.5	0.17
	8	01304000	69.9	0.26		8	5540160	65.4	0.39		8	01589330	14.2	0.40
	9	01377500	76.7	0.17		9	5530990	70.3	0.35		9	1583600	53.4	0.13
	10	01376800	79.5	0.12		10	5539900	72.4	0.35		10	1650500	54.6	0.10
	11	01405400	105	0.10		11	5551330	74.6	0.18		11	1591700	70.4	0.04
	12	01405030	116	0.20		12	5550500	90.9	0.28		12	1589300	84.4	0.20
	13	01403900	125	0.25		13	5536179	95.8	0.07		13	1651000	128	0.19
	14	01391500	141	0.17		14	5550300	101	0.12		14	1589352	165	0.28
	15	01377000	150	0.13		15	4095300	140	0.06		15	1649500	188	0.20
	16	01381800	177	0.15		16	5551700	177	0.13		16	1594000	255	0.09
	17	01305000	189	0.19		17	5536190	180	0.20	San Francisco, CA	1	11166000	16.5	0.14
Houston, TX	1	08075730	18.7	0.21		18	5536195	231	0.23		2	11465700	17.9	0.15
	2	08075770	19.4	0.23	Austin, TX	1	08155541	4.6	0.38		3	11465680	107	0.15
	3	08072730	21.4	0.05		2	08158380	13.5	0.56		4	11181040	121	0.12
	4	08076500	38.8	0.17		3	08156675	14.5	0.48		5	11466200	145	0.08
	5	08074760	41.7	0.18		4	08156800	31.9	0.43	Los Angeles, CA	1	11060400	30.9	0.09
	6	08072760	55.7	0.09		5	08154700	57.8	0.17		2	11120000	49.3	0.11
	7	08068400	63.7	0.10		6	08158860	59.8	0.12		3	11073300	83.6	0.07
	8	08076997	67.1	0.11		7	08158200	67.9	0.37		4	11073360	132	0.11
	9	08068450	74.3	0.11		8	08158970	71.5	0.29	Portland, OR	1	14211814	7.2	0.54
	10	08068325	84.7	0.07	Syracuse, NY	1	non-USGS	5.0	0.48		2	14142800	28.7	0.25
	11	08072300	89.4	0.05		2	non-USGS	10.0	0.36		3	14211400	38.6	0.10
	12	08075763	106	0.27		3	non-USGS	11.0	0.11		4	14211500	68.4	0.07
	13	08074150	164	0.31		4	04240120	72.0	0.34		5	14206950	80.3	0.40

Several storm events between October 2009 and September 2012 (about 40 events for western US cities, around 60 to 90 events for southern US cities, and about 100 events for northern US cities) were selected for analysis. I chose this window to match the 2011 National Land Cover Dataset (http://www.mrlc.gov/nlcd2011.php). Precipitation data for all cities except for Syracuse were obtained from the Phase 2 of the North American Land Data Assimilation System (NLDAS-2) using the HydroDesktop 1.4 software (Ames et al., 2012). Precipitation records for Syracuse sites were obtained from two locations: Metropolitan Syracuse Wastewater Treatment Plant (Metro) 5-min records and 1-hr records at Hancock International Airport (Table 4). The distance between Metro and Hancock is about 7 km (Figure 1). The storm-tracking results using NEXRAD Level 3 radar data from the National Oceanic and Atmospheric Administration at the study area showed that most storms with depth greater than 3 mm during the study period are from the Northwest. These stations show similar records with a short time lag, so the higher temporal resolution Metro records were used as the primary reference, and missing observations were filled from the Hancock record. Streamflow discharge records from water year 2009 to water year 2012 for all cities except for Syracuse were obtained from the corresponding USGS gages (Table 3). For Syracuse, USGS gage data were only used for site 4 and new gaging stations were established at the outlet of sites 1 to 3 and real-time stream-flow discharge monitoring were performed between October 2014 and January 2016 (as noted in section 3.1.2). Runoff components for each event were separated using the approach of Nathan and McMahon (1990).

Table 4. Descriptions of weather stations used in Syracuse, NY.

City	Raingage ID	NOAA station ID	Address	Location	Elevation (m)
Syracuse	H1	308383	Syracuse Hancock International Airport	43.1111°, -76.1038°	125.9
	H2	Non-NOAA	Syracuse Metropolitan water treamtment Plant (Metro)	43.0639°, -76.1778°	113.0

Land cover information for the study catchments was obtained from the National Land Cover Database (NLCD) 2011: Catchment boundaries were delineated using the USGS stream auto delineation tool (http://water.usgs.gov/osw/streamstats/) and used to clip the NLCD 2011 layer for the United States. The resulting raster files were converted to shape files of catchment area, impervious areas, and stream reaches to facilitate geometric analysis. Impervious areas were defined as medium to high density development. Fractional impervious area was calculated for each catchment on an area basis (Table 3).

To assess the impact of imperviousness distribution on flooding, the correlations between the runoff peak flow and nearness of the centroid of impervious areas to catchment outlet was determined.

3.2.2.2. RNICO index

I developed a new geometric index, RNICO, as follows:

$$RNICO = (1 - \frac{d_i}{d_c}) \quad \text{(Eq. 4)}$$

where d_i equals the distance between imperviousness centroid and the outlet, and d_c is the distance between the centroids of catchment and the outlet (Figure 7a).

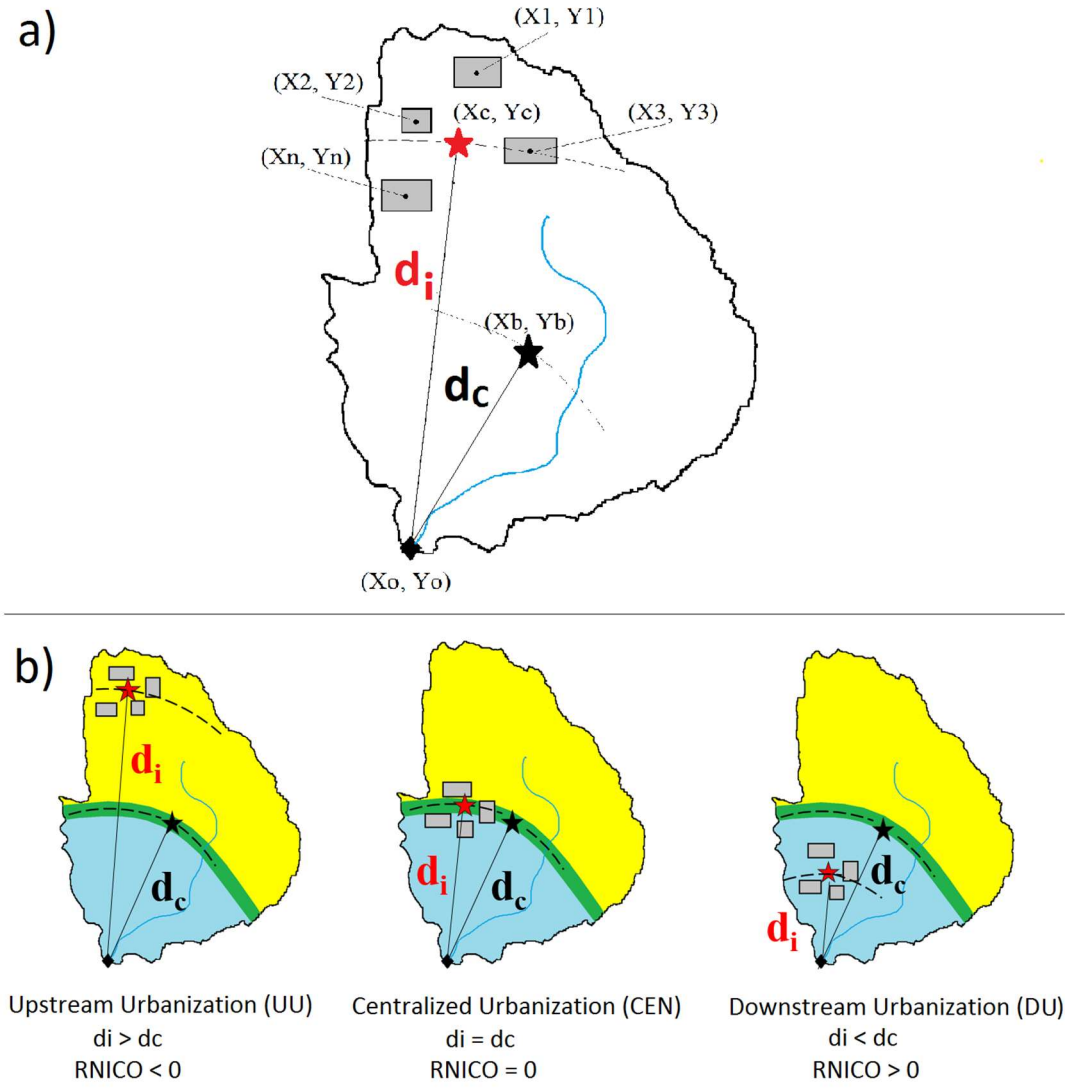

Figure 7. Schematic diagram of geometric parameters used for calculating (a) Relative Nearness of Imperviousness to the Catchment Outlet (RNICO) and (b) the three possible development pattern classes based on the RNICO index. (X1, Y1) to (Xn, Yn), impervious surface elements centroid location; (Xc, Yc), resultant geometric centroid location of all impervious surface elements in the catchment; (Xb, Yb), catchment centroid location; (Xo, Yo), catchment outlet location; di, distance between imperviousness centroid and the outlet; and dc, distance between the centroids of catchment and the outlet.

To remove the effect of catchment scale, the fractional distance (di/dc) between the centroid of imperviousness (Xc, Yc) and centroid of the catchment (Xb, Yb) and the catchment outlet (Xo, Yo) is calculated to represent relative remoteness of the imperviousness from the outlet (Figure 7). The calculated fraction is subtracted from one to indicate relative nearness to the outlet (Equation 2). ARCMAP 10.3 geometric calculation module is used to find the centroid of basin and impervious areas.

With the RNICO index, all development patterns are classified into three main classes (Figure 7b): upstream urbanization (UU; RNICO < 0), centralized urbanization (CEN; RNICO = 0), and downstream urbanization (DU; RNICO > 0). The maximum theoretical value of RNICO (1.0) occurs when all impervious areas are located at the catchment outlet.

3.3. Hydrologic modeling

In this phase of my dissertation, I used two physical hydrology models: SWMM 5.0 and SAC-SMA, and an ANFIS model for hydrologic modeling, and real-time deterministic and ensemble flood forecasting.

3.3.1. SWMM 5.0 model

SWMM model was first developed by Metcalf and Eddy (1971) to calculate surface runoff from catchment geometry. Catchment geometrical characteristics used in SWMM include the length of the plane (L), surface area (A), and runoff slope (J_0). United States Environmental Protection Agency (USEPA) has been improving the original SWMM model by adding groundwater, snowmelt and evapotranspiration components, and urban

drainage infrastructure design module through a free comprehensive software package (Rossman L., 2010).

3.3.2. SAC-SMA model

The SAC-SMA model is a physical hydrology model that was initially developed by Burnash et al. (1973) to distribute humidity characteristics at different levels of soil for an accurate streamflow simulation (Foehn et al., 2016). The Hydrology Laboratory of NOAA's NWS selected the SAC-SMA lumped model as a comparison baseline for participating distributed hydrologic models in the Distributed Model Intercomparison Project (DMIP), which aimed to identify the most suitable model for NWS streamflow prediction across the US (http://www.nws.noaa.gov/ohd/hrl/dmip/). More importantly, the NWS is currently using the lumped form of SAC-SMA for ensemble flood forecasting across the US (Emerton et al., 2016). For these reasons, I employ a lumped version of SAC-SMA. SAC-SMA requires precipitation and potential evapotranspiration as input to simulate streamflow. I use the Turc approach for calculating the potential evapotranspiration using air temperature data (Turc, 1955). However, I posit that changes in antecedent moisture due to ET may not greatly impact flood hydrographs due to the short time scale of flood events. The moisture accounting procedure used in the SAC-SMA model is structured based on a simple approximation of soil moisture (Burnash, 1995). SAC-SMA uses 17 parameters to represent upper and lower soil zones and catchment characteristics. The key parameters of the model include the upper and lower zone tension water capacity, free water capacity, and percolation parameters that should be adjusted during model calibration (Gan et al., 2014; Herman et al., 2013). Total computed surface runoff includes direct runoff from impervious surfaces and saturated

soils, and interflow resulting from free water storage and base flow components (Burnash, 1995) that can be modeled for a range of temporal resolutions from sub-hourly to monthly time steps.

SAC-SMA was calibrated using the Multi-Step Automatic Calibration Scheme (MACS; Hogue et al., 2000) that applies the procedure followed by NWS during manual calibration. In this procedure, all SAC-SMA model parameters were initially calibrated to minimize the RMSE of log-transformed streamflow observations and predictions. The upper zone parameters were then adjusted using the RMSE of the real data while lower zone parameter values remain fixed from the previous calibration. Finally, the lower zone parameters were re-adjusted using the RMSE of the log-transformed data while upper zone parameter values remained fixed from the previous step.

3.3.3. ANFIS model

ANFIS is a data-driven model that combines the human logic of fuzzy inference systems (FIS) with the adaptive capability of training artificial neural networks (ANNs) (Jang and Chuen-Tsai Sun, 1995). FIS is the theory of solving fuzzy processes (Zadeh, 1965) that are controlled by unclear, uncertain, or incomplete information using several if-then statements and numerical methods called membership functions. Membership functions define the degree of truth of each fuzzy statement using a value of between 0 and 1. Decisions on the number and shape of membership functions for a fuzzy system require the addition of human knowledge. However, ANN's training module can be used to create appropriate membership functions and if-then rules to approximate an output dataset. The FIS structure is unable to dynamically adjust with the environmental change

in datasets. To overcome this shortcoming, the learning capability of ANN was added to ANFIS.

FIS selection is an important part of an ANFIS model. Two widely used FIS functions in the literature are the Mamdani function (Mamdani and Assilian, 1999) and the Sugeno function (Takagi and Sugeno, 1983). This study applies the Sugeno FIS function as it has been commonly used for streamflow discharge forecasting in previous literature (Chang and Chang, 2006; Rezaeianzadeh et al., 2014; Shiri and Kisi, 2010). An example of a simple first-order Sugeno FIS with two inputs, two membership functions, and two rules is shown in Figure 8a. Figure 8b shows the equivalent ANFIS system for the same FIS. The if-then rules structure of the first-order FIS shown in Figure 8b can be expressed as (Farokhnia et al., 2011):

Rule 1: If x is A1 and y is B1 then f1=p1x+q1y+r1 (Eq. 5)

Rule 2: If x is A2 and y is B2 then f2=p2x+q2y+r2 (Eq. 6)

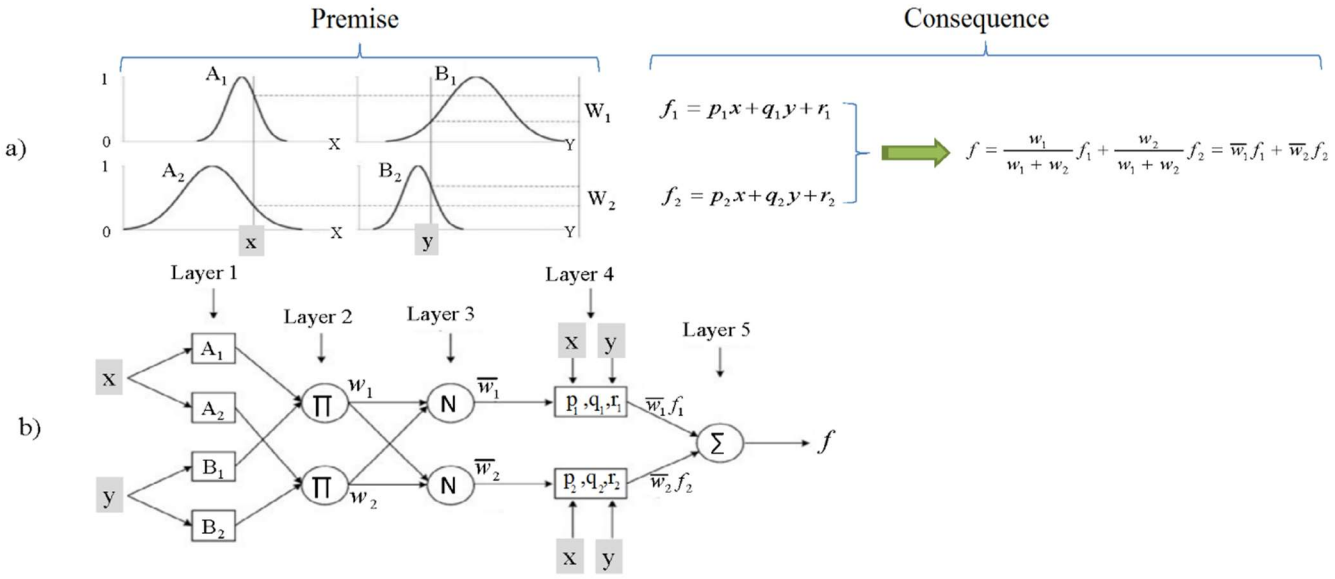

Figure 8. Sample of a first-order Sugeno FIS (a); and its equivalent ANFIS (b) (Farokhnia et al., 2011; Ghalkhani et al., 2013).

where Ai and Bi are the membership functions of inputs x and y, respectively; fi approximates output within the fuzzy region specified by the ith fuzzy rule and pi, qi, and ri are the parameter sets for calculating fi that are optimized alongside the membership function shape parameters during the training process.

ANFIS predicts an output parameter from input variable(s) through a multilayer structure (Figure 8b). In layer 1 (also called a Fuzzifier), input variables are translated to linguistic labels such as low, medium or high using membership functions. In layer 2 (Implication layer), the membership function values associated with different input variables from layer 1 are multiplied to represent the strength of different fuzzy rules (w_i). In layer 3, weights of different fuzzy rules are normalized. Finally in layer 4, the normalized weights from layer 3 are used to predict an output parameter using the pi, qi,

and ri parameter sets that are previously optimized using a gradient descent algorithm (Snyman, 2005).

AI models are typically trained using the input variables that have the highest Pearson correlation coefficient with the outputs (Sudheer et al., 2002). For hydrologic modeling, AI model input variables typically include the antecedent observed discharge and accumulated precipitation for lead times with the highest Pearson correlation coefficient. I trained ANFIS using the antecedent observed discharge and accumulated precipitation. This selection was based on the observation of greatest Pearson correlation coefficient values between the current discharge at each time step (Q_t) and the antecedent precipitation and discharge inputs (Q_{t-N}). I note that because the ANFIS model is dependent on antecedent observed discharge (Q_{t-N}) and forecast lead time, the model must be calibrated and validated for each lead time.

3.3.4. Effect of storm direction on the performance of ANFIS

Storm directions through the Ley Creek catchment were indicated by the dominant wind direction at the two weather stations in near Onondaga Lake (Figure 1). Dominant wind direction for a single storm event at each weather station is assumed as the most frequently reported direction from the beginning of the storm to the rainfall center of mass which is defined as the center of area under the hourly precipitation (mm) versus time (hours) plot. Only storm events with conclusive wind direction at the two stations are used in the study (for example, if the dominant wind direction in the two weather stations were the opposite for a storm event, it will be excluded from the analysis). I note that results of storm tracking using the NEXRAD Level 3 radar data for several storm events indicated an agreement between the wind directions in the two weather stations

and the actual direction of storm movements through the catchment. A total of 68 storm events between 24 June 2014 to 10 January 2016 were detected including 41 storms moving upstream to downstream (UD) and 28 storms moving downstream to upstream of the catchment (DU).

Three independent modeling scenarios were developed using different combinations of training data: 1) 20 UD storm events, 2) 10 DU+10 UD storms, and 3) 20 DU datasets. For all three scenarios, test periods included 5 DU+5 UD. For each modeling scenario, 100 independent combinations of storms were selected from the observed storms using the Sample function (in R programming language without replacement).

ANFIS was trained by water level data at the upstream station (Gage 2 in Table 1, Lemoyne Ave.) as input to predict discharge at the downstream station (Gage 8 in Table 1, Park St. USGS) for a lead time of 2-hours. Data at both stations were recorded at 15-min intervals. The highly correlated lagged input datasets (water levels at Lemoyne Ave station), $d_{t\text{-}2hrs}$, $d_{t\text{-}2.25hrs}$, and $d_{t\text{-}2.5hrs}$, were used to train the ANFIS model. Finally, the performance of the flood forecast model is assessed by MSE, RMSE, Mean Error (ME), and R^2 between observed and modeled values.

3.3.5. Real-time deterministic flood forecasting

The goal of this analysis is to compare the performance of ANFIS with two physical hydrology models, SAC-SMA and SWMM, for real-time deterministic flood forecasting at Ley Creek. Physical hydrology models are calibrated for observed discharge records during water years 2010 to 2013 using three different strategies (lumped, semi-lumped, and semi-distributed) and are validated for water years 2014 to 2015. Finally, different

statistical performance parameters for flood forecasting with lead times of one to six hours for different flow conditions (low, moderate, and high) are calculated and compared between ANFIS and all calibrated physical hydrology models.

3.3.5.1. Building multi-step-ahead forecasting models

All models were calibrated for water years 2010 to 2013 and validated for water years 2014 to 2015 using hourly observed discharge records at USGS gage number 04240120 at Park Street, Syracuse, NY. Hourly precipitation and temperature records are obtained from Hancock International Airport weather stations within the catchment. Three different strategies are used to calibrate physical hydrology modes: Lumped, Semi-Lumped, and Semi-Distributed (Figure 9). RS MINERVE hydrologic-hydraulic modeling package (Foehn et al., 2016) is used to simulate SAC-SMA and SWMM models. A degree-day snowmelt module in RS MINERVE (Snow-GSM) is used to simulate the snowmelt runoff. Evapotranspiration is calculated using Turc approach (1955). Kinematic Wave method is used to rout the stream-flow from source to the outlet through the channel (Miller, 1984).

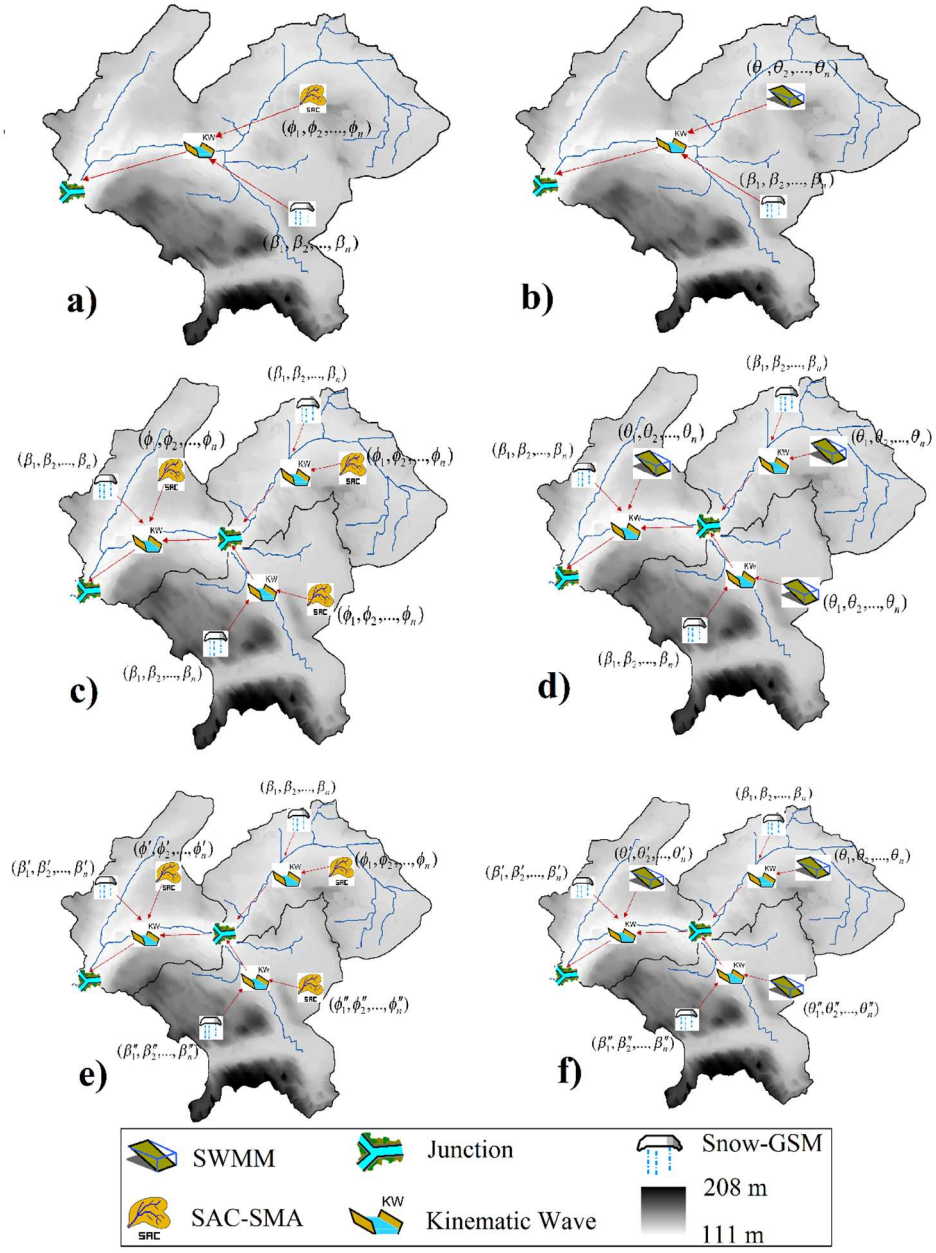

Figure 9. Schematic view of lumped (a and b) semi-lumped (c and d), and semi-distributed calibration strategies (e and f) used for SAC-SMA and SWMM models in RS MINERVE software. For all modeling scenarios, the Kinematic Wave and Snow-GSM degree-day approaches are used for flood routing and snowmelt runoff volume calculation, respectively. The lumped model assumes one parameter set for model calibration (ϕ_1, ϕ_2,…, ϕ_n) and does not divide the catchment into subcatchments. The

semi-lumped model divide the catchment in three subcatchments and assumes similar parameter sets for all subcatchments (ϕ_1, ϕ_2,…, ϕ_n). The semi-distributed model divides the catchment into three subcatchments and assumes different parameter sets for each subcatchment.

To build a real-time deterministic flood forecasting system, physical hydrology model predictions are updated using the observed discharge values (Figure 10). To perform this, the difference between the modeled future discharge (Q_{t+1}) and the current modeled discharge (Q_t) is added to the current observed discharge ($Q_{t,\ observed}$). This approach increases the real-time flood forecasting performance of the physical hydrology model by reducing the uncertainties and errors due to the modeling.

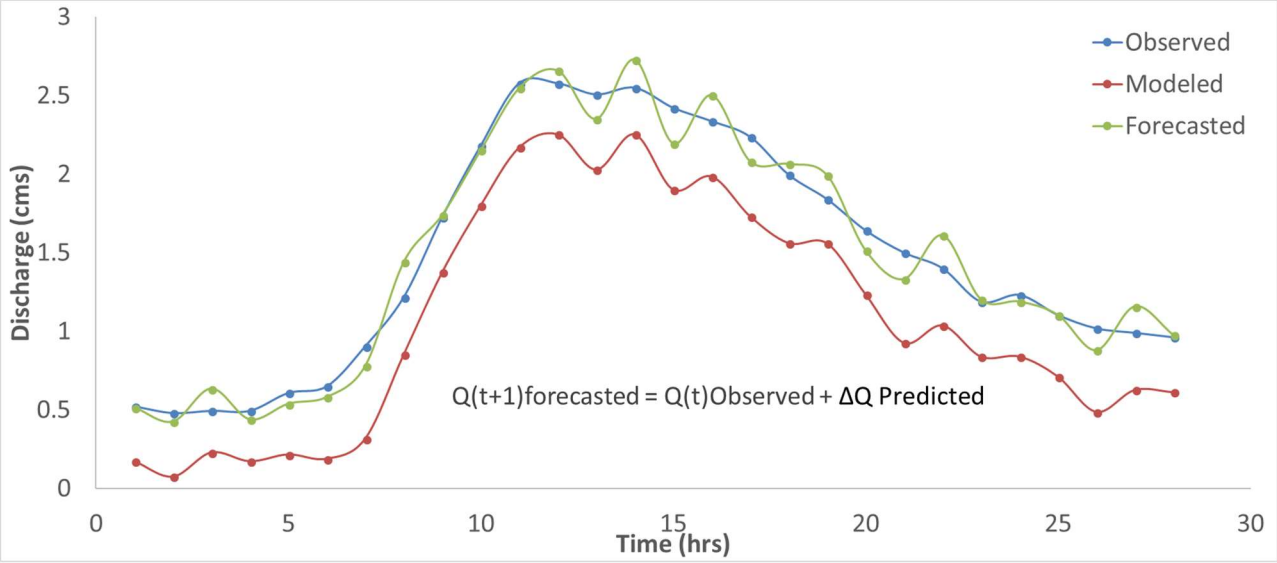

Figure 10. Real-time transformation of modeled discharge from SAC-SMA and SWMM.

The ANFIS real-time flood forecasting model was built in five steps: dataset creation, correlation analysis, optimization, calibration, and validation. First, discharge and

precipitation time series with lag times of one to 48 hours (Q_{t-1hr}, Q_{t-2hrs},…, $Q_{t-48hrs}$ and P_{t-1hr}, P_{t-2hrs},…, $P_{t-48hrs}$) are created. Second, the correlation coefficients between the current discharge and all lagged discharge and precipitation values are calculated. Next, a set of highly correlated discharge and precipitation lagged datasets are entered to Soccer League Competition (SLC) optimization algorithm (Moosavian and Roodsari, 2014a; Moosavian and Roodsari, 2014b) to find the five optimal lagged datasets with the minimum RMSE of the ANFIS model. Finally, ANFIS is calibrated and validated using the optimal discharge and precipitation lagged datasets.

3.3.6. Real-time ensemble flood forecasting

3.3.6.1. Study site description

In August 2011, Hurricane Irene caused several deaths and severe property damage to the eastern coast of the US. Property damage was approximated at about USD 1.5 billion in NY (http://www.fema.gov/ar/disaster/4020) and USD 1 billion in New Jersey (Saleh et al., 2016). During Hurricane Irene, a total of between 15 and 25 cm of accumulated precipitation occurred in a period of less than two days. Flood levels at most streams in proximity of NYC exceeded the major flood threshold defined by National Oceanic and Atmospheric Administration (NOAA) (Table 5). Emergency management agencies evacuated millions of people from the flood-prone regions to limit loss of life. Nevertheless, several deaths occurred in flooded areas during the event. I simulated the flood hydrographs for nine peri-urban catchments near NYC that were severely impacted by Hurricane Irene (Figure 11 and Table 5). Study catchment drainage areas range from small (17 km^2) to medium (150 km^2) sizes. The initial set of seventeen catchments for analysis was divided bases on careful inspection of land cover and catchment hydraulic

connectivity, which showed that eight catchments have stormwater reservoirs close to the outlet that dampen the outflow hydrograph during storm events. Therefore, nine catchments without stormwater control infrastructure were selected for analysis. These nine catchments are slightly to moderately developed, with impervious area ranges from 12% to 25%. The soil in the study area consists of approximately 40% silt, 10% clay, and 50% sand and has a high runoff potential (Falcone, 2011).

Table 5. Descriptions of the study sites in proximity of NYC.

Catchment ID	Subcatchment name	USGS gage number	Location	Area (km^2)	Channel length (km)	Fractional impervious area	Fractional urban area	Fractional forested area	NOAA Major flood threshold (m^3/s)
1	Saddle River at Lodi NJ	01391500	40°53'25" N, 74°04'50" W	141	207	0.17	0.75	0.12	53.8
2	Hackensack River at West Nyack NY	01376800	41°05'44" N, 73°57'50" W	80	93	0.12	0.62	0.27	-
3	Pascack Brook at Park Ridge NJ	01377370	41°02'12" N, 74°02'21" W	35	38	0.2	0.84	0.09	-
4	Hackensack River at Rivervale NJ	01377000	40°59'57" N, 73°59'21" W	150	167	0.13	0.65	0.24	-
5	Pascack Brook at Westwood NJ	01377500	40°59'34" N, 74°01'16" W	77	90	0.17	0.84	0.1	21
6	Peckman River at Little Falls NJ	01389550	40°52'19" N, 74°13'20" W	20	16	0.19	0.74	0.25	-
7	Bound Brook at Middlesex NJ	01403900	40°35'06" N, 74°30'28" W	125	144	0.25	0.71	0.16	62.6
8	Lawrence Brook at Westons Mills NJ	01405030	40°28'59" N, 74°24'46" W	116	152	0.2	0.56	0.18	60.9
9	Big Brook near Marlboro NJ	01407290	40°19'11" N, 74°12'51" W	17	27	0.12	0.5	0.16	28.1

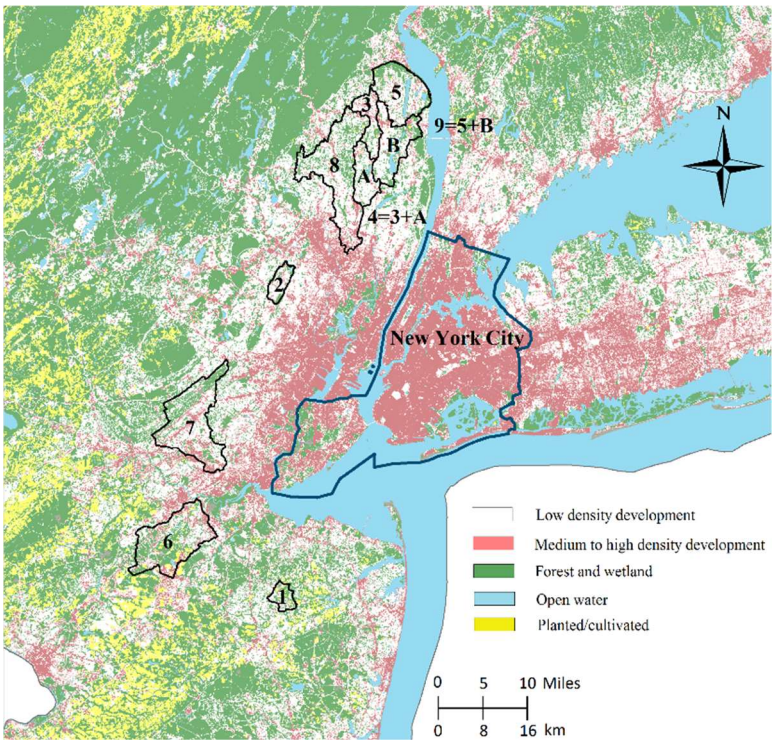

Figure 11. Land cover map of the study catchments. Land covers associated with low density development, medium- and high-density development, forest and wetland, open water, and planted/ cultivated are shown by white, red, green, blue, and yellow, respectively. Catchment ID numbers indicate drainage area, increases from 1 and 9. Table 5 provides detailed information about the study catchments.

Subcatchment drainage areas in Table 5 were calculated using the USGS StreamStats auto delineation tool (http://water.usgs.gov/osw/streamstats/). Statistics for calculating the mean historical annual gaged peak flow and the gaged peak flow during Hurricane Irene were obtained from the corresponding USGS gages. The NOAA major flood thresholds were obtained from the USGS website (http://waterwatch.usgs.gov). This threshold value, defined by the NWS, represents the volumetric discharge that, when exceeded, signifies a major flood event. Note that the NOAA major flood threshold

values that are presented in Table 5 were recently removed or changed at the USGS website for unknown reasons.

3.3.6.2. Model Input Data and Simulation Periods

Meteorological data including hourly precipitation and temperature data were obtained from Phase 2 of the North American Land Data Assimilation System (NLDAS-2) using the HydroDesktop version 1.4 software (Ames et al., 2012). I focus on model application to two different events: (1) Hurricane Irene, and (2) a smaller storm in NYC during September of 2011. The total accumulated precipitation for the small storm during 2011 was about 35 mm, which is approximately one-fifth of that for Hurricane Irene (160 mm), and the duration of small event was about half a day, which is around one-third of that for Hurricane Irene. The historical observed streamflow discharge records from 1 October 2004 to 1 October 2014 were obtained from the corresponding USGS gages (Table 5). Observed meteorological and discharge data from 1 October 2004 to 27 August 2011 were used for model calibration for Hurricane Irene. Similarly, observed datasets from 1 October 2004 to 23 September 2011 were used for model calibration for a small storm event that occurred a few weeks after Hurricane Irene. The calibrated models were then validated for the following three years to ensure robustness. Finally, the GEFS/R precipitation data inputs and the observed temperature and discharge records for the events 27-29 August 2011 and 23-25 September 2011 were used to force the calibrated/validated models for ensemble stream-flow prediction.

3.3.6.3. Real-time flood forecasting system

I implemented a real-time ensemble flood forecasting approach to re-forecast the flood discharge at nine USGS gages (Table 5) located at the outlet of the study sites for

Hurricane Irene and a smaller storm event that occurred a few weeks after Hurricane Irene. Eleven ensemble members of the GEFS/R precipitation (10 members + 1 control member) with a temporal resolution of three hours were used to force the calibrated models to forecast the streamflow discharge during the two study events. As the available GEFS/R precipitation data are produced only once daily at 00 Universal Time Coordinated (UTC), a meteorological and discharge data updating component was added to the system to update the precipitation and streamflow discharge inputs for sub-daily forecasts (lead times of three, six, and nine hours). For example, precipitation and streamflow data inputs corresponding to the forecasts for a lead time of three hours were updated at three-hour intervals using the observed data and models were re-run after every single update in the input database to correct the future discharge forecast. This updating component corrects the initial conditions of the predictor model (for SAC-SMA or ANFIS) for sub-daily predictions based on the most recent meteorological and streamflow observations within the forecast system. For SAC-SMA, a data-assimilation technique was used to update model parameters based on discharge observations. In this approach, SAC-SMA was re-calibrated at each update by allowing parameters to vary between 10% below and above the original parameter values to account for uncertainty in these estimates. This approach also supported real-time assimilation of observations, leading to improved agreement between modeled and observed discharge. This input data updating process also decreased the uncertainty and errors of the forecasted discharge values that arose from uncertainties in the daily GEFS/R meteorological predictions. Finally, the performance of the forecast models is assessed using the indices described in Table 6.

Table 6. Statistical indices used to assess model performance. Q_i^f and Q_i^o: the ith forecasted and observed discharge, respectively. N_P: number of time steps during the storm event that both the observed and predicted discharge (the average of eleven forecast ensemble members) are greater than the NOAA major flood threshold; and N_O: number of time steps during the storm event that the observed discharge values are greater than the NOAA major flood threshold. ARAD shows the average modeling error over the simulation period (Reilly and Kroll, 2003). For instance, ARAD=0.15 indicates that the model is on average 15 % different from the real observations regardless of over or underestimation.

Index title	Formula	min	max	best
Nash-Sutcliffe Efficiency (NSE)	$1 - \frac{\sum_{i=1}^{n} (Q_i^o - Q_i^f)^2}{\sum_{i=1}^{n} (Q_i^o - \overline{Q_i^o})^2}$	$-\infty$	1	1
Percent BIAS (PBIAS)	$100 \times \frac{\sum_{i=1}^{n} (Q_i^f - Q_i^o)}{\sum_{i=1}^{n} Q_i^o}$	$-\infty$	$+\infty$	0
Relative Bias (RelBIAS)	$\frac{\sum_{i=1}^{n} (\frac{Q_i^f - Q_i^o}{Q_i^o})}{n}$	$-\infty$	$+\infty$	0
Relative Mean Squared Error (RelMSE)	$\frac{\sum_{i=1}^{n} (\frac{Q_i^f - Q_i^o}{Q_i^o})^2}{n}$	0	$+\infty$	0
Average Relative Absolute Difference (ARAD)	$\frac{\sum_{i=1}^{n} \left\lvert \frac{Q_i^f - Q_i^o}{Q_i^o} \right\rvert}{n}$	0	$+\infty$	0
Prediction Reliability (PR)	$\frac{N_P}{N_O}$	0	1	1

To evaluate the effectiveness of models for predicting the major flood condition, I have developed a simple index, called "Prediction Reliability (*PR*)" (Table 6), similar to the Color-coded threshold exceedance diagram which was previously used by Saleh et al. (2016) in a similar study. The *PR* index is defined as the ratio of the number of time steps during the study storm event that both predicted and observed discharge values are greater than the NOAA major flood threshold (N_P) to the number of time steps with observed discharge greater than the NOAA major flood threshold (N_O). This index indicates the reliability of a real-time flood forecast model for emergency management conditions during extreme events which is necessary for evacuation and protection plans in urban catchments. Values near one represent greater predictability performance of the model and values near zero represent poor prediction. Note that this index is only meaningful for extreme events when the flood stage in the river exceeds the NOAA flood threshold. For example, in this study, *PR* is used only for Hurricane Irene and is not applicable for the small storm event. One problem with the *PR* index is that it favors models that generally overestimate floods.

4. Chapter 4 (Results and Discussion)

4.1. Seasonal change in urban runoff peak flows at Ley Creek

4.1.1. Results

Seasonal hydrographs resulting from cumulative precipitation depths of approximately one cm for the five subcatchments in Onondaga Creek Watersheds (Table 2) showed a relatively similar behavior for the wetland dominant (LOW1) and the most urbanized catchment with the retention pond (INT2) (Figures 12a and e). The greatest peak flows at these two sites occurred during late winter and spring, whereas summer peak flows were generally less. Furthermore, autumn peak flow in both catchments was significantly greater than summer peak flow. In contrast, the remaining sites (LOW2, LOW3, and INT1) had peak flows of about the same magnitude during summer and autumn (Figure 12b, c, and d). The spring peak flow was several times higher than winter peak flows in LOW2 and LOW3, and just slightly greater than the winter peak flow for INT1.

a)

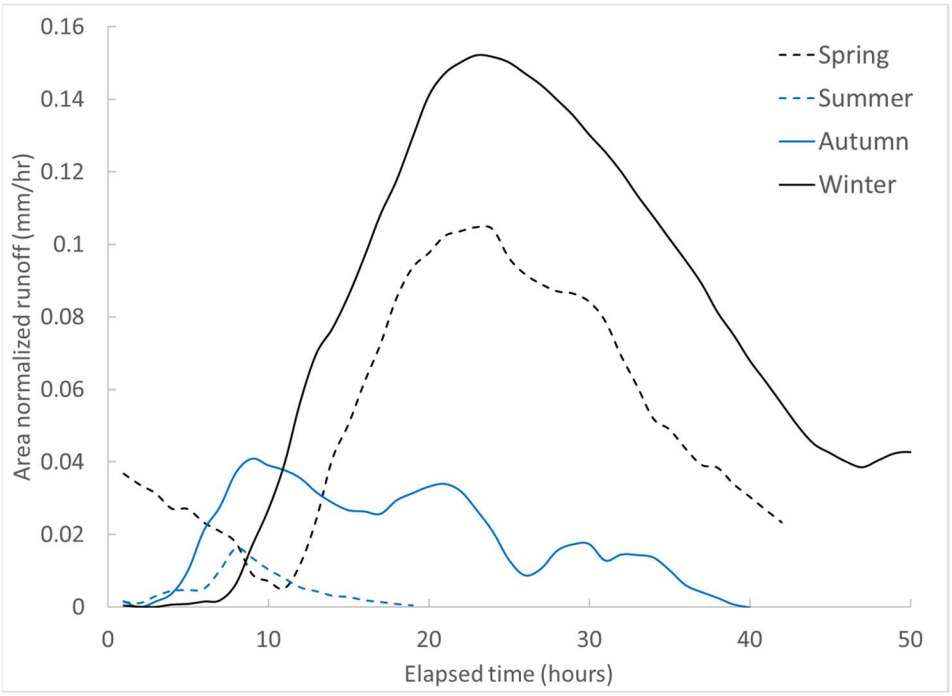

b)

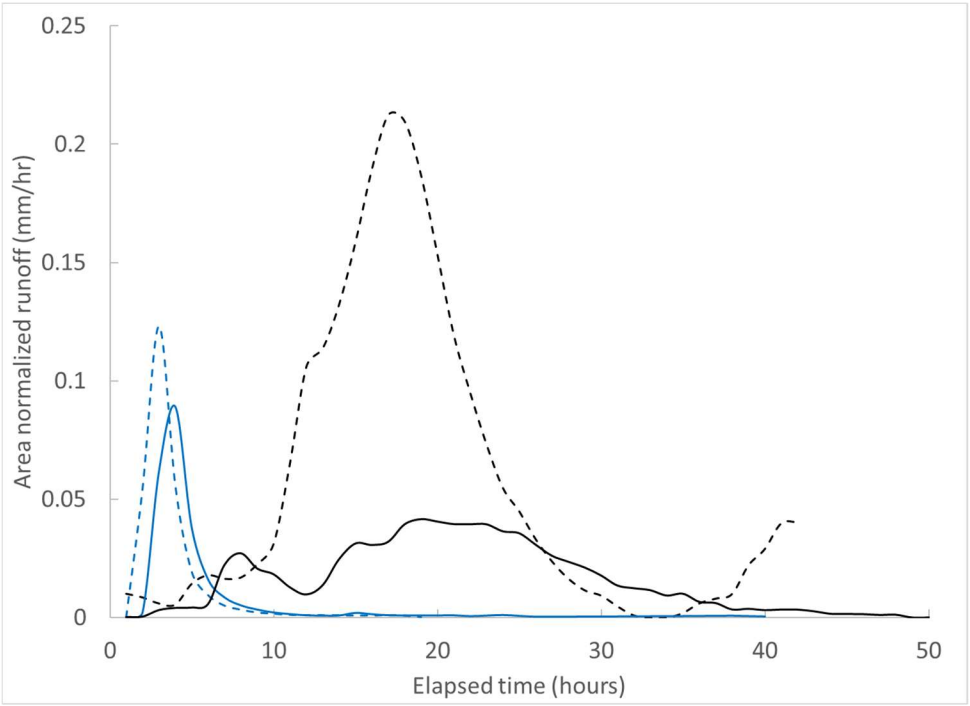

Figure 12. Seasonal hydrographs for a one cm rain event at LOW1 (a) and LOW2 (b). Events shown on the graph include 8 April 2015 (Spring), 28 October 2015 (Autumn), 20 August (Summer), and 27 December 2015.

c)

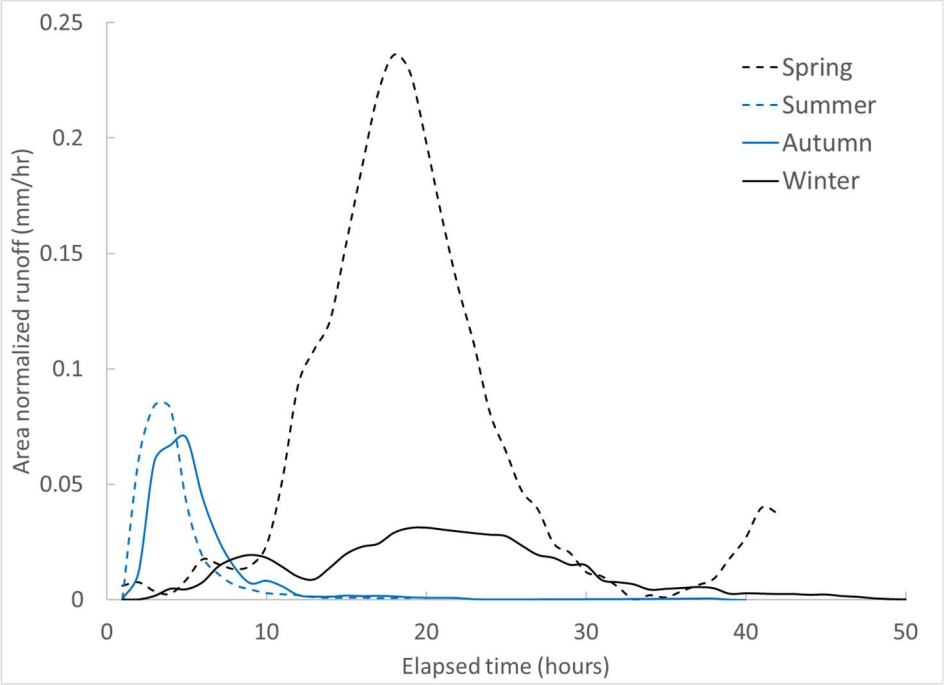

d)

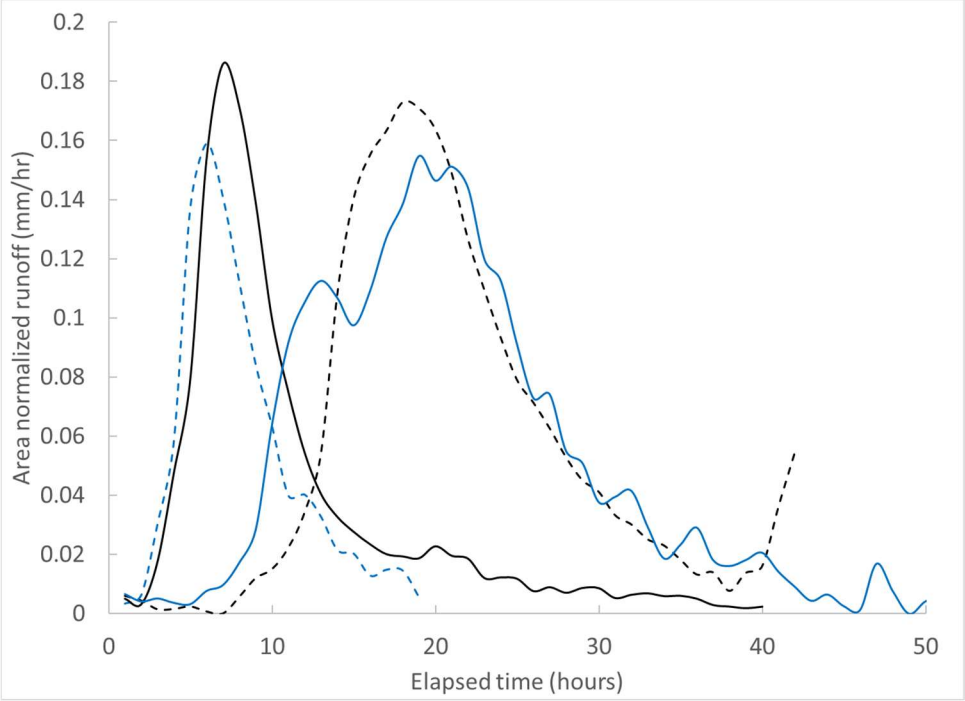

Figure 12 (continued). Seasonal hydrographs for 1 cm rain event at LOW3 (c) and INT1 (d). Events shown on the graph include 8 April 2015 (Spring), 28 October 2015 (Autumn), 20 August (Summer), and 27 December 2015.

e)

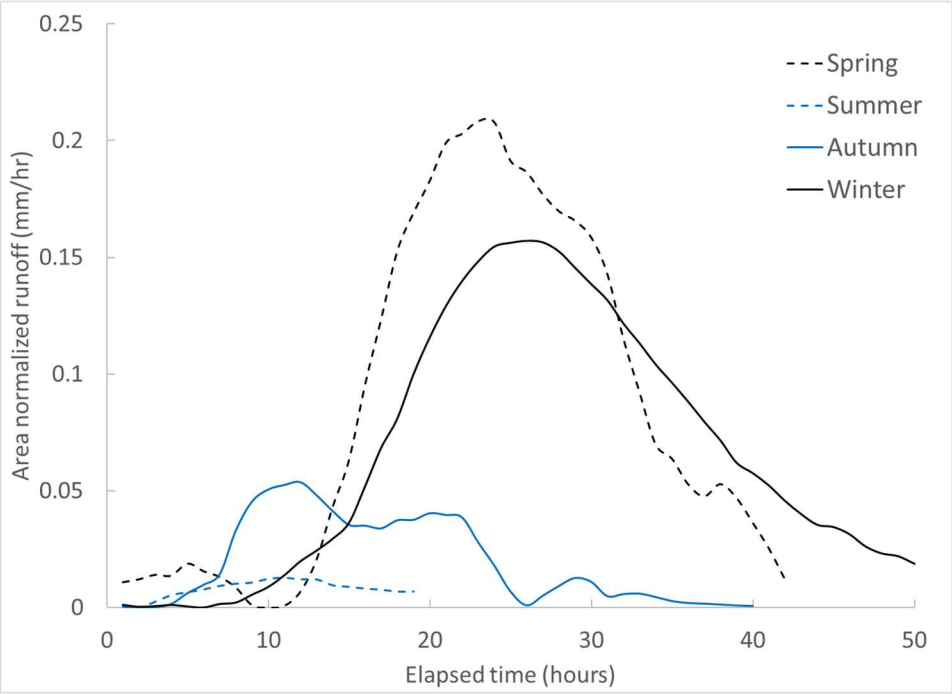

Figure 12 (continued). Seasonal hydrographs for 1 cm rain event at INT2 (e). Events shown on the graph include 8 April 2015 (Spring), 28 October 2015 (Autumn), 20 August (Summer), and 27 December 2015.

Urbanization increased surface runoff peak flows during all seasons, but the rate of increase was highly variable among seasons (Figure 13). For example, the average summer peak flow in the urbanized catchments were nearly three times greater than the natural catchment. For spring and autumn, the average urbanized catchment peak flow increased by 98 % and 73 % over the reference catchment, respectively, slightly less than the difference in annual average peak flow (105%). By contrast, this difference was only 6% for winter. Spring snowmelt in all catchments commenced in mid-March and concluded in early April. Ten snowmelt events were counted for all catchments except INT1 with has 16 melt events.

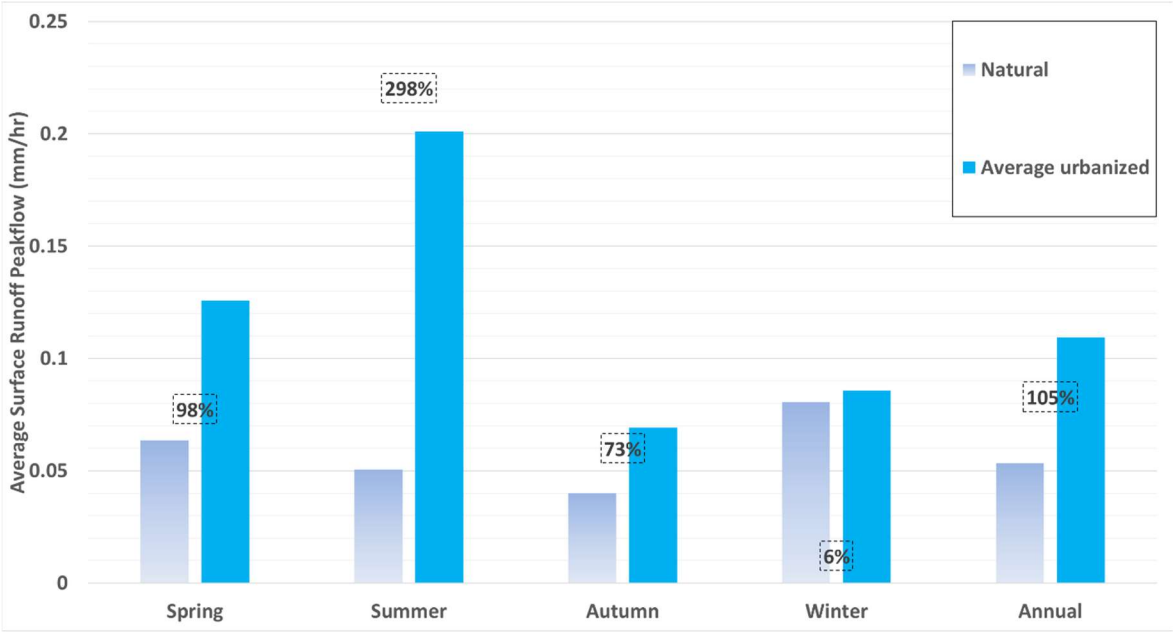

Figure 13. Average annual and seasonal runoff peak flows for wetland dominant (LOW1) and urbanized (the remaining) catchments. Values shown on the chart represent the difference between the natural catchment and the average of all urbanized catchments.

Annual peak flow differed by 0.04 mm/hr between LOW1 and LOW2 with an increase in imperviousness of only 1 % (Figure 14). Seasonality of peak flows (deviation from annual average) also increased significantly for this threshold of imperviousness.

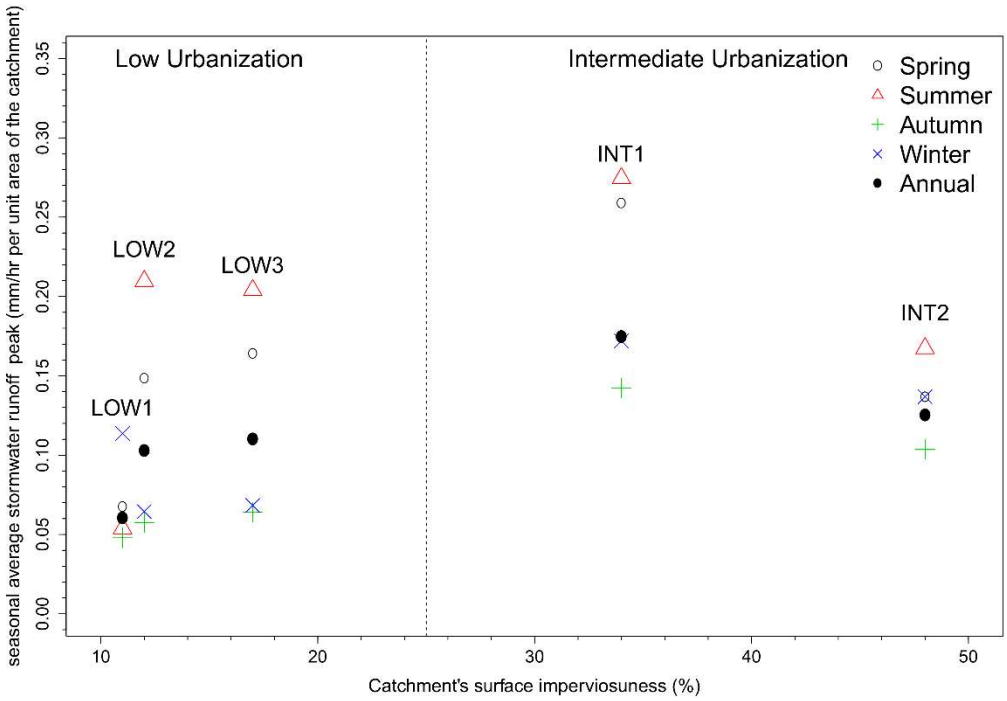

Figure 14. Average annual and seasonal runoff peak flows for the studied catchments as a function of imperviousness. Events associated with different seasons are plotted with open circle (Spring), open triangle (Summer), plus sign (Autumn), multiplication sign (Winter), and solid circle (Annual).

According to Figure 14, runoff peak flow in urbanized catchments did not necessarily increase with fractional impervious area: the most impervious catchment (48%) includes a relatively large stormwater pond at the outlet yet had smaller annual average peak flow compared to INT1 (34%). The seasonal deviation of peak flows from the annual average at the former catchment (INT2) was also less than that for INT1. This shows that the stormwater pond effectively reduces the impact of urbanization at INT2. Another possible explanation for the smaller peak flows at INT2 than INT1 may be the shorter channel length and greater contribution of the stormwater system to mitigating runoff peak flows at INT2. A great fraction of the stream-flow at INT2 receives precipitation runoff from the 690 highway, and local commercial districts. Stormwater network maps

are not available for Ley Creek, so it is difficult to approximate the runoff contribution from the commercial districts. Nevertheless, it is likely that some of the commercial properties at INT2 are connected to the urban stormwater system and not to the south branch of Ley Creek.

4.1.2. Discussion

The results suggest that the impact of urbanization on flooding is greater in summer than spring and winter. In addition, the annual average runoff peak flow in the study catchments increases with urbanization in agreement with previous findings (Arnold and Gibbons, 1996; Cheng et al., 2010; Valtanen et al., 2014). As hypothesized, the extent of this impact varies between seasons: average seasonal peak flows for urban catchments were almost three times greater than for the natural catchment while this difference was only 6% for winter. Similarly, previous literature reported greater (Buttle, 1990; Dougherty et al., 2006; Valtanen et al., 2014) impact of imperviousness on runoff volume in urbanized catchments during warm seasons. The water budget in LOW1 catchment during summer and fall is highly influenced by wetlands. In this catchment, evapotranspiration, infiltration, and soil storage capacity and lower ground water base depth in channel result in lower surface runoff rates. However, during winter, both pervious and impervious surfaces contribute to surface runoff due to the formation of large areas of saturated, compacted or frozen impervious soils. Therefore, differences between the hydrologic behaviors of natural and urbanized catchments is decreased during winter and spring. Average spring runoff peak flows were greater than the annual average in all catchments, but for the urbanized cases (imperviousness from 12 to 48%), they were considerably less than summer peak flows. This finding is in contrast with

results of Semádeni-Davies and Bengtsson (1999) who have indicated that the greatest discharge in urbanized catchments with 30 to 80% imperviousness occurs during spring. However, significant summer peak flows are common due to the extremely wet conditions during summer.

Furthermore, the results indicate that the snowmelt timing does not change for urbanized catchments in the studied range of imperviousness (11-48 %): snowmelt in all catchments initiated during mid-March 2015 and ended through early April. This is in contrast with results of Valtanen et al. (2014) who reported earlier-than-usual spring snowmelt peak flows at two urbanized catchments in Finland. In this study, the number of snowmelt events for the rural catchment (n=10) equaled those for the most urbanized catchment (imperviousness = 48%). However, the moderately urbanized catchments (imperviousness = 34%) had a greater number of snowmelt events (n=16). A smaller number of snowmelt events in the highly urbanized catchment is likely due to the moderating impact of the stormwater pond. The previous literature has also indicated a larger number of smaller melt events due to urbanization (Buttle, 1990; Semádeni-Davies, 2000). Changes in snowmelt timing and frequency are also associated with human disturbances such as snow redistribution, removal, ploughing, and transportation activities in urban catchments (Bengtsson and Westerström, 1992; Buttle and Xu, 1988; Semádeni-Davies and Bengtsson, 1999).

Analysis of seasonal and annual runoff peakflows, showed an imperviousness threshold of 11% for responsiveness of urban stream-flows, above this threshold, urban stream-flows experienced a substantial increase in annual average peak flows and greater seasonal changes in peak flow magnitudes. In this case, there was a substantial difference

in annual and seasonal runoff peak flows between LOW1 and LOW2 with imperviousness of 11 and 12%, respectively. Stream stability threshold data are limited, however, there is some evidence that the impact of imperviousness on urban streamflow can be detected when imperviousness exceeds 5-10 % (Schueler et al., 2009; Schueler, 1994; Valtanen et al., 2014). Interestingly, the seasonal variation of runoff peak flows was extremely high for all urbanized catchments with imperviousness of higher than the stability threshold (11%). The most highly impervious catchment (48%) had a large stormwater pond near the outlet and was an exception to this behavior. This difference in runoff response demonstrates the positive impact of appropriately designed detention storage ponds.

4.2. Impacts of urban development pattern on runoff peak flows

4.2.1. Results

To address the impact of impervious surface distribution on runoff peak flows, I investigated the correlation between RNICO with runoff peak flows and flow regime indices for ninety US peri-urban catchments (Table 3 and Figure 6). I present the results in two sections, climate and hydrology. The meteorological weather conditions including precipitation and temperature records for the study period at the study sites are reported in the climate section. The hydrology section describes the observed runoff peak flow analysis results, and the correlation analysis between RNICO with runoff peak flows and flow regime indices at the study sites are presented.

4.2.1.1. Climate

For all study locations, the probability density function (Kernel Density Estimates (Skorski, 2019)) of North American Land Data Assimilation System (NLDAS-2) radar

precipitation event's depth, duration, and average intensity were similar for the three-year study period, as were the long-term probability density function for event's precipitation depths less than one cm (see Figure 15 for Los Angeles and San Francisco). Furthermore, results of storm tracking using the NEXRAD Level 3 radar data at different study locations showed that most precipitation events with depths greater than one cm have nearly complete coverage of the relatively small study sites. For these reasons, we chose to use only storms with depth greater than one cm for this study. A total of 250, 550, and 750 storm events up to a depth of 60 cm were detected at western, southern, and northern US study sites, respectively. Screening by the one cm criterion reduced the event number to about 40, 75, and 100 precipitation events for analysis in western, southern, and northern US study sites, respectively.

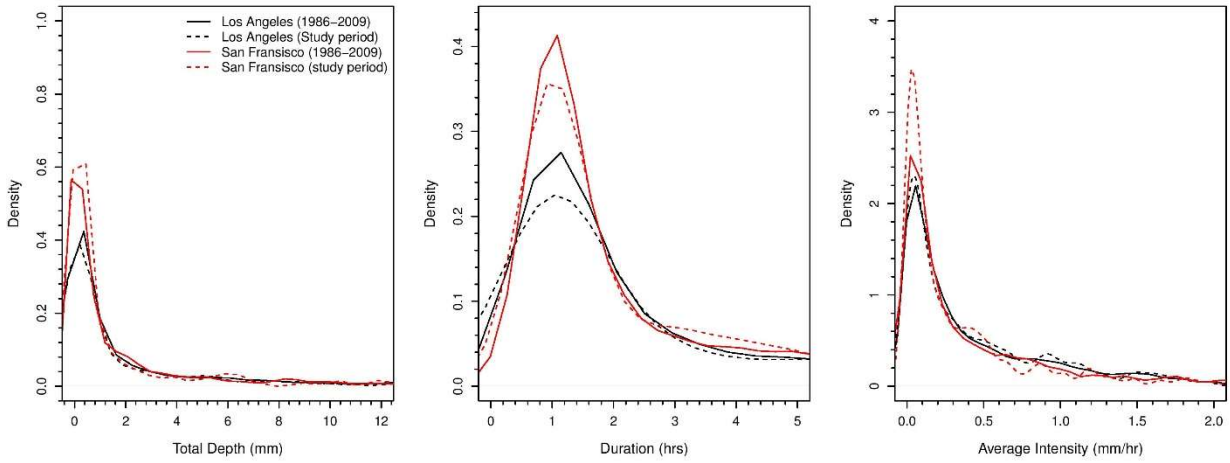

Figure 15. Smoothed probability density function (the Kernel Density Estimates (Skorski, 2019)) plot of NLDAS-2 radar precipitation depth (a), duration (b), and average intensity (c) for the study period (October 2009 to October 2012) and for October 1986 to October 2009 at San Francisco and Los Angeles. Plots are generated using the density function in R programming language. Note that the curve smoothing approach has caused meaningless negative values within all three figures. As a result, the area under the probability density functions on the positive side of the x-axis is not equal to 1, since a fraction of the smoothed plots are on the negative side of the x-axis are not shown. I preferred to use the smoothing approach for visualization because it better demonstrates the trend and shape of probability distributions, especially for the right-hand side tail of the plots which is the focus of this research.

4.2.1.2. Hydrology

Example hydrographs show differences between the peak flow response of catchments with different sizes and imperviousness (Figure 16). For the sites with similar fractional impervious area, streams in smaller catchments such as Site 13 show a flashier behavior

than in medium (Site 2) and larger catchments (Site 4) even for low-intensity precipitation. In contrast, for the sites with similar drainage area, streams of catchments with greater fractional impervious area such as Site 8 show greater flashiness than those of medium (Site 3) and less impervious catchments (Site 11). Time to peak flows in small, highly impervious catchments are less than in larger and lower impervious catchments (Gericke & Smithers, 2014; McCuen, Wong, & Rawls, 1984; McGlynn, McDonnell, Seibert, & Kendall, 2004). The magnitude and frequency of peak flows are also greater in the smaller and more impervious catchments due to the difference in time of concentration (Eimers & McDonald, 2015; Valtanen et al., 2014).

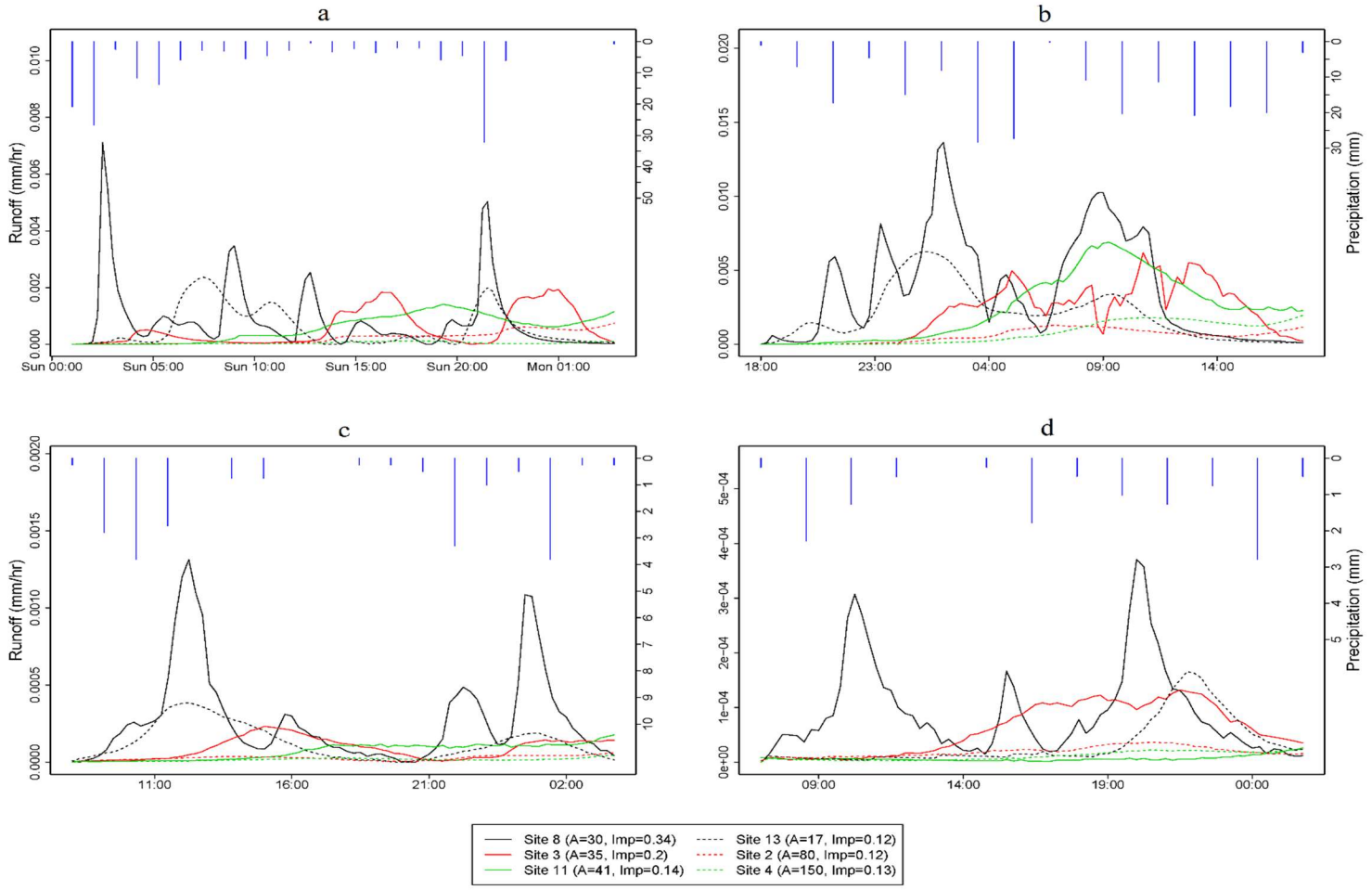

Figure 16. Flood hydrographs of six study catchments at NYC. Charts a, b, c, and d represent precipitation events on 14 August 2011 (160 mm), 27 August 2011 (230 mm), 19 October 2011 (25 mm), and 27 October 2011 (16 mm), respectively. The X- and Y-axis on the figure show time and runoff peak flow (mm/hr).

The RNICO index was positively correlated to runoff peak flows in all study sites, but the strength of this correlation was site- and scale-dependent (Figure 17). To understand the linkage between catchment size and the predictive power of RNICO, an area threshold value was defined to distinguish between small and large catchments. To calculate the area threshold value for each city, all study catchments for that city were sorted by descending drainage area. For each site, we evaluated the strength of the Pearson correlation coefficient between RNICO and average runoff peak flow, then selected an area threshold value based on a transition from strong to weak correlation. In this case, small catchments with upstream urbanization in Figure 4 had negative RNICO values which results in lesser runoff peak flows. For Chicago, NYC, Baltimore, Houston, and Austin, where there were a larger number of study catchments, catchment area threshold values of 55, 40, and 50, 42, and 32 km^2 were observed, respectively. RNICO values in catchments with drainage areas less than these area thresholds were strongly correlated to runoff peak flow magnitudes (Figures 17a-e). For these cases, the average runoff peak flows at the catchments with drainage area greater than the area threshold values remained relatively constant within the study sites. Syracuse, Portland, San Francisco, and Los Angeles had fewer number of study sites with no evident area threshold values. However, there was still a strong positive correlation between RNICO and runoff peak flows in these cities (Figures 17f-i).

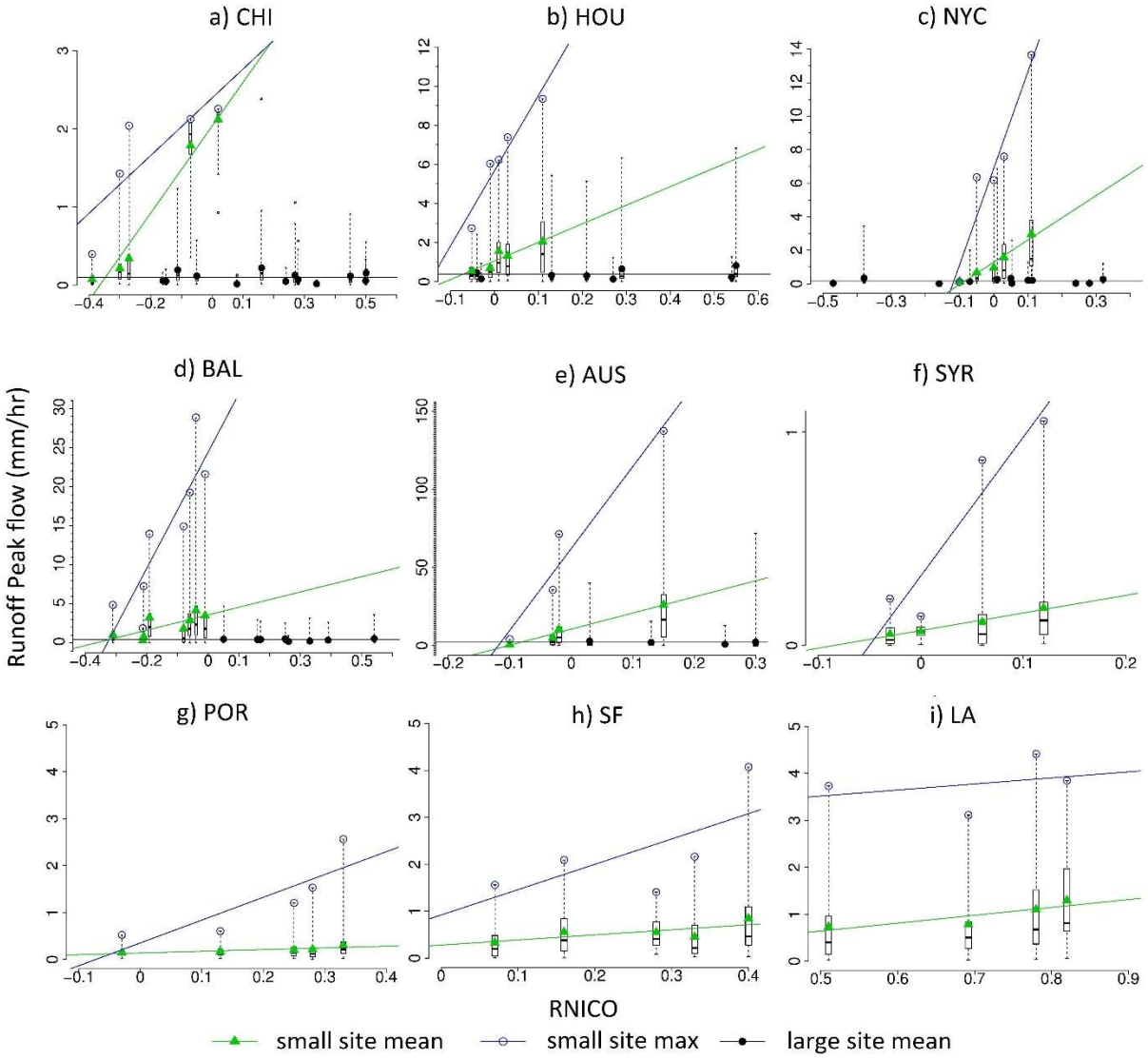

Figure 17. Box-and-whisker plot of runoff peak flows versus RNICO for Chicago, IL (CHI, 17a), Houston, TX (HOU, 17b), New York (NYC, 17c), Baltimore, MD (BAL, 17d), Austin, TX (AUS, 17e), Syracuse, NY (SYR, 17f), Portland, OR (POR, 17g), San Francisco, CA (SF, 17h), and Los Angeles, CA (LA, 17i). The values on the x-axis represent the RNICO index (see Section 3.2.2.2). The sites with negative RNICO are upstream urbanized (UU class in Figure 7b) and have lesser runoff peak flows. The three data series represent maximum runoff peak flows in small sites (black open circles),

average runoff peak flows for small sites (green solid triangles) and average runoff peak flows for large sites (black solid circles). Results for Syracuse, NY and NYC are reprinted from Roodsari and Chandler (2017). Equations of linear regressions are presented in Table Q1 in Appendix Q.

To investigate the impact of imperviousness distribution on stream-flow regime, the statistical correlation between RNICO and stream-flow regime indices including Richards-Baker Flashiness index (RBF) for Chicago, NYC, and Portland were studied (Figure 18). Similar analysis was performed for the coefficient of variation of mean daily flow (CV) (Figure Q1 in Appendix Q). Results indicated that RNICO can be a stronger predictor of stream-flow regime than fractional impervious area for the studied locations, especially for smaller catchments. For small catchments in NYC ($A<40$ km^2), both RNICO and imperviousness percentage had strong positive statistical correlation with flow regime indices ($R^2>0.7$; Figure 18b) (Roodsari and Chandler, 2017). For large study catchments in NYC ($A>40$ km^2) and Chicago ($A>55$ km^2), there were weak statistical correlations between RNICO and imperviousness percentage with stream-flow regime indices (Figures 18a and 18b). Due to the limited number of study catchments in Portland, I did not investigate the area threshold value for this city. Surprisingly, the percent imperviousness for Portland catchments with drainage areas ranging from 7 to 80 km^2 was negatively correlated with CV (Figure Q1, Q1c2) and showed weak statistical correlation with RBF ($R^2=0.02$; Figure 18c, 18c$_2$). On the other hand, RNICO of Portland study catchments was positively correlated with both RBF ($R^2=0.54$) and CV ($R^2=0.2$), indicating a higher influence of imperviousness distribution on stream-flow regime compared to development level in these sites. For small catchments in Chicago ($A< 55$

km^2; Figure 18a), the Pearson correlation coefficient between RNICO and RBF (R^2=0.41) was much greater than for those between the fractional impervious area and flow regime indices (R^2=0.41; Figure 18a, 18a2). Similarly, the Pearson correlation coefficient between RNICO and CV (R^2=0. 71) was much greater than for the Pearson correlation coefficients between the fractional impervious area and CV (R^2=0.41) (Figure Q1, Q1a).

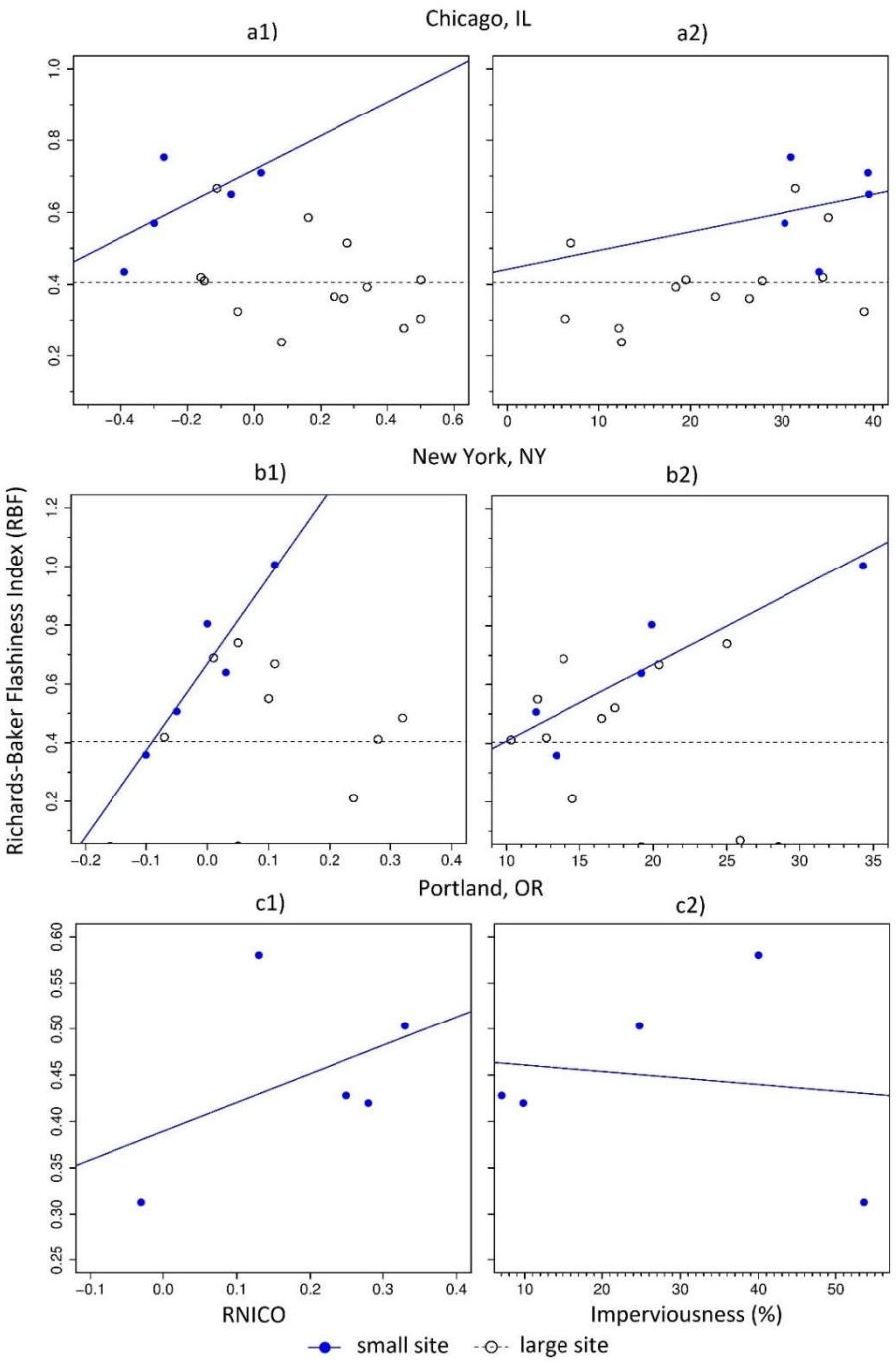

Figure 18. Plots of RNICO (18a1, 18b1, and 5c1) and imperviousness (18a2, 18b2, and 18c2) versus Richards-Baker flashiness index (RBF, solid circle) for Chicago, IL, New York, NY (Roodsari and Chandler, 2017), and Portland, OR. Blue and black symbols represent plotting points associated with small and large sites, respectively. Regression equations are presented in Table Q2.

Chicago had the greatest number of study catchments with variety of shapes, which could potentially lead to a great variation in time to peak flow. The impact of imperviousness distribution on time to peak flow was investigated for 18 study catchments in Chicago with drainage areas ranging from 20 to 230 km^2 (Figure 19). Time to peak flow was initially calculated as the time difference between the start of storm event to the time of maximum peak flow at the catchment outlet. To remove the influence of catchment scale, the approximate time to peak was normalized by the estimated maximum flow path distance to the outlet gage. The maximum flow path length was estimated using the USGS stream auto-delineation software. Results showed a negative correlation (R^2=0.41) between RNICO and the mean normalized time to peak of the 5 small study catchments (A<55 km^2). This may indicate that the downstream urbanization decreases the flood travel time within the small study sites in Chicago. For 13 large study catchments in Chicago (A>55 km^2), the normalized time to peak widely varied for most study sites, but the average normalized time to peak remained relatively constant.

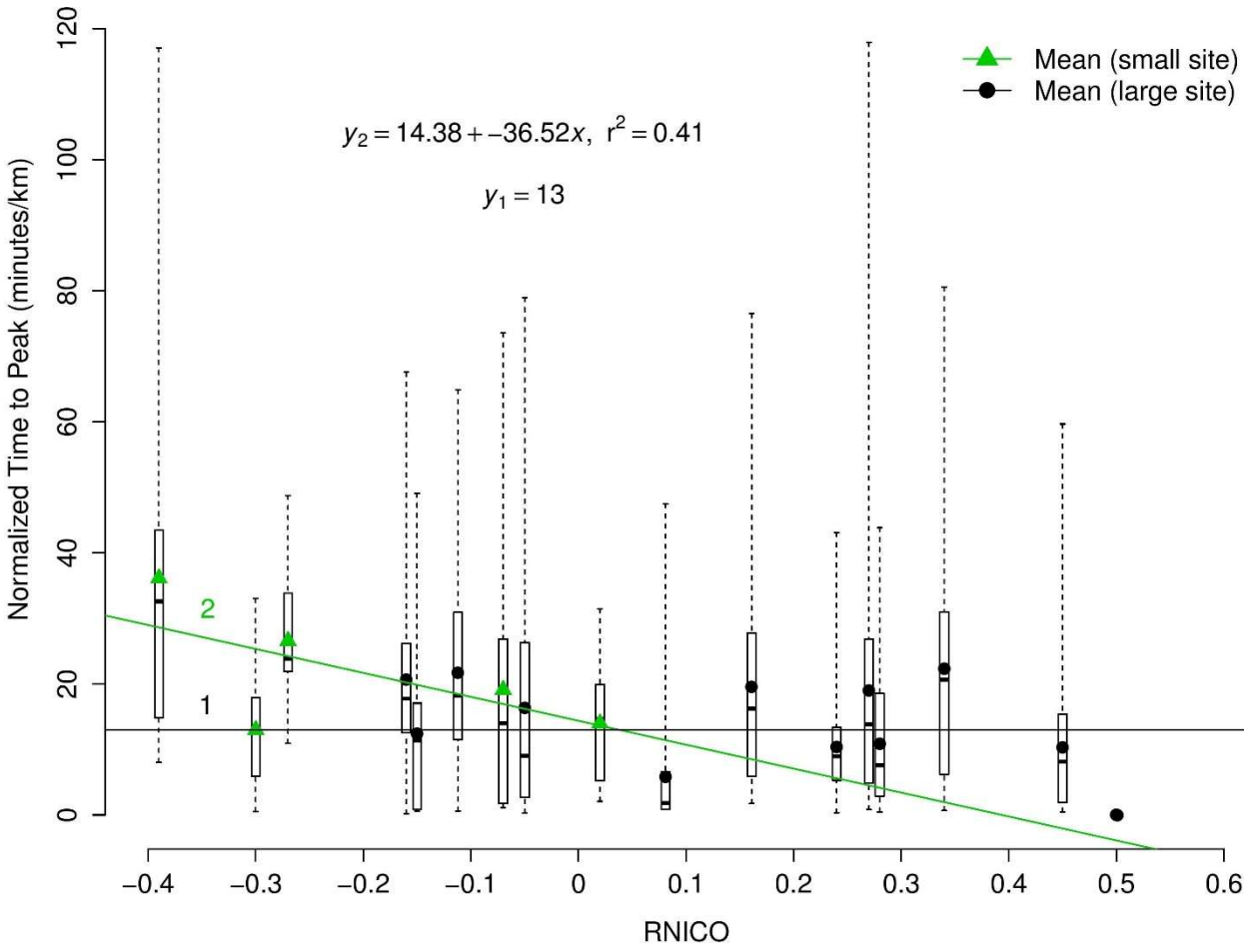

Figure 19. Box-and-whisker plot of normalized time to peak flow versus RNICO for Chicago, IL. Time to peak was measure as the time difference between the rainfall initiation and the time when the maximum runoff peak flows occurs in the catchment outlet point. To remove the impact of catchment scale, the measured time to peak was normalized by the maximum flow path length within the catchment.

The effectiveness of the RNICO index for urban development pattern classification was also tested by plotting the runoff peak flows and time to peak for the three development pattern classes (Figure 20). Results showed an obvious increase in runoff peak flows and

decrease in time to peak when moving from UU class to CEN and DU classes. This trend indicates that the RNICO index is an effective classification tool to represent the changes in runoff peak flow magnitude and timing in the NYC study catchments, despite the complexity of urban drainage systems within the study sites.

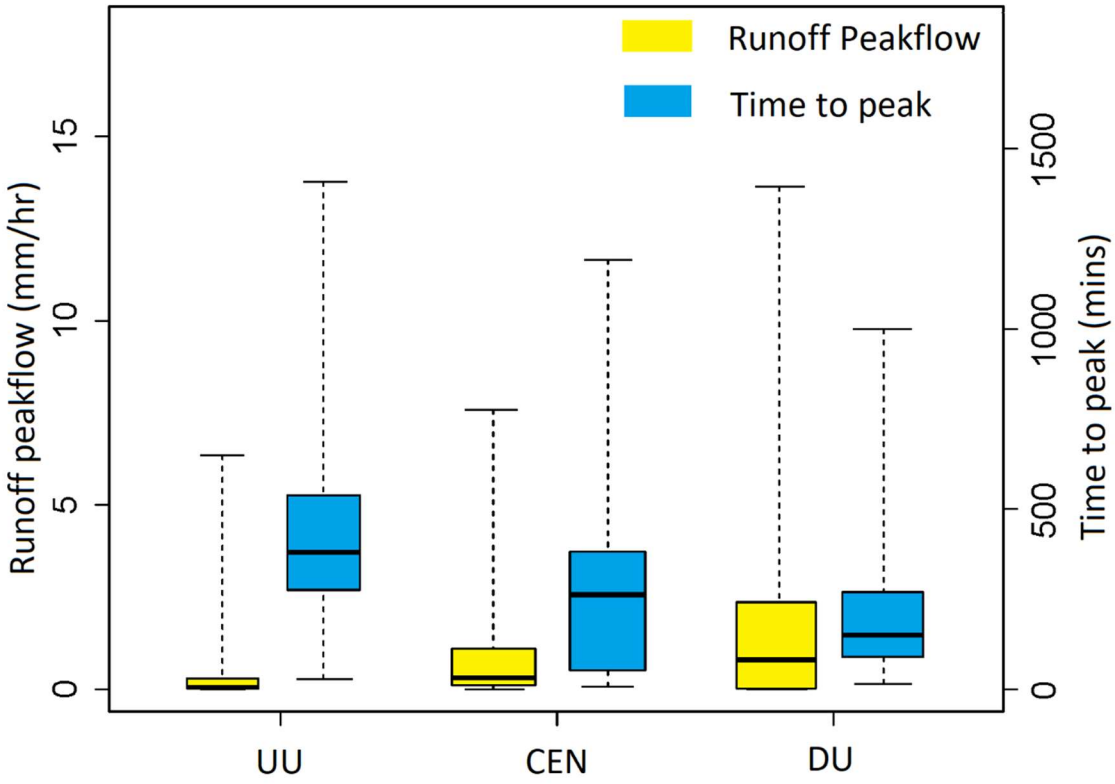

Figure 20. Runoff peak flows and time to peak versus RNICO for the three urbanization classes of NYC study catchments. Time to peak was calculated as the time between the occurrence times of maximum rainfall intensity and the runoff peak flow. UU, CEN, and DU represent upstream urbanization, centralized urbanization, and downstream urbanization.

To compare the peak flow response of study sites, rainfall total depth (cm) versus runoff peak flows (mm/hr) were plotted for the western and northern US study sites (Figure 21).

Black and red symbols in Figure 21 represent long precipitation events (storm duration> 6 hours) and flash floods (storm duration ≤ 6 hours), respectively. For the northern cities (Chicago, NYC, and Baltimore) where there were more study sites, triangle and circle symbols were used to represent small and large study sites, respectively (Figures 21a, 21b, and 21c). For Portland, San Francisco, and Los Angeles, only triangle symbols were used (Figures 21d, 21e, and 21f).

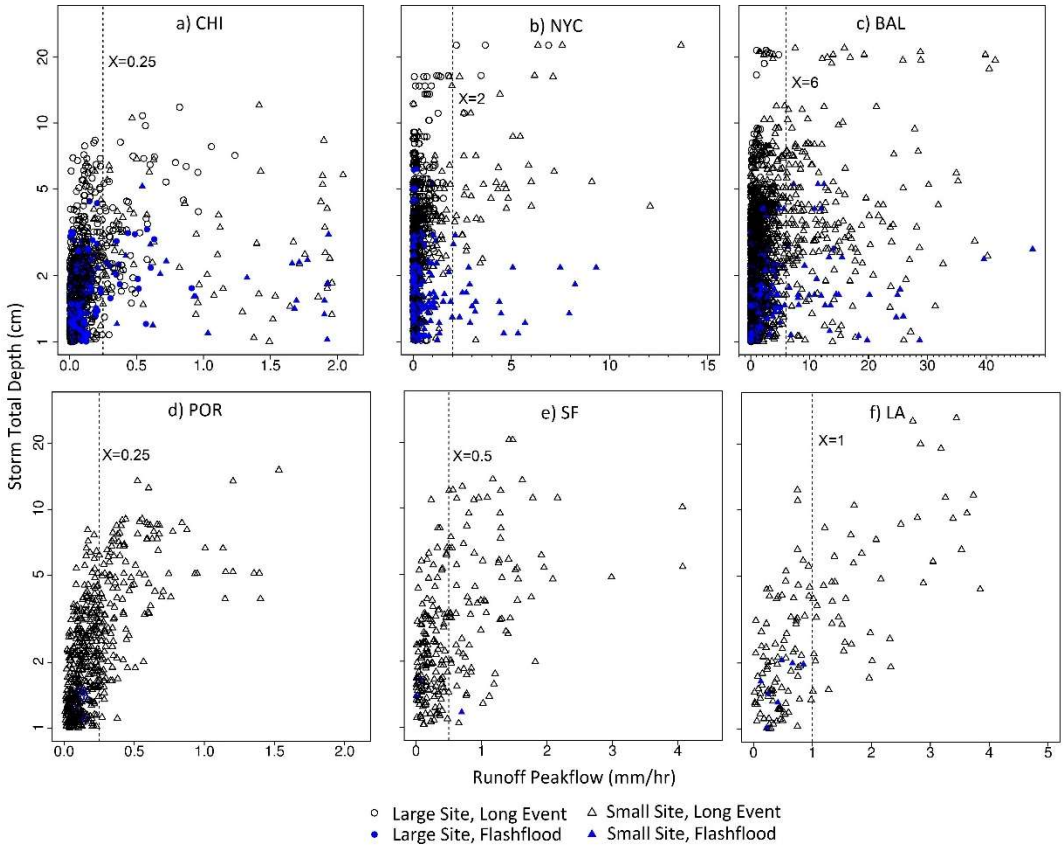

Figure 21. Scatter plots of runoff peak flows (mm/hr) versus storm depth (cm) for different cities. Black and blue symbols represent long precipitation events (duration > 6 hours) and flashfloods (duration ≤ 6 hours), respectively. Triangle and circle symbols were used to represent small and large study sites, respectively. For Portland, only triangle was used as there was a few study sites. The dashed lines indicate the 0.9

quantile of event peak flow depth which is rounded to the nearest quarter and is presented as an arbitrary threshold to flooding (X).

Comparison of scatter plots of precipitation depth versus peak flow suggested a difference between the hydrologic responses of northern and western US study sites (Figure 21). The 0.9 quantile was rounded to the nearest quarter and used to define an arbitrary flooding threshold (X) for different cities. The X values ranged from 0.25 (Chicago, IL) to 6 mm/hr (Baltimore, MD). For northern cities, small catchments (A< 55, 40, and 50 km^2 for Chicago, NYC, and Baltimore, respectively) were flooded by both flash floods and extended rainfall, but large catchments were flooded infrequently (Figures 21a-c). In eastern sites, flooding in large catchments resulted from precipitation events with duration greater than 24 hours and non-zero antecedent soil moisture values. In contrast, the western US study sites (Figures 21d-f) were often flooded during long precipitation events and were less responsive to flash flood events. This different behavior in the western US catchments likely reflects effect of the drier climate, longer time between storm events, and low antecedent soil moisture contents. In this case, a large fraction of flash flood precipitation is captured by the soil as initial abstraction. On the other hand, high runoff response of the western US catchments in Los Angeles and San Francisco during long precipitation events may be attributed to increased antecedent soil moisture contents and occasioned soil saturation. It is noteworthy that many natural settings in arid western settings are prone to extreme flash flooding.

4.2.2. Discussion

This study presents a new geometric index (RNICO), which is simply calculated from land cover and catchment geometry, as an approach to represent the hydrologic behavior of small peri-urban catchments. The results of analysis from several cities demonstrate that RNICO can be an effective tool for classifying the outcome of different urban development patterns on urban flooding behavior. The RNICO index allows all urban developments to be grouped into three main classes: UU, CEN, and DU (Figure 7). Results of applying this classification method on the NYC study sites showed the effectiveness of RNICO for representing changes in runoff peak flows and time to peak (Figures 19 and 20).

Previous studies have applied complex physical hydrology and numerical modeling approaches (Du et al., 2015; Yang et al., 2011; Yeo and Guldmann, 2006) to address the impact of development pattern on the hydrology of urban catchments. For example, a similar index has been developed by Du et al. (2015) to assess the distribution of imperviousness impact in urban catchments. A drawback of this method is that it requires Hydrologic Modeling System (HEC-HMS) model to calculate discharge before and after each hypothetical development scenario. This approach also requires additional parameter sets such as multi-temporal and multi-spectral satellite images, soil maps, and digital elevation models of the study area for HEC-HMS model calibration and validation. An advantage of the presented RNICO method is the reduced complexity compared to the traditional hydrologic modeling approaches.

A drawback of the RNICO index is an inability to account for the impact of stormwater systems and the complex hydrologic connectivity in urban catchments which can greatly increase stream flow flashiness. This limits the application of RNICO to macro-scale assessment of hydrologic behavior of low to moderately developed peri-urban catchments within a similar region. For longitudinal study of urban development in a single catchment, RNICO may fail to represent the impacts of contemporaneous changes in climate, land use/land cover, and imperviousness as longitudinal studies require detailed assessment of changes in hydraulic and hydrologic systems of the study catchment through time. For paired catchment studies, application of RNICO index may be limited to an ideal scenario in which two urban catchments with similar shape, soil properties, drainage area, imperviousness, and stormwater networks are present in one geographic location. For both longitudinal and paired studies, I suggest using physical hydrology modeling approaches.

The strength of the correlation between RNICO and runoff peak flows for several suburban catchments supports the concept that the impact of development pattern on flooding is dependent on scale and geology (Roodsari & Chandler, 2017; Yang et al., 2011). For instance, the studied catchments in NYC (Figure 17c) and Syracuse (Figure 17f) were selected at a range of scales and imperviousness with different catchment geology and physical properties. Syracuse catchments include glacial lacustrine deposits, and NYC sites are mostly metamorphosed sediments. The average clay content of Syracuse catchment soils (20%) is double that of NYC catchments (10%). In addition, the average amount of sand in NYC catchment soil (50%) is much greater than for Syracuse (30%). This difference emphasizes the much greater runoff production potential for

undeveloped land in Syracuse catchments compared to NYC. However, the observed runoff discharge at Syracuse sites was typically about one tenth of those at NYC sites (Figure 17a). One reason for the smaller observed peak flows for sites near Syracuse is the great channel modification in some relatively undeveloped corridors, which reduces the magnitude of peak flows. Furthermore, the range of storm precipitation depths over the study period was much less for Syracuse (3 mm to 7.6 cm) than for NYC (1 to 23 cm), which contributed to a large difference in peak flow for the two locations.

The range of runoff peak flows varied widely for all but the western study cities (Figure 17). For instance, the greatest observed runoff peak flow for NYC was 14 mm/hr. However, the greatest observed runoff peak flow for Portland, OR was less than 3 mm/hr. Detailed analysis of the study storms indicated that peak flows greater than 10 mm/hr, as observed in northern (Figure 17c) and southern (Figure 17b and 17e) cities followed by very large storms or hurricanes during the study period. For example, the maximum runoff peak flow for catchments near NYC (13.6 mm/hr) were at the Second River at Belleville, NJ, which occurred on August 28, 2011 during a tropical cyclone (Hurricane Irene). Tropical cyclones may strike Oceanic and Mediterranean climate cities in western US, but the wind force and destructive power of these storms can be greatly mitigated after landfall. The lack of destructive large storm events at the western US cities over the study period explains the smaller range of observed runoff peak flows in western cities.

Urban development pattern was a stronger predictor of RBF than percentage of imperviousness for small urban catchments (Figure 18). Traditionally, imperviousness percentage is used as a predictor of runoff peak flows and stream flow regime in urban catchments. However, the results for Portland showed a weak correlation of the percent

imperviousness with RBF (Figure 18c, 18c2). This indicates that the RNICO index can better represent the impact of urbanization on runoff peak flows in small catchments than the percent imperviousness due to the geometric analysis considerations in RNICO.

The time to peak flow for Chicago catchments was positively correlated to RNICO, but there was a great uncertainty associated with normalized time to peak within the study catchments (Figure 19). The normalized time to peak ranged from 1 to 120 minutes/km. The main source of uncertainty for time to peak flow in Chicago catchments can be due to the urban stormwater networks and artificial hydraulic pathways in these catchments. In addition, the storm direction through the catchment can increase this complexity by altering the flood travel time. Furthermore, Chicago is adjacent to a large lake and has a shallow groundwater table. This increases the complexity of hydrologic behavior of Chicago sites.

Comparison of the runoff peak flows versus precipitation total depth between western and northern US catchment indicated the marked impact of climate on hydrologic response of urban catchments (Figure 21). For northern cities, small catchments (A< 55, 40, and 50 km^2 for Chicago, NYC, and Baltimore, respectively) were flooded during both flash floods and long precipitation events, but large catchments were infrequently flooded (Figures 21a-c). In these cases, flooding in large catchments resulted from precipitation events longer than 24 hours and antecedent soil moisture content status greater than zero. In contrast, the western US study sites (e.g. Portland in Figures 21d) were often flooded during long precipitation events and flash flood events were less common. This contradictory behavior in the western US catchments is typical of drier climates and longer intervals between storm events. In this case, the runoff peak flow rate is expected

to decrease (Berthet et al., 2009; Grillakis et al., 2016). On the other hand, high runoff response of the western US catchments during long precipitation events may be driven by greater antecedent soil moisture content (McMillan et al., 2018; Zehe & Blöschl, 2004).

I found that the threshold of imperviousness used in previous literature (Schueler et al., 2009; Schueler, 1994; Valtanen et al., 2014) to distinguish between the impacted and less affected urban stream-flows may be scale dependent. Although stream stability threshold data are limited, there is some evidence that the impact of imperviousness on urban streams is shown for fractional impervious areas of 0.05‑0.1. In this study, large catchments such as 6, 14, and 15 in NYC with fractional impervious area from 0.15 to 0.26 were hydrologically stable, but small ($A < 40$ km^2) NYC catchments with fractional impervious area of greater than 0.12 showed greater peak flows and flashiness.

Correlation analysis among average runoff peak flows and stream R-B flashiness index with several physical and environmental factors (Falcone, 2011) indicated the great impact of urbanization on runoff peak flow and stream flow flashiness (Figure 22 and Table 3). Although several parameters showed strong correlation to runoff peak flows, only the parameters that make physical sense such as stream sinuosity, average sand content, artificial pathways, and land development were identified as significant parameters (Figure 8). Average soil sand content and land development can directly impact the runoff volume and peak flows by altering the infiltration rates. Stream sinuosity and artificial pathways can indirectly affect the runoff peak flow by changing the flood travel time. A complementary multilinear statistical analysis and corresponding diagnostic tests were also performed for the six cities in Figure 22, and in Appendix Q.

Results indicate that only urbanization parameters (IDs 11, 12, and 13) are strong predictors of the runoff peak flow.

The greatest influence of urban development pattern (RNICO) on peak flow magnitudes was observed in NYC, Los Angeles, and Chicago (Figure 22). For other study cities, RNICO was positively correlated to the runoff peak flows, but it was not the strongest predictor of runoff peak flows.

Correlation analysis results also indicated that catchment physical properties such as soil may be similarly important as land development (Table 4 and Figure 22). For example, the average soil sand content was negatively correlated with runoff peak flows in NYC (Figure 22). A similar analysis for San Francisco indicated the strong impact of soil permeability on runoff peak flows, in spite relatively high influence of RNICO and urbanization (Figure 22). Surprisingly, the stream sinuosity was the strongest predictor of runoff peak flows in Baltimore. For Portland, there were several parameters with higher Pearson correlation coefficient values and runoff peak flows than RNICO, but the nature of those correlations did not physically make sense.

Table 7. Environmental and physical parameters used in statistical analysis for six cities presented in Figure 22 (Falcone, 2011).

ID	Definition	Category
a	shape (compactness)	Morphology
b	stream density (km/km^2)	Hydraulics
c	stream sinuosity	
d	lakes/ponds (%)	
e	dam density (# of dams/100km^2)	
f	mean catchment slope (%)	Topography
g	mean catchment aspect (degrees)	
h	average permeability (in/hr)	Soil
i	average clay content (%)	
j	average sand content (%)	
k	artificial pathways (%)	Urbanization
l	land development (%)	
m	RNICO	

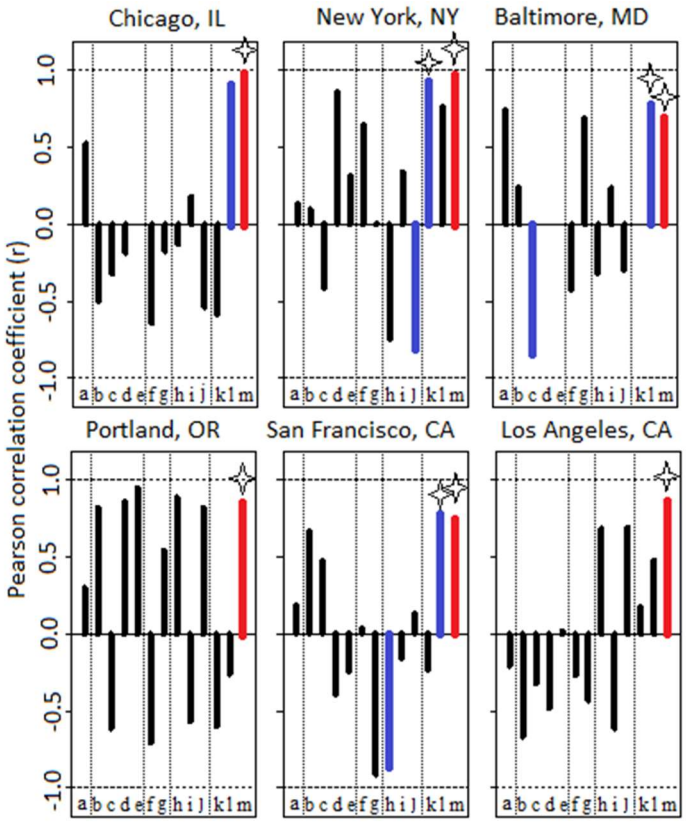

Figure 22. Pearson correlation coefficient (r) for average peak flow and several parameters including shape (a), stream density (b), stream sinuosity (c), lakes (d), dam density (e), mean catchment slope (f), mean catchment aspect (g), average permeability (h), average clay content (i), average sand content (j), artificial pathways (k), land development (l), RNICO (m) (Table 7). RNICO (red) and other parameters strongly correlated to runoff peak flow (blue) highlighted correlations make physical sense. These parameters can either directly impact the runoff peak flow by altering the infiltration rates (j and l) or indirectly affect the runoff peak flow and volume by changing the flood travel time (c and k). Statistically significant parameters are shown with star labels. The horizontal dashed line indicates the maximum (1) and minimum (-1) possible r values. The vertical dashed lines separate different categories of parameters explained in Table 7. For instance, parameters f and g are separated from other parameters as they are both

associated with the catchment topography. Stepwise regression analysis with diagnostic test results are presented in Appendix L.

4.3. Seasonal hydrologic performance of LID

4.3.1. Results and Discussion

Runoff reduction performance for bioretention systems decreased significantly between warm and cold seasons (Figure 23). However, this change was highly variable within different study locations, and the impact of season change on the total stormwater volume reduction was often marginal. The decrease in the runoff volume reduction performance, as reported in previous studies, can be explained by the decrease in plant cover and associated evapotranspiration during cold seasons. It should be noted that the impact of seasonal change in the performance of bioretention cells can be negligible if the sizing and capture volume of these systems satisfy the design requirements for both warm and cold seasons.

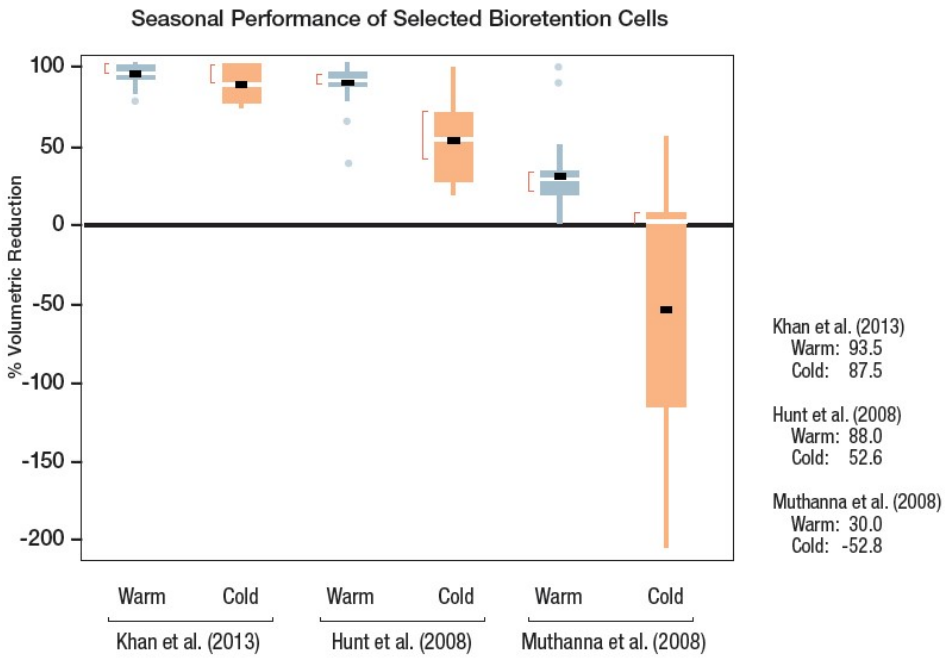

Figure 23. Summary of volumetric stormwater capture, loss and leakage during warm and cold seasons for bioretention cells based on studies in the literature, summarized as percent volume reduction of inflowing water. The values shown are of performance by individual events (Driscoll et al., 2015).

Among the available literature on seasonal performance of bioretention systems, Khan et al. (2013) reported the smallest decrease in hydrologic performance of these systems, which may be due to the overdesigning their site relative to their drainage area or an efficient site maintenance during the cold season. The overall stormwater retention volume of the sites presented in the other two studies were greatly decreasing from warm to cold season. The negative performance values for these two studies (Figure 23) is likely an outcome of poor winter maintenance of the parking areas in the study sites. Storage of snow piles on bioretention cells appears to decrease winter runoff reduction of these infrastructures due to the formation of compacted snow, ice and soil frost, which significantly decrease infiltration.

Furthermore, I found that the hydrologic performance of green roofs is more likely controlled by the event depth than the season (Carson et al., 2013; Schroll et al., 2011; Figure 24). Nevertheless, there was a small decrease in precipitation retention performance of green roofs from warm to cold season. This is likely a result of different evapotranspiration rates, ice formation in the growth media, and melt of accumulated snow and ice during rain-on-snow events.

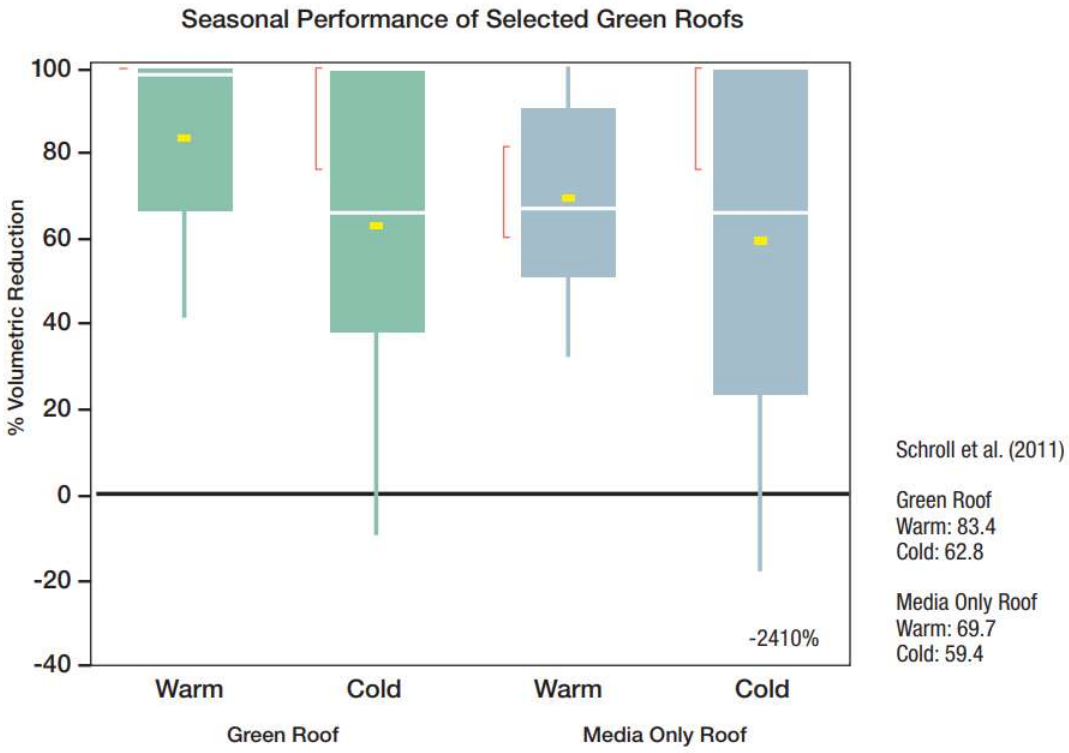

Figure 24. Representative summary of volumetric stormwater capture, loss and leakage during the warm and cold season from Schroll et al. (2011), summarized as percent volume reduction of rainfall. Data displays performance by individual events (Driscoll et al., 2015).

4.4. Effect of storm movement direction on the performance of ANFIS

4.4.1. Results and Discussion

The results indicated that the impact of storm movement direction on the performance of ANFIS model in Ley Creek catchment is marginal. Although, standard deviation of errors and RMSE of the three modeling scenarios were slightly different during the training period, all performance parameters were similar within the three study scenarios (Figure 25). Marginal impact of the storm movement direction on ANFIS model performance can be due to the relatively small drainage area of the catchment (78 km^2) and short time of concentration (2-6 hours) compared to the duration of storm movement through the catchment. I should note this impact could be more important for large catchments with greater time of concentration. In this case, water level or discharge data at the upstream stations (headwater streams) could be valuable for predicting the flood level at the catchment outlet.

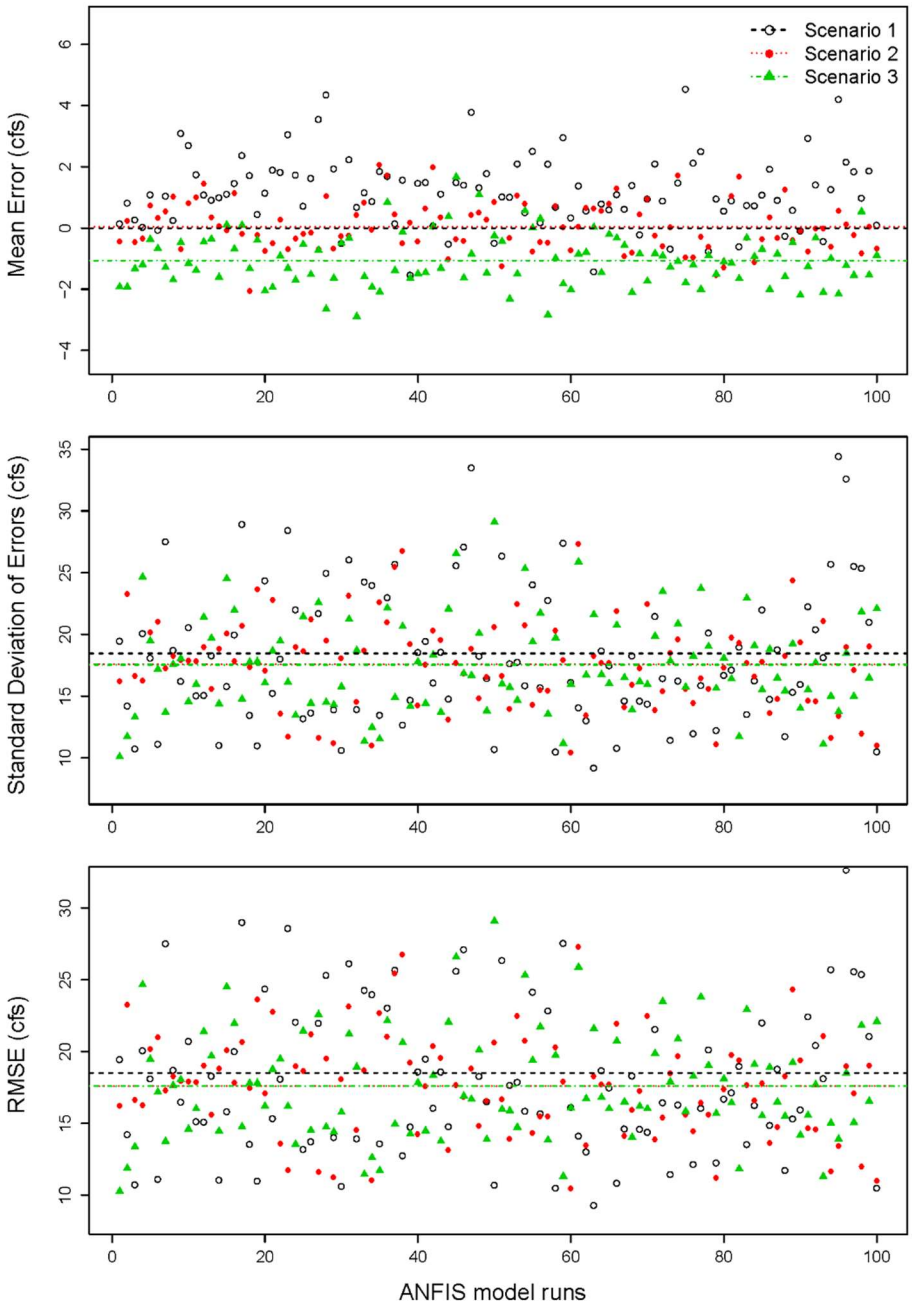

Figure 25. ANFIS model error indices for predicting the outflow discharge at Ley Creek catchment for the three wind direction scenarios show low variability within a similarly narrow range for the three storm direction scenarios. Three independent modeling scenarios include: 1) training data includes 20 upstream-downstream (UD) storm events, 2) training data includes 10 DU (downstream-upstream) +10 UD storms, and 3) training data include 20 DU datasets. For all three scenarios, test periods included 5 DU+5 UD.

For each modeling scenario, 100 independent combinations of storms were selected from the observed storms using the Sample function (in R programming language without replacement).

4.5. Real-time deterministic flood forecasting

4.5.1. Results and Discussion

Visual inspection of simulated versus observed flood hydrographs showed that all tested models (ANFIS, SAC-SMA, and SWMM) perform reasonably well during both calibration and validation periods (Figure 26). However, SWMM overestimated large peak flows during the calibration period relative to the other two models.

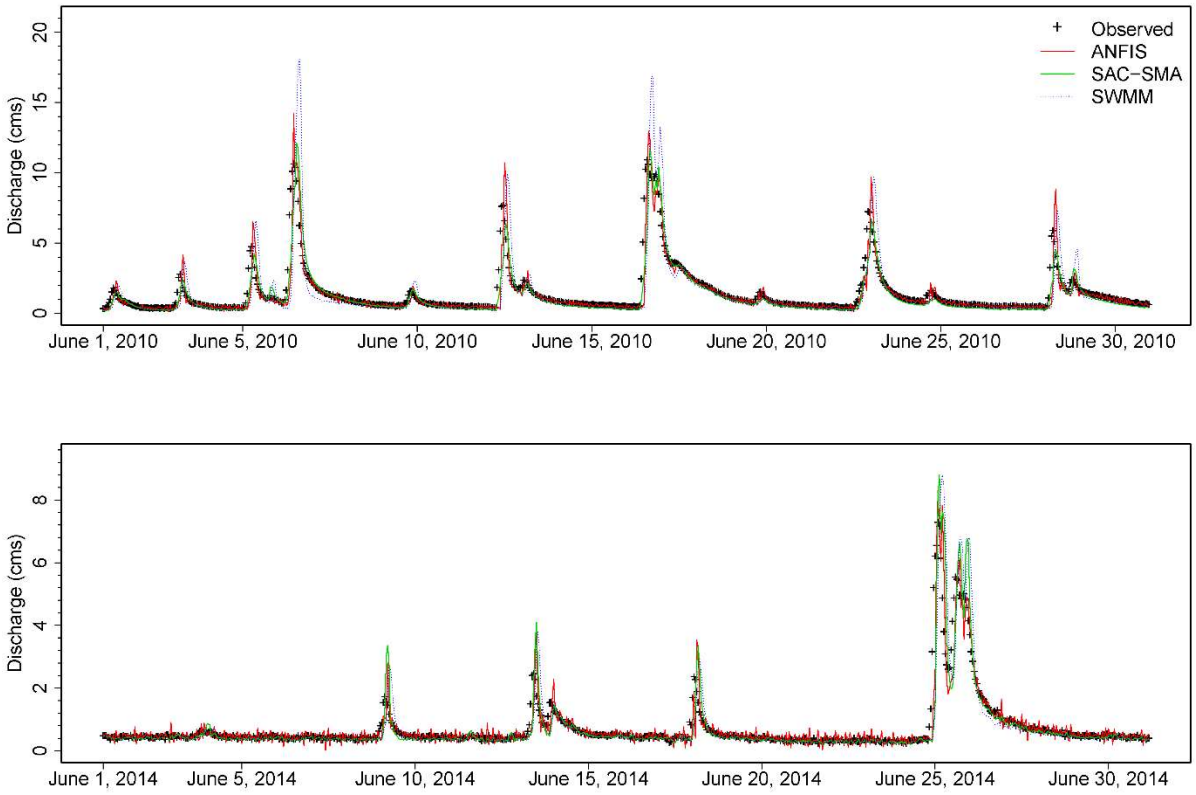

Figure 26. Simulated versus observed flood hydrographs during calibration (top) and validation (bottom) periods for three-hour advance forecasts from 1 June 2014 to 1 July 2014. Values for SAC-SMA and SWMM are the average of three calibration strategies.

Comparison analysis between the calculated statistical parameters for different calibrated models showed that all models perform better during high and moderate flow conditions compared to low flow conditions (Figures 27). NSE of high and moderate flow conditions ranged from 0.1 to 1.0, but for low flow conditions, NSE varied between -0.1 to 0.55 during calibration and -0.6 to 0.05 during validation period. Poor low flow representation in SWMM and ANFIS could be due to the absence of a groundwater

modeling component. SAC-SMA has a basic groundwater component that requires modifications for accurate low flow simulation (Matonse and Kroll, 2013).

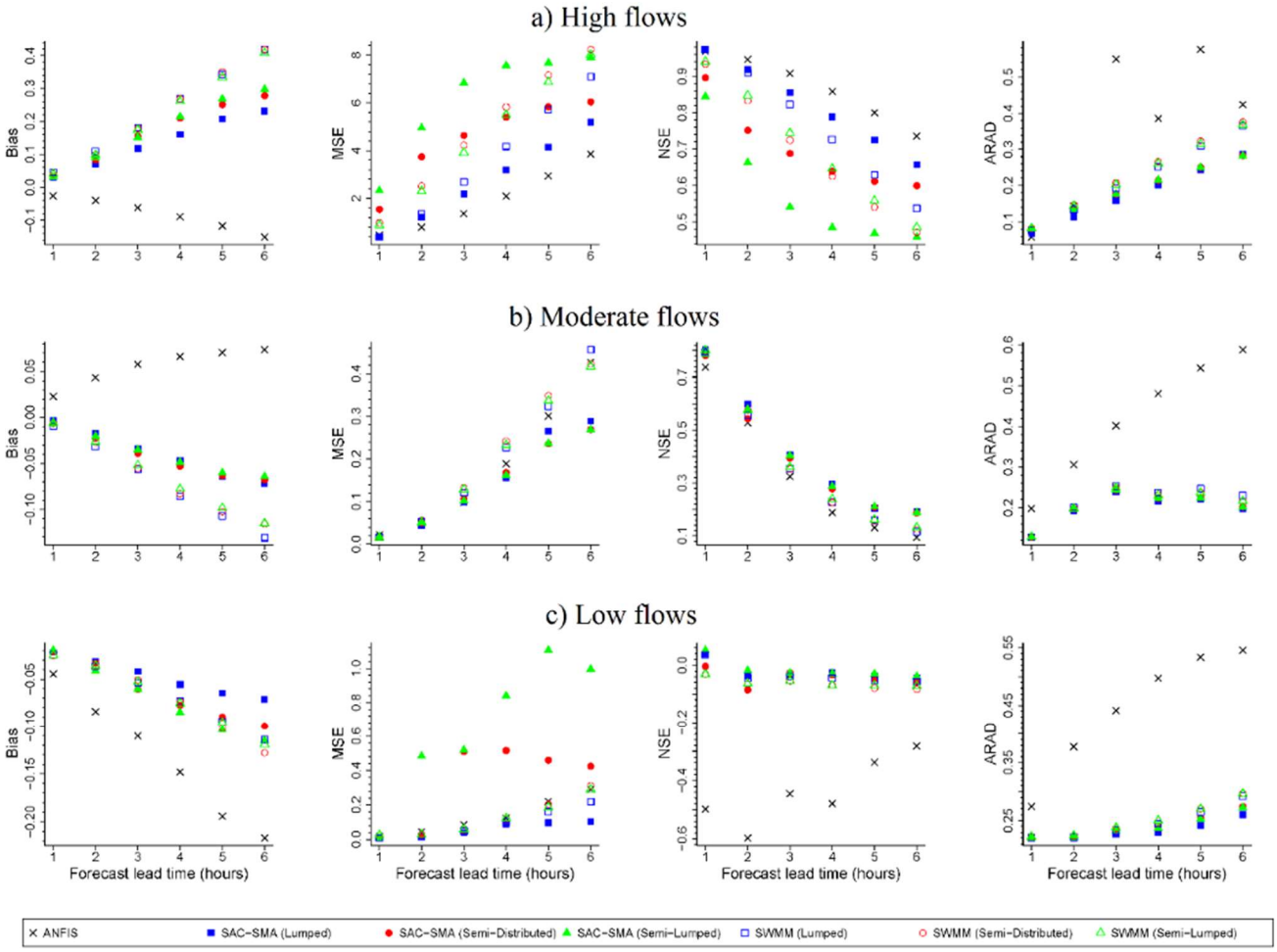

Figure 27. Performance analysis results for SAC-SMA, SWMM, and ANFIS for the validation period (water years 2014 to 2015). All performance parameters were calculated for lead times of one to six hours for three independent flow conditions: low flows, moderate flows, and high flows. Low flows were defined as periods in which observed discharge values were smaller than the first quartile (Q25%), moderate flows as the observed discharge values of between the first and third quartiles (Q75%), and high flows as observed discharge values of larger than the third quartile.

ANFIS was the least accurate model during the validation period, likely due to the large ARAD values (Figure 27). For moderate and high flow conditions in this period, MSE and NSE values of ANFIS varied in a relatively similar range with most physical hydrology models, but ARAD range for this model (0.1- 0.6) was much larger than that for physical hydrology models (0-0.28). The only condition in the validation period when ANFIS performed as well as physical hydrology models was for high flow condition forecast with lead times of less than three hours (Figure 27a). ANFIS has been little used for flood forecasting in small urban catchments, possibly due to the difficulty of modeling the short time of concentration and quick discharge variations in the rising limb of the flood hydrograph of small urban catchments with ANFIS. However, in contrast to our finding, results of applying ANFIS for large river basins have shown relatively strong performance of this model for flood forecasting with lead times of up to six hours (Campolo et al., 2003; Nayak et al., 2005).

4.6. Real-time ensemble flood forecasting

4.6.1. Results

4.6.1.1. Calibration/Validation

Across all catchments, both 3-hourly ANFIS and SAC-SMA models performed reasonably well in the calibration (2004-2011) and validation (2011-2014) periods. *NSE* values ranged from 0.72 to 0.87 (Table 8). *RelBIAS* values, SAC-SMA calibration datasets, and calibration hydrographs are presented for individual watersheds in Supplementary Material/Appendix (Table A1, Table A2, and Figure A1). Values presented in Table 8 represent average performance across the eleven forecast ensemble members for all study sites. Calibration and validation performance indices for ANFIS

decreased with forecast lead time for both events. This was consistent with the observed decrease in the statistical correlation between $Q_{t\text{-}lead\ time}$ and Q_t. Similarly, relative bias *(RelBIAS)* of the ANFIS model over the calibration period for Hurricane Irene increased from 0.08 to 0.15 when forecast lead time increased from three to 24 hours. For SAC-SMA, the most and least impervious study sites (sites 7 and 1) had the smallest and greatest RelBIAS values, respectively. However, I did not find any trends between performance indices (including RelBIAS) and either catchment imperviousness or drainage area. For ANFIS, performance indices varied within the sites and with lead time. For example, sites 3 and 8 for the 3-hour lead time, and sites 4 and 1 for the 24-hour lead time, had the smallest and greatest RelBIAS values for the calibration period, respectively.

Table 8. Average performance indices for the nine study sites near NYC over the calibration (1 October 2004 to 27 August 2011 for Hurricane Irene and 1 October 2004 to 23 September 2011 for the small event) and validation (27 August 2011 to 27 August 2014 for Hurricane Irene and 23 September 2011 to 23 September 2014 for the small event) periods.

Storm Event	Index	SAC-SMA		ANFIS							
		Calibration	Validation	Calibration				Validation			
				3 hrs	6 hrs	9 hrs	24 hrs	3 hrs	6 hrs	9 hrs	24 hrs
Hurricane Irene (27-29 Aug, 2011)	NSE	0.83	0.81	0.87	0.84	0.79	0.73	0.86	0.81	0.75	0.72
	PBIAS (%)	6.13	5.19	5.67	6.50	8.23	10.54	4.35	6.56	8.29	11.89
	RelBIAS	0.11	0.08	0.08	0.11	0.13	0.15	0.09	0.11	0.12	0.14
	RelMSE	0.15	0.11	0.19	0.22	0.27	0.34	0.18	0.25	0.37	0.45
	ARAD	0.14	0.13	0.17	0.23	0.29	0.36	0.19	0.25	0.39	0.48
Small event (23-25 Sep, 2011)	NSE	0.85	0.84	0.86	0.83	0.81	0.76	0.84	0.81	0.77	0.73
	PBIAS (%)	6.21	6.56	4.32	5.76	6.39	8.31	7.12	7.87	8.24	9.16
	RelBIAS	0.09	0.08	0.07	0.09	0.10	0.12	0.08	0.09	0.11	0.12
	RelMSE	0.18	0.19	0.15	0.19	0.27	0.39	0.16	0.22	0.35	0.46
	ARAD	0.12	0.15	0.13	0.26	0.38	0.45	0.15	0.19	0.24	0.36

4.6.1.2. Performance during extreme events

For simulated real-time flood forecasting, agreement between the observed and simulated hydrographs varied most between models for forecasts of Hurricane Irene; this makes sense given this extremely rare flood event. Forecasts are included for both ANFIS and SAC-SMA for Hurricane Irene (Figure 28a) and a small storm event (Figure 28b) for a single watershed (site 7). Flood forecast results for site 7 are shown in Figure 28 and hydrograph simulation patterns were similar across the other study sites. Note the difference in discharge magnitudes of these two storm events in Figure 28. Observed and ensemble forecasted flood hydrographs for the smallest and largest study sites (sites 1 and 9) and minimum, average, and maximum *RelBIAS* among the eleven forecasted ensemble members for individual catchments are presented in Supplementary Material/Appendix (Figure A2, Tables A2 and A3).

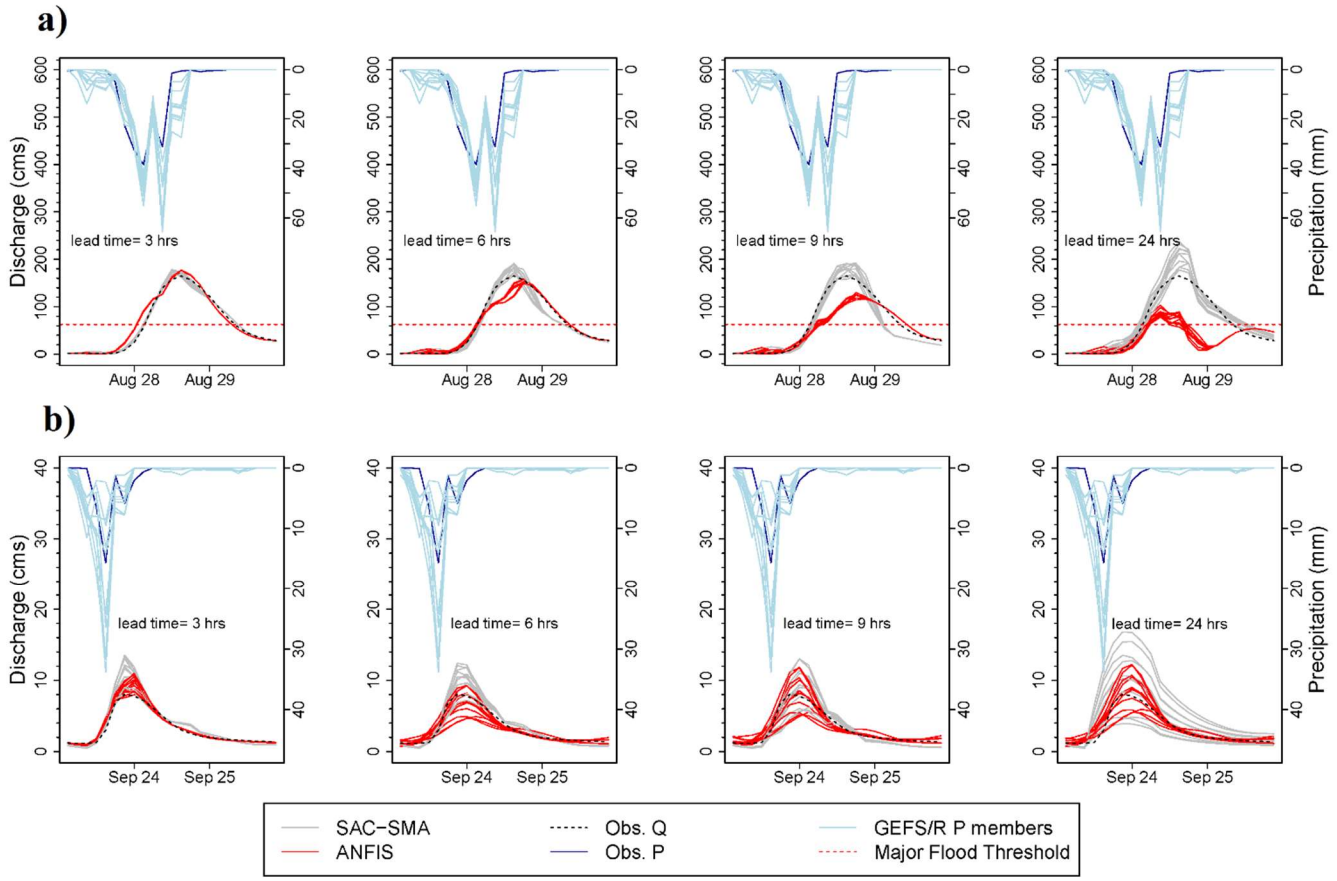

Figure 28. Observed and ensemble forecasted flood hydrographs of site 7 for Hurricane Irene (a) and the small storm event that occurred a few weeks after Hurricane Irene (b). Lead times for forecasting increase from left to right.

ANFIS-simulated real-time forecasted hydrographs for Hurricane Irene was best for the shortest lead times, and greatly decreased as the lead times approached 24 hours (Figure 29a). ANFIS forecast performance of Hurricane Irene declined in terms of average NSE (from 0.85 to 0.4) for increasing forecast lead times from three to 24 hours (Figure 32a). ANFIS largely under-predicted peak flow for Hurricane Irene for forecast lead times of 24 hours (Figure 29a). Accordingly, average *RelBIAS* values for ANFIS for 24-hour lead

time ranged from -0.45 to -1.1 (Table A3). However, when applied to simulate the flood hydrograph for a small storm event across three to 24-hour lead times, ANFIS performed reasonably well (Figure 29b). Average *RelBIAS* values for ANFIS for the small event ranged from -0.16 to 0.41 (Table A3). Although the ANFIS model failed to match the peak discharge for Hurricane Irene at the longest lead times (Figure 29a), the model performed reasonably well for the smaller storm event, bracketing streamflow observations.

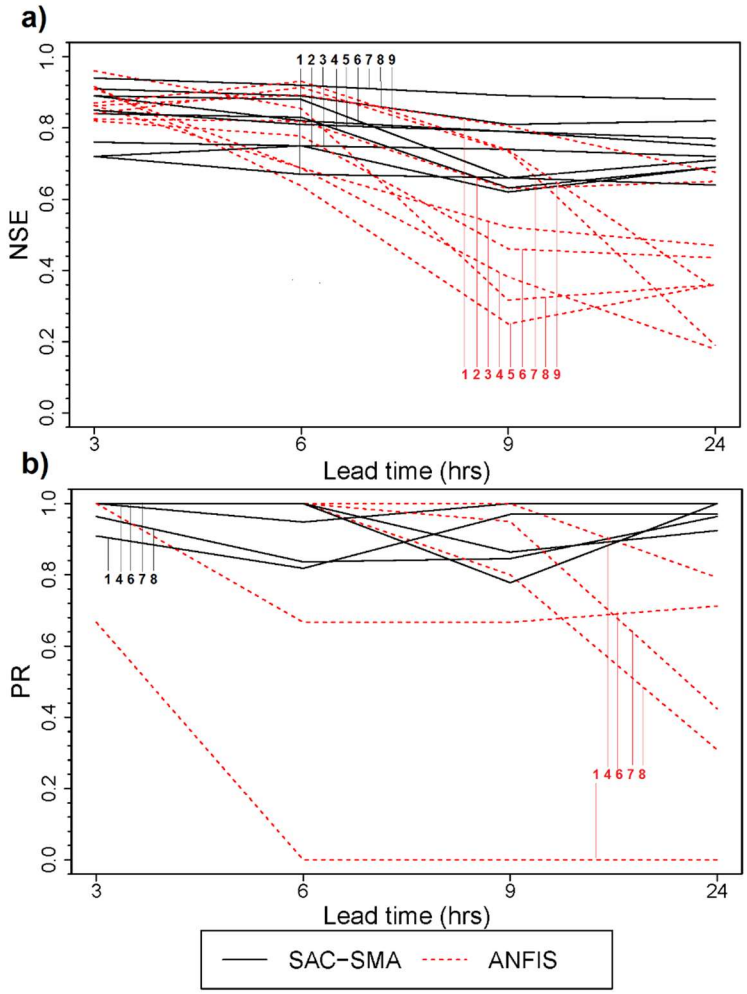

Figure 29. Model errors shown as (a) NSE coefficient and (b) Prediction Reliability (PR) index for SAC-SMA and ANFIS across the nine study catchments applied to simulate Hurricane Irene flood hydrographs. Numbers on each graph represents study site IDs (column 1 in Table 5) ordered by increasing drainage area. The PR index was calculated for the five study catchments for which the NOAA major flood threshold was exceeded (Table 5).

SAC-SMA performed well when simulating event hydrographs for both storms. Average *RelBIAS* values ranged from -0.2 to 0.48 (Table A4). Also, *NSE* values for Hurricane Irene ranged from 0.65 to 0.9 (Figure 30a). Figure 29 shows that SAC-SMA forecasts for

ensemble members tended to bracket streamflow observations regardless of lead time. However, at the longest lead times, SAC-SMA tended to over-predict peak discharge for both Hurricane Irene and the smaller event. This over-prediction decreased for shorter lead times.

For five catchments where NOAA major flood thresholds were reported (Table 5), the Prediction Reliability (*PR*) for SAC-SMA for Hurricane Irene did not change substantially with lead time, while *PR* for ANFIS decreased substantially with lead time for most sites (Figure 29b). For ANFIS, catchments 1 and 4 encompass the range of *PR* values. Note that *NSE* value of ANFIS for catchment 1 was the greatest among all study catchments. In this case, *PR* may better represent performance than *NSE*, as it can identify both under-prediction (in this case) and over-prediction of a flood hydrograph, important information for emergency management. I also present results of correlation analysis between *PR* and other indices used in this study (Table A4). The small Pearson correlation coefficient values between *PR* and other indices could indicate the independent nature of this index from other indices.

Finally, I sought to test whether catchment size or forecast lead time had greater impact on model performance (Figure 29) especially with respect to *NSE*. Both SAC-SMA and ANFIS models had strong *NSE* values for the lead times of 3 and 6 hours, but the *NSE* of ANFIS dramatically decreased over lead times between 9 to 24 hours. For example, *NSE* values for ANFIS for catchment 5 increased from 0.28 to 0.36 when forecast lead time increased from 9 to 24 hours, which was unexpected (Figure 29a). Similarly, *NSE* value for SAC-SMA for catchment 3 increased slightly between 9 to 24 hours lead time (Figure 29a).

Performance indices for both models were insensitive to catchment size and imperviousness but varied with forecast lead time. Figure 30 compares results for the average of 11 ensemble members versus catchment drainage areas for different forecast lead times with respect to *RelBIAS*, *RelMSE*, and *ARAD*. Similarly, performance results versus catchment imperviousness are shown in Supplementary Material/Appendix (Figures A4 and A5). While performance indices for both models varied in a relatively similar narrow range for forecast lead times of three to nine hours, I found performance diverged between models as lead times approached 24 hours. In particular, while performance indicators remained high for SAC-SMA, performance declined for ANFIS simulations with 24-hour lead times as compared to three, 6, or 9 hour lead times regardless of catchment size. For example, *ARAD* values of both model simulations of Hurricane Irene flood hydrographs ranged from 0 to 0.45 for lead times of three to nine hours, but increased to 0.7 for ANFIS when forecasted lead times reached 24 hours. The only observed influence of watershed size was with respect to SAC-SMA forecasts for longer lead times. I note that for lead times of both 9 hours and 24 hours, SAC-SMA performance tended to improve with watershed size (closer to 0) for *ARAD*, whereas this was not true for any other performance index. I found comparable results for ANFIS and SAC-SMA for short lead times for the smaller event. However, for the longest lead times, ANFIS outperformed SAC-SMA, with slightly lower values of performance indices regardless of watershed size.

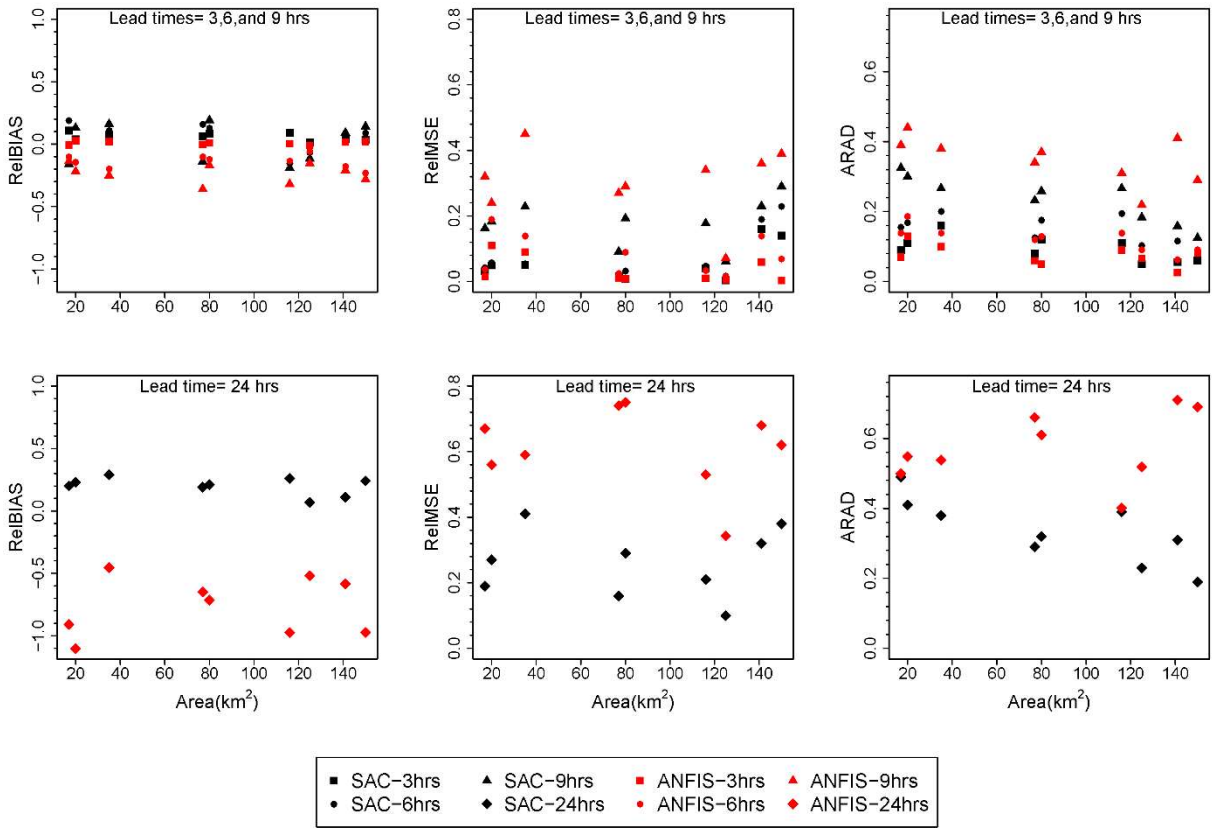

Figure 30. Performance indices for SAC-SMA and ANFIS averaged across the eleven ensemble members with varied lead times plotted against catchment drainage area. Results in this figure represent the Hurricane Irene flood hydrograph simulation. Plots for short lead times (3, 6, and 9 hours) are separated from the 24 hours. As can be seen, model performance indices for both models are insensitive to catchment size and imperviousness but vary with forecast lead time.

4.6.2. Discussion

4.6.2.1. Model performance and uncertainty outside of extreme event forecasts

Both SAC-SMA and ANFIS models performed reasonably well during calibration and validation periods with *NSE* values greater than 0.7. Deterministic flood forecasting applications of the SAC-SMA model in previous studies have shown both similar and

different performance results over a wide range of catchment scales and climate conditions when compared to my ensemble-based approach findings. For example, Ajami et al. (2004) and Reed et al. (2007) used a spatially distributed SAC-SMA model for streamflow forecasting in large US river basins. They found *NSE* and bias values similar to my findings (Table 7). Others have found larger estimated biases than I observed (e.g., Khakbaz et al. (2009)). Taken together, these studies indicate that the model performance in this study is comparable to other study applications of the SAC-SMA model in deterministic streamflow prediction.

To enable a real-world simulation of model forecasting, I do not investigate or compare the relative impacts of sources of uncertainty in this study, calibrating SAC-SMA following procedures used by the NWS. However, I recognize that different sources of uncertainty with respect to model parameters and input data ultimately shape results with respect to both models. It is noteworthy that the greater number of input parameters for SAC-SMA (17 parameters) as compared to ANFIS (3 parameters) increases the number of uncertainty sources and the risk of equifinality (Beven, 2006), an initial motivating factor for comparing these two models. For the ANFIS model, the main sources of uncertainty are intrinsic to: the measured precipitation and discharge values used for the model calibration; uncertainty due to the length of calibration period and the presence of events similar to the validation storm event; and the uncertainties of GEFS/R precipitation ensembles for the validation period, which was previously discussed as further sources of discrepancy between ANFIS and SAC-SMA performance. During the discussion of real-time forecasting, I posit that the most important sources of uncertainty in streamflow forecasts for both models are associated with the uncertainties of GEFS/R

precipitation ensembles. I note that this is in agreement with recent studies, which have also found high sensitivity of real-time flood forecasting models to the predicted precipitation inputs (Amengual et al., 2015; Liechti et al., 2013; Marty et al., 2013; Saleh et al., 2016).

4.6.2.2. How does model performance vary with lead time?

The presented study evaluates the performance of a lumped physical hydrology model (SAC-SMA) and an AI model (ANFIS) through a real-time ensemble flood forecasting approach. My results suggest that the forecast performance of both models decreases with forecast lead time, which is in agreement with results of previous findings (Campolo et al., 2003; Nayak et al., 2005; Saleh et al., 2016). For short lead times (three and six hours), precipitation input data updates, as I treated forecasts as a real-time exercise, likely resulted in smaller errors and uncertainties with respect to GEFS/R precipitation data inputs. In contrast, forecasts corresponding to longer lead times had poorer performance, likely given the relatively short time of concentration in the study catchments (1 hour to 6 hours). I note that accurate flood forecasting close to the event can be still valuable for emergency evacuation plans in small urban catchments, which require less time compared to large river basins.

Surprisingly, the predictive ability of models increased slightly between lead times of 9 to 24 hours. These unexpected increases in the performance of models for such lead times may be related to the underlying processes of the updating system or uncertainties of the GEFS/R precipitation inputs for 24-hour lead time due to variability in rainfall predictions. Also for this range of lead times, SAC-SMA generally over-estimated peak flow magnitudes as the GEFS/R precipitation data for both Hurricane Irene and the

smaller precipitation event were slightly greater than the observed precipitation amounts (Figure 28). Note that this over-prediction of peak flow magnitude is not necessarily detrimental, as it still correctly reports the major flood condition status in the catchment and may be similarly useful for emergency management.

4.6.2.3. Comparing ANFIS to SAC-SMA for extreme event forecasts

While forecast performance for ANFIS and SAC-SMA was similar for shorter lead times, performance diverged as lead times increased to 9 and 24 hours (Figure 30). At lead times of 24 hours, SAC-SMA outperformed ANFIS with respect to all performance indices. ANFIS under-estimated peak flow magnitude of Hurricane Irene for lead times greater than three hours. In addition, comparison of the *PR* index for the SAC-SMA and ANFIS models for Hurricane Irene indicated that SAC-SMA was more reliable than ANFIS for predicting the major flood condition and emergency management at the nine study sites (Figure 29b). For the five sites with reported NOAA major flood thresholds, SAC-SMA had a high *PR* coefficient for all lead times, while the *PR* index for ANFIS dramatically decreased with lead time. Thus, I expect ANFIS is most reliable for flood forecasting with short lead times (Figure 30).

An important consideration related to the poor performance of ANFIS for Hurricane Irene likely the dearth of very large storm events or hurricanes in the training period (2004-2011). Due to the learning nature of the ANFIS model, these types of models can only provide accurate predictions if the training period includes storms of magnitude equal to or greater than storms in the validation period. Unfortunately, continuous streamflow discharge data for the study sites were only available for a limited period (2004-2011) during which no other storms as large as Hurricane Irene occurred, and

represents a real-world scenario where data in small catchments may be limited. This also highlights the importance of ongoing streamflow discharge monitoring in small urban catchments, especially for extreme events, for more accurate future flood forecasting.

Poor performance of ANFIS for long lead times was likely also due to weak statistical correlations between the antecedent discharge ($Q_{t\text{-lead time}}$) and the observed discharge at each time step (Q_t) for the relatively short times of concentration in the study catchments (1 hour to 6 hrs). I infer that antecedent discharge is not an effective input parameter for ANFIS for lead times greater than three hours. In contrast to my finding, previous studies have found good predictability performance of AI models for large river basins with long times of concentration (Campolo et al., 2003; Khac-Tien Nguyen and Hock-Chye Chua, 2012; Nayak et al., 2005; Rezaeianzadeh et al., 2014). As there has been very limited focus on applying data-driven models for real-time flood forecasting in relatively small urban catchments in the previous literature, this study is one of the first to show potential tradeoffs in model frameworks for real-time flood forecasting.

I note that forecast performance was similar for ANFIS and SAC-SMA for the smaller storm (Figure A3). In this case, I found ANFIS outperformed SAC-SMA for long lead times. This suggests that both models can be reliable options for real-time flood forecasting in small urban catchments for predicting small storm events.

The presented results for Hurricane Irene suggest that the lumped SAC-SMA model in this study performs as well as a semi-distributed HEC-HMS model which was recently applied for real-time ensemble forecasting of Hurricane Irene in the Hudson River basin (Saleh et al., 2016). For example, Saleh et al. (2016) reported *NSE* values greater than

0.75 *PBIAS* less than 10% for most of their study catchments in the Hudson River basin, similar to performance in my study. Note that Saleh et al. (2016) used the 21 GEFS/R members that were briefly accessible from the NOAA website. This study applied only the 11 GEFS/R members that are currently available. In addition, Saleh et al. (2016) studied relatively large catchments with drainage areas ranging from 141 km^2 to 979 km^2 and forecast lead times of 24 to 72 hours, whereas this study considered smaller catchments (17 km^2 to 150 km^2) and shorter forecast lead times (three to 24 hours). Good performance of the lumped SAC-SMA model with a limited number of the GEFS/R precipitation members for daily and sub-daily flood forecasts in the relatively small catchments leads the conclusion: Lumped SAC-SMA may be a reliable option for local urban flood forecast, especially for events with forecast lead time of up to 24 hours is sufficient for implementing evacuation and rescue plans.

The model performance indices for the nine study catchments with drainage areas ranging from 17 to 150 km^2 and fractional impervious areas ranging from 12% to 25% indicate that the accuracy of both SAC-SMA and ANFIS models for ensemble flood prediction may not change significantly with catchment size and imperviousness (Figures 30, A4, and A5). I did not find a strong statistical correlation between model performance indices including *RelBIAS*, *RelMSE* and *ARAD* with catchment drainage area and fractional impervious area while these indices varied in a relatively similar range within the study sites (Figures 30, A4 and A5). However, the scope of my study has a limited climatic and spatial extent, and I caution that relationships between catchment size and imperviousness may differ for other areas. Due to the limited number of study catchments in this study, I suggest that applying SAC-SMA and ANFIS models for real-time flood

forecasting in a greater number of small suburban catchments over a wide range of fractional impervious area, drainage patterns, and climates should be made to assess the sensitivity of model performance indices on the different catchment characteristics.

5. Chapter 5 (Synthesis and conclusions)

5.1. Impacts of Urbanization on Flooding

The goal of the first phase of my dissertation studies was to understand the seasonal changes in hydrologic behavior of peri-urban catchments in Northern climates. For this, I monitored five peri-urban catchments in proximity of Syracuse, NY with imperviousness ranging from 11 to 48%. The least urbanized site (LOW1) is dominated by wetlands and other four study catchments are moderately urbanized. This gave me an opportunity to compare the peak flow response of natural and urban catchments. In addition, the most urbanized catchment (INT2) had a large stormwater pond near its outlet, which mitigates the impact of flooding. This also opened a new opportunity for me to address the effectiveness of such urban infrastructures in flood mitigation.

Seasonal peak flow results at the five subcathments of Ley Creek indicated that the impact of urbanization on flooding greatly increases for imperviousness greater than 11%. Historically, urban ecologists have used the average imperviousness as an indicator for assessing the stream ecological condition. They found an imperviousness threshold of 5-10% for stream ecological stability meaning that any imperviousness above this threshold can cause significant change in the stream ecosystem. Similarly, I investigated

the linkage between imperviousness and peak flow response of urban catchments. The results showed that increasing imperviousness to 11-12% is apparently a tipping point for peak flow response of urban catchments. I propose that an imperviousness threshold of 11% may be used as the hydrologic stream stability threshold. This threshold would indicate that the magnitude and seasonal variation of runoff peak flows in urban catchments are likely to increase for imperviousness 11%.

The stormwater pond at the outlet of INT2 greatly mitigated runoff peak flows in this catchment. Although INT2 had the greatest imperviousness (48 %), it had lesser runoff peak flows than other study catchments. Furthermore, INT2 had lesser peakflow variability between four seasons. This leads me to conclude that green stormwater infrastructures may be an effective solution for mitigating the impact of urbanization on flooding.

Comparison of mean seasonal and annual peak flows between natural (e.g. LOW1) and urbanized catchments (e.g. INT1) indicated that urbanization increases the magnitude of peak flows during all seasons. However, the percent increase in runoff peak flow magnitude greatly varies across warm and cold seasons. The greatest difference in peak flows was observed during summer (298%) and the least difference was observed during winter (6%). The greater peak flows of urban catchment compared to the natural catchment is associated with higher antecedent moisture condition in urban catchment soil. Higher summer ET rates in the natural catchment lowers the groundwater level and increase the soil storage capacity. Therefore, a great fraction of precipitation is stored in

the soil and less runoff is generated. In contrast, the difference between the runoff response of natural and urban catchments is minimized during winter due to the impact of frozen soil which behaves as an impervious area.

5.2. Impacts of Urban Development Pattern on Flooding

I addressed the impact of development pattern on flooding in peri-urban catchments in the second phase of my dissertation. I developed a new geometric index (RNICO) based on the distribution of impervious areas throughout the catchment. My results indicated that the RNICO index is a powerful tool for addressing the impact of urbanization on runoff peakflow and streamflow flashiness. Based on RNICO, all urban catchments can be classified into one of these three classes: UU, CEN, and DU. Comparison of the peak flow response of three urbanization classes in NYC sites indicated that RNICO is useful for urban development classification.

A potential application of RNICO is for sustainable urban planning in growing cities. For this purpose, the correlation between RNICO and a target variable such as runoff peak flow is assessed using the historical land cover information and data records of the target variable. Based on this correlation, an RNICO-target equation is generated. Then the future changes in the target variable due to a new development scenario is approximated using the RNICO-target equation. To perform this, the future RNICO is calculated from the hypothetical future land cover information and is used as input for the RNICO-target equation. This can help urban planners to select the most sustainable development scenario to minimize the impact of urbanization on a measurable parameter of interest.

My results also suggested that RNICO is a stronger predictor of peakflows in humid climates than for oceanic and semi-arid climates such as in the western US. Catchment soil in humid climate cities is often saturated. In this case, much of the precipitation contributes to runoff generation. However, the catchment soil in semi-arid and arid climates is often dry with a high storage capacity. Therefore, a great fraction of precipitation events is often stored in the soil and decreases flood response of urban catchments. Storm characteristics can also play an important role in runoff response of urban catchments. For instance, flooding in humid climate (e.g. in Syracuse, NY) often occurs during summer flashfloods when the soil is saturated. On the other hand, flooding in oceanic climate (e.g. in Portland, OR) often occurs during light drizzles over the course of several days. In this case flooding generally occurs due to slow infiltration which challenges the ability to predict runoff response due to the intermittent nature of the storm and slow response of the stream flow. The maximum gaged runoff peakflows in Portland exponentially increased with RNICO which was different from other study locations and requires further study (Figure 17).

5.6. Real-time ensemble flood forecasting

I applied a lumped physical hydrology model, SAC-SMA, and one of the most widely used data-driven models in hydrologic forecasting, ANFIS, to re-forecast streamflow discharge at several small to medium size peri-urban catchments near NYC during Hurricane Irene and another small storm event. Comparison of various statistical performance indices for SAC-SMA and ANFIS indicated that SAC-SMA performs reasonably well for flood prediction in relatively small urban catchments (drainage area < 150 km^2) with NSE values mostly greater than 0.75, but ANFIS largely under-predicted

the rising limb and the peak flow of Hurricane Irene flood hydrographs, especially for lead times greater than three hours. While ANFIS performance was poor when forecasting Hurricane Irene hydrographs, performance was relatively high when forecasting a smaller but still extreme storm event. It is inferred that the poor performance of ANFIS for Hurricane Irene is likely due to the absence of similarly large storms included in the training period.

This study also suggests that the flood forecasting performance of the lumped SAC-SMA and ANFIS models may not depend on the catchment scale and fractional impervious area for relatively small urban catchments. Quantitative performance parameters (RelBIAS, RelMSE, and ARAD) for both models varied in a relatively similar range for the nine study sites with drainage areas ranging from 17 to 150 km^2 and fractional impervious areas ranging from 12 to 25%. However, it is suggested to examine these models for real-time flood prediction systems in a greater number of small to medium-sized catchments with a wide range of imperviousness, drainage patterns, and climate to study the model's sensitivity to different characteristics of the catchments and their performance under varying conditions.

Despite better performance of SAC-SMA compared to ANFIS for predicting the flood hydrograph of Hurricane Irene in the nine study catchments, the use of AI models shows some promise as an alternative to physical hydrology models in local urban flood forecasting systems if a long training period with a wide range of storm scales from small to large are available for the site. An important benefit of AI models is the short training time that may require less data and expert knowledge. Furthermore, the small number of input parameters in AI models helps decrease the sources of uncertainty and the risk of

equifinality (Beven, 2006) which may be a concern for most physical hydrology models. Therefore, results of AI models with appropriately long training periods in small urban catchments could be used to provide simple real-time systems for urban flood warning systems and control outputs of physical hydrology models that are more computationally expensive and require significant expert knowledge for model calibration and validation. Indeed, the performance of ANFIS forecasts for short forecast lead times was comparable to SAC-SMA forecasts, despite the large increase in degrees of freedom associated with the large number of model parameters associated with SAC-SMA. However, the importance of applying physical hydrology models for the real-time flood forecasting systems is emphasized due to uncertain future climatic conditions and potential changing physical characteristics of a watershed. The streamflow hydrograph for the future extreme events may not be accurately predicted by AI models, which are learning algorithms that are highly dependent on past memory. Overall, this phase of the study demonstrates accurate flood forecasting in small watersheds requires long continuous periods of streamflow discharge monitoring and higher temporal resolution of predicted precipitation inputs. More importantly, flood hydrographs of extreme events in small catchments should be accurately and continuously recorded to increase the predictability power of both physical hydrology and data-driven real-time flood forecasting models.

6. Chapter 6 (Recommendations for future research)

In this dissertation, I provided new insights into statistical and modeling approaches for urban flood management. However, many more questions remain to be answered in future studies to complement my findings. In this section, I suggest some research directions for future studies.

6.1. Impacts of urbanization on flooding

Stormwater networks can greatly influence the seasonal peak flow response of peri-urban catchments by altering the hydraulic flow path lengths and travel times. However, information on stormwater networks in urban catchments are generally categorized as classified information and are generally inaccessible to the public. I suggest studying the impact of stormwater networks on peak flow magnitude and time-to-peak flow to complement my results.

6.2. Impacts of urban development pattern on flooding

The RNICO index cannot account for the interference of stormwater drainage networks on discharge. However, it is hypothesized that the impact of stormwater networks is negligible in low to moderately urbanized study catchments. This assumption may not be valid for highly developed catchments due to the considerable influence of drainage networks on the response of these catchments. To increase the effectiveness of RNICO for flood prediction in highly developed urban catchments with dense stormwater networks, the total length of stormwater conduits and/or the total area of stormwater catch basins may be used as weighting factors for RNICO.

The geometric distances used for calculating RNICO are defined based on straight line connections from the catchment outlet to the basin centroids (d_c) and areas of

imperviousness centroid (d_i). These lines do not closely represent the actual hydrologic pathways and lengths of catchment drainages. To increase the value of the RNICO index for catchments with irregular shapes, inclusion of known pipelines and channels for routing, or for variable source areas, may improve the index beyond the straight line approach developed here.

Another limitation was the relatively small number of USGS monitored peri-urban catchments in proximity of large growing cities. Especially in western US, most urban stream-flows are often intermittent. Secondly, there are fewer USGS stream-flow monitoring stations in the western US urban catchments compared to the northern US. Due to the limited number of small catchments in the western US, the correlation between RNICO and average runoff peak flow may be influenced by other physical properties such as fractional impervious area and urban drainage system. To decrease the uncertainty of analysis for western US study sites, an analysis of a greater sample number of small suburban catchments with a wide range of fractional impervious area and drainage patterns for the western US is suggested.

6.3. Impact of storm direction on flood forecasting performance of ANFIS

My results indicated a marginal impact of storm direction on the performance of ANFIS flood forecasting model in Ley Creek (78 km^2) due to the relatively short time of concentration (1-5 hours). This analysis was limited by the temporal resolution of discharge from the USGS gage (15 minutes). It is suggested to perform a similar analysis with a higher temporal resolution of discharge to more accurately approximate the peak flow magnitude and time to peak flow and address the impact of storm direction on flood forecasting. Also, I note that this impact can be more important in large river basins

(A>78 km^2), in which storm coverage area is typically smaller than the catchment drainage area. In this case, the storm location can affect the time of concentration and peak flow occurrence time, and water level data for the sub-branches of the catchment can be valuable inputs for an ANFIS model that is developed to predict flood level at the catchment outlet. I suggest applying the same methodology for flood forecasting in a large urbanized river basin to assess the impact of catchment scale for mentioned analysis.

6.4. Real-time ensemble flood forecasting

A limitation of the analysis in the second phase of this study was to access the historical numerical weather predictions that were used by NOAA for practical flood forecasting. Although this study used 11 GEFS/R precipitation ensemble members that are currently available from NOAA database, the actual precipitation prediction data used by NOAA include 21ensmeble members. To improve model performance and decrease the uncertainty of analysis, application of the 21 ensemble members is suggested. However, finding access to the 21 ensemble members from the NOAA database can be difficult without special permission from that organization.

Flood forecasting results for the nine NYC peri-urban catchments did not indicate a strong statistical correlation among model performance indices and catchment drainage area and imperviousness. As all study catchments are near NYC, this finding may be only valid for this study location and may differ for other geographic locations. Therefore, a similar analysis on different study locations with a wide range of imperviousness, climate, and drainage patterns is suggested.

As previously discussed in the results section, the ANFIS model performed poorly for predicting the Hurricane Irene flood hydrograph for lead times greater than 3 hours. I suggest that poor performance of ANFIS for predicting the flood hydrograph of Hurricane Irene is due to the lack of a similar large storm/hurricane in the training period (2004-2011). Data-driven models are training algorithms and their performance can be highly affected by the quality of training data inputs. To test the validity of my hypothesis, I suggest applying ANFIS for predicting the flood hydrograph of a more recent hurricane to extend the training period for this model and assess the impact of training data quality on the accuracy of predictions.

Appendix A: Real-time ensemble flood forecasting

Table A1: *RelBIAS* values for individual watersheds for calibration (2004-2011) and validation (2011-2014) periods.

Storm	Site ID	Calibration					Validation				
		SAC-SMA	ANFIS				SAC-SMA	ANFIS			
			3 hrs	6 hrs	9 hrs	24 hrs		3 hrs	6 hrs	9 hrs	24 hrs
Hurricane Irene (27-29 Aug, 2011)	1	0.16	0.06	0.09	0.15	0.20	0.11	0.07	0.09	0.14	0.15
	2	0.11	0.07	0.10	0.11	0.13	0.10	0.06	0.11	0.11	0.13
	3	0.13	0.06	0.14	0.15	0.15	0.08	0.07	0.14	0.14	0.15
	4	0.06	0.07	0.08	0.11	0.11	0.06	0.09	0.09	0.11	0.13
	5	0.10	0.10	0.11	0.12	0.13	0.06	0.10	0.12	0.13	0.14
	6	0.15	0.10	0.10	0.12	0.13	0.10	0.10	0.10	0.12	0.12
	7	0.04	0.07	0.08	0.13	0.15	0.05	0.09	0.08	0.11	0.12
	8	0.09	0.11	0.13	0.16	0.16	0.06	0.11	0.12	0.13	0.14
	9	0.15	0.11	0.13	0.14	0.16	0.11	0.12	0.13	0.13	0.16
Small event (23-25 Sep, 2011)	1	0.06	0.08	0.10	0.11	0.12	0.06	0.10	0.09	0.10	0.14
	2	0.05	0.07	0.08	0.09	0.11	0.07	0.06	0.08	0.10	0.12
	3	0.08	0.06	0.07	0.09	0.12	0.08	0.08	0.09	0.09	0.11
	4	0.08	0.05	0.07	0.08	0.10	0.07	0.06	0.08	0.10	0.12
	5	0.08	0.06	0.08	0.12	0.14	0.06	0.07	0.09	0.11	0.15
	6	0.10	0.07	0.10	0.10	0.12	0.08	0.10	0.11	0.11	0.13
	7	0.11	0.07	0.11	0.13	0.14	0.11	0.09	0.10	0.13	0.13
	8	0.20	0.08	0.10	0.12	0.15	0.15	0.09	0.12	0.12	0.13
	9	0.07	0.06	0.08	0.10	0.11	0.06	0.07	0.09	0.09	0.11

Table A2: Calibration datasets for the SAC-SMA model for the nine study catchments

Site ID	Uztwm	Uzfwm	Uzk	Adimp	Zperc	rexp	lztwm	lzfsm	lzfpm	lzsk	lzpk	pfree
1	14.54	62.76	0.27	0.16	139.62	3.90	353.62	13.64	415.33	0.16	0.01	0.57
2	15.51	1.21	0.14	0.20	78.51	4.98	97.96	13.78	717.97	0.14	0.02	0.55
3	31.03	34.30	0.50	0.40	78.98	4.04	495.33	232.66	998.72	0.01	0.02	0.01
4	51.42	11.28	0.12	0.01	171.09	1.49	482.46	42.59	11.09	0.02	0.01	0.60
5	37.17	63.31	0.50	0.17	249.98	0.00	493.79	42.38	42.01	0.24	0.03	0.12
6	15.26	1.37	0.12	0.01	131.70	0.77	432.60	35.66	1.25	0.24	0.02	0.42
7	45.14	147.65	0.47	0.00	44.39	4.82	496.78	1.37	271.46	0.07	0.01	0.35
8	11.51	149.63	0.25	0.01	246.33	4.83	335.82	74.01	412.76	0.24	0.02	0.46
9	98.83	62.70	0.35	0.15	68.91	4.34	450.10	508.59	994.25	0.08	0.01	0.00

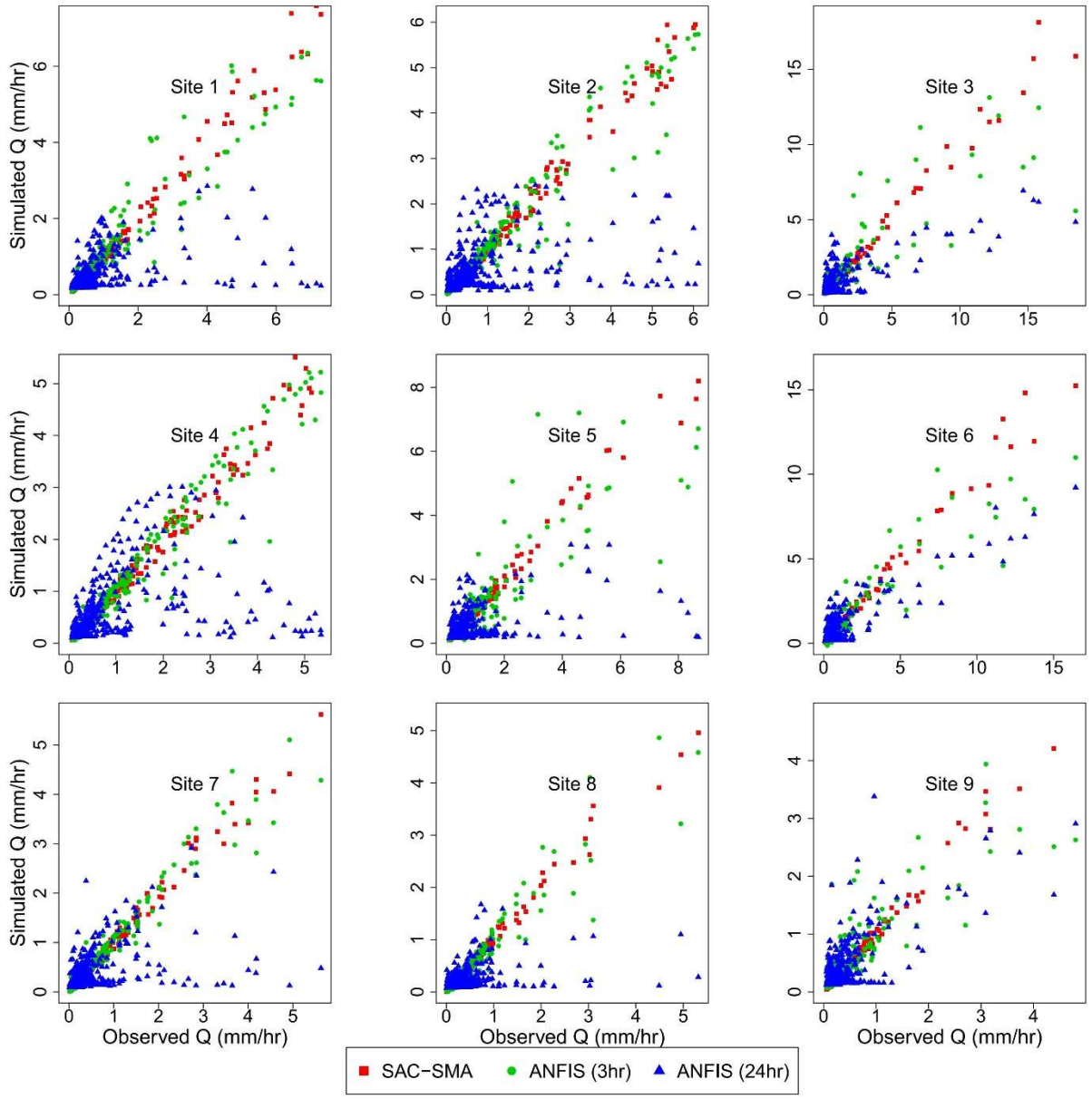

Figure A1: Observed versus simulated discharge values for SAC-SMA and ANFIS models for the calibration period. We focus on a 5-month period from 3/1/2011 to 8/1/2011 because of the difficulty in showing all data points for the 7-year calibration period for all sites. We note that the selected 5-month period includes the wettest and the driest part of the year in the study region.

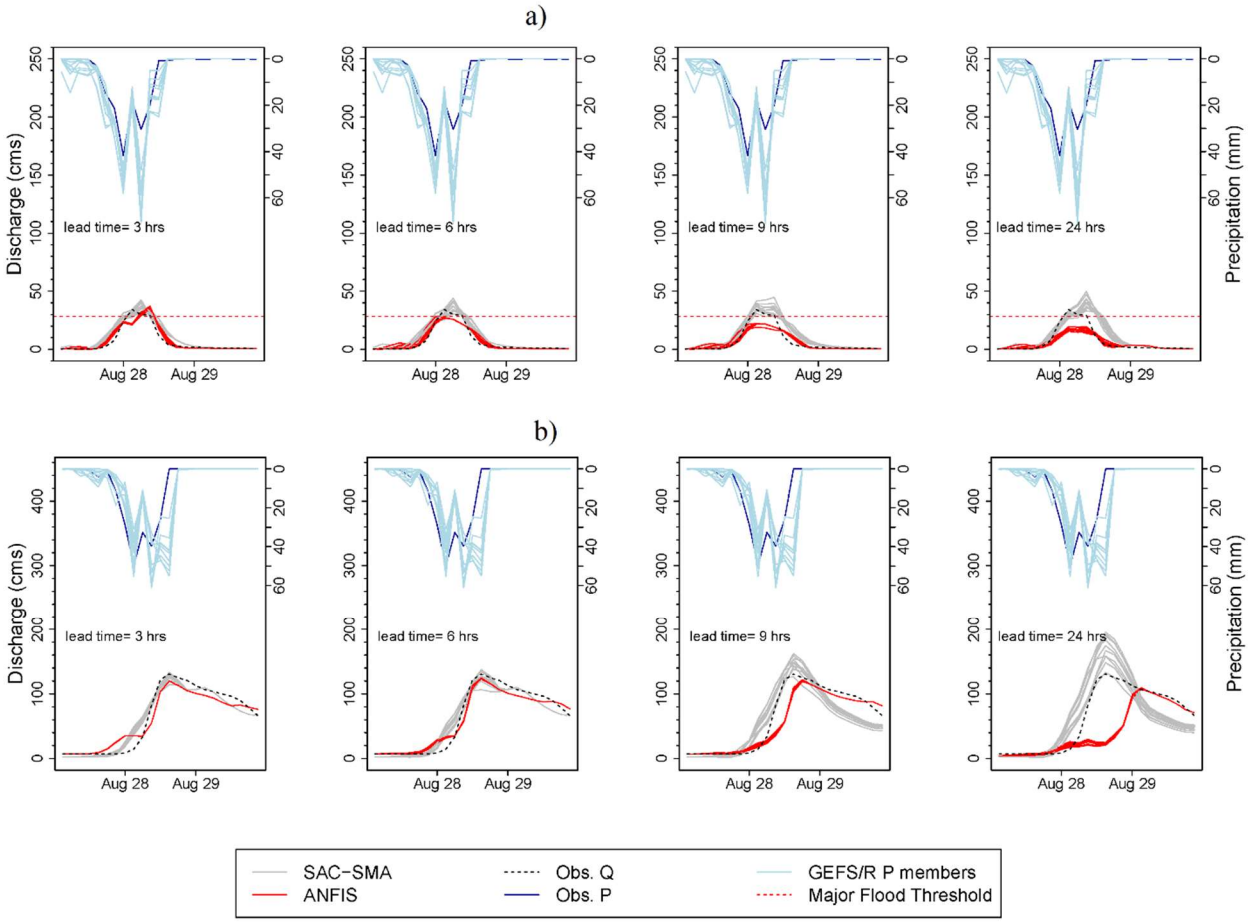

Figure A2: Observed and ensemble forecasted flood hydrographs of the smallest study site (site 1, Fig. A2-a) and the largest study site (site 9, Fig. A2-b) for Hurricane Irene. Lead times for forecasting increase from left to right

Table A3: *RelBIAS* values of ANFIS for predicting the Hurricane Irene and the small storm event flood hydrographs at the nine study catchments. Min, avg, and max values represent minimum, average, and maximum *RelBIAS* among the eleven forecasted ensemble members at the corresponding catchment.

Storm	Site ID	lead time= 3 hrs			lead time= 6 hrs			lead time= 9 hrs			lead time= 24 hrs		
		min	avg	max	min	avg	max	min	avg	max	min	avg	max
Hurricane Irene (27-29 Aug, 2011)	1	-0.01	-0.01	0.00	-0.13	-0.10	-0.04	-0.24	-0.14	-0.06	-1.26	-0.91	-0.85
	2	0.02	0.03	0.05	-0.17	-0.14	0.02	-0.33	-0.22	-0.11	-1.35	-1.10	-0.74
	3	0.01	0.02	0.04	-0.27	-0.20	-0.08	-0.40	-0.25	-0.18	-0.74	-0.45	-0.27
	4	-0.02	0.00	0.01	-0.12	-0.10	-0.02	-0.60	-0.36	-0.30	-0.94	-0.65	-0.41
	5	0.00	0.01	0.03	-0.17	-0.12	-0.08	-0.27	-0.17	-0.01	-0.99	-0.71	-0.52
	6	-0.01	0.00	0.01	-0.18	-0.13	-0.04	-0.42	-0.32	-0.13	-1.10	-0.97	-0.77
	7	-0.07	-0.01	0.09	-0.14	-0.05	-0.01	-0.29	-0.15	-0.01	-0.76	-0.52	-0.33
	8	0.00	0.02	0.06	-0.23	-0.18	-0.11	-0.35	-0.21	-0.11	-0.85	-0.58	-0.31
	9	0.01	0.02	0.03	-0.39	-0.23	-0.14	-0.41	-0.28	-0.14	-1.20	-0.97	-0.77
Small event (23-25 Sep, 2011)	1	0.06	0.15	0.22	0.13	0.26	0.40	0.05	0.21	0.36	0.21	0.41	0.63
	2	0.01	0.08	0.14	-0.14	-0.02	0.09	-0.12	-0.07	0.06	-0.06	0.03	0.04
	3	0.04	0.08	0.10	0.05	0.19	0.30	0.03	0.13	0.25	0.13	0.26	0.39
	4	0.02	0.05	0.09	0.14	0.23	0.39	0.01	0.17	0.24	0.17	0.34	0.54
	5	0.04	0.10	0.27	-0.11	-0.03	0.12	-0.21	-0.11	0.02	0.01	0.05	0.14
	6	0.07	0.13	0.20	-0.10	-0.03	0.05	-0.24	-0.12	0.00	-0.03	0.05	0.12
	7	0.03	0.10	0.19	-0.12	-0.06	0.03	-0.17	-0.05	0.10	-0.01	0.06	0.24
	8	0.07	0.14	0.17	-0.09	-0.03	0.03	-0.34	-0.15	0.02	0.00	0.03	0.09
	9	0.07	0.13	0.14	-0.12	-0.03	0.04	-0.16	-0.07	0.10	-0.02	0.07	0.09

Table A4: *RelBIAS* values of SAC-SMA for predicting the Hurricane Irene and the small storm event flood hydrographs at the nine study catchments.

Storm	Site ID	lead time= 3 hrs			lead time= 6 hrs			lead time= 9 hrs			lead time= 24 hrs		
		min	avg	max	min	avg	max	min	avg	max	min	avg	max
Hurricane Irene (27-29 Aug, 2011)	1	0.02	0.11	0.19	0.15	0.19	0.24	-0.22	-0.16	-0.09	0.15	0.20	0.27
	2	-0.07	0.04	0.12	-0.03	0.04	0.10	-0.07	0.13	0.23	0.16	0.23	0.31
	3	-0.02	0.08	0.18	0.02	0.11	0.20	0.00	0.16	0.26	0.21	0.29	0.38
	4	-0.05	0.06	0.16	0.10	0.16	0.22	0.06	-0.14	-0.06	0.11	0.19	0.27
	5	0.04	0.08	0.17	0.05	0.13	0.23	0.06	0.19	0.27	0.11	0.21	0.31
	6	0.08	0.09	0.16	-0.22	-0.15	-0.08	-0.25	-0.19	-0.08	0.17	0.26	0.37
	7	-0.04	0.01	0.09	-0.14	-0.07	0.02	-0.14	-0.12	-0.01	-0.01	0.07	0.15
	8	-0.02	0.04	0.16	-0.01	0.06	0.16	-0.01	0.09	0.17	0.04	0.11	0.18
	9	-0.08	0.04	0.08	-0.01	0.09	0.18	-0.01	0.14	0.24	0.17	0.24	0.32
Small event (23-25 Sep, 2011)	1	0.03	0.09	0.16	0.07	0.17	0.22	0.15	0.22	0.29	0.36	0.43	0.48
	2	-0.03	0.05	0.12	0.06	0.14	0.23	0.20	0.29	0.38	0.25	0.34	0.41
	3	0.07	0.17	0.26	0.22	0.27	0.35	0.24	0.31	0.41	0.33	0.38	0.46
	4	0.05	0.15	0.26	0.11	0.21	0.31	0.19	0.26	0.34	0.34	0.44	0.53
	5	-0.02	0.08	0.16	0.18	0.27	0.33	0.21	0.29	0.38	0.38	0.46	0.57
	6	0.12	0.21	0.32	0.19	0.30	0.39	0.22	0.32	0.38	0.35	0.42	0.52
	7	0.10	0.17	0.25	0.13	0.20	0.27	0.12	0.21	0.29	0.35	0.45	0.51
	8	0.12	0.20	0.26	0.22	0.32	0.40	0.21	0.32	0.43	0.39	0.48	0.59
	9	0.02	0.12	0.20	0.13	0.24	0.34	0.26	0.33	0.43	0.39	0.45	0.53

Table A5: Pearson correlation coefficient (*r*) between the *PR* index and other performance indices used in this study. We note that values in this table are calculated based on n=5 which equals the number of sites with NOAA flood threshold (Table 1).

		Lead time (hrs)			
		3	6	9	24
ANFIS	NSE	-0.48	-0.28	-0.58	-0.79
	RelBIAS	0.35	-0.08	-0.50	0.07
	RelMSE	0.14	0.21	-0.41	-0.03
	ARAD	-0.18	-0.66	0.99	0.00
SAC-SMA	NSE	-0.11	0.52	-0.99	0.19
	RelBIAS	-0.55	-0.73	-0.32	-0.65
	RelMSE	-0.23	-0.58	0.01	-0.53
	ARAD	-0.10	0.11	0.01	-0.55

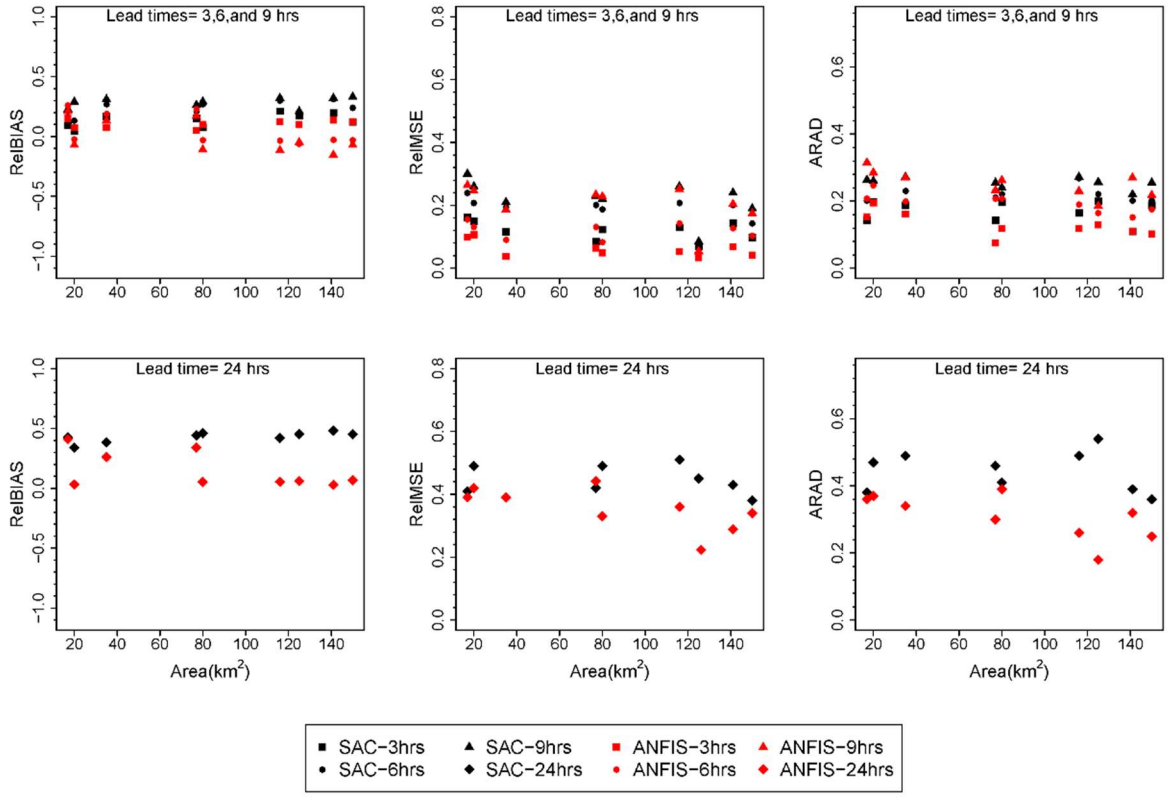

Figure A3. Performance indices for SAC-SMA and ANFIS averaged across the eleven ensemble members varied lead times plotted against catchment drainage area. Results in this figure represent the flood hydrograph simulation for the small storm event during September 2011.

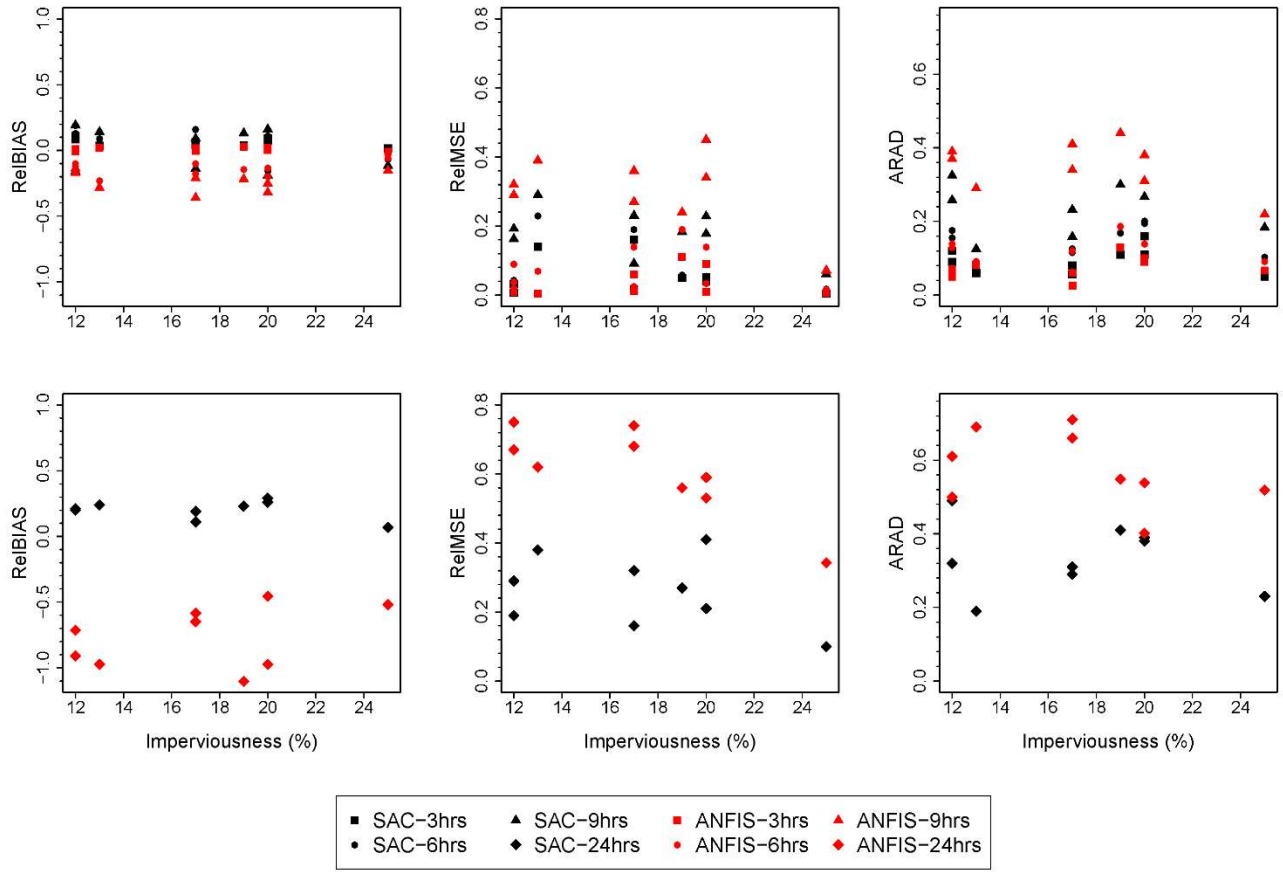

Figure A4. Performance indices for SAC-SMA and ANFIS averaged across the eleven ensemble members varied lead times plotted against catchment imperviousness. Results in this figure represent the flood hydrograph simulation for Hurricane Irene.

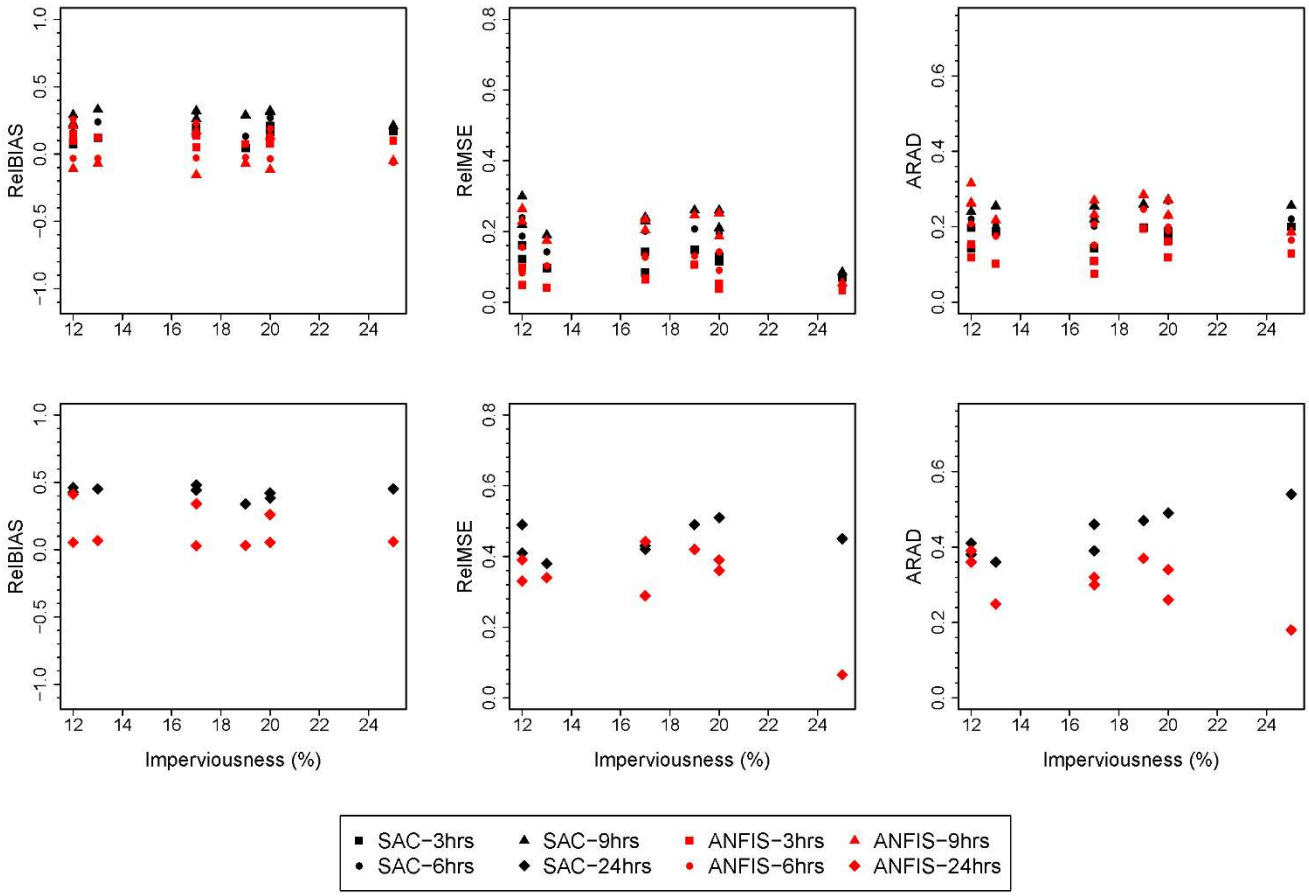

Figure A5. Performance indices for SAC-SMA and ANFIS averaged across the eleven ensemble members varied lead times plotted against catchment imperviousness. Results in this figure represent the flood hydrograph simulation for the small storm event during September 2011.

Appendix B: Culvert geometries for Ley Creek monitoring stations

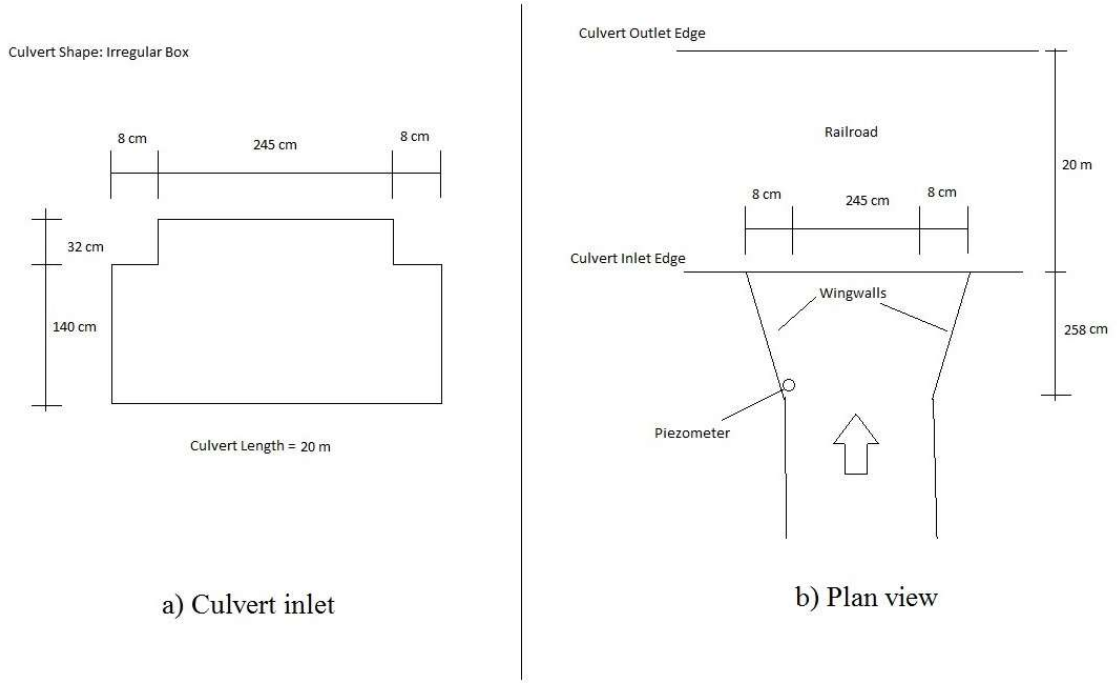

Figure B1. Monitoring station 1 at West 2nd St., East Syracuse, NY. Figures B1a and B1b show culvert inlet and plan views of this site, respectively.

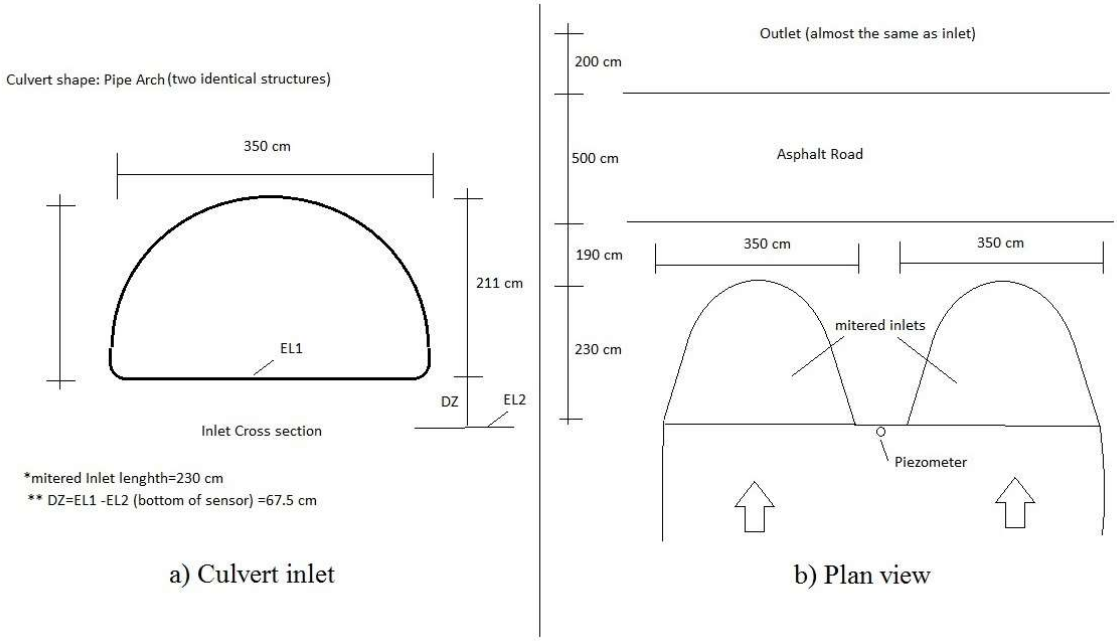

Figure B2. Monitoring station 2 at Beartrap Creek, Ley Creek Dr., Syracuse, NY. Figures B2a and B2b show culvert inlet and plan views of this site, respectively.

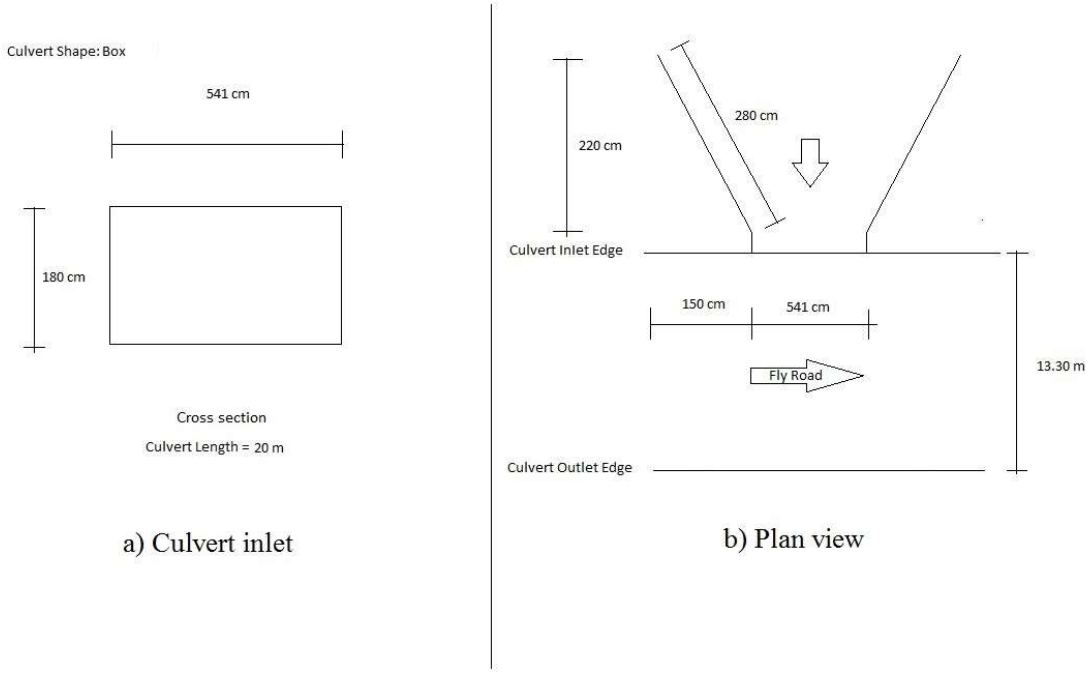

Figure B3. Monitoring station 3 at Fly Rd, Syracuse, NY. Figures B3a and B3b show culvert inlet and plan views of this site, respectively.

Appendix C: R script for correcting NLDAS radar precipitation data

```
setwd("C:/mott/Courses/THESIS papers/Paper3/4-Chicago/Step3-MetDataManipulation/PrecDataCorrection")

library("lubridate")
library(zoo)
Radar_IDs<-read.csv(file="RadarIDList.csv")

####################
#Create a loop to read out and correct hourly radar prec data
for (i in seq(1:dim(Radar_IDs)[1])){
  print(i)
    #PART A: HOURLY PRECIPITATION#####################################
    df_PrecHrly<-read.csv(file=paste(Radar_IDs[i,1],".csv",sep=""))
    df_PrecHrly<-df_PrecHrly[!duplicated(df_PrecHrly[,4]),]

    #read out dates
    date_PrecHrly<-as.POSIXct(df_PrecHrly[,4],format="%m/%d/%Y %H:%M", tz="EST")

    #calculating the length of date
    l_PrecHrly<-length(date_PrecHrly)

    #and the desired ones
    dates_desired<-seq(date_PrecHrly[1],date_PrecHrly[l_PrecHrly],by="1 hour")
    length_desired<-length(dates_desired)

    #using zoo to fill in the blanks
    mtx1 <- zoo(df_PrecHrly[,5],date_PrecHrly)
    zoo_merged <- merge(mtx1,zoo(,seq(start(mtx1),end(mtx1),by="1 hour")), all=TRUE)

    zoo_merged[is.na(zoo_merged)]<-0

    #converting zoo ts to dataframe
    #note that zoo destroys dates. Then we only save its values.
    df2 <-as.data.frame(as.numeric(zoo_merged[,2]))

    #Save total hourly Prec dataset
    PrecHrly<-df2

    ####################
    #PART B: WRITING DATASETS AS A CSV FILE#####################################
    #write a CSV for the hourly dataset (for use in SAC-SMA)
    #First, arrange dates in a proper way for reading in RS_MINERVE (SAC-SMA)
    X11<-paste(day(dates_desired),"/",month(dates_desired),"/",year(dates_desired),sep="")
    X22<-paste(hour(dates_desired),":00",sep="")
    X33<-paste(X11,X22)

    #Second, create outputs

    write.csv(output2,paste(Radar_IDs[i,1],"_PrecHourly.csv",sep=""),row.names = FALSE)
}
```

Appendix D: R script for precipitation event analysis: isolating individual precipitation events based on the corrected NLDAS precipitation input data.

```
setwd("C:/mott/Courses/THESIS papers/Paper3/4-Chicago/Step3-MetDataManipulation/EventAnalysis")

library("lubridate")

#This section should be filled by the user:
#Calib1 is the number of hours between rain events
Calib1<-3
#Define Start and End of the Study to limit the df of Radar Data
calib_win<-as.POSIXct(c("01/10/2009","01/10/2012"), format="%d/%m/%Y", tz="EST")
############read out the main information dataframe#############
#df_Info<-read.csv(file="Calif_Sites_Info.csv")
#attach(df_Info)
RadarIDs<-read.csv(file="RadarIDList.csv")
###################Event Analysis#################################
#I define a loop in which radars are called from the info file and analyzed
for(x in seq(292,305)){
  for(y in seq(131,140)){
    print(paste(x,y))
    if(paste("X",x,"-","Y",y,sep="") %in% RadarIDs[,1]){

      df<-read.csv(file=paste("X",x,"-","Y",y,"_PrecHourly.csv",sep=""))


      date1<-as.POSIXct(df[,1], format="%d/%m/%Y %H:%M", tz="EST")

       #now norrow down the df windo into the study period
       df<-df[date1 %in% date2,]

       PREC<-df[,2][df[,2]!=0]
       l_prec<-length(PREC)
       #and update date2
       date2<-date2[df[,2]!=0]

       #A PS flag is used to distinguish precipitation starts
       prec_flag<-array("PS",l_prec)
       prec_Index<-array(0,l_prec)

       #the first record is the start of first event but not
       #included in the later loops. it is introduced here.
       prec_Index[1]<-1

       #now walk through the dates and remove PS flag from
       #the positions that are less than or equal to Calib1 hrs different from the past event
       for (i in seq(2,l_prec)){

            if (as.numeric(difftime(date2[i], date2[i-1], tz,
                                    units = "hours"))<=Calib1){
              prec_flag[i]<-0
            }
            else{
              prec_Index[i]<-i
            }
          }

          #Now calculate the number of Precipitation events
          Num_PREC<-length(prec_flag[prec_flag=="PS"])

          #Also, prec_Index is shortened to the numebr of events.
          prec_Index<-prec_Index[prec_Index!=0]
```

```
        #precipitation start time date is saved here
        prec_Start<-date2[prec_Index]

        #precipitation end array has one less element cuse
        #the last event does not have enddate.
        prec_End<-prec_Start
        prec_End[1:(Num_PREC-1)]<-date2[(prec_Index-1)[2:Num_PREC]]

        #Now indices are used to sum the rainfal depths in hundreth of inch
        prec_Depths<-array(0,Num_PREC)

        #this array is used to record the maximum intensity of rain (mm/hr)
        prec_max_Intensity<-array(0,Num_PREC)
        #use a trick to make a copy of a dates dataframe (from date2)
        prec_max_Intensity_timdate<-date2[1:Num_PREC]

        #unit conversion from US to SI
        for (i in seq(1,(Num_PREC-1))){
          prec_Depths[i]<-sum(PREC[prec_Index[i]:(prec_Index[i+1]-1)])
          prec_max_Intensity[i]<-max(PREC[prec_Index[i]:(prec_Index[i+1]-1)])
          prec_max_Intensity_timdate[i]<-date2[date2>=prec_Start[i] &
    }

    #Calculating AMC5
    AMC5<-array(0,Num_PREC)

    for(i in seq(1:Num_PREC)){
      AMC5[i]<-sum(PREC[date2>(prec_Start[i]-5*24*60*60) & date2<prec_Start[i]])
    }

    #Precipitation Duration
    prec_Duration<-as.numeric(difftime(prec_End,prec_Start, tz,units ="hours" ))
    prec_Duration[prec_Duration==0]<-1
    #Precipipation Intensity (mm/hr)
    prec_Avg_Intensity<-prec_Depths/prec_Duration

    #creting output
    output1<-data.frame(prec_Index, prec_Start, prec_End, prec_max_Intensity_timdate,
                        prec_Duration, prec_Depths,prec_Avg_Intensity,
                        prec_max_Intensity, AMC5)
    colnames(output1)<-c("Prec Index","Start","End","Peak timedate","Duration (hrs)","Depth (mm)",
                         "Average Intensity (mm/hr)","Max Intensity (mm/hr)", "AMC5 (mm)")

    write.csv(output1, file = paste("X",x,"-","Y",y,"_PrecEvents.csv",sep=""),row.names = TRUE)


    #end of if
    }
 #end of y loop
  }

 #end of x loop
}
```

Appendix E: R script for peakflow analysis: extracting peak flow magnitude and timing for different precipitation events in the study period

```
#this program calculates runoff peak flow and time to peak for different events for NYC USGS gages
#Traveltime1: Start of precipitation to peak of discharge
#Travel time 2: Peak of prec to peak of discharge
setwd("C:/My files/Papers/Paper1/TimeToPeak/Step2-PeakFlowAnalysis")

#this function is used to seperate runoff from baseflow
library("EcoHydRology")

#The following threshold (mm) filters event based on total depth and
#only uses depths of greater than or equal to Prec_Thresh cm
Prec_Thresh<-10

################Read out Station file###########
#read the information dataframe
Stations_Info<-read.csv(file="NYC_Sites_Info.csv")
attach(Stations_Info)
#exclude stations without prec data
Stations_Info<-Stations_Info[is.na(Prec_Radar_ID)==FALSE,]

#convert catchment area from square mile to m2
Catch_Area_m2<-1e+6*Area_km2
#extracting the number of study stations
Num_Stations<-dim(Stations_Info)[1]
```

```
#building a matrix to save runoff peakflows for different stations at different events
#Since I dont know how many events at each station occured during the study period I specify
#500 hundred rows for the matrix
runoff_mtx<-matrix(NA,500,Num_Stations)
#Similarly, create a matrix for saving travel time
traveltime1_mtx<-matrix(NA,500,Num_Stations)
traveltime2_mtx<-matrix(NA,500,Num_Stations)

################Analyze Station data###########
for(i in seq(1:Num_Stations)){
  print(i)
  df_USGS<-read.csv(paste("0",Gage_ID[i],".csv",sep=""))
  date_USGS<-as.POSIXct(df_USGS[,3], format="%m/%d/%Y %H:%M", tz="EST")

  #reading the precipitation event file.
  df_Prec_Events<-read.csv(file=paste(Prec_Radar_ID[i],"_PREC_Events.csv",sep=""))
  #filter the dataset based on the event threshold
  df_Prec_Events<-df_Prec_Events[df_Prec_Events[,7]>=Prec_Thresh,]

  #calculating number of events
  Num_Events<-dim(df_Prec_Events)[1]
  #and update the first column (event number)
  df_Prec_Events[,1]<-seq(1,Num_Events)


 #setting the precipitation start timedate
 PREC_Start<-as.POSIXct(df_Prec_Events$Start, format="%Y-%m-%d %H:%M:%S", tz="EST")
 PREC_End<-as.POSIXct(df_Prec_Events$End, format="%Y-%m-%d %H:%M:%S", tz="EST")
 PREC_Peaktime<-as.POSIXct(df_Prec_Events$Peak.timedate, format="%Y-%m-%d %H:%M:%S", tz="EST")

 #then the following loop is used to calculate runoff peak for differnt events
 #before going through the loop, a PDF plot is created to include runoff changes fir
 #all events of each station
 pdf(paste("Runoff_ts_0",Stations_Info[i,1],".pdf",sep=""),180,14)
 par(mar=c(0.5, 0.5, 0.2, 0.2), mfrow=c(2,floor(Num_Events/2)+1),
     oma = c(4, 4, 0.2, 0.2))
```

```
    for (j in seq(1:Num_Events)){
      paste("Event",j)
      #the discharge records for the event period are isolated here
      EVENT_DATES<-date_USGS[date_USGS>PREC_Start[j]-3*3600 &
                               date_USGS<PREC_End[j]+3*3600]
      # to do the following method to remove NAs.
      EVENT_DATES<-EVENT_DATES[!is.na(EVENT_DATES)]
      #some stations have some missing data for some specific events. In order to continue
      #the program run when facing such cases I put the rest of the loop in the the if structure
      if (length(EVENT_DATES)>0){
        #make a dataframe of the discharge values over the event period.
        EVENT_DISCH<-df_USGS[,5][date_USGS>PREC_Start[j]-3*3600 &
                                   date_USGS<PREC_End[j]+3*3600]
        #same story for event discharge!
        EVENT_DISCH<-EVENT_DISCH[!is.na(EVENT_DISCH)]

        #then Runoff is sepperated (0.028316847*3600*1/Catch_Area_m2 is to convert cfs to mm/hr
        #for unit area of the catchment (each m2))
        RUNOFF<-0.028316847*1000*3600*1/Catch_Area_m2[i]*BaseflowSeparation(EVENT_DISCH,
                                                                            filter_parameter = 0.925,
                                                                            passes = 3)[,2]
        #then runoff peak flow is saved in the matrix
        runoff_mtx[j,i]<-max(RUNOFF)

        #calculate the peakflow time date
        Q_Peaktime<-EVENT_DATES[RUNOFF==max(RUNOFF)][1]

        #and calculate travel time as the time difference (min) between prec peak
        #and the discharge peak at the river
        traveltime1_mtx[j,i]<-difftime(Q_Peaktime,PREC_Start[j],units = "mins")
        traveltime2_mtx[j,i]<-difftime(Q_Peaktime,PREC_Peaktime[j],units = "mins")

        #use this condition to get rid of the runoff values that are 1-in the start of interval
        #2- at the end of interval 3- equal to the prevvious peak flow
        if(runoff_mtx[j,i] %in% c(RUNOFF[1], RUNOFF[length(RUNOFF)])){
          runoff_mtx[j,i]<-NA
          traveltime1_mtx[j,i]<-NA
          traveltime2_mtx[j,i]<-NA

        }

        if(j>1){
          if(is.na(runoff_mtx[j-1,i])==FALSE & is.na(runoff_mtx[j,i])==FALSE){
            if(runoff_mtx[j-1,i]==runoff_mtx[j,i]){
              runoff_mtx[j,i]<-NA

             traveltime1_mtx[j,i]<-NA
             traveltime2_mtx[j,i]<-NA

            }
          }
        }


        #and shown in the plot as a dashed line
        abline(v=EVENT_DATES[RUNOFF==max(RUNOFF)],lty=2)
        #and drop a label to know which event are we
        title(paste("station",Stations_Info[i,1],", event #",j),
              adj=0.5, line = -10, cex.main = 1.8)
      #end of if
      }
    #end of loop j
    }
    dev.off()
  #end of loop i
  }
            #write results into csv file
            colnames(runoff_mtx)<-c(paste("St_0",Stations_Info[,1],sep=""))
            write.csv(runoff_mtx,"Peakflow_Summary.csv",row.names = TRUE)
            write.csv(traveltime1_mtx,"Traveltime1_Summary.csv",row.names = TRUE)
            write.csv(traveltime2_mtx,"Traveltime2_Summary.csv",row.names = TRUE)
```

Appendix F: R script for plotting different figures of phase one of the study

```
#In this script, I plot results of RNICO for all cities. To do this,
# I create several functions that are called during the plots and create independant
#plots for different cities.
setwd("C:/mott/Courses/THESIS papers/Paper3/AllCityPlots")
library(Hmisc)
library(zoo)

source("Func1.R")

##########$$$$$$$$$$$$$$$$$$$$$$$$$$$$$$$$$$$$$$$$$$$$$$$$$$$$$$$$$$$$$$$$$$$$$$$
#1-PQ PLOTS:
pdf("PQ_All.pdf",18,14)
layout(matrix(c(1,2,3,4,5,6,7,7,7),ncol=3,byrow=TRUE),heights=c(6,6,1))
par(mai=rep(0.58, 4))

Chicago_PQ_Plt()
abline(v=0.25, lty=2)
NYC_PQ_Plt()
abline(v=2, lty=2)
Baltimore_PQ_Plt()
abline(v=6, lty=2)
Portland_PQ_Plt()
SF_PQ_Plt()
#after all plots are finished, a plot.new is opened to plot the legend at the last row.
par(mai=c(0,0,0,0))
plot.new()
legend(x="center",ncol=2,c("Large Site, Long Event","Large Site, Flashflood",
                           "Small Site, Long Event","Small Site, Flashflood"),bty="n",
       pch=c(1,1,2,2),pt.cex=2, col=c(1,2,1,2),cex=2.6)

dev.off()

##########$$$$$$$$$$$$$$$$$$$$$$$$$$$$$$$$$$$$$$$$$$$$$$$$$$$$$$$$$$$$$$$$$$$$$$$
#2-BOX PLOTS:
pdf(paste("BoxPlt_All.pdf", sep=""),21,19)

layout(matrix(c(seq(1:9),rep(10,3)),ncol=3,byrow=TRUE),heights=c(4,4,4,1))
par(cex.lab=1.4,cex.axis=1.5, mar=c(4, 2, 4, 4),
    oma = c(4, 4, 4, 4))

Chicago_BoxPlt()
NYC_BoxPlt()
Baltimore_BoxPlt()
Austin_BoxPlt()
Houston_BoxPlt()
SF_BoxPlt()
LA_BoxPlt()

#and a legend
par(mai=c(0,0,0,0))
plot.new()

legend("center",ncol=3,c("Mean (small site)", "Max (small site)","Mean (large site)"),
       col=c(3,3,2),bty="n", pch=c(17,1,16),lty=c(1,2,1),pt.cex=1.8,cex=3.5)

dev.off()
```

```
##########$$$$$$$$$$$$$$$##############$$$$$$$$$$$$##############
#3-Regime:

pdf("Regime_All.pdf",11,16)
layout(matrix(c(seq(1:6),rep(7,2)),ncol=2,byrow=TRUE),heights=c(5,5,5,1))
par(mai=rep(0.58, 4))

Chicago_Regime()
NYC_Regime()
Portland_Regime()


#and a legend
par(mai=c(0,0,0,0))
plot.new()

legend("center",ncol=2,c("RBF (small site)", "CV (small site)","RBF (large site)","CV (large large)"),
       col=c(3,3,1,1),bty="n", pch=c(2,16,2,16),lty=c(2,1,2,1),pt.cex=2.5,cex=3)

dev.off()
##########$$$$$$$$$$$$$$$##############$$$$$$$$$$$$##############
#4-Precipitation distribution:
pdf("PrecDist_plot.pdf",10,10)
layout(matrix(seq(1,4),ncol=2,byrow=TRUE),heights=c(4,4))

    Prec_Dist()

    #after all plots are finished, a plot.new is opened to plot the legend at the last row.
    par(mai=c(0,0,0,0))
    plot.new()
    legend(x="center",ncol=1,c("Los Angeles (1986-2009)","Los Angeles (Study period)",
                               "San Fransisco (1986-2009)","San Fransisco (study period)"),
           bty="n",lty=c(1,2,1,2),col=c(1,1,2,2),cex=2.2)
    dev.off()

    ##########$$$$$$$$$$$$$$$##############$$$$$$$$$$$$##############
    #5-Time to Peak:

    pdf(paste("Chi_ttp.pdf", sep=""),12,10)
    par(cex.lab=1.4,cex.axis=1.5, mar=c(2, 2, 2, 2), mfrow=c(1,1),
        oma = c(4, 4, 4, 4))
    Chicago_ttp()
    legend("topright",c("Mean (small site)","Mean (large site)"),
           col=c(3,2),bty="n", pch=c(17,16),lty=c(1,1),pt.cex=1.8,cex=1.7)

    dev.off()
```

Appendix G: R script of functions for plotting different figures of phase one of the study for Chicago, IL

```
Chicago_PQ_Plt<-function(){

  #define duration Tresholds to divide plots into smaller/larger than that Treshold
  Duration_Tresh<-6

  #read out the catchment information file.
  df0<-read.csv(file="Chicago_SiteInfo.csv")

  Num_Stations<-dim(df0)[1]

  ############################################################
  ####################PLOTTING PQ#####################################
  ############################################################
  #I define the plots as follows: color: red=flashflood(<6hrs) black=long
  #symbol: circle=Large sites  triangle=Small sites

  for (i in seq(1:Num_Stations)){
    print(i)

    #Initially Assume a small site
    Plt_Symb<-2
    #Change the symbol to northern using a condition
    if(df0$Site_Acr[i]=="CHI-L"){
      Plt_Symb<-1
      Plt_Cex<-1.9

    }

    #df1 contains the summary of precipitation records:
    df_PrecSummary<-read.csv(file=paste(df0$Radar_ID[i],"_PrecEvents.csv",sep=""))
    #and narrow it down to the events greater than 10 mm
    df_PrecSummary<-df_PrecSummary[df_PrecSummary$Depth..mm.>=10,]

    #df11:extract Prec Depths in a seperate dataset
    df11Depth<-0.1*df_PrecSummary$Depth..mm.

    #read out the peak flow summary file
    df_PeakSummary<-read.csv(file="Chicago_Peakflow_Summary.csv")
    #now extract data from peak flow summary file
    df11Peak<-df_PeakSummary[(1:length(df11Depth)),grepl(df0$STAID[i],colnames(df_PeakSummary))]

    #a)- Duration > 6hrs####################
    #now norrow down both Prec Depth & peak flow values to where both are not NA
    df12Depth<-df11Depth[is.na(df11Depth)==FALSE & is.na(df11Peak)==FALSE &
                           df_PrecSummary$Duration..hrs.>6]

    df12Peak<-df11Peak[is.na(df11Depth)==FALSE & is.na(df11Peak)==FALSE &
                         df_PrecSummary$Duration..hrs.>6]

    #b)- Duration <= 6hrs####################
    df13Depth<-df11Depth[is.na(df11Depth)==FALSE & is.na(df11Peak)==FALSE &
                           df_PrecSummary$Duration..hrs.<=6]

    df13Peak<-df11Peak[is.na(df11Depth)==FALSE & is.na(df11Peak)==FALSE &
                         df_PrecSummary$Duration..hrs.<=6]


    #plot short events with red color
    if(i==1){
      plot(df12Peak,df12Depth,log="y",xlim=range(0,2.7),ylim=c(1,15),
           xlab="Runoff Peakflow (mm/hr)",ylab="Storm Total Depth (cm)",type='p',col=1
           ,pch=Plt_Symb,cex.lab=2,cex.axis=2,cex=Plt_Cex)
```

```
      if(length(df13Depth)>0){
        points(df13Peak,df13Depth,col=2,pch=Plt_Symb,cex=Plt_Cex)
      }
    }

    else{
      points(df12Peak,df12Depth,col=1,pch=Plt_Symb,cex=Plt_Cex)
      if(length(df13Depth)>0){
        points(df13Peak,df13Depth,col=2,pch=Plt_Symb,cex=Plt_Cex)
      }
    }
  }

#}
Chicago_BoxPlt<-function(){

  #read out the sites information dataframe
  df1<-read.csv(file="Chicago_SiteInfo.csv")
  df_Info<-df1[df1$Good=="Y" & (df1$Site_Acr %in% c("CHI-S", "CHI-L")),]

  #read out the peak flow and the time to peak summary files
  df_PeakSummary<-read.csv(file="Chicago_Peakflow_Summary.csv")
  Num_Stations<-dim(df_Info)[1]

  #define BoxPlt Input arrays
  Peak_BoxInp<-array()
  RNICO_Peak_BoxInp<-array()

  #make the sites info dataframe sorted based on RNICO
  df_Info_Ordered<-df_Info[order(df_Info$RNICO),]
  #now define a loop in which the box plot input arrays are filled out
  #before that, define a couple of counters for use in peak and ttp
  Peak_Counter<-0
  for(i in seq(1:Num_Stations)){
    #N1 and N2 are the number of correct peaks(or ttps) for each station

    N1<-length(df_PeakSummary[is.na(df_PeakSummary[,grepl(df_Info_Ordered$STAID[i],
                                                          colnames(df_PeakSummary))])==FALSE,
                              grepl(df_Info_Ordered$STAID[i],colnames(df_PeakSummary))])

    #now substuite the values for peak flow box plot input arrays
    Peak_BoxInp[(Peak_Counter+1):(Peak_Counter+N1)]<-df_PeakSummary[is.na(df_PeakSummary[,
                                                    grepl(df_Info_Ordered$STAID[i],
                                                    colnames(df_PeakSummary))])==FALSE,
                                                    grepl(df_Info_Ordered$STAID[i],
                                                          colnames(df_PeakSummary))]
    RNICO_Peak_BoxInp[(Peak_Counter+1):(Peak_Counter+N1)]<-df_Info_Ordered$RNICO[i]

    #and at the end update the counters
    Peak_Counter<-Peak_Counter+N1
  }

  #save the Boxplt input files for later check
  Output_peak<-data.frame(Peak_BoxInp,RNICO_Peak_BoxInp)

  #calculating avg of values
  Peak_Avgs<-array()
  Peak_Maxs<-array()
```

```
for(i in seq(1:Num_Stations)){
  Peak_Avgs[i]<-mean(Peak_BoxInp[RNICO_Peak_BoxInp==df_Info_Ordered$RNICO[i]])
  Peak_Maxs[i]<-max(Peak_BoxInp[RNICO_Peak_BoxInp==df_Info_Ordered$RNICO[i]])
}

#plotting


#setting plotting locations on boxplots
At1<-df_Info_Ordered$RNICO
At1<-100*(At1+abs(min(df_Info_Ordered$RNICO)))+1

#########################################################
##############plot for Peak flow#################
Boxplot_Peak<-boxplot(Peak_BoxInp~RNICO_Peak_BoxInp, range = 10,
                      data=Output_peak,at =At1,ylim = c(0, 3))

#Adding the Mean points of Large sites with red color and circle symbol
points(Peak_Avgs[df_Info_Ordered$Site_Acr=="CHI-L"]~At1[df_Info_Ordered$Site_Acr=="CHI-L"],
       type='p',col=2,pch=16,cex=1.4)

#Adding the Mean points of small sites with green color and triangle symbol

  points(Peak_Avgs[df_Info_Ordered$Site_Acr=="CHI-L"]~At1[df_Info_Ordered$Site_Acr=="CHI-L"],
         type='p',col=2,pch=16,cex=1.4)

  #Adding the Mean points of small sites with green color and triangle symbol
  points(Peak_Avgs[df_Info_Ordered$Site_Acr=="CHI-S"]~At1[df_Info_Ordered$Site_Acr=="CHI-S"],
         type='p',col=3,pch=17,cex=1.4)

  #Adding the Max points of small sites with green color and triangle symbol
  #make a correction (the third site has a Max of greater than 75% quantile)
  Peak_Maxs[3]=2.04
  points(Peak_Maxs[df_Info_Ordered$Site_Acr=="CHI-S"]~At1[df_Info_Ordered$Site_Acr=="CHI-S"],
         type='p',col=3,pch=1,cex=1.4)

  ######Add regression line for avg peak flow (small site)
  fit_AvgPeak<-lm(Peak_Avgs[df_Info_Ordered$Site_Acr=="CHI-S"]~
                    df_Info_Ordered$RNICO[df_Info_Ordered$Site_Acr=="CHI-S"])

  coefs_AvgPeak<-coef(fit_AvgPeak)
  b0 <- round(coefs_AvgPeak[1], 2)
  b1 <- round(coefs_AvgPeak[2], 2)
  r2 <- round(summary(fit_AvgPeak)$r.squared, 2)

 eqn_AvgPeak<- bquote(italic(y[2]) == .(b0) + .(b1)*italic(x) * "," ~~
                        r^2 == .(r2))

 #create a fake line using At1 for demnstration on the plot screen
 fit_AvgPeak_fake<-lm(Peak_Avgs[df_Info_Ordered$Site_Acr=="CHI-S"]~
                        At1[df_Info_Ordered$Site_Acr=="CHI-S"])

 abline(fit_AvgPeak_fake,lty=1,col=3)

 ######Add regression line for Max peak flow (small site)
 fit_MaxPeak<-lm(Peak_Maxs[df_Info_Ordered$Site_Acr=="CHI-S"]~
                   df_Info_Ordered$RNICO[df_Info_Ordered$Site_Acr=="CHI-S"])

 coefs_MaxPeak<-coef(fit_MaxPeak)
 b0 <- round(coefs_MaxPeak[1], 2)
 b1 <- round(coefs_MaxPeak[2], 2)
 r2 <- round(summary(fit_MaxPeak)$r.squared, 2)

 eqn_MaxPeak<- bquote(italic(y[1]) == .(b0) + .(b1)*italic(x) * "," ~~
                        r^2 == .(r2))
```

```
    #create a fake line using At1 for demnstration on the plot screen
    fit_MaxPeak_fake<-lm(Peak_Maxs[df_Info_Ordered$Site_Acr=="CHI-S"]~
                           At1[df_Info_Ordered$Site_Acr=="CHI-S"])

    abline(fit_MaxPeak_fake,lty=2,col=3)


    #and add a n average line for the large sites
    abline(h=mean(Peak_Avgs[df_Info_Ordered$Site_Acr=="CHI-L"]),lty=1,col=2)

    #now add numbers of figures on plot
    text(18,c(0.2,0.9,1.7),c(3,2,1),col=c(2,3,3),cex=1.7)

    #and add equations

    text(70,2.7,eqn_MaxPeak,col=1, cex=1.7)
    text(70,2.1,eqn_AvgPeak,col=1, cex=1.7)
    eqn_Large<- bquote(italic(y[3]) == 0.1)
    text(70,1.5,eqn_Large,col=1, cex=1.7)


    #Adding axix labels
    mtext(text="RNICO", side=1,  las=0, line=3, cex=1.7)
    mtext(text="Runoff Peakflow (mm/hr)", side=2,  las=0, line=3, cex=1.7)


  }

########$$$$$$$$$##########$$$$$$$$$$############
Chicago_Regime<-function(){

  #define duration Tresholds to divide plots into smaller/larger than that Treshold
  Duration_Tresh<-6

  #read out the catchment information file.
  df0<-read.csv(file="Chicago_SiteInfo.csv")

  Num_Stations<-dim(df0)[1]

  ###PLOT2:RNICO BS FLOW REGIME INDICES#################################
  #First for large sites with black color
  plot(df0$RNICO[df0$Site_Acr=="CHI-L"],df0$CV[df0$Site_Acr=="CHI-L"],
       ylim=c(0.1,4.5),xlim=c(-0.5,0.6),xlab="RNICO",ylab="Flow Regime Index",
       type='p',col=1,pch=16,cex.lab=1.9,cex=1.7,
       cex.axis=1.5)

  points(df0$RNICO[df0$Site_Acr=="CHI-L"],df0$RBIndex[df0$Site_Acr=="CHI-L"],
         col=1,pch=2,cex=1.7)

  #Then for small sites with green color
  points(df0$RNICO[df0$Site_Acr=="CHI-S"],df0$CV[df0$Site_Acr=="CHI-S"],

                col=3,pch=16,cex=1.7)

        points(df0$RNICO[df0$Site_Acr=="CHI-S"],df0$RBIndex[df0$Site_Acr=="CHI-S"],
                col=3,pch=2,cex=1.7)
```

```
######Add average line for RBF (large sites)#####################
abline(h=mean(df0$RBIndex[df0$Site_Acr=="CHI-L"]),lty=2,col=1,untf=TRUE)

######Add average line for CV (Large sites)#####################
abline(h=mean(df0$CV[df0$Site_Acr=="CHI-L"]),lty=1,col=1,untf=TRUE)

######Add regression line for RBF (small sites)#####################
fit_RBF<-lm(df0$RBIndex[df0$Site_Acr=="CHI-S"]~df0$RNICO[df0$Site_Acr=="CHI-S"])

coefs_RBF<-coef(fit_RBF)
b0 <- round(coefs_RBF[1], 2)
b1 <- round(coefs_RBF[2], 2)
r2 <- round(summary(fit_RBF)$r.squared, 2)

eqn_RBF_S<- bquote(italic(y[3]) == .(b0) + .(b1)*italic(x) * "," ~~
                     r^2 == .(r2))

abline(fit_RBF,lty=2,col=3,untf=TRUE)

######Add regression line for CV (Small sites)#####################
fit_CV<-lm(df0$CV[df0$Site_Acr=="CHI-S"]~df0$RNICO[df0$Site_Acr=="CHI-S"])
 coefs_CV<-coef(fit_CV)
 b0 <- round(coefs_CV[1], 2)
 b1 <- round(coefs_CV[2], 2)
 r2 <- round(summary(fit_CV)$r.squared, 2)

 eqn_CV_S<- bquote(italic(y[1]) == .(b0) + .(b1)*italic(x) * "," ~~
                     r^2 == .(r2))

 abline(fit_CV,lty=1,col=3,untf=TRUE)

   #Now add line numbers on each of them
 text(0.6,c(3,1.9,0.8,0.1),c(1,2,3,4),col=c(3,1,3,1),cex=1.7)

 #Now add equations on the chart
 text(-0.1,4.5,eqn_CV_S,col=1, cex=1.7)
 eqn_CV_L<-bquote(italic(y[2]) ==1.8)
 text(-0.1,4,eqn_CV_L,col=1, cex=1.7)
 text(-0.1,3.5,eqn_RBF_S,col=1, cex=1.7)
 eqn_RBF_L<-bquote(italic(y[4]) ==0.4)
 text(-0.1,3,eqn_RBF_L,col=1, cex=1.7)


###PLOT3:RNICO BS IMPERVIOUSNESS###################################
#First for large sites with black color

plot(df0$NLCD11_Imp[df0$Site_Acr=="CHI-L"],df0$CV[df0$Site_Acr=="CHI-L"],
     ylim=c(0.1,4.5),xlim=c(0,40),xlab="Imperviousness (%)",ylab="Flow Regime Index",
     type='p',col=1,pch=16,cex.lab=1.9,cex=1.7,cex.axis=1.5)

points(df0$NLCD11_Imp[df0$Site_Acr=="CHI-L"],df0$RBIndex[df0$Site_Acr=="CHI-L"],
       col=1,pch=2,cex=1.7)

#Then for Southern sites with green color
points(df0$NLCD11_Imp[df0$Site_Acr=="CHI-S"],df0$CV[df0$Site_Acr=="CHI-S"],
       col=3,pch=16,cex=1.7)

points(df0$NLCD11_Imp[df0$Site_Acr=="CHI-S"],df0$RBIndex[df0$Site_Acr=="CHI-S"],
       col=3,pch=2,cex=1.7)

######Add average line for RBF (large sites)#####################
abline(h=mean(df0$RBIndex[df0$Site_Acr=="CHI-L"]),lty=2,col=1,untf=TRUE)

######Add average line for CV (Large sites)#####################
abline(h=mean(df0$CV[df0$Site_Acr=="CHI-L"]),lty=1,col=1,untf=TRUE)
```

```
  ######Add regression line for RBF (Small sites)#####################
  fit_RBF<-lm(df0$RBIndex[df0$Site_Acr=="CHI-S"]~df0$NLCD11_Imp[df0$Site_Acr=="CHI-S"])

  coefs_RBF<-coef(fit_RBF)
  b0 <- round(coefs_RBF[1], 2)
  b1 <- round(coefs_RBF[2], 2)
  r2 <- round(summary(fit_RBF)$r.squared, 2)

  eqn_RBF_S<- bquote(italic(y[3]) == .(b0) + .(b1)*italic(x) * "," ~~
                       r^2 == .(r2))

  abline(fit_RBF,lty=2,col=3,untf=TRUE)

  ######Add regression line for CV (Small sites)#####################
  fit_CV<-lm(df0$CV[df0$Site_Acr=="CHI-S"]~df0$NLCD11_Imp[df0$Site_Acr=="CHI-S"])

  coefs_CV<-coef(fit_CV)
  b0 <- round(coefs_CV[1], 2)
  b1 <- round(coefs_CV[2], 2)
  r2 <- round(summary(fit_CV)$r.squared, 2)

  eqn_CV_S<- bquote(italic(y[1]) == .(b0) + .(b1)*italic(x) * "," ~~
                      r^2 == .(r2))

   abline(fit_CV,lty=1,col=3,untf=TRUE)

   #Now add line numbers on each of them
   text(2,c(1.9,1.4,1,0.1),c(1,2,3,4),col=c(3,1,3,1),cex=1.7)

   #Now add equations on the chart
   text(11,4.5,eqn_CV_S,col=1, cex=1.7)
   eqn_CV_L<-bquote(italic(y[2]) ==1.8)
   text(11,4,eqn_CV_L,col=1, cex=1.7)
   text(11,3.5,eqn_RBF_S,col=1, cex=1.7)
   eqn_RBF_L<-bquote(italic(y[4]) ==0.4)
   text(11,3,eqn_RBF_L,col=1, cex=1.7)
 }

#########$$$$$$$$$$##########$$$$$$$$$$############
Prec_Dist<-function(){

  #read out the input data
  df<-read.csv(file="precdep_Input.csv")


  #define these code to facilitate the distinguishing between 30yr and SP
  xlims<-c(4,5,2,1.5)
  ylims<-c(0.43,0.25,2,1.1)
  xLabels<-c("Total Depth (mm)","Duration (hrs)",
             "Average Intensity (mm/hr)","Maximum Intensity (mm/hr)")

  for (i in seq(1:3)){

    d1 <- density(df[,i][is.na(df[,i])==FALSE])
    d2 <- density(df[,i+4][is.na(df[,i+4])==FALSE])
    d3 <- density(df[,i+8][is.na(df[,i+8])==FALSE])
    d4 <- density(df[,i+12][is.na(df[,i+12])==FALSE])

    plot(d1,xlim=c(-0.1,xlims[i]),ylim=c(0,ylims[i]),col=1, main=NA,xlab=NA,ylab=NA, cex.axis=1.8)
    lines(d2,col=1,lty=2)
    lines(d3,col=2,lty=1)
```

```
    lines(d4,col=2,lty=2)

    mtext(text=xLabels[i], side=1, las=0, line=3, cex=1.4)

    mtext(text="Density", side=2, las=0, line=2.5, cex=1.3)

    #putting minor labels on the axis
    minor.tick(nx=5,ny=5)
  }

}

#########$$$$$$$$$$##########$$$$$$$$$$#############
Chicago_ttp<-function(){
  #read out the sites information dataframe
  df1<-read.csv(file="Chicago_SiteInfo.csv")
  df_Info<-df1[df1$Good=="Y" & (df1$Site_Acr %in% c("CHI-S", "CHI-L")),]

  #read out the peak flow and the time to peak summary files
  df_ttpSummary<-read.csv(file="Chicago_Traveltime_Summary.csv")
  Num_Stations<-dim(df_Info)[1]
  #define BoxPlt Input arrays
  ttp_BoxInp<-array()
  RNICO_ttp_BoxInp<-array()

  #make the sites info dataframe sorted based on RNICO
  df_Info_Ordered<-df_Info[order(df_Info$RNICO),]
  #now define a loop in which the box plot input arrays are filled out
  #before that, define a couple of counters for use in peak and ttp
  ttp_Counter<-0
  for(i in seq(1:Num_Stations)){
    #N2 is the number of correct peaks(or ttps) for each station
    N2<-length(df_ttpSummary[is.na(df_ttpSummary[,grepl(df_Info_Ordered$STAID[i],
                                                        colnames(df_ttpSummary))])==FALSE,
                             grepl(df_Info_Ordered$STAID[i],colnames(df_ttpSummary))])

    #and for the ttp box plot input arrays
    ttp_BoxInp[(ttp_Counter+1):(ttp_Counter+N2)]<-(df_ttpSummary[is.na(df_ttpSummary[,
                                                  grepl(df_Info_Ordered$STAID[i],
                                                  colnames(df_ttpSummary))])==FALSE,
                                                  grepl(df_Info_Ordered$STAID[i],
                                          colnames(df_ttpSummary))])/df_Info_Ordered$Longest_Flowpath_km[i]
    RNICO_ttp_BoxInp[(ttp_Counter+1):(ttp_Counter+N2)]<-df_Info_Ordered$RNICO[i]

    #and at the end update the counters
    ttp_Counter<-ttp_Counter+N2
  }

  #save the Boxplt input files for later check
  Output_ttp<-data.frame(ttp_BoxInp,RNICO_ttp_BoxInp)

  #calculating avg of values
  ttp_Avgs<-array()
  ttp_Maxs<-array()

  for(i in seq(1:Num_Stations)){
    ttp_Avgs[i]<-mean(ttp_BoxInp[RNICO_ttp_BoxInp==df_Info_Ordered$RNICO[i]])
    ttp_Maxs[i]<-max(ttp_BoxInp[RNICO_ttp_BoxInp==df_Info_Ordered$RNICO[i]])
  }

  #setting plotting locations on boxplots
  At1<-df_Info_Ordered$RNICO
  At1<-100*(At1+abs(min(df_Info_Ordered$RNICO)))+1

  ##############plot for time to peak#################
  Boxplot_ttp<-boxplot(ttp_BoxInp~RNICO_ttp_BoxInp, range = 10,
                       data=Output_ttp,at =At1,ylim = c(0, 130))
```

```
  #Adding the Mean points of Large sites with red color and circle symbol
  points(ttp_Avgs[df_Info_Ordered$Site_Acr=="CHI-L"]~At1[df_Info_Ordered$Site_Acr=="CHI-L"],
         type='p',col=2,pch=16,cex=1.4)

  #Adding the Mean points of small sites with green color and triangle symbol
  points(ttp_Avgs[df_Info_Ordered$Site_Acr=="CHI-S"]~At1[df_Info_Ordered$Site_Acr=="CHI-S"],
         type='p',col=3,pch=17,cex=1.4)

  ######Add regression line for avg ttp (small site)
  fit_Avgttp<-lm(ttp_Avgs[df_Info_Ordered$Site_Acr=="CHI-S"]~
                   df_Info_Ordered$RNICO[df_Info_Ordered$Site_Acr=="CHI-S"])

  coefs_Avgttp<-coef(fit_Avgttp)
  b0 <- round(coefs_Avgttp[1], 2)
  b1 <- round(coefs_Avgttp[2], 2)
  r2 <- round(summary(fit_Avgttp)$r.squared, 2)

  eqn_Avgttp<- bquote(italic(y[2]) == .(b0) + .(b1)*italic(x) * "," ~~
                        r^2 == .(r2))

  #create a fake line using At1 for demnstration on the plot screen
  fit_Avgttp_fake<-lm(ttp_Avgs[df_Info_Ordered$Site_Acr=="CHI-S"]~
                        At1[df_Info_Ordered$Site_Acr=="CHI-S"])

   abline(fit_Avgttp_fake,lty=1,col=3)

   #and add an average line for the large sites
   abline(h=mean(ttp_Avgs[df_Info_Ordered$Site_Acr=="CHI-L"]),lty=1,col=2)


   #now add numbers of figures on plot
   text(40,c(35,20),c(2,1),col=c(3,2),cex=1.7)

   #and add equations
   text(35,125,eqn_Avgttp,col=1, cex=1.7)
   eqn_Large<- bquote(italic(y[1]) == 13)
   text(35,115,eqn_Large,col=1, cex=1.7)

   #Adding axix labels
   mtext(text="RNICO", side=1,  las=0, line=3, cex=1.7)
   mtext(text="Normalized Time to Peak (minutes/km)", side=2,  las=0, line=3, cex=1.7)

}
```

Appendix H: R script for correlation analysis between mean runoff peak flows and different physical parameters

```
#This program reads out the information for the study sites in Paper 3 and calculates
#the correlation coef between mean runoff value and different parameters such as
#morphologica, topological, soil, land cover, and ...

setwd("C:/mott/Courses/THESIS papers/Paper3/AllCorrelationAnalysis/VarsVSPeak/CorAnalysis
InpVar_df<-read.csv("VarInpData.csv")
Varnames<-read.csv("Vars.csv")
City_Abrs<-c("Chicago","NYC", "Portland","Baltimore","SF","LA")
City_Names<-c("Chicago","New York", "Portland","Baltimore","San Fransisco","Los Angeles")

#create three matrices to save correlations coefs for AvgPeak, RBF, and CV.
AvgPeak_CorMat<-matrix(NA, length(City_Abrs),(length(Varnames)+1))
rownames(AvgPeak_CorMat)<-City_Abrs
colnames(AvgPeak_CorMat)<-c(colnames(Varnames),"NLCD11Dev")

RBF_CorMat<-AvgPeak_CorMat
CV_CorMat<-AvgPeak_CorMat

#create a loop in which correlation analysis is done.
for(i in seq(1:length(City_Abrs))){

  #First, I walk through the site information files for different cities and calculate
  #the average runoff peak flows.
 df0<-read.csv(paste(City_Abrs[i],"_SiteInfo.csv",sep=""))
 df1<-read.csv(paste(City_Abrs[i],"_Peakflow_Summary.csv",sep=""))
 #create an array to save the Calculated Avg Peak flows of different stations
 Calc_AvgPeak<-array(NA,dim(df0)[1])

 for(j in seq(1:dim(df0)[1])){
   Calc_AvgPeak[j]<-mean(df1[is.na(df1[,grepl(df0$STAID[j],colnames(df1))])==FALSE,
                             grepl(df0$STAID[j],colnames(df1))])
 }

 InpVar_df1<-InpVar_df[InpVar_df$STAID %in% df0$STAID,
                       colnames(InpVar_df) %in% colnames(Varnames)]
 attach(InpVar_df1)

 #arrane columns for the later plotting
 InpVar_df2<-data.frame(BAS_COMPACTNESS,InpVar_df1[,1:2],WATERNLCD06, DDENS_2009,
                        SLOPE_PCT,ASPECT_DEGREES, PERMAVE,CLAYAVE,SANDAVE,ARTIFPATH_PCT,
                        df0$NLCD11_Dev[df0$STAID %in% InpVar_df$STAID])

 #now calculate the correlation coeficient with differnt parameters
 AvgPeak_CorMat[i,]<-cor(Calc_AvgPeak[df0$STAID %in% InpVar_df$STAID],InpVar_df2)
 RBF_CorMat[i,]<-cor(df0$RBIndex[df0$STAID %in% InpVar_df$STAID],InpVar_df2)
 CV_CorMat[i,]<-cor(df0$CV[df0$STAID %in% InpVar_df$STAID],InpVar_df2)
}

#save correlation table
write.csv(AvgPeak_CorMat, file = "AvgPeak_CorMat.csv",row.names = TRUE)
write.csv(RBF_CorMat, file = "RBF_CorMat.csv",row.names = TRUE)
write.csv(CV_CorMat, file = "CV_CorMat.csv",row.names = TRUE)


#Plotting
pdf("correlationplots.pdf",10,27)
layout(matrix(c(1,2,3),ncol=1,byrow=TRUE),heights=c(9,9,2))

par(mar=c(10, 2, 2, 2),oma = c(10, 2, 2, 4))

Bar_Plt_Labels<-c("shape (compactness)","stream density (km/km2)","stream sinuosity",
                  "lakes/ponds (%)","dam density (# of dams/100km2)",
                  "mean catchment slope (%)","mean catchment aspect (degrees)",
                  "average permeability (in/hr)","average clay content (%)",
                  "average sand content (%)","artificial pathways (%)",
                  "land development (%)")
```

```
x1<-seq(1:12)-0.3
x2<-seq(1:12)-0.2
x3<-seq(1:12)-0.1
x4<-seq(1:12)
x5<-seq(1:12)+0.1
x6<-seq(1:12)+0.2
x0<-(x3+x4)/2
######################Plotting for avg peak flows#################
#first plot correlation values between mean  peak flow indices
plot(AvgPeak_CorMat[1,]~x1,type="h",xaxt="n",xlab=NA,ylab="r (x, mean peak flow)",lwd=3,
     cex.lab=1.5, cex.axis=2.8, cex.main=1.5, cex.sub=1.5,col=1,xlim=c(0.5,12.5),ylim=c(-1.1,1.1))

axis(1, at=x0, labels=NA, las=2,cex.axis=1.5)

lines(AvgPeak_CorMat[2,]~x2,type="h",lwd=3, cex=3, cex.lab=2,
      cex.axis=2, cex.main=2, cex.sub=2,col=2)
lines(AvgPeak_CorMat[3,]~x3,type="h",lwd=3, cex=3, cex.lab=2,
      cex.axis=2, cex.main=2, cex.sub=2,col=3)
lines(AvgPeak_CorMat[4,]~x4,type="h",lwd=3, cex=3, cex.lab=2,
      cex.axis=2, cex.main=2, cex.sub=2,col=4)
lines(AvgPeak_CorMat[5,]~x5,type="h",lwd=3, cex=3, cex.lab=2,
      cex.axis=2, cex.main=2, cex.sub=2,col=5)
lines(AvgPeak_CorMat[6,]~x6,type="h",lwd=3, cex=3, cex.lab=2,
      cex.axis=2, cex.main=2, cex.sub=2,col=6)

#adding information on the plot
text(c(0.5,3.5,6.5,9,11.5),-0.75,c("Morphology","Hydraulics","Topography","Soil","Urbanization"),
     cex=2.8,srt=90)

abline(h=c(0,1,-1),lty=c(1,2,2))
abline(v=c(1.5,5.5,7.5,10.5),lty=3)

######################Plotting for flashiness#################
plot(RBF_CorMat[1,]~x1,type="h",xaxt="n",xlab=NA,ylab="r (x, RBF)",lwd=3,
     cex.lab=1.5, cex.axis=2.8, cex.main=1.5, cex.sub=1.5,col=1,xlim=c(0.5,12.5),ylim=c(-1.1,1.1))

axis(1, at=x0, labels=NA, las=2,cex.axis=1.5)

lines(RBF_CorMat[2,]~x2,type="h",lwd=3, cex=3, cex.lab=2,
      cex.axis=2, cex.main=2, cex.sub=2,col=2)
lines(RBF_CorMat[3,]~x3,type="h",lwd=3, cex=3, cex.lab=2,
      cex.axis=2, cex.main=2, cex.sub=2,col=3)
lines(RBF_CorMat[4,]~x4,type="h",lwd=3, cex=3, cex.lab=2,
      cex.axis=2, cex.main=2, cex.sub=2,col=4)
lines(RBF_CorMat[5,]~x5,type="h",lwd=3, cex=3, cex.lab=2,
      cex.axis=2, cex.main=2, cex.sub=2,col=5)
lines(RBF_CorMat[6,]~x6,type="h",lwd=3, cex=3, cex.lab=2,
      cex.axis=2, cex.main=2, cex.sub=2,col=6)


#adding information on the plot
text(c(0.5,3.5,6.5,9.5,11.5),-0.75,c("Morphology","Hydraulics","Topography","Soil","Urbanization"),
     cex=2.8,srt=90)

abline(h=c(0,1,-1),lty=c(1,2,2))
abline(v=c(1.5,5.5,7.5,10.5),lty=3)


#after all plots are finished, a plot.new is opened to plot the legend at the last row.
par(mai=c(0,0,0,0))
plot.new()
legend(x="center",ncol=3,bty="n",City_Names,lty=1,lwd=6,col=seq(1:6),cex=2.8)

dev.off()
```

Appendix I: R script for plotting flood hydrographs of four NYC study catchments

```
setwd("C:/mott/Courses/research/PROPOSAL/Analysis/Extreme_Event_cities_analysis/MULTICITY_PLOTS/New folder

#call this function to sepperate runoff from discharge later on
library("EcoHydRology")

#these should bedefined by user:
#input the city name group of interest (e.g. NYCG1, ...)
City_Name<-"NYCG2"
#input catchment area
Catch_Area_m2<-2.59e+6*c(7.82,48.4)
#input event #s that needs to be plotted(minimum of 2
#and maximum of 4 events are allowed).
Event_Numbers<-c(4,11,24,50)
#input precipitation file name:
Prec_file_name<-"286026"
#input the two USGS gages of interst,
USGS_gages_Numbers<-c(01389550,01403900)
##########READING PRECIPITATION (df0 & df1)##############
#reading out the precipitation records,
df0<-read.csv(file=paste(Prec_file_name,".csv",sep=""))
attach(df0)
PREC_df0<-HPCP[HPCP!=999.99 & HPCP!=0]
date_df0<-as.POSIXct(DATE[HPCP!=999.99 & HPCP!=0], format="%Y%m%d %H:%M", tz="EST")

#reading the precipitation summary file.
df1<-read.csv(file=paste(City_Name,"_PREC_Events.csv",sep=""))

#setting the precipitation summary start and end timedates
PREC_Start<-as.POSIXct(df1$prec_Start, format="%m/%d/%Y %H:%M", tz="EST")
PREC_End<-as.POSIXct(df1$prec_End, format="%m/%d/%Y %H:%M", tz="EST")


##########READING DISCHARGE (df2 & df3)##############
#USGS discharge data files (df2 is for the small and df3 is for the large catchment)
df2<-read.csv(file=paste("0",USGS_gages_Numbers[1],".csv",sep=""))
df3<-read.csv(file=paste("0",USGS_gages_Numbers[2],".csv",sep=""))

#and their dates,
date_df2<-as.POSIXct(df2[,3], format="%m/%d/%Y %H:%M", tz="EST")
date_df3<-as.POSIXct(df3[,3], format="%m/%d/%Y %H:%M", tz="EST")

##########PLOTTING##############
pdf("Hydrographs.pdf",20,14)
#set the plot screen based on the number of events defined by the user
Plot_Screen_Set<-c(2,1)
if(length(Event_Numbers)==4){
  Plot_Screen_Set<-c(2,2)
}
par(mar=c(2, 2, 2, 2), mfrow=Plot_Screen_Set,
    oma = c(4, 4, 4, 4))

#The purpose is to compare the hydrographs of a small
#(df2 or 01389550) and a large (df3 or 01381800) catchment
#for the two events (or four based on Event_Numbers).

#these setting values were found by try and error (for precipitation plots or axis 4)
Label_At_End<-c(10,8,40,25)
Label_At_Step<-c(2,2,10,5)


for (i in seq(1:length(Event_Numbers))){

  j<-Event_Numbers[i]
```

```
  #First, event dates are created (df0 is for precipitation records and df2, df3 are discharge),
  EVENT_DATES_df0<-date_df0[(date_df0>=PREC_Start[j]) & (date_df0<= PREC_End[j])]
  EVENT_DATES_df2<-date_df2[(date_df2>=PREC_Start[j]) & (date_df2< (PREC_End[j]+5*3600))]
  EVENT_DATES_df3<-date_df3[(date_df3>=PREC_Start[j]) & (date_df3< (PREC_End[j]+5*3600))]


  #make a dataframe of the precipitaton and discharge values over the event period.
  EVENT_PREC_df0<-PREC_df0[(date_df0>=(PREC_Start[j])) & (date_df0<= PREC_End[j])]
  EVENT_DISCH_df2<-df2[,5][(date_df2>=PREC_Start[j]) & (date_df2< (PREC_End[j]+5*3600))]
  EVENT_DISCH_df3<-df3[,5][(date_df3>=PREC_Start[j]) & (date_df3< (PREC_End[j]+5*3600))]


  #calculating runoff,
  RUNOFF_df2<-0.028316847*3600*1/Catch_Area_m2[1]*BaseflowSeparation(EVENT_DISCH_df2,
                                                                     filter_parameter = 0.925,
                                                                     passes = 3)[,2]
  RUNOFF_df3<-0.028316847*3600*1/Catch_Area_m2[2]*BaseflowSeparation(EVENT_DISCH_df3,
                                                                     filter_parameter = 0.925,
                                                                     passes = 3)[,2]

#Initiating plot with df2 (small catchment),
  plot(EVENT_DATES_df2,RUNOFF_df2,type="l",col=1,cex.lab=1.5, cex.axis=1.3, cex.main=1.5,
       cex.sub=1.5,ylim=c(0,1.5*max(RUNOFF_df2)))

#adding df3 (large cathment),
  lines(EVENT_DATES_df3,RUNOFF_df3,col=2)


#adding axis titles. write it on only first and 3rd plot (for plot's beauty)
  if(i %in% c(1,3)){
    mtext(text="Runoff (mm/hr)", side=2,  las=0, line=3, cex=1.5)
  }


  |

#adding chart titles. It is placed on the two third of the precipitation duration
#from the begining of the event.

text(EVENT_DATES_df2[1]+3/4*3600*df1[j,6],0.7*max(RUNOFF_df2),
       paste("Rainfall depth=", round(df1$prec_Depths[j],1),"cm","\nEvent date:",
             substr(PREC_Start[j],1,10)),
             cex=1.5)

#adding precipitatin plot on the second axis
par(new=TRUE)
plot(-25.4*EVENT_PREC_df0~EVENT_DATES_df0, type='h',xaxt="n",yaxt="n",xlab="",


     ylim=c(-25.4*3*max(EVENT_PREC_df0),0),col=4,pch=15,cex=1.5)
 axis(4,at=seq(-Label_At_End[i],0,Label_At_Step[i]),
     labels=as.character(rev(seq(0,Label_At_End[i],Label_At_Step[i]))), cex.axis=1.3)
 #axis(4, cex.axis=1.3)

 #i only put axis name for plots 2 and 4 for the beauty.
 if(i %in% c(2,4)){
   mtext(text="Precipitation (mm)", side=4,  las=0, line=3, cex=1.5)

 }

 #now, adding a legend for the plot (for only the first plot)
  if (i==2){
   legend("topright",c(paste("Catchment 7 (A=",round(Catch_Area_m2[1]/10^6,0),"km2)"),
                       paste("Catchment 9 (A=",round(Catch_Area_m2[2]/10^6,0),"km2)"),
                       "Precipitation (mm)"),col=c(1,2,4),lty=c(1,1,0),bty="n",
          pch=c(NA,NA,15),pt.cex=1.5,cex=1.5)
    }


 }

 dev.off()
```

Appendix J: R script for importing GEFS/R precipitation and temperature ensemble files from NETCDF format to Excel

```
#in this file, ensembles of Precipitation and Temperature for two historical
#events that are already donwloaded from
#   http://www.esrl.noaa.gov/psd/forecasts/reforecast2/download.html
#are read out from netCDF file. Then they are plotted and a csv file is created.

#########################LIBRARY AND DIRECTORY#############################
setwd("C:/mott/Courses/THESIS papers/Paper2/analysis/14/PEC_LT_01389550/Step2-GEFSR checking/Read out Prec


library("ncdf4")
library("lubridate")
library("Hmisc")

#defining start and end dates.
Start_date<-as.POSIXct(c("08/24/2011 00:00"),format="%m/%d/%Y %H:%M", tz="EST")
End_date<-as.POSIXct(c("08/31/2011 00:00"),format="%m/%d/%Y %H:%M", tz="EST")

#create a sequence of dates
Ev_Dates<-seq(Start_date, End_date, 3*3600)

#Enter netCDF4 file name here,
netCDF_name<-"apcp_sfc_gaussian_all_20110824_20110830_baba8qjnDx.nc"


#Read Precipitation ensemble members (the first colum is the Control member)
All_P<-nc_open(netCDF_name, write=FALSE, readunlim=TRUE, verbose=FALSE,
               auto_GMT=TRUE, suppress_dimvals=FALSE )

All_P<-ncvar_get(All_P, varid=NA, start=NA, count=NA, verbose=FALSE,
                 signedbyte=TRUE, collapse_degen=TRUE)

#Number of event days are exxtracted from open netCDF arrays
Num_Ev_Days<-dim(All_P)[3]

#create matrices to save  P ensembles in it
Ev_mtx_P<-matrix(NA,length(Ev_Dates),(dim(All_P)[2]))
colnames(Ev_mtx_P)<-c("Ens_Control",paste("Ens_",seq(1:10),sep=""))

#using a row counter for floowing the matrix rows while filling it up with ensembles
row_counter=0
for (i in seq(1:Num_Ev_Days)){
  #the first prediction in all ensembles is 0. Then the first line starts from
  #zero. But, for the next days, this zero is not used because the forecast of the
  #previous day at t=24 hrs is used instead. Therefore, an if-else is used here.
  if(i==1){
    #the first day has 9 elements for times 0, 3, ..., 24
    Ev_mtx_P[seq(1,9),]<-All_P[,,i]
  }

  else{
    #but next days has 8 elements iuncluding 3, 6, ..., 24
    Ev_mtx_P[seq((10+(i-2)*8),(17+(i-2)*8)),]<-All_P[2:dim(All_P)[1],,i]

  }

}

 ########################OUTPUT CREATION#################################
 #write results in a csv file
 X1<-paste(day(Ev_Dates),"/",month(Ev_Dates),"/",year(Ev_Dates),sep="")
 X2<-paste(hour(Ev_Dates),":00",sep="")
 X3<-paste(X1,X2)
 output1<-data.frame(X3,Ev_mtx_P)
 colnames(output1)<-c("date",paste(colnames(Ev_mtx_P),"_P_mm",sep=""))
 write.csv(output1,"GEFSR_Prec_mm.csv",row.names = FALSE)
```

Appendix K: R script for correcting stream-flow discharge data of the USGS gages

```
library("lubridate")
library(zoo)
Station_ID<-"01389550-PECLT"
#PART A: DATA READ OUT#####################################
#read out the data
#Before everything, make sure that
#1)-the first date has Hour=1 and the last date is a fraction of 3 (e.g. 3,6,9,12,15,18,21,0). because
#I later want to aggregate hours to three as follows:
#1,2,3---4,5,6---7,8,9---10,11,12---13,14,15---16,17,18---19,20,21---22,23,00
#2)- there is no none-numeric in values in the discharge column of excel input file (e.g. ICE)
df1<-read.csv(file=paste(Station_ID,".csv",sep=""))
#read out dates. I use EST time which is not true for Illinoise River, but doesn't matter
date_USGS<-as.POSIXct(df1[,3],format="%m/%d/%Y %H:%M", tz="EST")

#get rid of the duplicated records here before getting error at zoo!
df1<-df1[!duplicated(date_USGS),]
date_USGS<-date_USGS[!duplicated(date_USGS)]
#calculating the length of date USGS
l_USGS<-length(date_USGS)

#PART B: FILLING MISSED OBS#####################################
dates_desired<-seq(date_USGS[4],date_USGS[l_USGS],by="1 hour")
length_desired<-length(dates_desired)

#Now, i'll only include the measurement on exact hours
df11<-df1[date_USGS %in% dates_desired,]
date_USGS<-date_USGS[date_USGS %in% dates_desired]

#length desired =! The length of data file.
#tehreofore ,a correction in zoo is needed!
mtx1 <- zoo(df11[,5],date_USGS)
# !!$$$$!!
#mtx11 <- zoo(df11[,7],date_USGS)


zoo_merged1 <- merge(mtx1,zoo(,seq(start(mtx1),end(mtx1),by="1 hour")), all=TRUE)
# !!$$$$!!
#zoo_merged11 <- merge(mtx11,zoo(,seq(start(mtx11),end(mtx11),by="1 hour")), all=TRUE)


zoo_merged1 <- merge(mtx1,zoo(,dates_desired), all=TRUE)
# !!$$$$!!
#zoo_merged11 <- merge(mtx11,zoo(,dates_desired), all=TRUE)


mtx2<-na.approx(zoo_merged1, na.rm = FALSE)

# !!$$$$!!
#mtx22<-na.approx(zoo_merged11, na.rm = FALSE)

#converting zoo ts to dataframe
#note that zoo destroys dates. Then we only save its values.
df2 <- as.data.frame(as.numeric(mtx2[,2]))

# !!$$$$!!
#df22 <- as.data.frame(as.numeric(mtx22[,2]))


#now write datasets into the csv files for use in SAC-SMA model
#First, arrange dates in a proper way for reading in RS_MINERVE (SAC-SMA)
X1<-paste(day(dates_desired),"/",month(dates_desired),"/",year(dates_desired),sep="")
X2<-paste(hour(dates_desired),":00",sep="")
X3<-paste(X1,X2)

Q<-0.028316847*df2

# !!$$$$!!
#Prec_USGS<-25.4*df22
```

```
#Second, create outputs
output1<-data.frame(X3,Q)

# !!$$$$!!
#output11<-data.frame(X3,Prec_USGS)


colnames(output1)<-c("date","Q_cms")

# !!$$$$!!
#colnames(output11)<-c("date","Prec_mm")


write.csv(output1,paste(Station_ID,"_Q_USGS_hourly_cms.csv",sep=""),row.names = FALSE)

# !!$$$$!!
#write.csv(output11,paste(Station_ID,"_Prec_USGS_hourly_cms.csv",sep=""),row.names = FALSE)

#PART C: AGGREGATING Q FROM 1HR TO 3HR(for use in ANFIS)##########################
dates_desired_Agg3hr<-seq(dates_desired[3],dates_desired[length_desired],by="3 hour")
Q_Agg3hr<-array(0,length(dates_desired_Agg3hr))

# !!$$$$!!
#PrecUSGS_Agg3hr<-array(0,length(dates_desired_Agg3hr))

for(i in seq(1:length_desired)){
  if(i%%3==0){
    #0.028316847 for converting cfs to cms
    Q_Agg3hr[i/3]<-mean(Q[(i-2):i,1])

    # !!$$$$!!
    #PrecUSGS_Agg3hr[i/3]<-sum(Prec_USGS[(i-2):i,1])

  }

}

#arranging dates in SAC-SMA format just in case! (i think I use this aggregated
#data only for ANFIS)
X1<-paste(day(dates_desired_Agg3hr),"/",month(dates_desired_Agg3hr),"/",year(dates_desired_Agg3hr),sep="")
X2<-paste(hour(dates_desired_Agg3hr),":00",sep="")
X3<-paste(X1,X2)

#Second, create outputs
output2<-data.frame(X3,Q_Agg3hr)

# !!$$$$!!
#output22<-data.frame(X3,PrecUSGS_Agg3hr)

colnames(output2)<-c("date","Q_cms")

# !!$$$$!!
#colnames(output22)<-c("date","Prec_mm")

write.csv(output2,paste(Station_ID,"_Q_USGS_Agg3hr_cms.csv",sep=""),row.names = FALSE)

# !!$$$$!!
#write.csv(output22,paste(Station_ID,"_Prec_USGS_Agg3hr_cms.csv",sep=""),row.names = FALSE)
```

Appendix L: R script for NLDAS2 precipitation and temperature data manipulation for calibrating/validating flood forecasting models

```
library("lubridate")
library(zoo)
Station_ID<-"X406-Y127"

#PART A: TEMPERATURE AT 2 M#####################################
df_Temp2mhrly<-read.csv(file=paste(Station_ID,"_Temp2mhrly.csv",sep=""))
df_Temp2mhrly<-df_Temp2mhrly[!duplicated(df_Temp2mhrly[,1]),]

#read out dates
date_Temp2mhrly<-as.POSIXct(df_Temp2mhrly[,1],format="%m/%d/%Y %H:%M", tz="EST")

#calculating the length of date
l_Temp2mhrly<-length(date_Temp2mhrly)

#and the desired ones
dates_desired<-seq(date_Temp2mhrly[1],date_Temp2mhrly[l_Temp2mhrly],by="1 hour")
length_desired<-length(dates_desired)

#using zoo to fill in the blanks
mtx1 <- zoo(df_Temp2mhrly[,2],date_Temp2mhrly)
zoo_merged <- merge(mtx1,zoo(,seq(start(mtx1),end(mtx1),by="1 hour")), all=TRUE)
mtx2<-na.approx(zoo_merged, na.rm = FALSE)

#converting zoo ts to dataframe
#note that zoo destroys dates. Then we only save its values.
df2 <- as.data.frame(as.numeric(mtx2[,2]))

#Save hourly temp dataset (in C) before aggregating
Temp2mhrly<-df2-273.15

#Aggregating the dataset
dates_desired_Agg3hr<-seq(date_Temp2mhrly[3],date_Temp2mhrly[l_Temp2mhrly],by="3 hour")
Temp2mhrly_Agg3hr<-array(0,length(dates_desired_Agg3hr))

for(i in seq(1:length_desired)){
  if(i%%3==0){
    #-273.15 is to convert from Kelvin to C
    Temp2mhrly_Agg3hr[i/3]<-mean(df2[(i-2):i,1])-273.15
  }

}
####################
####################
####################
#PART B: HOURLY PRECIPITATION#####################################
df_PrecHrly<-df_PrecHrly[!duplicated(df_PrecHrly[,1]),]

#read out dates
date_PrecHrly<-as.POSIXct(df_PrecHrly[,1],format="%m/%d/%Y %H:%M", tz="EST")

#calculating the length of date
l_PrecHrly<-length(date_PrecHrly)

#and the desired ones
dates_desired<-seq(date_PrecHrly[1],date_PrecHrly[l_PrecHrly],by="1 hour")
length_desired<-length(dates_desired)

#using zoo to fill in the blanks
mtx1 <- zoo(df_PrecHrly[,2],date_PrecHrly)
zoo_merged <- merge(mtx1,zoo(,seq(start(mtx1),end(mtx1),by="1 hour")), all=TRUE)

zoo_merged[is.na(zoo_merged)]<-0

#converting zoo ts to dataframe
#note that zoo destroys dates. Then we only save its values.
df2 <-as.data.frame(as.numeric(zoo_merged[,2]))
```

```
#Save total hourly Prec dataset
PrecHrly<-df2
#sepperate liquid and snow precipitation based on temp (> or < zero)
LiqPrecHrly<-PrecHrly
SnowPrecHrly<-PrecHrly

LiqPrecHrly[Temp2mhrly<0]<-0
SnowPrecHrly[Temp2mhrly>0]<-0


}
####################
####################
####################
#PART D: WRITING DATASETS AS A CSV FILE#####################################
#First, arrange dates in a proper way for reading in RS_MINERVE (SAC-SMA)
X1<-paste(day(dates_desired_Agg3hr),"/",month(dates_desired_Agg3hr),"/",year(dates_desired_Agg3hr),sep="")
X2<-paste(hour(dates_desired_Agg3hr),":00",sep="")
X3<-paste(X1,X2)

#Second, create outputs
output1<-data.frame(X3,PrecHrly_Agg3hr,LiqPrecHrly_Agg3hr,SnowPrecHrly_Agg3hr,
                    Temp2mhrly_Agg3hr)
colnames(output1)<-c("Dates","Total Prec (mmp3hr)","Liquid Prec (mmp3hr)",
                     "Snowfall Prec (mmp3hr)","Temp (C)")

write.csv(output1,paste(Station_ID,"_Met_Agg3hr.csv",sep=""),row.names = FALSE)

#%%%%%%%%%%%%%
#same story for hourly datasets

#write a CSV for the hourly dataset (for use in SAC-SMA)
#First, arrange dates in a proper way for reading in RS_MINERVE (SAC-SMA)

X11<-paste(day(dates_desired),"/",month(dates_desired),"/",year(dates_desired),sep="")
X22<-paste(hour(dates_desired),":00",sep="")
X33<-paste(X11,X22)

#Second, create outputs
output2<-data.frame(X33,PrecHrly,LiqPrecHrly,SnowPrecHrly,Temp2mhrly)
colnames(output2)<-c("Dates","Total Prec (mmphr)","Liquid Prec (mmphr)",
                     "Snowfall Prec (mmphr)","Temp (C)")

write.csv(output2,paste(Station_ID,"_Met_hourly.csv",sep=""),row.names = FALSE)
```

Appendix M: R script for finding periods of missing discharge records for study

USGS gages

```
library("lubridate")

USGS_Station_ID<-"01389550-PECLT"
Radar_ID<-"X406-Y127_Met_hourly"
#PART A: DATA READ OUT#####################################
df1<-read.csv(file=paste(USGS_Station_ID,".csv",sep=""))
df2<-read.csv(file=paste(Radar_ID,".csv",sep=""))

#read out dates. I use EST time which is not true for Illinoise River, but doesn't matter
date_USGS<-as.POSIXct(df1[,3],format="%m/%d/%Y %H:%M", tz="EST")
date_NOAA<-as.POSIXct(df2[,1],format="%d/%m/%Y %H:%M", tz="EST")

#calculating the length of date USGS
l_USGS<-length(date_USGS)
l_NOAA<-length(date_NOAA)

#############USGS DATA ANALYSIS (FINDING MISSING Q PERIODS)###################
#Create arrays with undefined number of rows to save start
#Also, a counter is used to keep track of the number of Start_Ind row number
Start_Ind<-array()
Counter<-1
for(i in seq(98658,(l_USGS-1))){
  if(as.numeric(difftime(date_USGS[i+1],date_USGS[i],units ="hours"))>5){



    print(i)
    Start_Ind[Counter]<-i
    Counter<-Counter+1
  }
}
#Now create Date datasets from indices
Start_Miss_Dates<-date_USGS[Start_Ind]
End_Miss_Dates<-date_USGS[Start_Ind+1]
Length_Miss_Period<-as.numeric(difftime(End_Miss_Dates,Start_Miss_Dates,units ="days"))

#PART B: NOAA DATA ANALYSIS (FINDING PREC AMOUNT IN MISSING PERIODS)#####################################
#Now I calculate the amount of precipitation fell in the missed period
#this will help me to decide whether or not this period is important.
Prec_Amounts<-array(0,length(Start_Miss_Dates))
for(i in seq(1:length(Prec_Amounts))){

  Prec_Amounts[i]<-sum(as.numeric(df2[,2][date_NOAA>Start_Miss_Dates[i] & date_NOAA<End_Miss_Dates[i]]))
}


#PART C: OUTPUT CREATION#####################################
#create outputs
output<-data.frame(Start_Miss_Dates,End_Miss_Dates,Length_Miss_Period,Prec_Amounts)
colnames(output)<-c("Start", "End", "Length of missing period (days)", "Prec amount (mm)")
write.csv(output,paste(USGS_Station_ID,"_Missing_USGS_Periods.csv",sep=""),row.names = FALSE)
```

Appendix N: R script for generating spaghetti plots

```
library("Hmisc")

#########Datasets Readout & User defined parameters###########
#introduce lead times
Lead_times<-c(3,6,9,24)

#read out the site info
df_Site_Info<-read.csv(file="Sites_Info.csv")
#read some useful info from the sit_info file.
Site_Abb_Name<-df_Site_Info[,3]
Site_Maj_Fl_Thresh<-df_Site_Info[,9]
YMAX<-df_Site_Info[,10]
Site_Area_m2<-10^6*df_Site_Info[,6]
#define start and end indices for plots with different lead times
Col_Start_Ind<-c(3,15,27,39)
Col_End_Ind<-c(13,25,37,49)

#########Plotting###########
#Setting Plot x axis date labels
Real_Date_Labels<-as.POSIXct(c("28/08/2011 00:00", "29/08/2011 00:00"),
                             format="%d/%m/%Y %H:%M", tz="EST")
My_Date_Labels<-c("Aug 28","Aug 29")

Real_Date_Labels2<-as.POSIXct(c("24/09/2011 00:00","25/09/2011 00:00"),
                              format="%d/%m/%Y %H:%M", tz="EST")
My_Date_Labels2<-c("Sep 24","Sep 25")

#define the location of labels on the two rows of plots
Label_X_Loc<-c(7,12)
Label_Y_Loc_Coef<-c(0.4,0.45)
pdf("Models_Spag_Plots.pdf",16,11)
layout(matrix(c(seq(1,8),rep(9,4)),ncol=4,byrow=TRUE),heights=c(4,4,1))

for(i in seq(1:2)){
  #first figure out the plot date labels
  if(i==2){
    My_Date_Labels<-My_Date_Labels2
    Real_Date_Labels<-Real_Date_Labels2
  }

  #read out the SAC and ANFIS ensembles for the corresponding site
  df0_SAC<-read.csv(file=paste(Site_Abb_Name[i],"_Smooth_SAC.csv",sep=""))
  df0_ANFIS<-read.csv(file=paste(Site_Abb_Name[i],"_Smooth_ANFIS.csv",sep=""))
  df0_Prec<-read.csv(file=paste(Site_Abb_Name[i],"_Phase3_GEFSR_Prec_mm.csv",sep=""))
  Obs_Prec_mm<-df0_Prec[,14]
  Obs_Q_cms<-Site_Area_m2[i]*1/3/3600/1000*df0_Prec[,15]
  Dates<-as.POSIXct(df0_Prec[,1],format="%d/%m/%Y %H:%M", tz="EST")

  for(j in seq(1:length(Lead_times))){
    #first sepperate the deired ensembles
    df1_SAC<-df0_SAC[,Col_Start_Ind[j]:Col_End_Ind[j]]
    df1_ANFIS<-df0_ANFIS[,Col_Start_Ind[j]:Col_End_Ind[j]]

    #plot ensmebles one by one
    for(k in seq(1:11)){

      if(k==1){
        #start with plot command
        par(mai=c(0.6,0.65,0.6,0.65))
        plot(df1_SAC[,1]~Dates,xlab="",ylab="",xaxt = "n",ylim=c(0,YMAX[i]),
             type='l',col="grey",cex.axis=1.8, cex.main=1.8, cex.sub=1.5)
```

```
      lines(df1_ANFIS[,1]~Dates,col="red",lty=1,cex=1.7)
      axis(1, at=Real_Date_Labels, labels=My_Date_Labels,cex.axis=1.8)

    }

    else{
      lines(df1_SAC[,k]~Dates,col="grey",lty=1,cex=1.7)
      lines(df1_ANFIS[,k]~Dates,col="red",lty=1,cex=1.7)

    }

  #end of k loop
  }

  #Adding Observed Q line
  lines(Obs_Q_cms~Dates,col=1,lty=2,cex=1.7)

  #adding minor ticks and y axis title
  minor.tick(nx=1,ny=5)

  #Adding legend for Y axis
  if(j==1){
    mtext("Discharge (cms)", side=2,  las=0, line=3, cex=1.5)


  }

  #Adding plot labels
  text(Dates[Label_X_Loc[i]],Label_Y_Loc_Coef[i]*YMAX[i],paste("lead time=",Lead_times[j],"hrs"),cex=1.6)

  #Adding Major Flood Threshold Line (if it is available)

  if(i==1 & is.na(df_Site_Info[i,9])==FALSE){
    abline(h = df_Site_Info[i,9], col = 2, lty = 2)
  }

  #####adding precipitatin plot on the fourth axis
  par(new=TRUE)
  ####first add the observed precipitation
  plot(-Obs_Prec_mm~Dates, type='l',xaxt="n",yaxt="n",xlab="",ylab=NA,ylim=c(-3*max(Obs_Prec_mm),0),
       col="dark blue",cex=1.8)
  axis(4,at=seq(-60,0,10),labels=as.character(rev(seq(0,60,10))), cex.axis=1.8)

  #now add the precipitation forecast ensembles
  for(t in seq(3,12)){
    lines(-df0_Prec[,t]~Dates, type='l',xaxt="n",yaxt="n",xlab="",ylab=NA,
          col="light blue",cex=1.8)
  #End of t loop
  }
   #i only put axis name for plots 2 and 4 for the beauty.
   if(j==4){
     mtext(text="Precipitation (mm)", side=4,  las=0, line=3, cex=1.5)
   }

 #End of j loop
 }

#End of i loop
}

#after all plots are finished, a plot.new is opened to plot the legend at the last row.
par(mai=c(0,0,0,0))
plot.new()
legend(x="center",ncol=3,c("SAC-SMA","ANFIS","Obs. Q","Obs. P", "GEFS/R P members",
                           "Major Flood Threshold"),lty=c(1,1,2,1,1,2),
       col=c("grey","red",1,"dark blue","light blue","red"),cex=2.2)

dev.off()
```

Appendix O: R script for input data manipulation for the ANFIS model

```
library("hydromad")
library("zoo")
library("lubridate")

#"USER CHANGE"###### Enter info from previous steps (Calibration means Training)
City_Abb_Name<-"SAD"
Calib_Win<-c("2007-10-01","2011-08-27")

#Are your Q in M3/S (If you have already make this convrsion from m3/s to mm in Excel then enter No)
is_cms_Unit<-"Yes"

#if you answer is Yes, make sure to correct the catchemt Area below
Catch_Area_m2<-1.4608e+8

###################General Data Inputs#################
Calib_Win_Dates<-as.POSIXct(Calib_Win,format="%Y-%m-%d", tz="EST")
#MET data also include the observed Q. All valuea are in  mm.
df_MET<-read.csv(file=paste(City_Abb_Name,"_Phase3_3hrMET_Inps.csv",sep=""))
Date_MET<-as.POSIXct(df_MET[,1],format="%d/%m/%Y %H:%M", tz="EST")

####Correct Q units if they are in m3/s unit######
if (is_cms_Unit=="Yes"){
  df_MET$Q<-3*3600*1000/Catch_Area_m2*df_MET$Q
}
##########

df_Ens<-read.csv(file=paste(City_Abb_Name,"_Phase3_GEFSR_Prec_mm.csv",sep=""))
Date_Ens<-as.POSIXct(df_Ens[,1],format="%d/%m/%Y %H:%M", tz="EST")
df_Forecasted_Ens<-read.csv(file=paste(City_Abb_Name,"_SAC_Forecasted_Ensembles.csv",sep=""))

# I also need to run the calibrated SAC model
#First,create dates for the training reference dataset
Date_Train<-Date_MET[Date_MET>=Calib_Win_Dates[1] & Date_MET<=Calib_Win_Dates[2]]
x<- zoo(df_MET[(Date_MET %in% Date_Train),2:4],Date_Train)

#"USER CHANGE"###### Second, paste the final calibrated model parameters from step 5 here.
#(from file Model_Summary.txt)
fitx3<-hydromad(DATA = x, tau_s = 35.7374, tau_q = 3.73065, v_s = 0.0159433, pctim = 0.165,
                uztwm = 11.5078, uzfwm = 150, uzk = 0.248567, adimp = 0, zperc = 250, rexp = 5,
                sma = "sacramento", routing = "expuh", lztwm = 335.817, lzfsm = 74.0133,
                lzfpm = 412.756, lzsk = 0.25, lzpk = 0.00262689, pfree = 0.464728)

###################STEP1: TRAINING INPs#################
#Training inputs includes the Accumulated Prec of 3 and 6  and antecedent discharge
#Pacc3 hrs is already exists in the input file. Thefore, the 6 acc are calculated

#I create a reference matrix for Training period inputs:
Nrow1<-dim(df_MET[(Date_MET %in% Date_Train),])[1]
Ncol1<-8
Cailb_Inp_Ref_mtx<-matrix(NA,Nrow1,Ncol1)
colnames(Cailb_Inp_Ref_mtx)<-c("ObsQ_mm","Qt-3hrs_mm","Qt-6hrs_mm","Qt-9hrs_mm","Qt-24hrs_mm",
                               "AccP3hrs_mm","AccP6hrs_mm","QSim_SAC")

#Second, fill out the known columns (e.g. Q Obs and Acc3hrsP which is the
#original aggregated 3 hrs P)
Cailb_Inp_Ref_mtx[,1]<-df_MET[Date_MET %in% Date_Train,3]
Cailb_Inp_Ref_mtx[,6]<-df_MET[Date_MET %in% Date_Train,2]
#Last column is the SAC sma simulated Q values.
Cailb_Inp_Ref_mtx[,8]<-coredata(predict(fitx3,x))


#Column 2,3,4,5 Qt-3 to t-24:
Cailb_Inp_Ref_mtx[2:dim(Cailb_Inp_Ref_mtx)[1],2]<-Cailb_Inp_Ref_mtx[1:(dim(Cailb_Inp_Ref_mtx)[1]-1),1]
Cailb_Inp_Ref_mtx[3:dim(Cailb_Inp_Ref_mtx)[1],3]<-Cailb_Inp_Ref_mtx[1:(dim(Cailb_Inp_Ref_mtx)[1]-2),1]
Cailb_Inp_Ref_mtx[4:dim(Cailb_Inp_Ref_mtx)[1],4]<-Cailb_Inp_Ref_mtx[1:(dim(Cailb_Inp_Ref_mtx)[1]-3),1]
Cailb_Inp_Ref_mtx[9:dim(Cailb_Inp_Ref_mtx)[1],5]<-Cailb_Inp_Ref_mtx[1:(dim(Cailb_Inp_Ref_mtx)[1]-8),1]

#to fill out the 6 hour accumulated prec values I need to use a loop
for (i in seq(1:dim(Cailb_Inp_Ref_mtx)[1])){
```

```
 if(i>=2){
   Cailb_Inp_Ref_mtx[i,7]<-sum(Cailb_Inp_Ref_mtx[((i-1):i),6])
 }
}

#Now write the Training Ref file and create required inputs for ANFIS (for different lead times)
Out_Train_Ref<-data.frame(Date_Train,Cailb_Inp_Ref_mtx)
#and create a csv file containing this source
write.csv(Out_Train_Ref,paste(City_Abb_Name,"_ANFIS_Train_Inp_Reference.csv",sep=""),row.names=FALSE)

#WRITING ANFIS INPUTS (WITHOUT SAC): write Training file for different lead times
write.csv(Out_Train_Ref[(2:dim(Out_Train_Ref)[1]),c(1,3,7,8)],
          paste(City_Abb_Name,"_ANFIS_Train_Inp_3hrsLead.csv",sep=""),row.names=FALSE)
write.csv(Out_Train_Ref[(3:dim(Out_Train_Ref)[1]),c(1,4,7,8)],
          paste(City_Abb_Name,"_ANFIS_Train_Inp_6hrsLead.csv",sep=""),row.names=FALSE)
write.csv(Out_Train_Ref[(4:dim(Out_Train_Ref)[1]),c(1,5,7,8)],
          paste(City_Abb_Name,"_ANFIS_Train_Inp_9hrsLead.csv",sep=""),row.names=FALSE)
write.csv(Out_Train_Ref[(9:dim(Out_Train_Ref)[1]),c(1,6,7,8)],
          paste(City_Abb_Name,"_ANFIS_Train_Inp_24hrsLead.csv",sep=""),row.names=FALSE)

#WRITING ANFIS INPUTS (WITH SAC): write Training file for different lead times
write.csv(Out_Train_Ref[(2:dim(Out_Train_Ref)[1]),c(1,3,7,8,9)],
          paste(City_Abb_Name,"_ANFIS_Train_Inp_with_SAC_3hrsLead.csv",sep=""),row.names=FALSE)
write.csv(Out_Train_Ref[(3:dim(Out_Train_Ref)[1]),c(1,4,7,8,9)],
          paste(City_Abb_Name,"_ANFIS_Train_Inp_with_SAC_6hrsLead.csv",sep=""),row.names=FALSE)
write.csv(Out_Train_Ref[(4:dim(Out_Train_Ref)[1]),c(1,5,7,8,9)],
          paste(City_Abb_Name,"_ANFIS_Train_Inp_with_SAC_9hrsLead.csv",sep=""),row.names=FALSE)
write.csv(Out_Train_Ref[(9:dim(Out_Train_Ref)[1]),c(1,6,7,8,9)],
          paste(City_Abb_Name,"_ANFIS_Train_Inp_with_SAC_24hrsLead.csv",sep=""),row.names=FALSE)

#And TRAINING TARGETS
write.csv(Out_Train_Ref[(2:dim(Out_Train_Ref)[1]),c(1,2)],
          paste(City_Abb_Name,"_ANFIS_Train_Targ_3hrsLead.csv",sep=""),row.names=FALSE)
write.csv(Out_Train_Ref[(3:dim(Out_Train_Ref)[1]),c(1,2)],
          paste(City_Abb_Name,"_ANFIS_Train_Targ_6hrsLead.csv",sep=""),row.names=FALSE)
write.csv(Out_Train_Ref[(4:dim(Out_Train_Ref)[1]),c(1,2)],
          paste(City_Abb_Name,"_ANFIS_Train_Targ_9hrsLead.csv",sep=""),row.names=FALSE)
write.csv(Out_Train_Ref[(9:dim(Out_Train_Ref)[1]),c(1,2)],
          paste(City_Abb_Name,"_ANFIS_Train_Targ_24hrsLead.csv",sep=""),row.names=FALSE)

##################STEP2: TESTING INPs#################
#The reference testing matrix will have 89 columns:
#Col1:ObsQ--- Col2-5: Qt-3, t-6, t-9, and t-24
#Col6-17 PEns-Acc3hrs---Col18-29: PEns-Acc6hrs---Col30-41:QEnsSimSAC3hrs
#Col 42-53: QEnsSimSAC6hrs---Col 54-65:QEnsSimSAC9hrs ---Col 56-77:QEnsSimSAC24hrs ,
#Col 78-89 Acc6hrs_for_GT3hrsLead (GT: Greater than)

Test_Inp_Ref_mtx<-matrix(NA,length(Date_Ens),89)
colnames(Test_Inp_Ref_mtx)<-c("ObsQ_mm","Qt-3hrs_mm","Qt-6hrs_mm","Qt-9hrs_mm","Qt-24hrs_mm",
                              paste(rep(c("EnsCon",paste("Ens",seq(1:10)),"Ens_Avg"),4),
                                    c(rep("_AccP3hrs",12),rep("_AccP6hrsLead3hr",12),
                                      rep("_QSimSAC3hrs",12), rep("_QSimSAC6hrs",12),
                                      rep("_QSimSAC9hrs",12),rep("_QSimSAC24hrs",12),
                                      rep("_AccP6hrsLeadGT3hr",12)),sep=""))

#first fill out the easy columns that doesn't need data manipulation
#######Col1
Test_Inp_Ref_mtx[,1]<-df_MET$Q[Date_MET %in% Date_Ens]

#######Col2-5:
#To simplify the Qt-leadtime look up for the testing period, I create an original
#Q dataset (from df_MET) with as many columns as the number of lead times (here 4) and nrow= nrow (df_MET)
Tempor_Q<-matrix(NA,length(Date_MET),5)
colnames(Tempor_Q)<-c("QObs","Qt-3hrs","Qt-6hrs","Qt-9hrs","Qt-24hrs")
Tempor_Q[,1]<-df_MET$Q
Tempor_Q[(2:length(Date_MET)),2]<-df_MET$Q[1:(length(Date_MET)-1)]
Tempor_Q[(3:length(Date_MET)),3]<-df_MET$Q[1:(length(Date_MET)-2)]
```

```
Tempor_Q[(4:length(Date_MET)),4]<-df_MET$Q[1:(length(Date_MET)-3)]
Tempor_Q[(9:length(Date_MET)),5]<-df_MET$Q[1:(length(Date_MET)-8)]

#then filter this dataset based on the Ens dates period
for(i in seq(1:4)){
  Test_Inp_Ref_mtx[,(i+1)]<-Tempor_Q[(Date_MET %in% Date_Ens),(i+1)]
}

#########Col 6:17 PEns-Acc3hrs
for(i in seq(1:12)){
  Test_Inp_Ref_mtx[,(i+5)]<-df_Ens[,(i+1)]

}

#########Col 30:77 QEnsSimSAC for different lead times which is the output of Step5
for (i in seq(1:(dim(df_Forecasted_Ens)[2]-1))){
  Test_Inp_Ref_mtx[,(i+29)]<-df_Forecasted_Ens[,(i+1)]
}

#########Col18-29 & 78-89 Acc 6 hrs Prec for 3 and GT3 lead times
#The computation time I limit the dates to 24 hours before the testing period which is enouh
Date_Tempor<-Date_MET[(Date_MET>=Date_Ens[1]-24*3600) & Date_MET<=Date_Ens[length(Date_Ens)]]
#I create a temporary matrix to save the Col1= Pobs, Col2=PAcc3hrs(with replaced Ensemble),
# Col3=PAc6hrsLead3, and Col4=PAc6hrsLeadGT3
P1<-matrix(NA,length(Date_Tempor),4)
P1[,(1:2)]<-df_MET$P[Date_MET %in% Date_Tempor]

for(i in seq(1:12)){
#insert the 3 hourly ensemble prec (i.e. Pacc 3hrs) into the Col2 of P1
  P1[Date_Tempor %in% Date_Ens,2]<-Test_Inp_Ref_mtx[,(i+5)]
  #calculate Acc Prec of 6 and 9 hours
  for(j in seq(1:dim(P1)[1])){
    if(j>=2){
      #Only updating with Obs Prec for Lead=3hrs
      P1[j,3]<-P1[(j-1),1]+P1[j,2]
      P1[j,4]<-sum(P1[((j-1):j),2])
    }
   }
  #Now insert the calculated datasets (Acc 6hrs) in the right place
  Test_Inp_Ref_mtx[,(i+17)]<-P1[Date_Tempor %in% Date_Ens,3]
  Test_Inp_Ref_mtx[,(i+77)]<-P1[Date_Tempor %in% Date_Ens,4]
}


#Now write the Testing Ref file and create required inputs for ANFIS (for different lead times)
Out_Test_Ref<-data.frame(Date_Ens,Test_Inp_Ref_mtx)


#and create a csv file containing this source
write.csv(Out_Test_Ref,paste(City_Abb_Name,"_ANFIS_Test_Inp_Reference.csv",sep=""),row.names=FALSE)

#WRITING ANFIS INPUTS (WITHOUT SAC): write Testing file for different lead times
write.csv(Out_Test_Ref[,c(1,3,7:30)],paste(City_Abb_Name,
                                           "_ANFIS_Test_Inp_3hrsLead.csv",sep=""),row.names=FALSE)
write.csv(Out_Test_Ref[,c(1,4,7:18,79:90)],paste(City_Abb_Name,
                                                 "_ANFIS_Test_Inp_6hrsLead.csv",sep=""),row.names=FALSE)
write.csv(Out_Test_Ref[,c(1,5,7:18,79:90)],paste(City_Abb_Name,
                                                 "_ANFIS_Test_Inp_9hrsLead.csv",sep=""),row.names=FALSE)
write.csv(Out_Test_Ref[,c(1,6,7:18,79:90)],paste(City_Abb_Name,
                                                 "_ANFIS_Test_Inp_24hrsLead.csv",sep=""),row.names=FALSE)


#WRITING ANFIS INPUTS (WITH SAC): write Training file for different lead times
write.csv(Out_Test_Ref[,c(1,3,7:42)],paste(City_Abb_Name,
                                           "_ANFIS_Test_Inp_With_SAC_3hrsLead.csv",sep=""),row.names=FALSE)
write.csv(Out_Test_Ref[,c(1,4,7:18,79:90,43:54)],
          paste(City_Abb_Name,"_ANFIS_Test_Inp_With_SAC_6hrsLead.csv",sep=""),row.names=FALSE)
write.csv(Out_Test_Ref[,c(1,5,7:18,79:90,55:66)],
          paste(City_Abb_Name,"_ANFIS_Test_Inp_With_SAC_9hrsLead.csv",sep=""),row.names=FALSE)
write.csv(Out_Test_Ref[,c(1,6,7:18,79:90,67:78)],
          paste(City_Abb_Name,"_ANFIS_Test_Inp_With_SAC_24hrsLead.csv",sep=""),row.names=FALSE)
#And TESTING TARGETS
write.csv(Out_Test_Ref[,c(1,2)],paste(City_Abb_Name,"_ANFIS_Test_Targ.csv",sep=""),row.names=FALSE)

#create an output of calibration MET df
ZZ<-df_MET[Date_MET %in% Date_Train,]
write.csv(ZZ,"ZZ.csv")
```

Appendix P: MATLAB script for training and testing the ANFIS flood forecasting model

```
clc;
clear;
close all;

%load data
TrainTargets=load('BBMID_ANFIS_Train_Targ_24hrsLead.csv');
TrainInputs=load('BBMID_ANFIS_Train_Inp_24hrsLead.csv');

TestTargets=load('BBMID_ANFIS_Test_Targ.csv');
TestInputs_Source=load('BBMID_ANFIS_Test_Inp_24hrsLead.csv');

%count the number of elements
nData=numel(TestTargets);

%create an empty matrix to save test outputs for 12 different ensembles
%(the last one is the Mean of all ensembles)
%% Design ANFIS
%first create ANFIS based on training data
fis=genfis3(TrainInputs,TrainTargets,'sugeno',5);

%create train outputs
TrainOutputs=evalfis(TrainInputs,fis);

%then use a loop to calculate outputs for the validation period resulted
%from 11 different ensembles of GEFS/R data.
for i=1:12

%create a matrix to save Test input datasets (3 columns are for antecedent Q
%and Acc prec 3 and 6 hrs
%Antecedent Q column
TestInputs(:,1)=TestInputs_Source(:,1);

%accumulated prec 3 hrs (which is original GEFS/R of each ensemble)
TestInputs(:,2)=TestInputs_Source(:,(i+1));

%accumulated prec 6 hrs
TestInputs(:,3)=TestInputs_Source(:,(i+13));

%and create the output
TestOutputs(:,i)=evalfis(TestInputs,fis);

end
```

Appendix Q: complementary tables and figures for RNICO analysis

Table Q1. Linear equations (Y=aX + b) for nine cities presented in Figure 4. Parameters X and Y represent RNICO and Runoff peak flows, respectively.

City	Dependent variable (Y)	Regression parameters		R^2
		a	b	
Chicago, IL (CHI)	Max. Peak, small site	3.68	2.39	0.67
	Avg. Peak, small site	5.57	2.03	0.97
	Avg. Peak, large site	-	0.1	-
New York, NY (NYC)	Max. Peak, small site	57.61	6.89	0.91
	Avg. Peak, small site	13.27	1.28	0.95
	Avg. Peak, large site	-	0.15	-
Baltimore, MD (BAL)	Max. Peak, small site	74.46	24.46	0.75
	Avg. Peak, small site	9.79	3.61	0.55
	Avg. Peak, large site	-	0.43	-
Portland, OR (POR)	Max. Peak	4.86	0.35	0.72
	Avg. Peak	0.36	0.14	0.7
Houston, TX (HOU)	Max. Peak, small site	5.67	38.44	0.91
	Avg. Peak, small site	9.5	1.06	0.85
	Avg. Peak, large site	-	0.4	-
Austin, TX (AUS)	Max. Peak, small site	523.29	62.07	0.94
	Avg. Peak, small site	103.03	10.53	0.97
	Avg. Peak, large site	-	2	-
Syracuse, NY (SYR)	Max. Peak	0.11	0.04	0.86
	Avg. Peak	0.82	0.07	0.97
San Francisco, CA (SF)	Max. Peak	5.4	0.92	0.45
	Avg. Peak	1.08	0.28	0.56
Los Angeles, CA (LA)	Max. Peak	1.29	2.88	0.11
	Avg. Peak	1.67	-0.19	0.75

Table Q2. linear equations (Y=aX + b) for three cities presented in Figure 18a. Parameters X and Y represent RNICO (or imperviousness) and R-B flashiness index, respectively.

City name	Equation #	Site scale	X	equation parameters		R^2
				a	b	
Chicago, IL (CHI)	1	small	RNICO	0.47	0.7	0.4
	2	large	RNICO	-	0.4	-
	1	small	Imperviouness (%)	0.01	0.4	0
	2	large	Imperviouness (%)	-	0.4	-
New York, NY (NYC)	1	small	RNICO	2.95	0.7	0.9
	2	large	RNICO	-	0.4	-
	1	small	Imperviouness (%)	0.03	0.2	0.8
	2	large	Imperviouness (%)	-	0.4	-
Portland, OR (POR)	-	small	RNICO	0.31	0.4	0.2
	-	small	Imperviouness (%)	-	0.5	-

Table Q3. linear equations (Y=aX + b) for three cities presented in Figure 18b. Parameters X and Y represent RNICO (or imperviousness) and coefficient of variation of daily mean discharge values, respectively.

City name	Equation #	Site scale	X	equation parameters		R^2
				a	b	
Chicago, IL (CHI)	1	small	RNICO	1.7	2.6	0.7
	2	large	RNICO	-	1.8	-
	1	small	Imperviouness (%)	0.05	0.5	0.4
	2	large	Imperviouness (%)	-	1.8	-
New York, NY (NYC)	1	small	RNICO	8.18	2.2	0.7
	2	large	RNICO	-	1.7	-
	1	small	Imperviouness (%)	0.08	0.6	0.8
	2	large	Imperviouness (%)	0	1.7	0.4
Portland, OR (POR)	-	small	RNICO	2.01	1.2	0.5
	-	small	Imperviouness (%)	-0.01	1.9	0.4

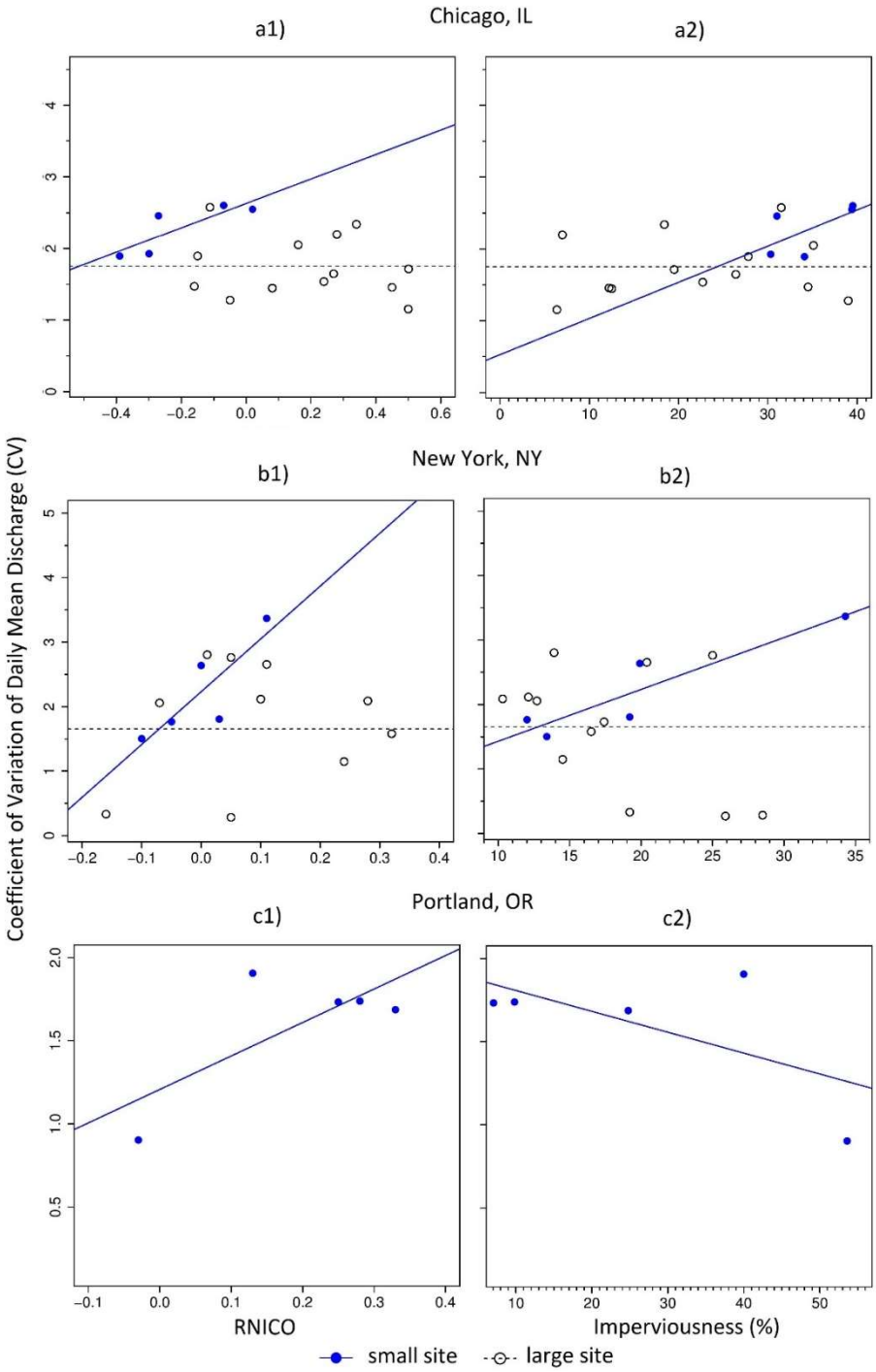

Figure Q1. Plots of RNICO and imperviousness versus the coefficient of variation of daily mean discharge values (CV, $\frac{ft^3}{s}$) for Chicago, IL, New York, NY (Roodsari and Chandler, 2017), and Portland, OR. Equations of linear regressions are presented in Table Q3.

Appendix R: Multilinear regression analysis and diagnostic test results for average runoff peak flow and physical and environmental parameters

Table L1. Results for stepwise regression among significant environmental physical parameters (X_i) and the average runoff peak flow (Y), and diagnostic tests for the six cities in Figure 22.

City name	Significant parameter (s)	Regression equation (Y represents average runoff peak flow (mm/hr) and X_n is an input defined in Table 7)	Adjusted R^2	variance-inflation factor (VIF) (typically, values less than 10 are desirable)	Probability Plot Correlation Coefficient (PPCC) test results		
					Number of data points (n)	$r_{\alpha=0.05}$	Calculated r value
Chicago	X_m	$Y=5.57X_m+2.03$	0.96	NA	5	0.879	0.970
NYC	X_m, X_k	$Y=7.16e\text{-}03\ X_m+2.08e\text{-}05X_k+9.034e\text{-}04$	0.91	4.44	4	0.867	0.996
Baltimore	X_m, X_l	$Y=6.77\ X_m+0.04X_l-0.23$	0.68	1.15	7	0.897	0.998
Portland	X_m	$Y=0.36\ X_m+0.14$	0.60	NA	5	0.879	0.936
San Francisco	X_m, X_l	$Y=0.98\ X_m+0.002X_l-0.120$	0.99	2.11	5	0.879	0.992
Los Angeles	X_m	$Y=1.67\ X_m-0.195$	0.63	NA	4	0.867	0.960

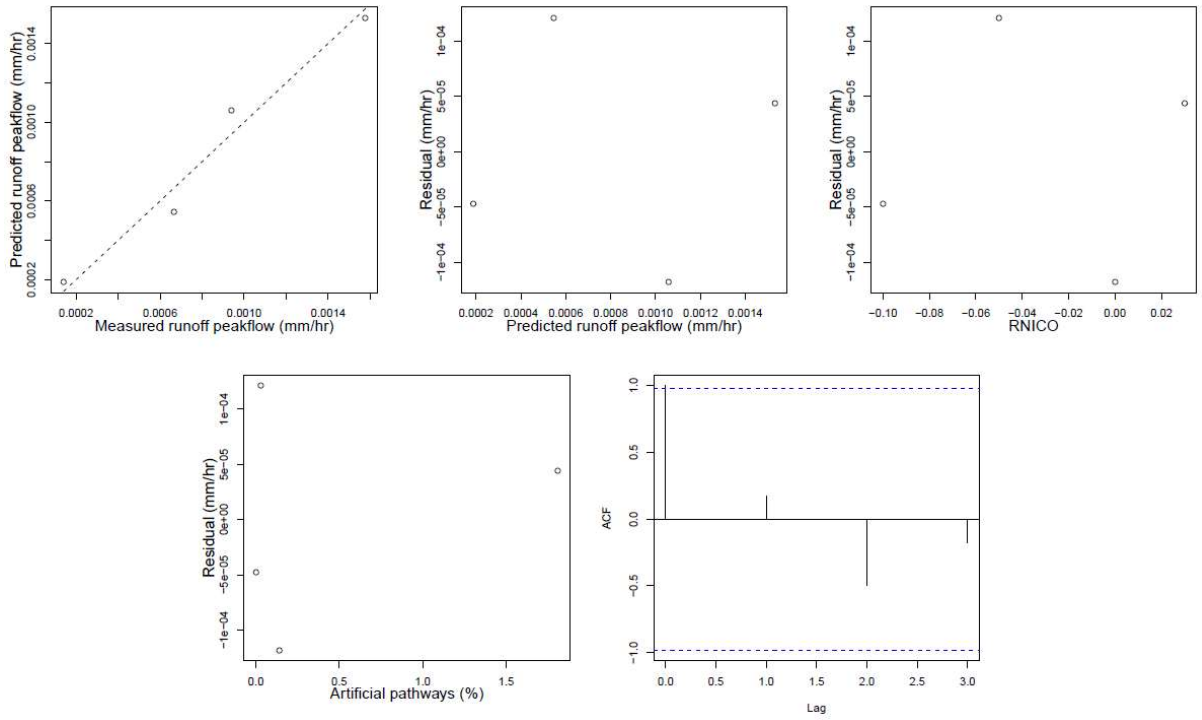

Figure L1. Diagnostic tests for the multilinear regression equation for NYC presented in Table L1.

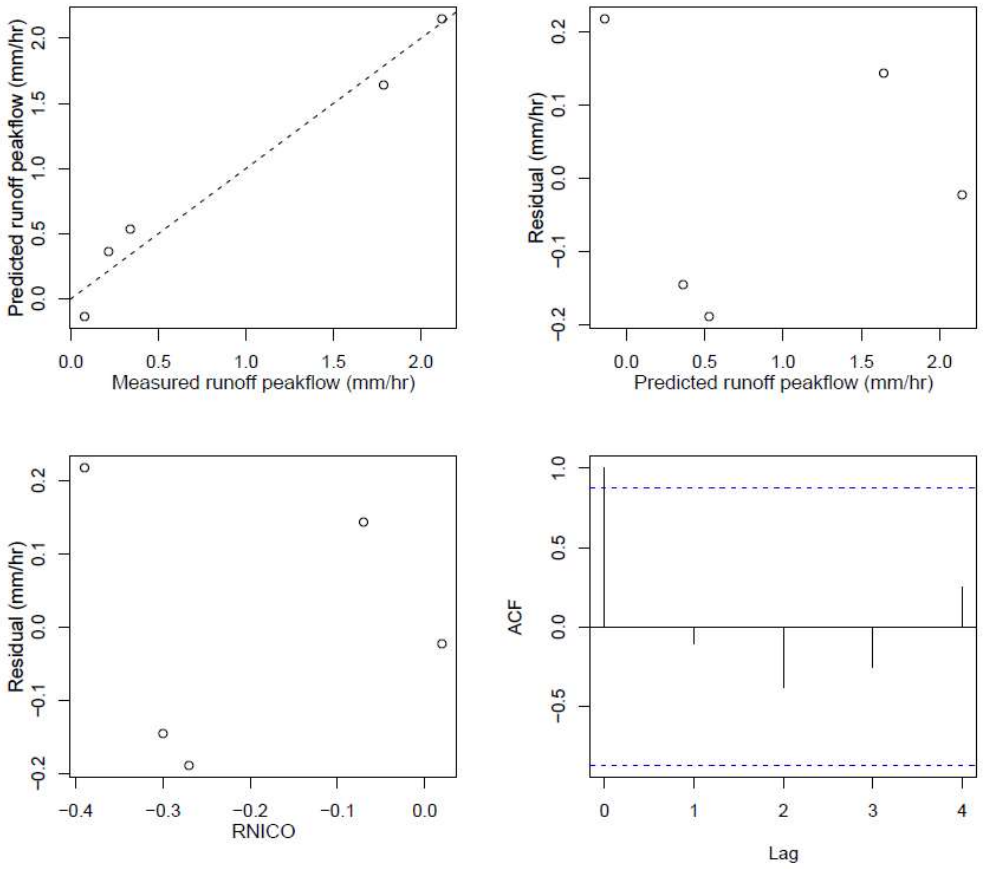

Figure L2. Diagnostic tests for the linear regression equation for Chicago, IL presented in Table L1.

Appendix S: Marginal research questions

Question 1: Does the scale of a peri-urban catchment matter for assessing the impact of the distribution of surface imperviousness on runoff peak flows? If so, what is the catchment drainage area threshold value associated with this assessment? Does this area threshold value vary substantially with the catchment's geographic location?

Question 2: Do climate and geographic location of peri-urban catchments impact the connectivity of urban development pattern with runoff peak flows and stream flashiness? If so, in which climates may we expect to find a stronger linkage between the urban development pattern and peak flow response of small peri-urban catchments?

Question 3: How do measurable surface properties including morphologic, hydrologic, and topographic parameters affect runoff peak flows in peri-urban catchments?

Question 4: Based on the previous literature, how do the hydrologic performance of varying LIDs such as green roof and bioretention systems change from warm to cold season?

Question 5: Does the storm movement direction relative to the catchment drainage orientation impact the performance of data-driven models for flood forecasting in small peri-urban catchments?

References

Adamowski, J.F., 2008. River flow forecasting using wavelet and cross-wavelet transform models. Hydrol. Process. 22, 4877–4891. https://doi.org/10.1002/hyp.7107

Alves, A., Gersonius, B., Sanchez, A., Vojinovic, Z., Kapelan, Z., 2018. Multi-criteria Approach for Selection of Green and Grey Infrastructure to Reduce Flood Risk and Increase CO-benefits. Water Resour. Manag. 32, 2505–2522. https://doi.org/10.1007/s11269-018-1943-3

Amengual, A., Homar, V., Jaume, O., 2015. Potential of a probabilistic hydrometeorological forecasting approach for the 28 September 2012 extreme flash flood in Murcia, Spain. Atmospheric Res. 166, 10–23. https://doi.org/10.1016/j.atmosres.2015.06.012

Ames, D.P., Horsburgh, J.S., Cao, Y., Kadlec, J., Whiteaker, T., Valentine, D., 2012. HydroDesktop: Web services-based software for hydrologic data discovery, download, visualization, and analysis. Environ. Model. Softw. 37, 146–156. https://doi.org/10.1016/j.envsoft.2012.03.013

Arnold, C.L., Gibbons, C.J., 1996. Impervious Surface Coverage: The Emergence of a Key Environmental Indicator. J. Am. Plann. Assoc. 62, 243–258. https://doi.org/10.1080/01944369608975688

Baker, D.B., Richards, R.P., Loftus, T.T., Kramer, J.W., 2004. A New Flashiness Index: Characteristics and Applications to Midwestern Rivers and Streams1. JAWRA J. Am. Water Resour. Assoc. 40, 503–522. https://doi.org/10.1111/j.1752-1688.2004.tb01046.x

Berthet, L., Andréassian, V., Perrin, C., Javelle, P., 2009. How crucial is it to account for the antecedent moisture conditions in flood forecasting? Comparison of event-based and continuous approaches on 178 catchments. Hydrol. Earth Syst. Sci. Katlenburg-Lindau 13, 819.

Bengtsson, L., Westerström, G., 1992. Urban snowmelt and runoff in northern Sweden. Hydrol. Sci. J. 37, 263–275. https://doi.org/10.1080/02626669209492586

Beven, K., 2006. A manifesto for the equifinality thesis. J. Hydrol. 320, 18–36. https://doi.org/10.1016/j.jhydrol.2005.07.007

Beven, K.J., 2018. On hypothesis testing in hydrology: Why falsification of models is still a really good idea. Wiley Interdiscip. Rev. Water 5, e1278. https://doi.org/10.1002/wat2.1278

Bhaskar, A.S., Welty, C., 2012. Water Balances along an Urban-to-Rural Gradient of Metropolitan Baltimore, 2001-2009. Environ. Eng. Geosci. Vol. XVIII, No. 1, 37–50.

Biggs, C., Ryan, C., Wiseman, J., Kristen, L., 2009. Distributed Water Systems: A Networked and Localised Approach for Sustainable Water Services. Vic. Eco-Innov. Lab VEIL Univ. Melb. Melb. Aust. 31.

Buchanan T. J., Somers W. P., 1969. Discharge Measurement at Gaging Stations, in: Applications of Hydraulics. United States Geological Survey.

Burnash, R., 1995. The NWS River Forecast System -- Catchment Modeling, in: Singh, V. (Ed.), Computer Models of Watershed Hydrology. Water Resources Publications.

Burnash, R.J.C., Ferral, R.L., McGuire, Robert A., McGuire, Richard A., 1973. A Generalized Streamflow Simulation System: Conceptual Modeling for Digital Computers. U.S. Department of Commerce, National Weather Service, and State of California, Department of Water Resources.

Buttle, J.M., 1990. Effects of suburbanization upon snowmelt runoff. Hydrol. Sci. J. 35, 285–302.

Buttle, J.M., Xu, F., 1988. Snowmelt Runoff in Suburban Environments. Hydrol. Res. 19, 19–40.

Campolo, M., Soldati, A., Andreussi, P., 2003. Artificial neural network approach to flood forecasting in the River Arno. Hydrol. Sci. J. 48, 381–398. https://doi.org/10.1623/hysj.48.3.381.45286

Carpenter, T.M., Georgakakos, K.P., 2006. Discretization scale dependencies of the ensemble flow range versus catchment area relationship in distributed hydrologic modeling. J. Hydrol., Measurement and Parameterization of Rainfall Microstructure 328, 242–257. https://doi.org/10.1016/j.jhydrol.2005.12.008

Carson, T.B., Marasco, D.E., Culligan, P.J., McGillis, W.R., 2013. Hydrological performance of extensive green roofs in New York City: observations and multi-year modeling of three full-scale systems. Environ. Res. Lett. 8, 024036. https://doi.org/10.1088/1748-9326/8/2/024036

Chang, F.-J., Chang, Y.-T., 2006. Adaptive neuro-fuzzy inference system for prediction of water level in reservoir. Adv. Water Resour. 29, 1–10. https://doi.org/10.1016/j.advwatres.2005.04.015

Chang, F.-J., Chiang, Y.-M., Chang, L.-C., 2007. Multi-step-ahead neural networks for flood forecasting. Hydrol. Sci. J. 52, 114–130. https://doi.org/10.1623/hysj.52.1.114

Cheng, S., Lee, C., Lee, J., 2010. Effects of Urbanization Factors on Model Parameters. Water Resour. Manag. 24, 775–794. https://doi.org/10.1007/s11269-009-9471-9

Chiang, Y.-M., Hsu, K.-L., Chang, F.-J., Hong, Y., Sorooshian, S., 2007. Merging multiple precipitation sources for flash flood forecasting. J. Hydrol. 340, 183–196. https://doi.org/10.1016/j.jhydrol.2007.04.007

Cloke, H.L., Pappenberger, F., 2009. Ensemble flood forecasting: A review. J. Hydrol. 375, 613–626. https://doi.org/10.1016/j.jhydrol.2009.06.005

Day, G.N., 1985. Extended Streamflow Forecasting Using NWSRFS. J. Water Resour. Plan. Manag. 111, 157–170. https://doi.org/10.1061/(ASCE)0733-9496(1985)111:2(157)

Deshmukh, R.P., Ghatol, A.A., 2010. Short term flood forecasting using general recurrent neural network modeling a comparative study. Int. J. Comput. Appl. 8, 5–9.

Dietz Michael E., Arnold Chester L., 2018. Can Green Infrastructure Provide Both Water Quality and Flood Reduction Benefits? J. Sustain. Water Built Environ. 4, 02518001. https://doi.org/10.1061/JSWBAY.0000856

Domínguez, I., Ward, S., Mendoza, J.G., Rincón, C.I., Oviedo-Ocaña, E.R., 2017. End-User Cost-Benefit Prioritization for Selecting Rainwater Harvesting and Greywater Reuse in Social Housing. Water 9, 516.

Dougherty, M., Dymond, R.L., Grizzard, T.J., Godrej, A.N., Zipper, C.E., Randolph, J., Anderson-Cook, C.M., 2006. Empirical Modeling of Hydrologic and Nfs Pollutant Flux in an Urbanizing Basin1. JAWRA J. Am. Water Resour. Assoc. 42, 1405–1419. https://doi.org/10.1111/j.1752-1688.2006.tb05309.x

Driscoll, C.T., Eger, C.G., Chandler, D.G., Davidson, C.I., Roodsari, B.K., Flynn, C.D., Lambert, K.F., Bettez, N.D., Groffman, P.M., 2015. Green Infrastructure: Lessons from Science and Practice.

Du, S., Shi, P., Van Rompaey, A., Wen, J., 2015. Quantifying the impact of impervious surface location on flood peak discharge in urban areas. Nat. Hazards 76, 1457–1471. https://doi.org/10.1007/s11069-014-1463-2

Eimers, M.C., McDonald, E.C., 2015. Hydrologic changes resulting from urban cover in seasonally snow-covered catchments: URBAN EFFECTS ON STREAMFLOW. Hydrol. Process. 29, 1280–1288. https://doi.org/10.1002/hyp.10250

Emerton, R.E., Stephens, E.M., Pappenberger, F., Pagano, T.C., Weerts, A.H., Wood, A.W., Salamon, P., Brown, J.D., Hjerdt, N., Donnelly, C., Baugh, C.A., Cloke, H.L., 2016. Continental and global scale flood forecasting systems. Wiley Interdiscip. Rev. Water 3, 391–418. https://doi.org/10.1002/wat2.1137

Epstein, D.M., Kelso, J.E., Baker, M.A., 2016. Beyond the urban stream syndrome: organic matter budget for diagnostics and restoration of an impaired urban river. Urban Ecosyst. 19, 1041–1061. https://doi.org/10.1007/s11252-016-0557-x

Falcone, J., 2011. GAGES-II: Geospatial Attributes of Gages for Evaluating Streamflow.

Farokhnia, A., Morid, S., Byun, H.-R., 2011. Application of global SST and SLP data for drought forecasting on Tehran plain using data mining and ANFIS techniques. Theor. Appl. Climatol. 104, 71–81. https://doi.org/10.1007/s00704-010-0317-4

Federal Emergency Management Agency (FEMA), 2012. Flood Insurance Studies: Onondaga County, New York (All Jurisdictions).

Foehn, A., Hernandez, J.G., Roquier, B., Arquiola, J.P., 2016. RS MINERVE - User's Manual v2.4.

Foulon, É., Rousseau, A.N., 2018. Equifinality and automatic calibration: What is the impact of hypothesizing an optimal parameter set on modelled hydrological processes? Can. Water Resour. J. Rev. Can. Ressour. Hydr. 0, 1–21. https://doi.org/10.1080/07011784.2018.1430620

Gan, Y., Duan, Q., Gong, W., Tong, C., Sun, Y., Chu, W., Ye, A., Miao, C., Di, Z., 2014. A comprehensive evaluation of various sensitivity analysis methods: A case study with a hydrological model. Environ. Model. Softw. 51, 269–285. https://doi.org/10.1016/j.envsoft.2013.09.031

Gouweleeuw, B., Thielen Del Pozo, J., Franchello, G., De Roo, A., Buizza, R., 2005. Flood Forecasting Using Medium-Range Probabilistic Weather Prediction. Hydrol. Earth Syst. Sci. 9, 365–380.

Grayson, R.B., Moore, I.D., McMahon, T.A., 1992. Physically based hydrologic modeling: 2. Is the concept realistic? Water Resour. Res. 28, 2659–2666. https://doi.org/10.1029/92WR01259

Grillakis, M.G., Koutroulis, A.G., Komma, J., Tsanis, I.K., Wagner, W., Blöschl, G., 2016. Initial soil moisture effects on flash flood generation – A comparison between basins of contrasting hydro-climatic conditions. J. Hydrol., Flash floods, hydro-geomorphic response and risk management 541, 206–217. https://doi.org/10.1016/j.jhydrol.2016.03.007

Grimmond, C.S.B., Oke, T.R., 1999. Evapotranspiration rates in urban areas: Impacts of Urban Growth on Surface Water and Groundwater Quality (Proceedings of IUGG 99 Symposium HS5) Vol. IAHS, Publ. No. 259, 235–243.

Haderlie, G.M., Tullis, B.P., 2008. Hydraulics of Multibarrel Culverts under Inlet Control. J. Irrig. Drain. Eng. 134, 507–514. https://doi.org/10.1061/(ASCE)0733-9437(2008)134:4(507)

Hally, A., Caumont, O., Garrote, L., Richard, E., Weerts, A., Delogu, F., Fiori, E., Rebora, N., Parodi, A., Mihalović, A., Ivković, M., Dekić, L., van Verseveld, W., Nuissier, O., Ducrocq, V., D'Agostino, D., Galizia, A., Danovaro, E., Clematis, A., 2015. Hydrometeorological multi-model ensemble simulations of the 4 November 2011 flash flood event in Genoa, Italy, in the framework of the DRIHM project. Nat Hazards Earth Syst Sci 15, 537–555. https://doi.org/10.5194/nhess-15-537-2015

Hamill, T.M., Bates, G.T., Whitaker, J.S., Murray, D.R., Fiorino, M., Galarneau, T.J., Zhu, Y., Lapenta, W., 2013. NOAA's Second-Generation Global Medium-Range Ensemble Reforecast Dataset. Bull. Am. Meteorol. Soc. 94, 1553–1565. https://doi.org/10.1175/BAMS-D-12-00014.1

Hammond, M.J., Chen, A.S., Djordjević, S., Butler, D., Mark, O., 2015. Urban flood impact assessment: A state-of-the-art review. Urban Water J. 12, 14–29. https://doi.org/10.1080/1573062X.2013.857421

Heino, R., Hellsten, E., 1983. Tilastoja Suomen ilmastosta 1961–1980.

Herath, H.M.P.I.K., Halwatura, R.U., Jayasinghe, G.Y., 2018. Evaluation of green infrastructure effects on tropical Sri Lankan urban context as an urban heat island adaptation strategy. Urban For. Urban Green., Wild urban ecosystems: challenges and opportunities for urban development 29, 212–222. https://doi.org/10.1016/j.ufug.2017.11.013

Herman, J.D., Reed, P.M., Wagener, T., 2013. Time-varying sensitivity analysis clarifies the effects of watershed model formulation on model behavior. Water Resour. Res. 49, 1400–1414. https://doi.org/10.1002/wrcr.20124
Ho, C.L.I., Valeo, C., 2005. Observations of urban snow properties in Calgary, Canada. Hydrol. Process. 19, 459–473. https://doi.org/10.1002/hyp.5544
Hogue, T.S., Sorooshian, S., Gupta, H., Holz, A., Braatz, D., 2000. A Multistep Automatic Calibration Scheme for River Forecasting Models. J. Hydrometeorol. 1, 524–542. https://doi.org/10.1175/1525-7541(2000)001<0524:AMACSF>2.0.CO;2
Jain, A., Varshney, A.K., Joshi, U.C., 2001. Short-term water demand forecast modelling at IIT Kanpur using artificial neural networks. Water Resour. Manag. 15, 299–321.
Jakeman, A.J., Hornberger, G.M., 1993. How much complexity is warranted in a rainfall-runoff model? Water Resour. Res. 29, 2637–2649. https://doi.org/10.1029/93WR00877
Jang, J.-S.R., Chuen-Tsai Sun, 1995. Neuro-fuzzy modeling and control. Proc. IEEE 83, 378–406. https://doi.org/10.1109/5.364486
Jayawardena, A.W., Perera, E.D.P., Zhu, B., Amarasekara, J.D., Vereivalu, V., 2014. A comparative study of fuzzy logic systems approach for river discharge prediction. J. Hydrol. 514, 85–101. https://doi.org/10.1016/j.jhydrol.2014.03.064
Jha, A.K., Bloch, R., Lamond, J., 2012. Cities and Flooding: A Guide to Integrated Urban Flood Risk Management for the 21st Century. The World Bank, Washington, D.C.
Julian, J.P., Gardner, R.H., 2014. Land cover effects on runoff patterns in eastern Piedmont (USA) watersheds. Hydrol. Process. 28, 1525–1538. https://doi.org/10.1002/hyp.9692
K. Ajami, N., Gupta, H., Wagener, T., Sorooshian, S., 2004. Calibration of a semi-distributed hydrologic model for streamflow estimation along a river system. J. Hydrol., The Distributed Model Intercomparison Project (DMIP) 298, 112–135. https://doi.org/10.1016/j.jhydrol.2004.03.033
Khac-Tien Nguyen, P., Hock-Chye Chua, L., 2012. The data-driven approach as an operational real-time flood forecasting model. Hydrol. Process. 26, 2878–2893. https://doi.org/10.1002/hyp.8347
Khakbaz, B., Imam, B., Hsu, K., Sorooshian, S., 2009. From lumped to distributed via semi-distributed: Calibration strategies for semi-distributed hydrologic models. J. Hydrol., The Distributed Model Intercomparison Project (DMIP) - Phase 2 Experiments in the Oklahoma Region, USA 418–419, 61–77. https://doi.org/10.1016/j.jhydrol.2009.02.021
Khan, U.T., Valeo, C., Chu, A., He, J., 2013. A Data Driven Approach to Bioretention Cell Performance: Prediction and Design. Water 5, 13–28. https://doi.org/10.3390/w5010013
Knijff, J.M.V.D., Younis, J., Roo, A.P.J.D., 2010. LISFLOOD: a GIS-based distributed model for river basin scale water balance and flood simulation. Int. J. Geogr. Inf. Sci. 24, 189–212. https://doi.org/10.1080/13658810802549154
Koivusalo, H., Kokkonen, T., Laurén, A., Ahtiainen, M., Karvonen, T., Mannerkoski, H., Penttinen, S., Seuna, P., Starr, M., Finér, L., 2006. Parameterisation and application of a hillslope hydrological model to assess impacts of a forest clear-cutting on runoff generation. Environ. Model. Softw., Integrative Modelling of Climatic, Terrestrial and Fluvial SystemsIntegrative Modelling of Climatic, Terrestrial and Fluvial Systems 21, 1324–1339. https://doi.org/10.1016/j.envsoft.2005.04.020
Koren, V.I., Finnerty, B.D., Schaake, J.C., Smith, M.B., Seo, D.-J., Duan, Q.-Y., 1999. Scale dependencies of hydrologic models to spatial variability of precipitation. J. Hydrol. 217, 285–302. https://doi.org/10.1016/S0022-1694(98)00231-5
Lamberti, P., Pilati, S., 1996. Flood propagation models for real-time forecasting. J. Hydrol. 175, 239–265.
Liebe, J.R., van de Giesen, N., Andreini, M., Walter, M.T., Steenhuis, T.S., 2009. Determining watershed response in data poor environments with remotely sensed small reservoirs as runoff gauges. Water Resour. Res. 45, W07410. https://doi.org/10.1029/2008WR007369

Liechti, K., Panziera, L., Germann, U., Zappa, M., 2013. The potential of radar-based ensemble forecasts for flash-flood early warning in the southern Swiss Alps. Hydrol Earth Syst Sci 17, 3853–3869. https://doi.org/10.5194/hess-17-3853-2013

Liechti, Katharina, Zappa, M., Fundel, F., Germann, U., 2013. Probabilistic evaluation of ensemble discharge nowcasts in two nested Alpine basins prone to flash floods. Hydrol. Process. 27, 5–17. https://doi.org/10.1002/hyp.9458

Lindström, G., Pers, C., Rosberg, J., Strömqvist, J., Arheimer, B., 2010. Development and testing of the HYPE (Hydrological Predictions for the Environment) water quality model for different spatial scales. Hydrol. Res. 41, 295–319. https://doi.org/10.2166/nh.2010.007

Mamdani, E.H., Assilian, S., 1999. An Experiment in Linguistic Synthesis with a Fuzzy Logic Controller. Int. J. Hum.-Comput. Stud. 51, 135–147. https://doi.org/10.1006/ijhc.1973.0303

Mao, X., Jia, H., Yu, S.L., 2017. Assessing the ecological benefits of aggregate LID-BMPs through modelling. Ecol. Model., Special Issue of China-Korea Joint Seminars on multi-disciplinary and multi-method approaches toward sustainable human and nature interactions 353, 139–149. https://doi.org/10.1016/j.ecolmodel.2016.10.018

Markantonis, V., Meyer, V., Lienhoop, N., 2013. Evaluation of the environmental impacts of extreme floods in the Evros River basin using Contingent Valuation Method. Nat. Hazards 69, 1535–1549. https://doi.org/10.1007/s11069-013-0762-3

McMillan, S.K., Wilson, H.F., Tague, C.L., Hanes, D.M., Inamdar, S., Karwan, D.L., Loecke, T., Morrison, J., Murphy, S.F., Vidon, P., 2018. Before the storm: antecedent conditions as regulators of hydrologic and biogeochemical response to extreme climate events. Biogeochemistry. https://doi.org/10.1007/s10533-018-0482-6

Marty, R., Zin, I., Obled, C., 2013. Sensitivity of hydrological ensemble forecasts to different sources and temporal resolutions of probabilistic quantitative precipitation forecasts: flash flood case studies in the Cévennes-Vivarais region (Southern France). Hydrol. Process. 27, 33–44. https://doi.org/10.1002/hyp.9543

Matonse, A.H., Kroll, C.N., 2013. Applying hillslope-storage models to improve low flow estimates with limited streamflow data at a watershed scale. J. Hydrol. 494, 20–31. https://doi.org/10.1016/j.jhydrol.2013.04.032

Meierdiercks, K.L., Smith, J.A., Baeck, M.L., Miller, A.J., 2010. Analyses of Urban Drainage Network Structure and its Impact on Hydrologic Response1. JAWRA J. Am. Water Resour. Assoc. 46, 932–943. https://doi.org/10.1111/j.1752-1688.2010.00465.x

Mejía, A.I., Moglen, G.E., 2010a. Spatial distribution of imperviousness and the space-time variability of rainfall, runoff generation, and routing: SPATIAL DISTRIBUTION OF IMPERVIOUSNESS. Water Resour. Res. 46, n/a-n/a. https://doi.org/10.1029/2009WR008568

Mejía, A.I., Moglen, G.E., 2010b. Impact of the spatial distribution of imperviousness on the hydrologic response of an urbanizing basin. Hydrol. Process. 24, 3359–3373. https://doi.org/10.1002/hyp.7755

Mejía, A.I., Moglen, G.E., 2009. Spatial patterns of urban development from optimization of flood peaks and imperviousness-based measures. J. Hydrol. Eng. 14, 416–424.

Metcalf and Eddy, Inc., University of Florida, and Water Resources Engineers, Inc., 1971. Storm Water Management Model, Vol. I. Final Report 11024DOC07/71 (NTIS PB-203289). https://doi.org/U.S. EPA, Washington, DC, 20460

Miguez, M.G., Veról, A.P., de Sousa, M.M., Rezende, O.M., 2015. Urban Floods in Lowlands—Levee Systems, Unplanned Urban Growth and River Restoration Alternative: A Case Study in Brazil. Sustainability 7, 11068–11097. https://doi.org/10.3390/su70811068

Miller, J.D., Kim, H., Kjeldsen, T.R., Packman, J., Grebby, S., Dearden, R., 2014. Assessing the impact of urbanization on storm runoff in a peri-urban catchment using historical change in impervious cover. J. Hydrol. 515, 59–70. https://doi.org/10.1016/j.jhydrol.2014.04.011

Miller, J.E., 1984. Basic concepts of kinematic-wave models (USGS Numbered Series No. 1302), Professional Paper.
Moosavian, N., 2015. Soccer league competition algorithm for solving knapsack problems. Swarm Evol. Comput. 20, 14–22. https://doi.org/10.1016/j.swevo.2014.10.002
Moosavian, N., Kasaee Roodsari, B., 2014. Soccer league competition algorithm: A novel meta-heuristic algorithm for optimal design of water distribution networks. Swarm Evol. Comput. 17, 14–24. https://doi.org/10.1016/j.swevo.2014.02.002
Moosavian, N., Roodsari, B.K., 2014. Soccer League Competition Algorithm, a New Method for Solving Systems of Nonlinear Equations. Int. J. Intell. Sci. 04, 7–16. https://doi.org/10.4236/ijis.2014.41002
Muthanna, T.M., Viklander, M., Thorolfsson, S.T., 2008. Seasonal climatic effects on the hydrology of a rain garden. Hydrol. Process. 22, 1640–1649. https://doi.org/10.1002/hyp.6732
Napolitano, G., See, L., Calvo, B., Savi, F., Heppenstall, A., 2010. A conceptual and neural network model for real-time flood forecasting of the Tiber River in Rome. Phys. Chem. Earth Parts ABC, Modelling and simulation of dangerous phenomena, and innovative techniques for hazard mapping and mitigation 35, 187–194. https://doi.org/10.1016/j.pce.2009.12.004
Nathan, R.J., McMahon, T.A., 1990. Evaluation of automated techniques for base flow and recession analyses. Water Resour. Res. 26, 1465–1473. https://doi.org/10.1029/WR026i007p01465
Nayak, P.C., Sudheer, K.P., Rangan, D.M., Ramasastri, K.S., 2005. Short-term flood forecasting with a neurofuzzy model. Water Resour. Res. 41, n/a-n/a. https://doi.org/10.1029/2004WR003562
Nicótina, L., Alessi Celegon, E., Rinaldo, A., Marani, M., 2008. On the impact of rainfall patterns on the hydrologic response. Water Resour. Res. 44, W12401. https://doi.org/10.1029/2007WR006654
Nirupama, N., Simonovic, S.P., 2007. Increase of Flood Risk due to Urbanisation: A Canadian Example. Nat. Hazards 40, 25–41. https://doi.org/10.1007/s11069-006-0003-0
NOAA, 2000. Climatography of the united states no. 81 monthly station normals of temperature, precipitation, and heating and cooling degree days 1971–2000.
Norman J. M., Houghtalen R. J., and Johnston W. J., 2001. Hydraulic Design of Highway Culverts, Second Edition (No. FHWA –NHI-01-020 HDS No. 5). Federal Highway Administration.
Nourani, V., Hosseini Baghanam, A., Adamowski, J., Kisi, O., 2014. Applications of hybrid wavelet–Artificial Intelligence models in hydrology: A review. J. Hydrol. 514, 358–377. https://doi.org/10.1016/j.jhydrol.2014.03.057
Patel, D., Parekh, D.F., 2014. Flood forecasting using adaptive neuro-fuzzy inference system (ANFIS). Int. J. Eng. Trends Technol. 12, 510–514.
Rantz S. E. et al., 1982. Measurement and Computationof Streamflow: Volume 1. Measurement of Stage and Discharge.
Reed, S., Schaake, J., Zhang, Z., 2007. A distributed hydrologic model and threshold frequency-based method for flash flood forecasting at ungauged locations. J. Hydrol. 337, 402–420. https://doi.org/10.1016/j.jhydrol.2007.02.015
Reilly, C.F., Kroll, C.N., 2003. Estimation of 7-day, 10-year low-streamflow statistics using baseflow correlation. Water Resour. Res. 39, 1236. https://doi.org/10.1029/2002WR001740
Rezaeianzadeh, M., Tabari, H., Arabi Yazdi, A., Isik, S., Kalin, L., 2014. Flood flow forecasting using ANN, ANFIS and regression models. Neural Comput. Appl. 25, 25–37. https://doi.org/10.1007/s00521-013-1443-6

Roodsari, B.K., Chandler, D.G., 2017. Distribution of surface imperviousness in small urban catchments predicts runoff peak flows and stream flashiness. Hydrological Processes 31, 2990–3002. https://doi.org/10.1002/hyp.11230

Roodsari, B.K., Chandler, D.G., Kelleher, C., Kroll, C.N., 2018. A comparison of SAC-SMA and Adaptive Neuro-fuzzy Inference System for real-time flood forecasting in small urban catchments. Journal of Flood Risk Management 0, e12492. https://doi.org/10.1111/jfr3.12492

Rose, S., Peters, N.E., 2001. Effects of urbanization on streamflow in the Atlanta area (Georgia, USA): a comparative hydrological approach. Hydrol. Process. 15, 1441–1457. https://doi.org/10.1002/hyp.218

Roseen, R.M., Ballestero, T.P., Houle, J.J., Avellaneda, P., Briggs, J., Fowler, G., Wildey, R., 2009. Seasonal performance variations for storm-water management systems in cold climate conditions. J. Environ. Eng.

Rossman, L.A., 2010. Storm water management model user's manual, version 5.0. National Risk Management Research Laboratory, Office of Research and Development, US Environmental Protection Agency Cincinnati.

Saleh, F., Ramaswamy, V., Georgas, N., Blumberg, A.F., Pullen, J., 2016. A retrospective streamflow ensemble forecast for an extreme hydrologic event: a case study of Hurricane Irene and on the Hudson River basin. Hydrol Earth Syst Sci 20, 2649–2667. https://doi.org/10.5194/hess-20-2649-2016

Sapkota, M., Arora, M., Malano, H., Moglia, M., Sharma, A., George, B., Pamminger, F., 2014. An Overview of Hybrid Water Supply Systems in the Context of Urban Water Management: Challenges and Opportunities. Water 7, 153–174. https://doi.org/10.3390/w7010153

Sapriza-Azuri, G., Jódar, J., Navarro, V., Slooten, L.J., Carrera, J., Gupta, H.V., 2015. Impacts of rainfall spatial variability on hydrogeological response. Water Resour. Res. 51, 1300–1314. https://doi.org/10.1002/2014WR016168

Schroll, E., Lambrinos, J., Righetti, T., Sandrock, D., 2011. The role of vegetation in regulating stormwater runoff from green roofs in a winter rainfall climate. Ecol. Eng. 37, 595–600. https://doi.org/10.1016/j.ecoleng.2010.12.020

Schueler, T., Fraley-McNeal, L., Cappiella, K., 2009. Is Impervious Cover Still Important? Review of Recent Research. J. Hydrol. Eng. 14, 309–315. https://doi.org/10.1061/(ASCE)1084-0699(2009)14:4(309)

Schueler, T., 1994. The importance of Imperviousness. Watershed Prot. Tech. 1(3), 100–111.

Semádeni-Davies, A.F., 2000. Representation of snow in urban drainage models. J. Hydrol. Eng. 5, 363–370.

Semádeni-Davies, A.F., Bengtsson, L., 1999. The water balance of a sub-Arctic town. Hydrol. Process. 13, 1871–1885. https://doi.org/10.1002/(SICI)1099-1085(199909)13:12/13<1871::AID-HYP878>3.0.CO;2-M

Seo, Y., Kim, S., Singh, V.P., 2015. Multistep-ahead flood forecasting using wavelet and data-driven methods. KSCE J. Civ. Eng. 19, 401–417. https://doi.org/10.1007/s12205-015-1483-9

Seo, Y., Schmidt, A.R., Sivapalan, M., 2012. Effect of storm movement on flood peaks: Analysis framework based on characteristic timescales. Water Resour. Res. 48. https://doi.org/10.1029/2011WR011761

Shiri, J., Kisi, O., 2010. Short-term and long-term streamflow forecasting using a wavelet and neuro-fuzzy conjunction model. J. Hydrol. 394, 486–493. https://doi.org/10.1016/j.jhydrol.2010.10.008

Sillanpää, N., Koivusalo, H., 2015. Impacts of urban development on runoff event characteristics and unit hydrographs across warm and cold seasons in high latitudes. J. Hydrol. 521, 328–340. https://doi.org/10.1016/j.jhydrol.2014.12.008

Skorski, M., 2019. Kernel Density Estimation Bias under Minimal Assumptions. ArXiv190100331 Cs Math Stat.

Singh, S.K., Dutta, S., 2017. Observational uncertainty in hydrological modelling using data depth. Glob. Nest J. 19, 489–497.

Smith, J.A., Baeck, M.L., Meierdiercks, K.L., Nelson, P.A., Miller, A.J., Holland, E.J., 2005. Field studies of the storm event hydrologic response in an urbanizing watershed. Water Resour. Res. 41, W10413. https://doi.org/10.1029/2004WR003712

Snyman, J., 2005. Practical Mathematical Optimization: An Introduction to Basic Optimization Theory and Classical and New Gradient-Based Algorithms. Springer Science & Business Media.

Sojka, S., Younos, T., Crawford, D., 2016. Modern Urban Rainwater Harvesting Systems: Design, Case Studies, and Impacts, in: Sustainable Water Management in Urban Environments, The Handbook of Environmental Chemistry. Springer, Cham, pp. 209–234. https://doi.org/10.1007/978-3-319-29337-0_7

Solomatine, D.P., Ostfeld, A., 2008. Data-driven modelling: some past experiences and new approaches. J. Hydroinformatics 10, 3. https://doi.org/10.2166/hydro.2008.015

Su, W., Ye, G., Yao, S., Yang, G., 2014. Urban Land Pattern Impacts on Floods in a New District of China. Sustainability 6, 6488–6508. https://doi.org/10.3390/su6106488

Sudheer, K.P., Gosain, A.K., Ramasastri, K.S., 2002. A data-driven algorithm for constructing artificial neural network rainfall-runoff models. Hydrol. Process. 16, 1325–1330. https://doi.org/10.1002/hyp.554

Suriya, S., Mudgal, B.V., 2012. Impact of urbanization on flooding: The Thirusoolam sub watershed – A case study. J. Hydrol. 412–413, 210–219. https://doi.org/10.1016/j.jhydrol.2011.05.008

Takagi, T., Sugeno, M., 1983. Derivation of Fuzzy Control Rules from Human Operator's Control Actions. Proc IFAC Symp Fuzzy Inf. Knowl. Represent. Decis. Anal. 55–60.

Taylor, C.H., 1982. The Effect on Storm Runoff Response of Seasonal Variations in Contributing Zones in Small Watersheds. Hydrol. Res. 13, 165–182.

Taylor, C.H., 1977. Seasonal variations in the impact of suburban development on runoff response: Peterborough, Ontario. Water Resour. Res. 13, 464–467. https://doi.org/10.1029/WR013i002p00464

Tiwari, M.K., Chatterjee, C., 2010. Uncertainty assessment and ensemble flood forecasting using bootstrap based artificial neural networks (BANNs). J. Hydrol. 382, 20–33. https://doi.org/10.1016/j.jhydrol.2009.12.013

Tjandraatmadja, G., Burn, S., McLaughlin, M., Biswas, T., 2005. Rethinking urban water systems – revisiting concepts in urban wastewater collection and treatment to ensure infrastructure sustainability. Water Sci. Technol. Water Supply 5, 145–154.

Tullis, B.P., Anderson, D., 2010. Slip-Lined Culvert Inlet End Treatment Hydraulics. J. Irrig. Drain. Eng. 136, 31–36. https://doi.org/10.1061/(ASCE)IR.1943-4774.0000113

Turc, L., 1955. Le bilan de l'eau des sols. Relations entre les precipitations, l'evaporation et l'ecoulement. Ann Agro 6, 5–152. https://doi.org/INRA

United Nations, 2010. World urbanization prospects: the 2009 revision.

United States Environmental Protection Agency (USEPA), 2014. Final Feasibility Study Report: Lower Ley Creek Subsite of the Onondaga Lake Superfund Site, Syracuse, New York.

Valtanen, M., Sillanpää, N., Setälä, H., 2014. Effects of land use intensity on stormwater runoff and its temporal occurrence in cold climates. Hydrol. Process. 28, 2639–2650. https://doi.org/10.1002/hyp.9819

van Roon, M., 2007. Water localisation and reclamation: Steps towards low impact urban design and development. J. Environ. Manage. 83, 437–447. https://doi.org/10.1016/j.jenvman.2006.04.008

Walsh, C.J., Roy, A.H., Feminella, J.W., Cottingham, P.D., Groffman, P.M., Morgan, R.P., 2005. The urban stream syndrome: current knowledge and the search for a cure. J. North Am. Benthol. Soc. 24, 706–723. https://doi.org/10.1899/04-028.1

Wang, Y., Yang, X., 2013. Land use/cover change effects on floods with different return periods: a case study of Beijing, China. Front. Environ. Sci. Eng. 7, 769–776. https://doi.org/10.1007/s11783-013-0542-z

Wilson, C.B., Valdes, J.B., Rodriguez-Iturbe, I., 1979. On the influence of the spatial distribution of rainfall on storm runoff. Water Resour. Res. 15, 321–328. https://doi.org/10.1029/WR015i002p00321

Wood, A.W., Clark, M.P., Nijssen, B., 2017. The Rise of Complexity in Flood Forecasting: Opportunities, Challenges and Tradeoffs. AGU Fall Meet. Abstr. 51.

World Bank, 2013. World Development Report 2014: Risk and Opportunity - Managing Risk for Development. The World Bank.

Yang, G., Bowling, L.C., Cherkauer, K.A., Pijanowski, B.C., 2011. The impact of urban development on hydrologic regime from catchment to basin scales. Landsc. Urban Plan. 103, 237–247. https://doi.org/10.1016/j.landurbplan.2011.08.003

Yen, H., Hoque, Y., Harmel, R.D., Jeong, J., 2015. The impact of considering uncertainty in measured calibration/validation data during auto-calibration of hydrologic and water quality models. Stoch. Environ. Res. Risk Assess. 29, 1891–1901. https://doi.org/10.1007/s00477-015-1047-z

Yeo, I.-Y., Guldmann, J.-M., 2006. Land-Use Optimization for Controlling Peak Flow Discharge and Nonpoint Source Water Pollution. Environ. Plan. B Plan. Des. 33, 903–921. https://doi.org/10.1068/b31185

Younos, T., 2011. Paradigm shift: Holistic approach for water management in urban environments. Front. Earth Sci. 5, 421–427. https://doi.org/10.1007/s11707-011-0209-7

Zadeh, L.A., 1965. Fuzzy sets. Inf. Control 8, 338–353. https://doi.org/10.1016/S0019-9958(65)90241-X

Zehe, E., Blöschl, G., 2004. Predictability of hydrologic response at the plot and catchment scales: Role of initial conditions. Water Resour. Res. 40. https://doi.org/10.1029/2003WR002869

Zhang, Y., Shuster, W., 2014. Impacts of Spatial Distribution of Impervious Areas on Runoff Response of Hillslope Catchments: Simulation Study. J. Hydrol. Eng. 19, 1089–1100. https://doi.org/10.1061/(ASCE)HE.1943-5584.0000905

Zope, P.E., Eldho, T.I., Jothiprakash, V., 2015. Impacts of urbanization on flooding of a coastal urban catchment: a case study of Mumbai City, India. Nat. Hazards 75, 887–908. https://doi.org/10.1007/s11069-014-1356-4

Vita

Babak Kasaee Roodsari

|Philadelphia, PA|312-340-7277|bkasaeer@syr.edu|https://www.linkedin.com/in/babak-kasaee-roodsari|

Education

SYRACUSE UNIVERSITY — SYRACUSE, NY

Ph.D., Civil & Environmental Engineering (CGPA: 3.92/4.00) — **2013-2019**

Thesis: Impacts of Urbanization on Hydrologic Response of Peri-urban Catchments.

- Awarded "*Water Initiative Fellowship (2013-2015)*" from Syracuse University.
- Performed research on seasonal changes in hydrologic performance of green infrastructures.
- Used HOBO U20-L sensors to monitor water level in several urban streams in Syracuse, NY.
- Used Sontek Flow Tracker for stream gaging in several urban catchments in Syracuse, NY.
- Calibrated SWMM for a peri-urban catchment in Syracuse, NY.
- Performed intensive data manipulation in R, Python, MATLAB, and ARCGIS.
- Performed parametric and nonparametric statistical tests in R and Excel.
- Developed a real-time ensemble flood forecasting system in R using SAC-SMA and ANFIS.
- Developed a new geometric index (RNICO) to assess the impact of urban development pattern on peak flows and stream flashiness in peri-urban catchments.

FERDOWSI UNIVERSITY MASHHAD, IRAN

M.Sc., Hydraulic Structures **2005-2008**

B.Sc., Civil Engineering **2001-2005**

Publications:

Roodsari, B.K. and D. G. Chandler (2017). *Distribution of Surface Imperviousness in Small Urban Catchments Predicts Runoff Peak flows and Stream Flashiness.* doi: 10.1002/hyp.11230. Hydrological Processes.

Roodsari, B.K., Chandler, D.G., C. Kelleher., and C.N. Kroll (2018). *A Comparison of SAC-SMA and Adaptive Neuro-fuzzy Inference System for Real-time Flood Forecasting in Small Urban Catchments.* https://doi.org/10.1111/jfr3.12492. Journal of Flood Risk Management.

Roodsari, B.K. and D. G. Chandler (under review). *RNICO: a new geometric index for assessing the impact of urban development pattern on runoff peak flows and stream flashiness is small peri-urban* catchments. Hydrological Processes.

Pu, G., Roodsari, B.K., Hamilton, K.A., Stillwell, C., Haas, F., F.A. Montalto (manuscript in preparation). *Reducing urban runoff on ultra-urban private land: performance of a Bronx River lined stormwater treatment wetland.*

Roodsari, B.K., Chen, W., DiGiovanni, K., and F.A. Montalto (manuscript in preparation) *Monitoring and Modeling the hydrologic performance of a right-of-way bioswale in NYC*.

Roodsari, B.K., Yu, Z., White, S., Fritsch, M., Brown, C., and F.A. Montalto (2018). *Green Infrastructure Living Laboratory White Paper 1: Monitoring of a Rainwater Harvesting Cistern in Philadelphia, PA.* Philadelphia. Water Department Research project.

Driscoll, C.T., Eger, C.G., Chandler, D.G., Davidson, C. I., Roodsari, B.K., Flynn, C.D., Lambert, K.F., Bettez, N.D., and P.M. Groffman (2015). *Green Infrastructure: Lessons from Science and Practice*. A publication of the Science Policy Exchange. 32 pages.

Moosavian, N. and B.K. Roodsari (2014). *Soccer League Competition Algorithm: A Novel Meta-heuristic Algorithm for Optimal Design of Water Distribution Networks*. Swarm and Evolutionary Computation 17, 14–24. doi: 10.1016/j.swevo.2014.02.002.

Moosavian, N. and B.K. Roodsari (2014). *Soccer League Competition Algorithm, a New Method for Solving Systems of Nonlinear Equations*. International Journal of Intelligence Science 4, 7–16. doi:10.4236/ijis.2014.41002.

Eger, C.G., Chandler, D.G., Roodsari, B.K., and C.T. Driscoll (2014). *Water Budget Triangle. A New Conceptual Framework for Comparison of Green and Gray Infrastructure*. International Conference on Sustainable Infrastructure 2014. DOI: 10.1061/9780784478745.095.

Roodsari B. K., Sharifi M.B., and B. Ghahraman (2010). *Study the Rain gage Density and Spatial Analysis for Annual Rainfall in Khorasan Province using Geostatistical methods*, Iranian Journal of watershed Management, Science & Engineering.Vol4, No10.

Farzanegan H., Roodsari B. K., and N. Moosavian (2009). *Simulating the Variation of Water Quality of Dam Reservoirs Using HEC-5Q Model*, International Conference on Water Resources.

Moosavian N., Roodsari B. K., and H. Farzanegan (2009). *Evaluation of Control & Telemetry Systems Application in Water Distribution Networks (A Case Study of Mashhad WDS)*, International Conference on Water Resources.

Roodsari B.K., Moosavian N., and H., Farzanegan (2009). *A Case Study of GIS Application in Rain gage Network Optimization Using Geostatistical Methods*, International Conference on Water Resources.

Roodsari, B.K., and H. Teimoori (2007). *Reservoir Storage Curve Estimation based on RS method*, First National Conference on Dam & Hydraulic Structures, Karaj, Iran.

Sharifi M.B., and B.K. Roodsari (2007). *A Review of the Methods for Estimating Areal Reduction Factors for Design Rainfalls*, Journal of Design and Construction. Vol2, No4, Iran.

Professional Work Experience

DREXEL UNIVERSITY PHILADELPHIA, PA

Research Scientist **2017-Present**

- Managing the Green Infrastructure Living Laboratory (GILL) project for real-time monitoring of Green Infrastructure sites on private properties in Philadelphia, PA.
- Real-time monitoring of soil moisture, ET, and inflow/outflow in rain gardens.
- Performing Simulated Runoff Tests (SRTs) at rain gardens.
- Monitoring water level in a rainwater harvesting cistern at Drexel University campus.
- Assessing the hydraulic performance of the Rec. Center rainwater harvesting cistern.
- Coordinating meetings and writing technical reports for Philadelphia Water Department.

- Monitoring equipment installation in several green infrastructure sites in NYC.

PAZHOUHAB SHARGH CONSULTING ENGINEERS CO. MASHHAD, IRAN

Head of Water Engineering Office **2007-2013**

- Visited water engineering project sites to record project elements.
- Studied the history of population growth and water consumption in the city.
- Modeled existing water networks and reported the current network problems to the investor.
- Applied mathematical methods to predict future population and water consumption.
- Applied the predicted future population and water demand for future water network.
- Anticipated water resources management strategies for future years.
- Modeled the future water distribution network in EPANET and WATERGEMS.
- Developed technical reports for the current and future conditions of water networks.
- Developed design drawings in AUTOCAD in collaboration with the project architects.
- Submitted project reports through official letters to the investor.
- Organized and planned time schedules for each project in MS project.
- Defined daily, weekly, and monthly duties for the project members.
- Developed contract documents for the tenders.
- Estimated an initial project cost and calculated the suggested value based on cost estimation.
- *Sum of eight project budgets: USD 32 million.*

METARAH CONSTRUCTION CO. MASHHAD, IRAN

Civil Engineer **2005-2007**

- Visited the three railroad project sites to update project construction costs.
- Performed weekly cost analysis for the new constructions (e.g. railroad, bridge, and building).
- Developed official payment request reports and submitted to the investor office for review and payment.
- *Sum of three project budgets: USD 56 million.*

Presentations & Posters:

Roodsari, B.K., Chen, W., DiGiovanni, K., and F.A. Montalto (oral presentation). *Case Study: Monitoring and Modeling the Hydrologic Performance of a Right-of-Way Bioswale in NYC.* International Low Impact Development Conference 2018.

Roodsari, B.K., Pu, G., Hamilton, K.A., Stillwell, C., Haas, F., and F.A. Montalto (poster presentation). *Case Study: Water Quantity and Quality Mitigation Performance of a Constructed Wetland in NYC*. International Low Impact Development Conference 2018.

Soldner, K., Roodsari, B.K., Yu, Z., Fritch, M., and F.A. Montalto (oral presentation). *Reducing costs of Green Stormwater Infrastructure monitoring data collection to inform site maintenance decisions with real-time soil moisture sensing technologies and the Internet of Things*. International Low Impact Development Conference 2018.

Roodsari, B. K. and D. G. Chandler (2016). *RNICO: A New Simple Geometric Index for Assessing the Impact of Urban Development Pattern on Peak flows in Urban Catchments*. Oral presentation at the American Geophysical Union Annual Fall Meeting.

Roodsari, B. K. and D. G. Chandler (2016). *Impacts of Imperviousness on Seasonal Runoff Peak flows in Northern Urban Catchments*. Syracuse University's College of Engineering and Computer Science's annual Nunan Lecture and Research Day.

Roodsari, B. K. and D. G. Chandler (2015). *A Hybrid Data-driven Model for Real-time Urban Flood Forecasting*. American Geophysical Union Annual Fall Meeting.

Roodsari, B. K. and D. G. Chandler (2014). *Green Infrastructures Performance in Cold Climates*. Syracuse University's College of Engineering and Computer Science's annual Nunan Lecture and Research Day.

Roodsari, B. K. and D.G. Chandler (2014). *Green Infrastructures Performance in Cold Climates*. 15th Annual Onondaga Lake Scientific Forum (OLSF), Sponsored by Upstate Freshwater Institution, State University of New York college of Science & Forestry(SUNY-ESF) and Syracuse University.

Roodsari, B. K., Eger, C., Ma, J., and D. G. Chandler (2014). *Low Impact Development for Cold Regions: Evaluation of SWMM 5.0 Snowmelt Model Against Seasonal Change*. 14th American Ecological Engineering Society Meeting, Charleston, SC.

Teaching Experience

SYRACUSE UNIVERSITY SYRACUSE, NY

Teaching Assistant **2014-2017**

Courses: *Fluid Mechanics, Water Resources Management, and Introduction to Geomatics and BIM.*

SADJAD UNIVERSITY MASHHAD, IRAN

Part Time Faculty Member **2007-2013**

Courses: *Hydraulic Structures, Fluid Mechanics, Statics, and Strength of Materials.*

FERDOWSI UNIVERSITY SYRACUSE, NY

Teaching Assistant **2007-2008**

Courses: *Fluid Mechanics, and Water & Wastewater Engineering.*

Computer Skills

Hydrologic/Hydraulic Modeling: SWMM, SAC-SMA, HSPF, EPANET, Water GEMS, Water Hammer, HEC-HMS, HEC-RAS, HEC-GEORAS, HEC-GEOHMS, RS-MINERVE, Sewer CAD, BASINS, and UVQ.

Data management: R, ARCGIS, EXCEL, MATLAB, Python, ACCESS, SPSS, Minitab, Surfer, and SigmaStat.

Other: AUTOCAD, Word, MS Project, and Trimble Realworks.

Memberships and Positions

Drexel University	Research Scientist/Project Manager	**2017-Present**
Syracuse University	Water Initiative Fellow	**2013-2015**
Syracuse Univ. Graduate Student Org.	Inter. Res. Committee member	**2013-2015**
American Society of Civil Engineers (ASCE)	Member	**2013-Present**
American Geophysical Union (AGU)	Member	**2014-2017**
Iranian Construction Engineering Organization	Construction Inspector	**2010-Present**

Pazhouhab Consulting Engineers Co.	Head of Water Engineering Office	**2008-2013**
Scientific Association of Ferdowsi University	Head	**2001-2003**